FACULTY OF TEXTILE ENGINEERING TUL

Dissertation Thesis

Multi-Layer Phase Change Materials System for Thermal Energy Storage

Study programme:	P3106 Textile Engineering
Study branch:	Textile Technics and Materials Engineering

Author:	**Kai Yang, M.Eng.**
Thesis Supervisor:	prof. Ing. Jiří Militký, CSc. Department of material engineering

Liberec 2023

Declaration

I hereby certify, I, myself, have written my dissertation as an original and primary work using the literature listed below and consulting it with my thesis supervisor and my thesis counsellor.

I acknowledge that my dissertation is fully governed by Act No. 121/2000 Coll., the Copyright Act, in particular Article 60 – School Work.

I acknowledge that the Technical University of Liberec does not infringe my copyrights by using my dissertation for internal purposes of the Technical University of Liberec.

I am aware of my obligation to inform the Technical University of Liberec on having used or granted license to use the results of my dissertation; in such a case the Technical University of Liberec may require reimbursement of the costs incurred for creating the result up to their actual amount.

At the same time, I honestly declare that the text of the printed version of my dissertation is identical with the text of the electronic version uploaded into the IS/STAG.

I acknowledge that the Technical University of Liberec will make my dissertation public in accordance with paragraph 47b of Act No. 111/1998 Coll., on Higher Education Institutions and on Amendment to Other Acts (the Higher Education Act), as amended.

I am aware of the consequences which may under the Higher Education Act result from a breach of this declaration.

December 18, 2023 Kai Yang, M.Eng.

Acknowledgements

Having handed in this dissertation, I owe an immense amount of gratitude to a large number of individuals for their invaluable assistance. I would like to begin by expressing my utmost gratitude and appreciation to my supervisor, Prof. Ing. Jiří Militký, CSc. EURING, for being extremely supportive and helpful during the entire process of my research and study program. Having him as my mentor has played a vital role in shaping me as a researcher and accomplishing my objectives at every stage of my tenure at the Technical University of Liberec. My sincere thanks to the co-supervisor, Dr. Mohanapriya Venkataraman for her invaluable support towards my research work. I also would like to thank prof. Dr. Jakub Wiener, for supporting me during the whole PhD study. I truly thank them for their encouragement, cooperation, and concentrated discussions throughout this work. They have helped me realize the significance of condensing and presenting my ideas in a coherent and approachable fashion.

I am grateful to all of those with whom I have had the pleasure to work. I would like to thank Dr. Miroslava Pechočiaková, and Dr. Blanka Tomková (Head of Department, KMI) for their insightful comments throughout the course of my research. I would also like to thank Dr. Iva Mertová (Vice-Dean for Development and Ph.D. Studies) for her crucial guidance. I would also like to thank from the bottom of my heart the laboratory personnel in the Department of material engineering, who were always available to assist me. It will be incomplete, without my special thanks to Ing. Hana Musilová and Mrs. Bohumila Keilová, for their relentless support every step of the way, since my very first day at the Technical University of Liberec. I am especially grateful to Ing. Lenka Martinkova (INOTEX company, Czech Republic) for granting me the exceptional opportunity in the industry, under her expert supervision and guidance.

Finally, I would like to express my heartfelt gratitude to my dear friend Ms. Xiuling Zhang. She has been always supporting my study and life. Without her support, I could not imagine my PhD study life. Besides, I thank my close friends Mr. Yuanfeng Wang, Mr. Shi Hu, Ms. Dan Wang, Mr. Xiaodong Tan, Ms. Qingyan Peng and Dr. Xiaoman Xiong. I also sincerely appreciate my family, my father and my mother. I also owe an enormous debt of gratitude to the people who have been my closest friends and trusted associates over the years, for their ongoing support and inspiration.

Abstract

The aim of the dissertation work is to prepare and characterize a multi-layer fabric for buffering thermal shocks from the environment using a phase change material (PCM) and protection against leakage of PCM in the liquid state (above and in the phase change region)

Although there have been various PCM contained textiles, there are still some problems with their practical use. The amount of PCM in fibers or fabric is limited when they significantly deteriorate other properties (e.g., mechanical property, breathability etc.). The multi-layer fabric is composed from PCM-loaded layer, barrier layer and protective layer. By controlling the interfacial adhesion of melting PCMs on barrier layer or protection layer, the leakage phenomena were totally avoided. The PEG and paraffin wax were selected as PCMs in such multi-layer fabric. The maximum loading amount of PCMs in the multi-layer fabric was 45 wt%. Correspondingly, the overall enthalpy value of the multi-layer fabric was high as 78 J/g, which supported thermal buffering effects

Besides, the introduction of metal microparticles in the PCM-loaded layer was able to enhance heat transfer through the whole multi-layer fabric.

Furthermore, the breathability of the multi-layer fabric was also realized by modifying PCM-loaded layer. The PCM-loaded layer was split to system of air pockets and PCM pockets. However, the heat transfer through the breathable multi-layer fabric became complicated. The size of air pockets was strongly connected to the mutual heat transfer between PCM pockets and air pockets.

The research work not only provided an alternative to have a textile containing PCM, but also extended the application of nanofibrous membranes in smart textiles. It has been verified that the nanofibrous PUR membrane incorporated into the multilayer textiles meets the requirements of preventing PCM leakage during phase changes and ensures their practical use.

Keywords: *PCM, PUR nanofibrous membrane, PCM leakage, interfacial adhesion, thermal energy storage, thermal buffering effect, metal particles, breathability*

Abstrakt

Cílem disertační práce je připravit a charakterizovat vícevrstvou tkaninu pro tlumení tepelných šoků z okolí s využitím materiálu s fázovou změnou (PCM) a ochranu před únikem PCM v kapalném stavu (nad a v oblasti změny fáze). Ačkoli jsou známy textilie obsahující PCM v různé formě (obvykle zapouzdřených v mikro kapsulích), existují stále problémy s jejich praktickým použitím. Množství PCM ve vláknech nebo tkaninách je omezené, protože se významně zhoršují jiné vlastnosti (např. mechanické vlastnosti, prodyšnost atd.). Navržená vícevrstvá textilie se skládá z vrstvy plněné PCM, bariérové vrstvy a ochranné vrstvy. Řízením mezifázové adheze roztavených PCM na bariérové vrstvě nebo ochranné vrstvě bylo zcela zabráněno jevu úniku. PEG a parafínový vosk byly vybrány jako vhodné PCM v připravené vícevrstvé textilii. Maximální množství PCM v připravené vícevrstvé tkanině bylo 45 % hmotnostních procent, což výrazně převyšuje množství kapsulí PCM na textiliích. Celková hodnota entalpie vícevrstvé tkaniny byla také vysoká, tj. 78 J/g, což podporovalo tepelné tlumící efekty.

Kromě toho zavedení kovových mikročástic do vrstvy plněné PCM o zvýšilo přenos tepla celou vícevrstvou textilii.

Zlepšení prodyšnosti připravené vícevrstvé tkaniny byl také realizováno úpravou vrstvy plněné PCM. Vrstva plněná PCM byla rozdělena na vzduchové kapsy a kapsy obsahující PCM. Zkomplikoval se však přenos tepla prodyšnější vícevrstvou textilií. Optimální velikost vzduchových kapes byla silně ovlivněna vzájemným přenosem tepla mezi PCM obsahující kapsami a vzduchovými kapsami.

Výzkumná práce poskytla nejen novou alternativu k přípravě textilií obsahující PCM, ale také rozšířila aplikaci speciálních nanovlákenných membrán v inteligentních textiliích. Bylo ověřeno, že nanovlákenná PUR membrána začleněná do vícevrstvé textilie splňuje požadavky zabránění úniku PCM při fázových změnách a zajišťuje jejich praktické použití.

Klíčová slova: *PCM, PUR nanovlákenná membrána, únik PCM*, *mezifázová adheze, akumulace tepelné energie, tepelný tlumicí efekt, kovové částice, prodyšnost*

摘要

本论文成功提出一种纤维多层相变材料（PCM）系统，并用于缓冲环境中的热冲击及熔融 PCM 的泄漏。尽管已经出现了多种载有 PCM 的纺织品，但在实际使用过程中仍存在一些问题，尤其是纤维或织物中的 PCM 负载量受到限制。当 PCM 负载量增加时，负载 PCM 的纺织品的其他性能会受到影响（例如机械性能、透气性等）。该论文所提出的纤维多层 PCM 系统由 PCM 负载层、阻隔层和保护层组成。通过控制熔融相变材料在阻挡层或保护层上的界面粘附行为，PCM 的泄漏得以控制。在这种纤维多层 PCM 系统中，选择聚乙二醇和石蜡作为相变材料。纤维多层 PCM 系统中 PCM 的最大负载量为 45wt%，且纤维多层 PCM 系统的总焓值高达 78 J/g，足以支撑热缓冲效应。通过使用不同分子量的 PCM，可以调节纤维多层 PCM 系统的工作温度。另外，在 PCM 负载层中引入金属微粒能够增强整个纤维多层 PCM 系统的传热。 此外，通过改进 PCM 负载层的结构，将 PCM 负载层被分成气穴和 PCM 穴，从而使得纤维多层 PCM 系统的透气性得以改善。但是，该透气纤维多层 PCM 系统的热传递行为比较复杂，并与气穴及 PCM 穴的大小相关。

该研究工作不仅为含有 PCM 的纺织品提供了替代方案，而且扩展了纳米纤维膜在智能纺织品中的应用。尤其是，含有纳米纤维 PUR 膜的多层纺织品中的满足相变过程中防止 PCM 泄漏的要求，保证了其实际使用。

关键词：PCM，PUR 纳米纤维膜，PCM 渗漏，界面粘附，热能储存，热缓冲效应，金属颗粒，透气性

Content

Figure List

List of Tables

List of abbreviation

BN: boron nitride

CA: capric acid

CNF: cellulose nanofiber

CS: chitosan

EG: expanded graphite

FSPCM: form-stable PCM

H-SiC-modified MF: hydrophobic-silicon carbide modified melamine-formaldehyde

GO: graphene oxide

LA: lauric acid

MA: myristic acid

MES: methyl stearate

MF: melamine-formaldehyde resin

MP: metal particle

MPF: melamine-paraformaldehyde

MPCM: PCM capsule

MUF: melamine-urea-formaldehyde

MWCNT: multi-walled carbon nanotube

MP: methyl palmitate

PAN: polyacrylonitrile

PCM: phase change material

PDMS: polydimethylsiloxane

PEG: polyethylene glycol

PET: polyester

PMMA: poly(methyl methacrylate)

PP: polypropylene

PU: polyurethane

PVA: polyvinyl alcohol

PVDF: polyvinylidene fluoride

PVP: polyvinylpyrrolidone

PW: paraffin wax

SA: stearic acid

SWCNT: single-wall carbon nanotube

TD: tetradecyl alcohol

UF: urea formaldehyde

List of Symbols

Bi: Biot number

D_0: length of PCM pocket before heating/cooling cycles

D_1: length of PCM pocket after heating/cooling cycles

h: free convection coefficient (W m^{-2} K^{-1})

I: thermal insulation value

k: thermal conductivity (W m^{-1} K^{-1})

L: thickness of the sample (mm)

L_0: thickness of PCM pocket before heating/cooling cycles

L_1: thickness of PCM pocket after heating/cooling cycles

p: PCM loading amount (wt%)

$p_{overall}$: overall PCM loading amount in fibrous multi-layer PCM system (wt%)

R_{PEG}: mass ratio of PEG to viscose fabric

t: time (s)

$t_{h,65}$: time to reach 65 °C during heating process (s)

$t_{c,40}$: time to reach 40 °C during cooling process (s)

t_{phase}: time for phase transition (s)

T: temperature (°C)

T_f: the final temperature of sample (°C)

T_i: the initial temperature of sample (°C)

T_s: is the sample temperature with time t (°C)

T_{phase}: temperature for phase transition (°C)

τ: is the cooling (heating) rate constant (°C/s)

χ_0: predicted relative crystalline degree according to database (%)

χ: experimental relative crystalline degree according to measurement (%)

$\Delta H_{m,sample}$: measured melting enthalpy value of sample (J/g)

$\Delta H_{m,PCM}^{T}$: theoretical melting enthalpy value of PCM (J/g)

$\Delta H_{m,PCM}$: measured melting enthalpy value of the measured PCM (J/g)

$\Delta H_{m,overall}$: overall enthalpy value of sample (J/g)

η: PCM encapsulation efficiency (%)

1. Introduction

Phase change materials (PCM) are a group of materials that adsorb/release thermal energy during their phase transition. The PCM could be applied in various fields, including building materials, solar energy storage, the thermal management of the electronic system, food storage, smart textiles, and so on [1–6]. The discussions of the PCM related to the PCMs classification, the preparation of PCMs, the application of PCM have been reviewed in various published works [2,7–14]. Besides, the toxicity, health hazards, and commercialization of PCMs are reviewed by S.S. Chandel et al [15]. It is also reported that the market revenue of the PCMs is increasing with rate of 19 % and can reaches 5.1 billion dollars, which is shown in **Figure 1 (A)**.

Especially, the PCM-incorporated textiles have attracted more and more attention even from academics (**Figure 1 (B)**) (PCMs publications are determined by search 'phase change material' for 'abstract' or 'title' or 'keyword', and PCM-incorporated textile publications are determined by search 'phase change material' and 'textile' or 'fabric' or 'yarn' or 'fiber' for 'abstract' or 'title' or 'keyword'). It is well known that the first introduction of PCM into textiles was realized from NASA in the early 1980s, which was aimed to improve the thermal protection against the extreme temperature fluctuation in the outer space. The basic working principal of PCM-incorporated textiles is the realization of thermal energy storage when the phase transition of PCM between the solid and liquid phase while the temperature of PCM during the phase transition is little altered. Besides, the thermal resistance of the PCM-incorporated textiles is enhanced when there is the phase transition of PCM. Now, there are various commercial PCM-incorporated textile products over the globe (e.g., air condition thermal fiber from Outlast company, Smartskin fabric, Triangle R&D and so on), which is shown in **Figure 1 (C)**. The main function of the PCM-incorporated textiles includes thermal regulation, heat protection, thermal energy harvesting and so on (**Figure 1 (D)**).

The main reasons for the rapid development of the PCM textiles could be two aspects:

1) The first aspect is based on the various functional applications of textiles. It is indicated that the concept of 'textile structures' include fiber, yarn, and fabric [16]. Since the successful fabrication of the ultrafine fibers via the advanced technologies, the flexibility of the ultrafine fibers supports the high compatibility with various other materials. Besides, the yarns are considered a special structure where the twist enhances the mechanical property. The release/store of the mechanical property in the yarns could be realized. In addition, the fabric is a stable porous structure. By modifying the fabric, various applications are proposed, including the antibacterial

property, oil/water separation, particle filtration, thermal regulation, Joule heating property, optical property, EMI shielding etc. [17–26].

2) The second aspect is based on the usage of the PCM. The usage of the PCM is proposed to enhance the thermal regulation and thermal energy storage, and also supports the light radiation-thermal energy conversion, solar-thermal energy conversion, and so on [27].

Although there has been a great achievement in PCM-incorporated textiles, there are still some challenges. The limited thermal energy storage of PCM-incorporated textiles is found, which is caused by limited mass of PCMs in the textiles and confined crystallization of PCMs in the textiles. So, how to effectively increase thermal energy storage and thermal buffering effect of PCM-incorporated textiles should be focused on. Besides, the thermal energy storage efficiency of PCM-incorporated textiles is low. Enhancing the thermal energy storage efficiency of PCM textiles can support other applications, which is also necessary to be solved.

This dissertation work is in the form of commented set of published scientific papers dealing with preparation, characterization and testing of multi-layer fabric for buffering thermal shocks from the environment by using of PCM. Full texts of four most important papers where I am first author are in appendix. In total, the set of scientific paper contains 20 research works published in impact factor journals and 17 conference paper. There were 5 published chapters in scientific books.

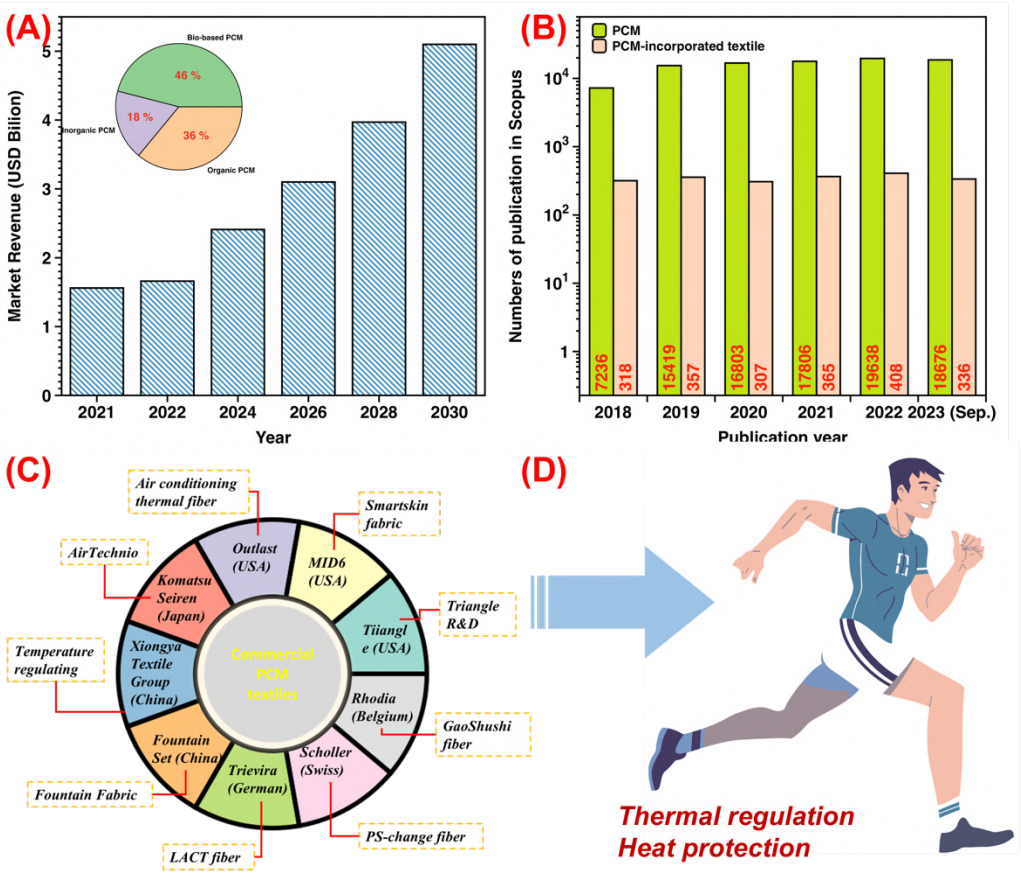

Figure 1 Necessity to develop PCM-incorporated textiles (A: Current market revenue of PCMs and their podcast, B: publications related to PCMs and PCM-incorporated textiles from Scopus, C: famous commercial products, and D: function of PCM-incorporated textiles for human

2. State of the Art

2.1 Suitable PCM for textiles

It is well known that the PCM is classified into two types: inorganic PCM and organic PCM [28]. However, the phase separation and corrosion property of inorganic PCM are found, which make inorganic PCMs unsuitable for textiles. So, the organic PCM are used for textiles, which includes paraffin wax, fatty acid, polyethylene glycol and so on. However, the leakage and low thermal conductivity of the organic PCM are the main problems for the practical applications. To avoid leakage, microencapsulated PCMs (MPCM) and form-stable PCMs (FSPCM) have been proposed [29–31].

- PCM capsules (MPCM)

MPCM has been the most industrial technology and its application in textiles has been studied for decades [32,33]. The summary for the MPCM is shown in **Figure 2 (A)**. The MPCM consists of supporting materials as shell and PCM as core, where stability

of thermal energy storage and phase transition of MPCM is enhanced [34]. The biggest advantage of MPCM is the good encapsulation of PCMs. Besides, there are various preparation methods for development of MPCM, such as suspension-like polymerization, photo-induced microencapsulation, interfacial polymerization etc. According to the shell type of MPCM, there are three MPCM, including organic MPCM, ceramic MPCM and metallic MPCM. Among three MPCM, the organic MPCM are usually for textiles since they have no corrosion and easy control. However, the poor mechanical property of the organic MPCM is found, which results in unexpected destroy of MPCM during their coating on fabrics. Besides, the overall thermal conductivity of the MPCM reduces the heat transfer efficiency. In addition, the encapsulation efficiency of MPCM requires modification and the reproducibility of the MPCM is difficult [33].

- Form-stable PCM (FSPCM)

FSPCM is an alternative to avoid leakage of PCM and realize thermal energy storage, which is shown in **Figure 2 (B)**. FSPCM is usually prepared by filling PCM into porous materials (e.g., zeolite, aerogel, foam etc.) [29,35–38]. Although the leakage of molten PCMs can be avoided, the self-crystalline behavior of the encapsulated PCM in the FSPCM is significantly confined and thermal energy storage and phase transition behavior of the FSPCM is different from pure PCM [39,40]. Besides, the environment could have a side effect on the phase transition behavior and thermal energy storage of FSPCM. For example, our recent work revealed that a significant side effect of hot and humid environment resulted in a reduced overall thermal energy storage of PCM/expanded graphite composites [41].

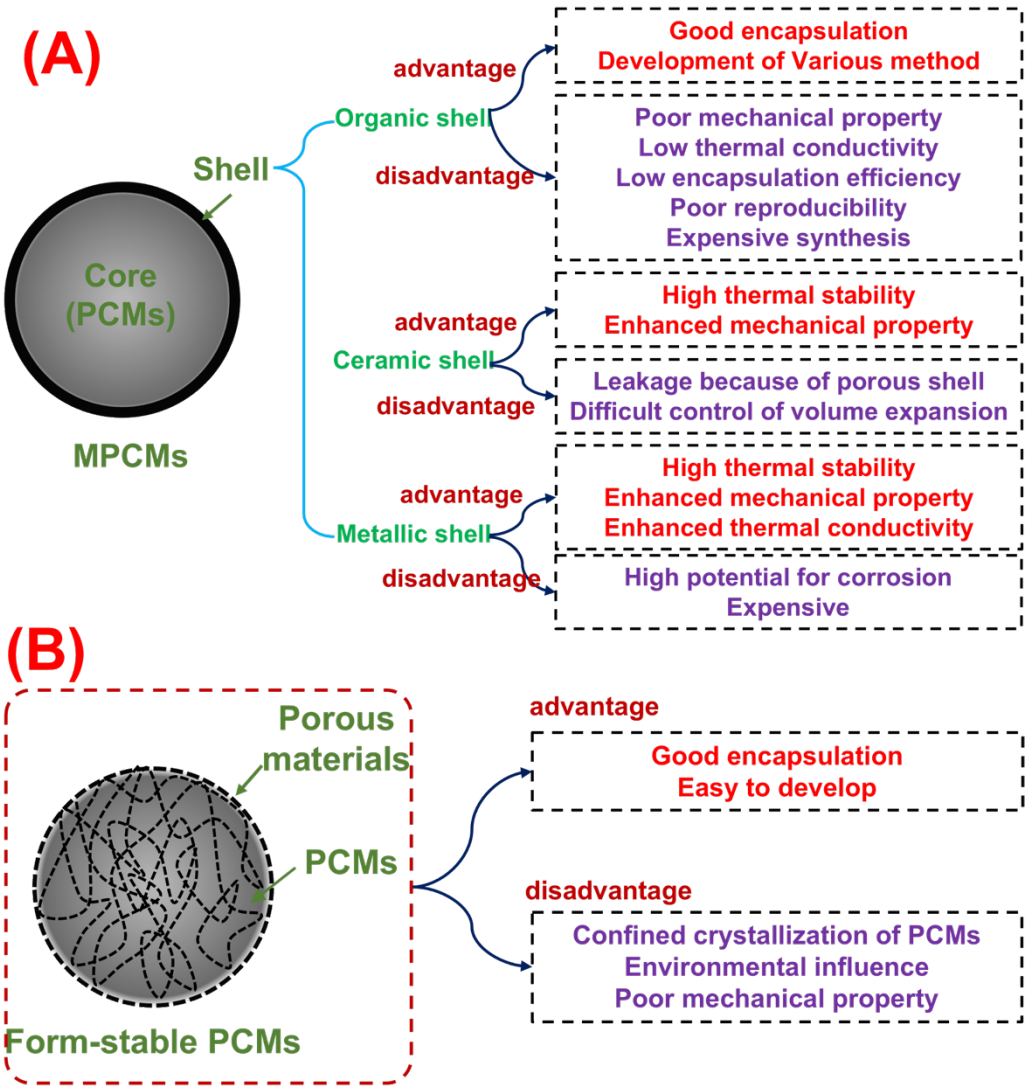

Figure 2 Current problems of PCM (A: MPCM, and B: FSPCM)

2.2 Incorporation of PCMs into textiles

2.2.1 PCM containing fibers

For PCM containing fibers, the PCM are trapped in the fiber matrix. Various technologies are used to prepare the PCM containing fibers, including electrospinning, centrifugal spinning, molten spinning, solution spinning, dry-jet quenching spinning, interfacial polyelectrolyte complex spinning, vacuum impregnation, and injection spinning [44]. Then, the various polymers have been successfully used as the supporting materials for the storage of the different PCMs, including polyester (PET), polyvinyl alcohol (PVA), polyurethane (PUR), and etc. Although there is a great achievement in PCM incorporated fibers, some drawbacks or problems remain to be solved.

As shown in **Figure 3 (A)**, two key factors are taken into consideration for the PCM

containing fibers. Firstly, the PCM loading amount of the PCM containing fibers is limited, which is related to the mechanical property. Higher PCM loading amount reduces the mechanical property of PCM containing fibers although increase the thermal energy storage. Especial for MPCM containing fibers, the recommended maximum MPCM loading amount is 10 wt% [28]. Secondly, there is a strong confinement of PCM inside the PCM containing fibers, which results in reduced thermal energy storage. Besides, it is reported that the PCM containing fibers have a stable phase transition behavior after heating/cooling cycles. However, the mechanical property of the PCM containing fibers after heating/cooling cycles should be different from the one without heating/cooling cycles since the crystalline structure of the PCM inside the PCM containing fibers is altered, although there are no research works to report.

The PCM containing fibers are also for fabrication of PCM-incorporated yarns or PCM containing fabrics. In this case, the similar problems are found as described.

Apart from such PCM containing fibers, the coating of PCM on the fibers is an alternative. However, it is not standard as PCM containing fibers and there are few works related to such topic.

2.2.2 PCM containing fabrics

For PCM containing fabrics, the pad-dry-cure coating method is the most popular to have a coating of MPCM (or FSPCM) on the fabric [5,42,43]. To enhance the ability of MPCM (or FSPCM) on the fabric, the binder is necessary to be used. Then, such MPCM (or FSPCM)-coated fabrics have thermal regulation behavior. Although there are some achievements in the MPCM-coated fabrics, some problems remain to be solved, which is shown in **Figure 3 (B)**.

Firstly, the MPCM loading amount on the fabric is limited and shorter thermal buffering effect is suggested. Secondly, the surface chemistry and mechanical property of MPCM-coated fabrics are changed since there is a coating by using binders. The type of binders significantly affects thermal comfort (e.g., moisture management etc.). Thirdly, the breathability (e.g., air permeability, water vapor permeability) is reduced since there is a MPCM (or FSPCM) coating layer on the fabric surface. Fourthly, loss or damage of MPCM possibly happens because of external mechanical damage (e.g., due to washing, abrasion). The leakage of the MPCM also possibly happens during the coating process.

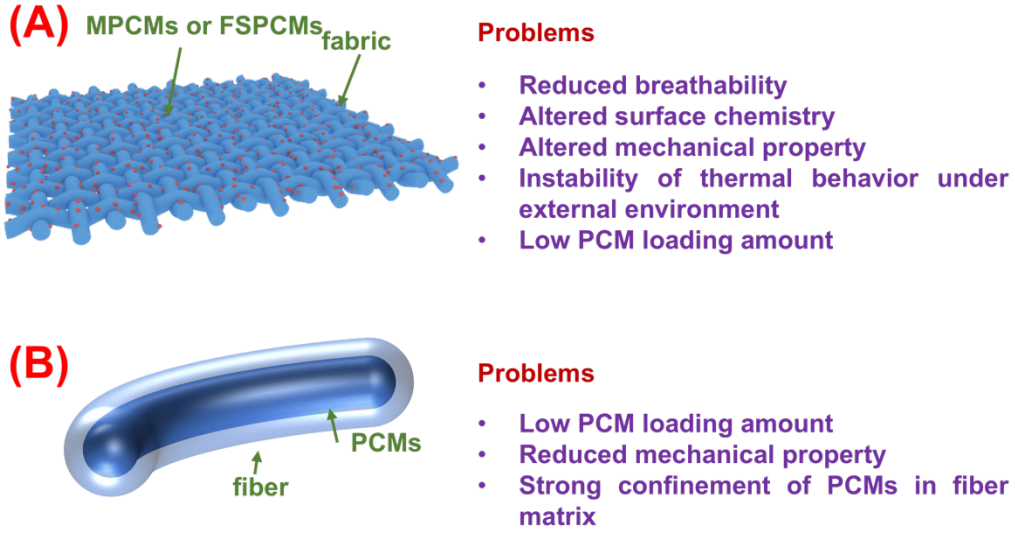

Figure 3 Current problems of PCM-incorporated textiles (A: PCM containing fibers, and B: PCM containing fabrics)

2.2.3 Characterization of PCM-incorporated textiles

There are various methods to characterize thermal buffering effect of PCM-incorporated textiles (Details are given in **9.5** in **APPENDIX 1**). Among all the methods, the temperature-time curve (T-history) is the most convenient one to characterize thermal buffering effect. The whole T-history or selected points only can be used for characterization of thermal buffering effect of PCM [42,45]. Besides, the protection time of the PCM-incorporated textiles has been proposed. This time is determined by the time corresponding to half of difference of final and initial temperature [46]. However, such characterization of T-history cannot provide the exact thermal buffering effect range of the PCM-incorporated textiles.

Kinetics of temperature changes are formally expressed as rate equation of first order is equivalent to so-called Newton's cooling law (used of course for both cooling and heating), which is expressed by **equation (1)**.

$$\frac{dT}{dt} = -(T - T_i)/\tau \tag{1}$$

Where, T_f is the final temperature of sample (for $t \to \infty$), T_i is the initial temperature of sample, T is the sample temperature in time t and τ is the cooling (heating) rate constant.

By integrating of this differential equation in suitable limits (from t=0 where T= T_i till time t where temperature is T), the integral form is expressed in **equation (2)**.

$$T_f - T = (T_f - T_i)e^{-t/\tau} \tag{2}$$

Formal linearization of **equation (2)** is expressed by **equation (3)**:

$$\ln[(T_f - T)] = \ln[(T_f - T_i)] - t/\tau \quad (3)$$

The τ can be therefore approximately related to slope of dependence y = ln (T -T_f) on $x = t$ by linear least squares method.

Figure 4 (A) and **(A')** present one example for standard application of Newton's cooling law. For the common fabric, the temperature-time curve (T-history) is classic, and the parameters of Newton's cooling law are interpretated with physical meaning, and the relevant thermal property of fabric (e.g., thermal conductivity, thermal resistance etc.) can be estimated [27]. To extend the application of this model for better fitting of complex T-history curves with different parts, the different models are proposed for individual parts [28]. As a result, the calculated heating or cooling constants corresponds to different parts of T-history. For PCM-incorporated textiles, the T-history curve consists of three parts, including first sensitive heat storage part with solid PCM, latent heat storage part with solid-liquid PCM and second sensitive heat storage part with liquid PCM. By formal splitting of kinetic **equation (2)** into the three parts of T-history of PCM-incorporated textiles can be estimated. More precise is to integrate rate **equation (1)** for different parts of T history in different limits.

For *Part I*, obviously the lower limit is $t = 0$ and $T = T_i$. This part is bounded by end point (t_1. T_1) which is constraint. Then, the modified **equation (4)** is obtained.

$$\frac{T-T_f}{T_i-T_f} = e^{-(t)/\tau} \quad (4)$$

For *Part II*, the lower limit starts from the point of $t = t_1$ and $T = T_i$ and ends at the point of $t = t_2$ and $T = T_2$. Then, the modified **equation (5)** is obtained.

$$\frac{T-T_f}{T_2-T_f} = e^{-(t-t_2)/\tau} \quad (5)$$

For *Part III*, the lower limit is at point of $t = t_2$ and $T = T_2$ and higher limit could be at point of $t = t_3$ and $T = T_f$. Then, the modified **equation (6)** is obtained.

$$\frac{T-T_f}{T_3-T_f} = e^{-(t-t_3)/\tau} \quad (6)$$

It should be noticed that the use of **equation (1)** assumes here that for all parts have an equilibrium temperature (e.g., T_f). To having the turning points for three parts, the plot of $\ln[(T - T_f)]$ against t can be used. By observing the three linear segments in this plot, the three parts corresponding to solid phase state of textile and PCM, phase transition state of PCM and liquid phase state of PCM are suggested. A pure empirical model based on exponential model expressed in **equation (7)** is proposed. The A is the

factor, and the parameter with subscript *1*, *2*, *3* in **equation (7)** represents three parts of PCMs (solid phase state, phase transition state and liquid phase state).

$$T_f = \begin{cases} T_i + A_1 e^{-\frac{t_1}{\tau_1}} \\ T_2 + A_2 e^{-\frac{t_2}{\tau_2}} \\ T_3 + A_3 e^{-\frac{t_3}{\tau_3}} \end{cases} \quad (7)$$

However, it is hard to obtain the turning points for three parts from T-history curve. By having logarithm for **equation (7),** the three linear parts can be obtained. By observing the linear segments in the plot of $\ln[(T_f - T)]$ aganist *t*, the three parts corresponding to solid phase state, phase transition state and liquid phase state are suggested. After having linear fitting for each part of $\ln[(T_f - T)]$ aganist *t*, the parameters including *A* and τ can be found. By having intersection points of adjacent linear equations, the turning points at time *t* are found. Then, the nonlinear fitting models according to **equation (7)** for full heating T history is used. By taking errors into consideration, the theoretical turning points (time and temperature) for phase transition are estimated by having the intersection points of adjacent nonlinear model in **equation (7)**. **Figure 4 (B)** and **(B')** present one example for standard application of modified Newton's cooling law.

Besides, the thermal insulation (*I*) can provide the potential overheat injury of PCM-incorporated textiles when the PCM-incorporated textiles reach heat balance during heating process, which is expressed in **equation (8)**. The T_h is the temperature of the heater and T_r is the environmental temperature.

$$I = (T_h - T_f)/(T_h - T_r) \quad (8)$$

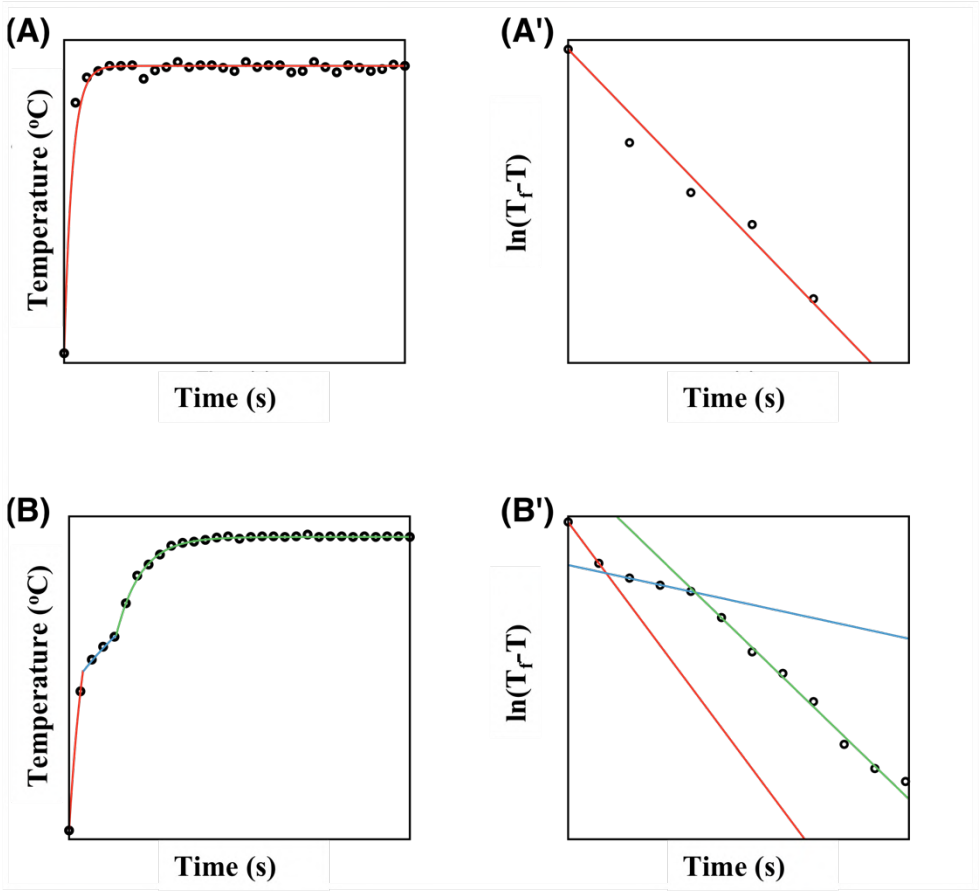

Figure 4 Example for application of Newton's cooling law (A: heating curve with standard Newton's cooling law, A': standard plot of $\ln[(T_f - T)]$ against *t*, B: heating curve with modified Newton's cooling law, and B': nonlinear regression model for $\ln[(T_f - T)]$ against *t*)

3. Motivation and aims

It is well known that the leakage of PCM during heating/cooling cycles is governed by viscosity of molten PCMs and interfacial adhesion between molten PCMs and fabrics if the pure PCMs are coated on fabrics directly. From this point of view, the multi-layer fabric structure with barrier layers covering the PCM-loaded layer (pure PCM-coated fabrics) is promising to avoid leakage [47]. For the selection of the barrier layers, the nanofibrous membranes are advantageous. There are two reasons:

1) By controlling porosity and surface chemistry, various nanofibrous membranes have been applied for oil/water separation, air filtration etc. [48–52].
2) The high resistance against mass transfer of nanofibrous membrane-coated fabrics have been proposed [53,54].

From this point of view, the nanofibrous membranes can be used as barrier layer to resist against the penetration of molten PCMs.

In this work, we first tried to use nanofibrous membranes in the fibrous multi-layer PCM system. As shown in **Figure 5**, the fibrous multi-layer PCM system consists of PCM-loaded layer, barrier layer and protection layer. The PCM-loaded layer is PCM-coated fabric. The viscose nonwoven fabric was selected as substrate for coating of various organic PCM (e.g., PEG, PW, myristic acid etc.) since the viscose nonwoven fabric is porous and has a good interfacial adhesion with organic PCM. The PCM-coated fabrics have a mass percentage of PCMs ranging from 80 wt% to 90 wt%. The nanofibrous membrane is used for barrier layer as described. Because of weak mechanical property of barrier layer (nanofibrous membrane), the protection layer was used to avoid damage of barrier layer under external environment. The commercial PET knitted fabric was selected for protection layer. Still, it is necessary to avoid the effect of liquid on the PCM inside the fibrous multi-layer PCM system. Although net PET film has a low surface energy and hydrophobic property, the fibrous structure of PET fabric would result in wicking of solution. Then, the alternatively commercial PET fabric with hydrophobic coating (5 μL water contact angle of 122°) is also selected as protection layer. The details about used fibrous materials are given in **Table 1**, and their structure and morphology are shown in **Figure 6**.

The main objectives of this work include four aims by following strategy as shown in **Figure 5**:

- The first objective is to find suitable multi-layer fabric structures to contain PCM. The multi-layer fabric structure is composed of PCM-loaded layer, barrier layer and protection layer and stabilized by using commercial fibrous tape to connect each layer. Firstly, three different organic PCMs with similar melting/solidifying points are used, including PEG 6000, paraffin wax (PW) and myristic acid (MA) (**Table 2**). Besides, the different fibrous multi-layer PCM systems with different structures are prepared, which is given in **Table 4**. After investigating leakage phenomena of PCM from the fibrous multi-layer PCM system, the selected fibrous materials in the multi-layer fabric containing PCM will be proven. The wetting behavior of molten PCM on various fibrous materials will be also estimated, which are considered for leakage phenomena.
- The second objective is complex characterization of thermal property of the prepared fibrous multi-layer PCM system. The thermal energy storage and phase transition behavior of the suitable fibrous multi-layer PCM system will be

investigated by using differential scanning calorimetry (DSC). In addition, the thermal buffering effect will be evaluated by recording heating/cooling T-history curves. Especially, the application of Newton's cooling law is to characterize heating T-history of the fibrous multi-layer PCM system.

- The third objective is to improve the thermal energy storage efficiency of the suitable fibrous multi-layer PCM system. Different metal particles (MP) including copper (Cu), aluminum (Al), silver (Ag), iron (Fe), and zinc (Zn) will be introduced in PCM-loaded layer to increase thermal conductivity supporting energy storage efficiency (Details of MP are given in **Table 3**). Correspondingly, thermal energy storage, phase transition behavior and thermal buffering effect of the MP-incorporated fibrous multi-layer PCM system will be investigated.
- The fourth objective is to improve the breathability of the fibrous multi-layer PCM system. The PCM-loaded layer of the fibrous multi-layer PCM system will be modified and consists of PCM pocket and air pocket. The breathability, thermal energy storage, phase transition behavior and thermal buffering effect of the multi-layer PCM fabrics will be investigated.

Table 1 Details for fibrous materials (mean±standard error)

Fibrous materials	Areal density	Thickness	Diameter of fiber	Water contact angle*	Surface porosity (%)
Viscose nonwoven fabric	47±1.21g/m^2	0.33 ± 0.02mm	13.8±4.79μm	0^o	15.5 ± 1.3
PET knitted fabric	200±2.35g/m^2	0.57 ± 0.01mm	12.5±1.49m	0^o	4.1±1.2
PET knitted fabric with hydrophobic coating	212±2.51g/m^2	0.54 ± 0.01mm	13.57 ± 1.05 μm	122±2.1^o	6.3±1.1
PU nanofibrous membrane	6.0±1.02g/m^2	0.1±0.01mm	292±132nm	131±2.1^o	3.5±1.2

*: water contact angle values were measured after 5 min deposition

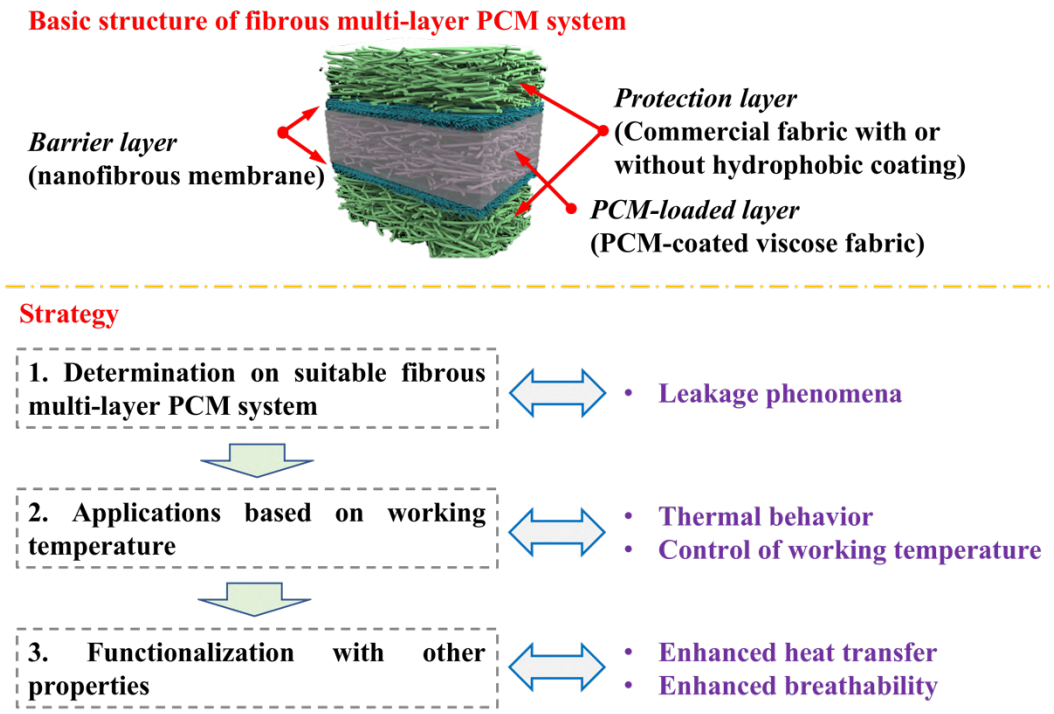

Figure 5 Basic structure of a fibrous multi-layer PCM system and development strategy

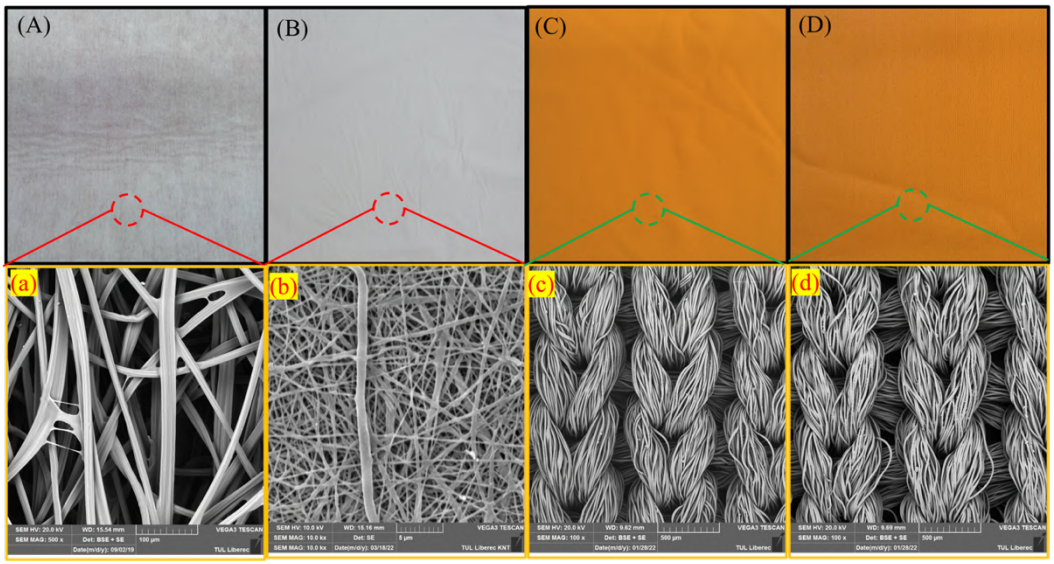

Figure 6 Structure and morphology of used fibrous materials (A, B, C, D: macroscopical images of viscose nonwoven fabric, PU nanofibrous membrane, PET fabric and PET fabric with hydrophobic coating; a, b, c, and d: SEM images of viscose nonwoven fabric, PU nanofibrous membrane, PET fabric and PET fabric with hydrophobic coating)

Table 2 Details of used organic PCMs

Label	Materials	Melting point from Sigma

		Aldrich datasheet (°C)
PEG 600	Polyethylene glycol with molecular weight of 600	17-22
PEG 1000	Polyethylene glycol with molecular weight of 1000	33-40
PEG 1500	Polyethylene glycol with molecular weight of 1500	43-49
PEG 4000	Polyethylene glycol with molecular weight of 4000	53-58
PEG 6000	Polyethylene glycol with molecular weight of 6000	58-63
PW	Paraffin wax	58-62
MA	Myristic acid	52-54

Table 3 Details of metal particles (MP)

MP type	Diameter (D50) (μm)
Cu	35.00
Al	51.47
Ag	23.00
Fe	25.00
Zn	3.60

Table 4 Description of multi-layer PCM fabrics

Sample code	Protection layer	Barrier layer	PCM-loaded layer
$C1_{MA}$	PET fabric	-	MA-coated viscose fabric
$C2_{MA}$	PET fabric	PU nanofibrous membrane	
$C3_{MA}$	PEG fabric with hydrophobic coating	-	
$C4_{MA}$	PEG fabric with hydrophobic coating	PU nanofibrous membrane	
$C1_{PW}$	PET fabric	-	PW-coated viscose fabric
$C2_{PW}$	PET fabric	PU nanofibrous membrane	
$C3_{PW}$	PEG fabric with hydrophobic coating	-	
$C4_{PW}$	PEG fabric with hydrophobic coating	PU nanofibrous membrane	
$C1_{PEG}$	PET fabric	-	PEG-coated viscose fabric
$C2_{PEG}$	PET fabric	PU nanofibrous membrane	
$C3_{PEG}$	PEG fabric with	-	

	hydrophobic coating	
$C4_{PEG}$	PEG fabric with hydrophobic coating	PU nanofibrous membrane

4. Construction of A Fibrous Multi-layer PCM System

Various fibrous multi-layer PCM systems have been developed according to **Table 4**. At first, the leakage of PCM textiles should be solved. After checking leakage phenomena of different combinations of fibrous multi-layer PCM system, two structure of the fibrous multi-layer PCM systems without leakage were successfully obtained. The first one ($C4_{(PW)}$) was the sample consisting of polyester fabric with hydrophobic coating as protection layer, PU nanofibrous membrane as barrier layer and PEG-coated viscose fabric as PCM-loaded layer. The second one ($C4_{(PEG)}$) was the sample consisting of polyester fabric with hydrophobic coating as protection layer, PU nanofibrous membrane as barrier layer and PEG-coated viscose fabric as PCM-loaded layer.

4.1 Mechanism to avoid leakage

It is noticed that the leakage phenomena could be a result of interfacial adhesion between molten PCMs and fibrous materials. The contact angle of molten PCM droplets on the fibrous membrane were investigated. As a result, molten PW droplets can be only on the PU nanofibrous membrane and have a stable contact angle of 110°. Molten PEG droplets can be only on the PU nanofibrous membrane and have a stable contact angle of 130°. The weak interfacial adhesion between molten PW and PU nanofibrous membrane was found, and the weak interfacial adhesion between molten PEG and PET fabric with hydrophobic coating was found (**Figure 7**). Especially for $C4_{(PEG)}$, the successful barrier for resistance of molten PEG was realized by both PET knitted fabric with hydrophobic coating as protection layer and PU nanofibrous membrane as barrier layers (More details are shown in published work **9.1**, **9.2** and **9.4** in **APPENDIX 1**).

So, a combination of weak interfacial adhesion of molten PCMs and fibrous materials and the use of nanofibrous membrane in fibrous multi-layer system accounted for no leakage phenomena.

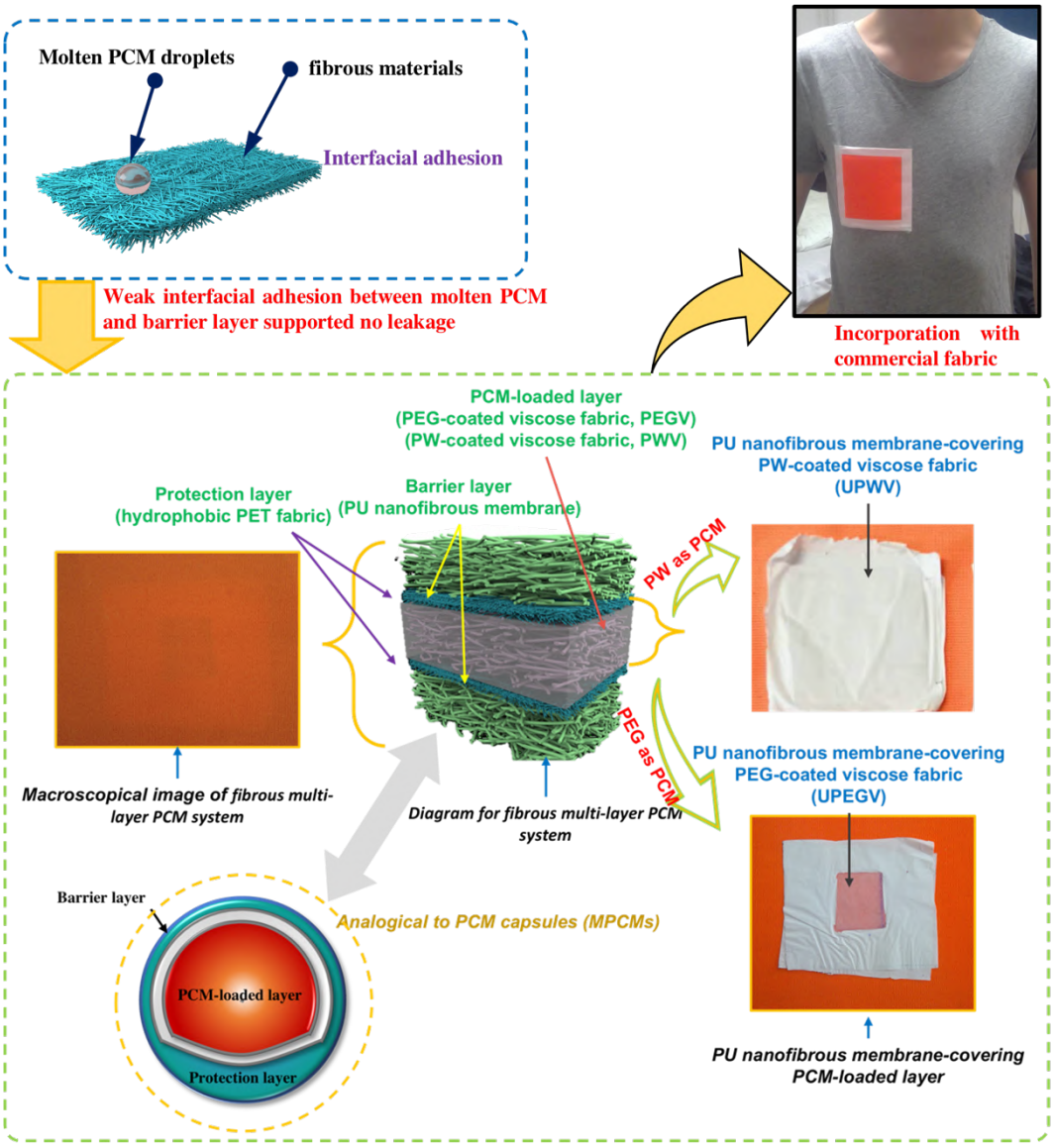

Figure 7 PCM loading situation inside the fibrous multi-layer PCM system and analogy of fibrous multi-layer PCM system to MPCMs

Besides, the PCM (including PEG and PW) were well kept inside the sample C4 fibrous multi-layer PCM system containing PET fabric with hydrophobic coating as protection layer. So, the fibrous multi-layer PCM system can resist the side effects from external environment (e.g., rubbing, water pouring etc.).

For MPCM-coated fabrics, we have reported that the MPCMs are possibly destroyed during padding-coating-drying method. For example, the phase transition and enthalpy values are changed when compared with net MPCMs. It is proposed that the leakage of MPCMs happens because of unexpected mechanical property of their shells. However, the fibrous multi-layer PCM system should be a relatively better control of phase transition and enthalpy values under different external environments because of PET

fabric with hydrophobic coating as protection layer.

4.2 High PCM loading performance in the fibrous multi-layer PCM system

The PCM loading performance is essential for thermal behavior of the PCM-incorporated materials, including encapsulation efficiency, PCM loading amount, relative crystalline degree and working temperature range.

The PCM loading amount (p) is directly related to the thermal energy storage, and higher PCM loading amount supports the higher thermal energy storage. Besides, the self-crystalline behavior of the PCM inside the PCM-incorporated materials is altered because of the confined space for crystallization (e.g., MPCMs, PCM containing fibers, form-stable PCM etc.). The predicted relative crystalline degree (χ_0) of the PCM in the PCM-incorporated materials also supports the higher thermal energy storage. The DSC method is usually for the relative crystalline degree by using **equation (9)**, where $\Delta H_{m,sample}$ is the measured melting enthalpy value of sample (J/g), p is the PCM loading amount and $\Delta H_{m,PCM}^{T}$ is the theoretical melting enthalpy value of PCM. The calculation of the relative crystalline degree is based on the PCM loading amount. It is noticed that paraffin wax has a solid-solid phase transition and solid-liquid phase transition. So, the **equation (10)** modified from **equation (9)** could be used to reveal characterize the experimental relative crystalline degree (χ), where $\Delta H_{m,PCM}$ is the measured melting enthalpy value of the PCM. The experimental relative crystalline degree obtained from **equation (10)** only reveals the effect of PCM-incorporated textile on the self-crystalline behavior of PCM. Indeed, it is difficult to determine the practical PCM loading amount in PCM containing fibers, MPCMs and other PCM-incorporated composites. Instead of the PCM loading amount, the encapsulation efficiency (η) is proposed as a result of PCM loading amount and relative crystalline degree of encapsulated PCMs, which is the ratio of the measured enthalpy value (ΔH_{sample}) of the PCM-incorporated materials to the measured enthalpy value (ΔH_{PCM}) of net PCMs (**equation (11)**). Besides, the overall enthalpy value ($\Delta H_{m,overall}$) of the fibrous multi-layer PCM system is calculated according to **equation (12)**. The $p_{overall}$ is the PCM loading amount of the whole fibrous multi-layer PCM system.

$$\chi_0 = \frac{\Delta H_{m,sample}}{\Delta H_{m,PCM}^{T} \times p} \tag{9}$$

$$\chi = \frac{\Delta H_{m,sample}}{\Delta H_{m,PCM} \times p} \tag{10}$$

$$\eta = \frac{\Delta H_{sample}}{\Delta H_{PCM}} \times 100\% \tag{11}$$

$$\Delta H_{m,overall} = \frac{\Delta H_{m,sample}}{p} \times p_{overall} \quad (12)$$

Especially, there were several characterizations of the fibrous multi-layer PCM system. The first one was that the fibrous multi-layer PCM system had a similar structure as MPCMs and was analogical to the MPCMs as shown in **Figure 5**. From this point, the fibrous multi-layer PCM system was in fact the 'big' PCM encapsulations. The second one was that the fibrous multi-layer PCM system was already a composite fabric and can be incorporated into commercial textiles. So, the overall PCM performance of the fibrous multi-layer PCM system was presented and compared with current reported PCM products (including MPCMs, PCM containing fibers, and PCM containing fabrics) for the advantages.

4.2.1 Encapsulation efficiency of the fibrous multi-layer PCM system and current PCM products

The encapsulation efficiency and molten enthalpy values of the fibrous multi-layer PCM system ($C4_{(PW)}$ and $C4_{(PEG,6000)}$) was 55 % and 73 J/g, and 44 % and 78 J/g, respectively. As shown in **Figure 8 (A)**, the fibrous multi-layer PCM system had a relative low encapsulation efficiency and molten enthalpy values when compared with MPCMs [55–70] (All values are given in **Table 10-1** in **APPENDIX 2**). According to **equation (11)**, the encapsulation efficiency is strongly influenced by $\Delta H_{m,sample}$ and $\Delta H_{m,sample}$ is significantly affected by PCM loading amount. So, the encapsulation efficiency can be increased by having relatively higher PCM loading amount in the fibrous multi-layer PCM system containing protection layers with small areal density. The ideal maximum encapsulation efficiency of the fibrous multi-layer PCM system was infinitely close to the fibrous multi-layer PCM system without protection layer (e.g., UPWV) with encapsulation efficiency of 78.9 %, which is comparable with reported MPCMs. The ideal maximum molten enthalpy value of the fibrous multi-layer PCM system ($C4_{(PW)}$) can reach 105 J/g and have a medium center in the **Figure 8 (A)**. The fibrous multi-layer PCM system also has a comparable encapsulation efficiency with PCM containing fibers. As shown in **Figure 8 (B)**, the encapsulation efficiency of the fibrous multi-layer PCM system ($C4_{(PEG,6000)}$ and $C4_{(PW)}$) is higher than most reported PCM-reported fibers [71–82]. The encapsulation efficiency can be increased by using thin fibrous materials (e.g., ultrafine nonwoven fabric) as protection layers. The ideal maximum encapsulation efficiency of the fibrous multi-layer PCM system ($C4_{(PW)}$) is close to UPWV and the highest among the samples in **Figure 8 (B)**.

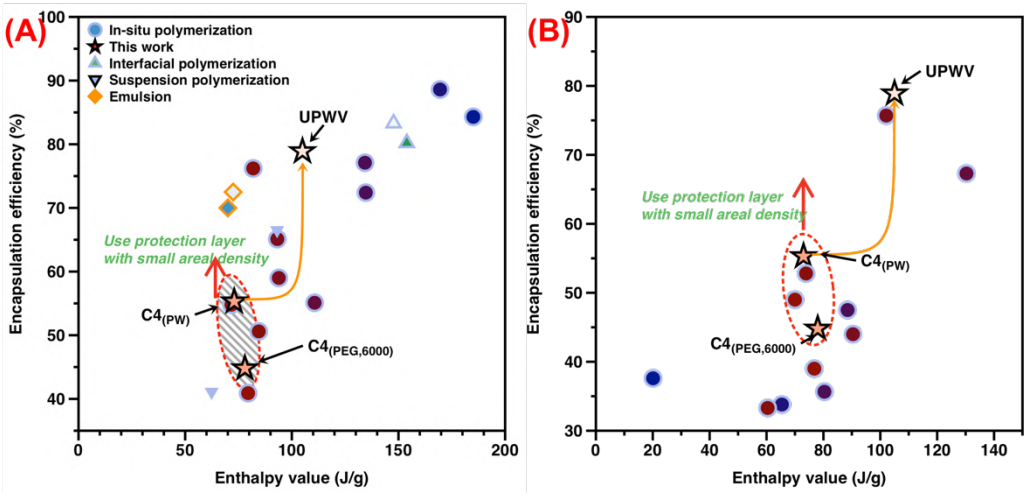

Figure 8 Comparison of this work with MPCM (A) and PCM containing fibers (B) in PCM encapsulation efficiency

4.2.2 PCM loading amount of the fibrous multi-layer PCM system and current PCM products

As described in published work (**9.1**, **9.2**, and **9.3** in **APPENDIX 1**), the optimal maximum loading amount of PW and PEG in the PCM-loaded layer is around 90 wt%. By taking the mass of nanofibrous membranes and PET fabrics with hydrophobic coating, the optimal maximum loading amount of PW and PEG in the fibrous multi-layer PCM system reached 46 wt%.

As shown in **Figure 9 (A)**, the PCM loading amount in the fibrous multi-layer PCM system is very close to most of PCM containing fibers [72,78,81–84] (All values are given in **Table 10-2** and **APPENDIX 2**). Besides, the PCM loading amount in the fibrous multi-layer PCM system is much higher than PCM containing fabrics as shown in **Figure 9 (B)**. So, the high PCM loading amount in the fibrous multi-layer PCM system was found.

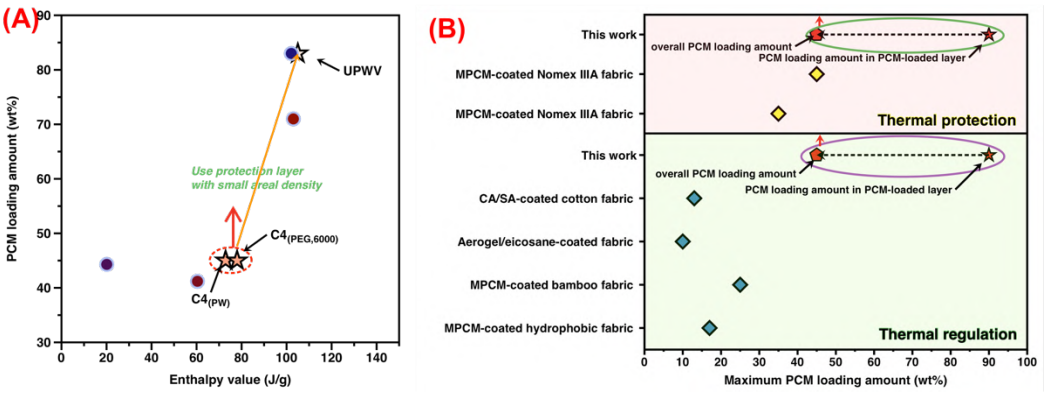

Figure 9 Comparison of this work with PCM containing fibers in PCM loading amount

(A) and with PCM containing fabric for potential applications (B)

4.2.3 Experimental relative crystalline degree ratio of PCM in the fibrous multi-layer PCM system and current PCM products

The experimental relative crystalline degree ratios of PCM in the fibrous multi-layer PCM system and current PCM products are shown in **Figure 10**. [73,78,80,82,85–88] (All values are given in **Table 10-3** in **APPENDIX 2**). Obviously, the PCMs in the fibrous multi-layer PCM system have highest relative crystalline degree ratio (>95%). The little confinement of the fibrous multi-layer PCM system on the self-crystalline behavior was found.

The reason is that the PCM-loaded layer is the PCM-coated viscose nonwoven fabric and PU nanofibrous membrane just slightly affected the self-crystalline behavior of PCM. In contrast, the supporting materials for other PCM products resulted in a strong confinement. For PCM containing fibers, the self-crystalline behavior of the PCM in the fiber matrix was affected by the fiber diameter and interfacial adhesion between PCMs and fiber materials. The similar reason was also for MPCMs and other form-stable PCMs (e.g., PCM/aerogel composites).

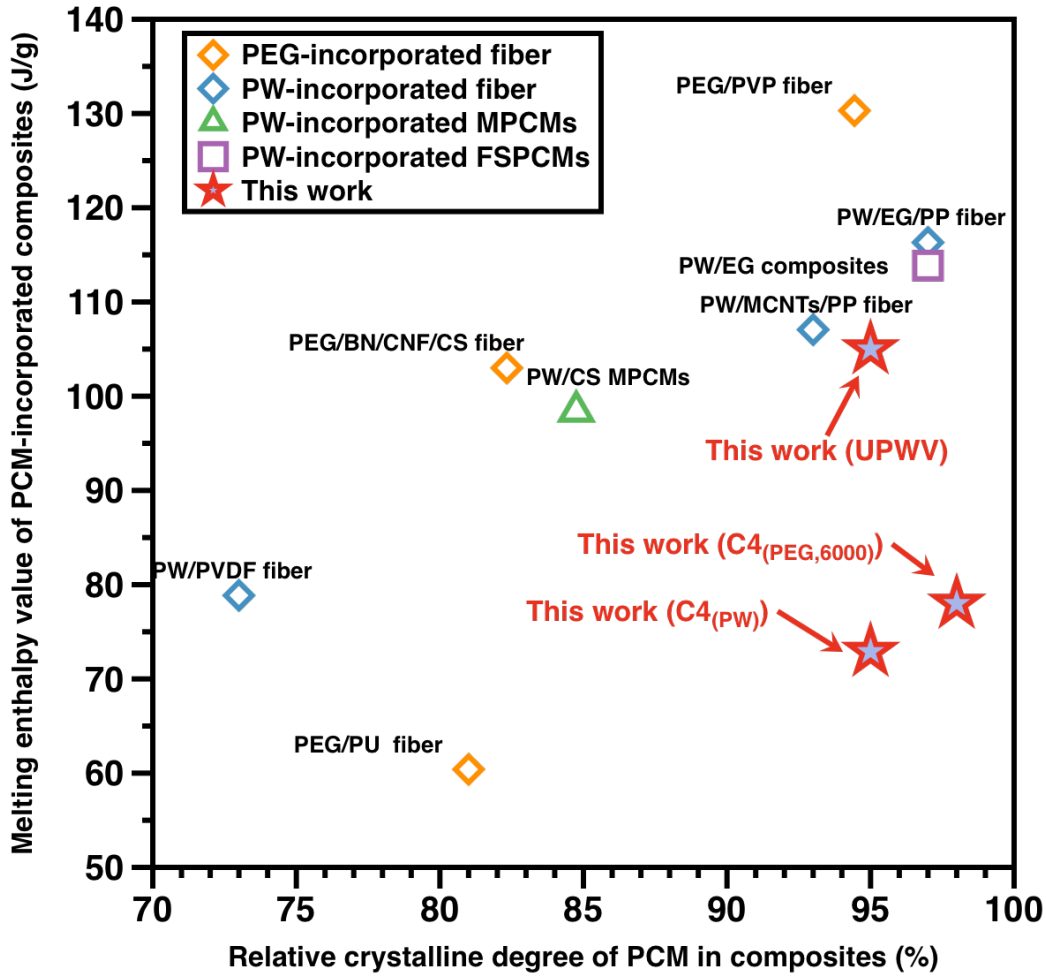

Figure 10 Comparison of this work with other reported work in crystallinity of PCM

4.2.4 Controlled working temperature range and selected applications

It had been proved that the PEG and PW were suitable in the proposed fibrous multi-layer PCM system. The thermal behavior (including phase transition and enthalpy value) of PEG was up to the molecular weight and the thermal behavior of PW was up to the carbon numbers. In this case, various PEGs with different molecular weights were used as PCMs in the fibrous multi-layer PCM system.

As shown in **Figure 11**, the working temperature ranges of the fibrous multi-layer PCM system was successfully controlled by using different PEGs while the enthalpy values were very close although there was a slight increase when the PEG with higher molecular weight was used (All values are given in **Table 10-4** in **APPENDIX 2**).

The enthalpy values of the fibrous multi-layer PCM system were higher than the PCM products from famous Outlast company while the working temperature range of the fibrous multi-layer PCM system were easier to be controlled.

Besides, enthalpy values of the fibrous multi-layer PCM system were smaller than the

PCM-incorporated materials from literature. However, the overall thermal energy storage of the fibrous multi-layer PCM system can be increased by having relatively higher PCM loading amount in the fibrous multi-layer PCM system containing protection layers with small areal density.

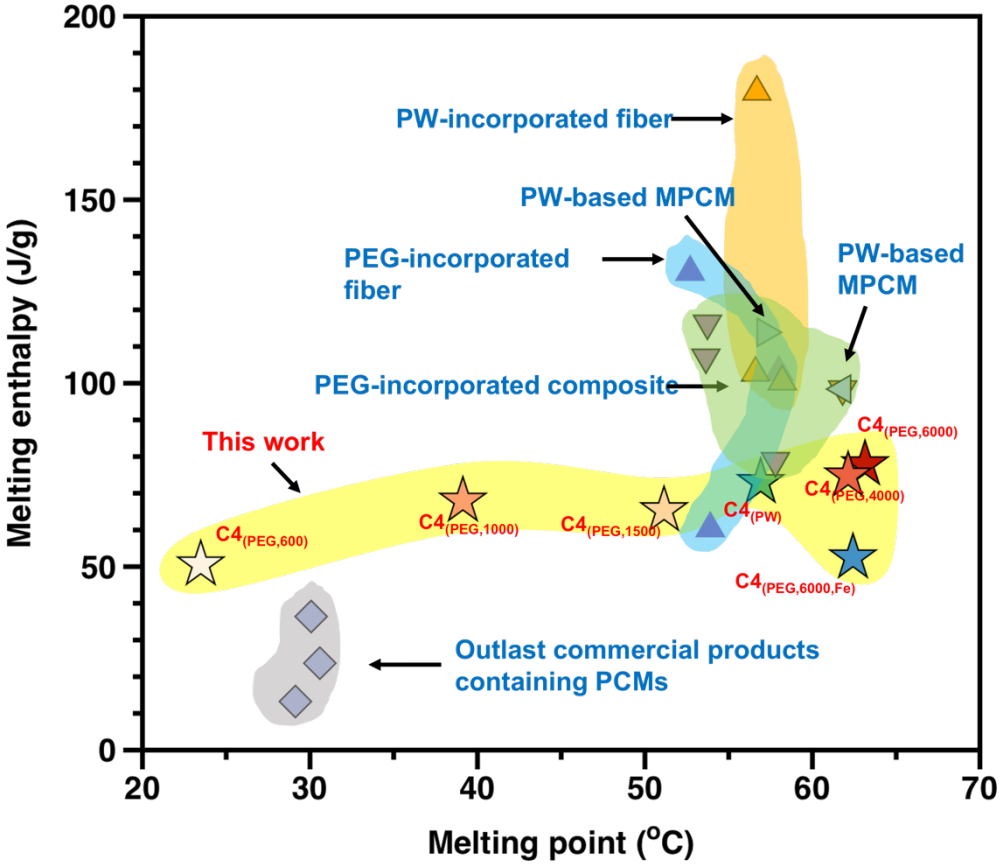

Figure 11 Comparison of this work with current PCM-incorporated products in the field of working temperature range and enthalpy values

4.2.5 Thermal buffering effect of the fibrous multi-layer PCM system

To reveal thermal buffering effect of the fibrous multi-layer PCM system, PEG 6000 and PW were selected as PCM, respectively. The higher melting point of PEG 6000 and PW than room temperature could provide an understanding of thermal buffering effect. **Figure 12 (A)** present full T-history of multi-layer fabric without PCM (reference sample), multi-layer fabric with PEG 6000 ($C4_{PEG,6000}$) and multi-layer fabric with PW ($C4_{PW}$). Obviously, the thermal buffering effect was found in the $C4_{(PEG,6000)}$ and $C4_{PW}$ samples when compared with $C4_{reference}$ sample without PCMs. Generally, the time for each sample to reach selected temperature during T-history was available to characterize thermal buffering effect. By taking phase transition of PCM into

consideration, both the time to reach 65 °C during heating process ($t_{h,65}$), and the time to reach 40 °C during cooling process were selected ($t_{c,40}$). The $t_{c,40}$ value of reference sample, $C4_{(PEG,6000)}$, and $C4_{PW}$ was 4s, 207s and 108s, respectively. From this point of view, the sample $C4_{(PEG,6000)}$ had the better thermal buffering effect than $C4_{(PW)}$.

To further reveal the temperature increasing rate in each part in the heating T-history curves of all the samples, the modified Newton's cooling law was used to characterize by referring **equation (4)-(7)**.

Especially, the application of modified Newton's cooling of to characterize the heating T-history was valid only when Biot number (*Bi*) of the sample should be smaller than 0.1. Since T-history for the samples was measured under room temperature, the free convection was taken into consideration. Then, the free convection coefficient (h) was chosen as 8 W m^{-2} K^{-1}. According to **equation (13)**, *Bi* number was calculated. The L (mm) was the thickness of the sample, and the k (W m^{-1} K^{-1}) was the thermal conductivity of the sample. Both L and k were measured by using ALAMBETA setup a [41]. As a result, the calculated *Bi* number value of $C4_{(reference)}$, $C4_{(PEG,6000)}$, and $C4_{(PW)}$ ranged from 0.1 to 0.2. So, the modified Newton's cooling las could roughly evaluate the heating T-history [42].

$$Bi = \frac{hL}{k} \tag{13}$$

As shown in **Figure 12 (B)**, good fittings for three linear parts including solid phase, phase transition phase and liquid phase were found. After having the intersection points of estimated x and y values from **Figure 12 (B)**, the fittings for heating T-history curves were found and shown in **Figure 12 (C)**. By calculating the intersection points of estimated t and T values, the time (t_{phase}) and temperature (T_{phase}) for phase transition range of multi-layer PCM fabrics were determined.

As shown in **Figure 12 (D)**, the sample $C4_{(PEG,6000)}$ had higher t_{phase} and T_{phase} values than the sample $C4_{PW}$, which also supported that $C4_{PEG}$ sample had better thermal buffering effect than $C4_{PW}$.

In addition, the thermal insulation values (I) of all the samples were calculated according to **equation (8)**, and were schemed in **Figure 12 (E)**. The T_h was the heating temperature of 80 °C and T_r was the room temperature. As a result, both sample $C4_{(PEG,6000)}$ and $C4_{PW}$ had lower I values than $C4_{reference}$ from heating T-history, which was caused by large amount of still air in $C4_{reference}$ sample.

By comparing with other methods of reported work (**9.5** in **APPENDIX 1**), the application of Newton's cooling law can not only exactly determine the thermal buffering effect but also predict the T-history.

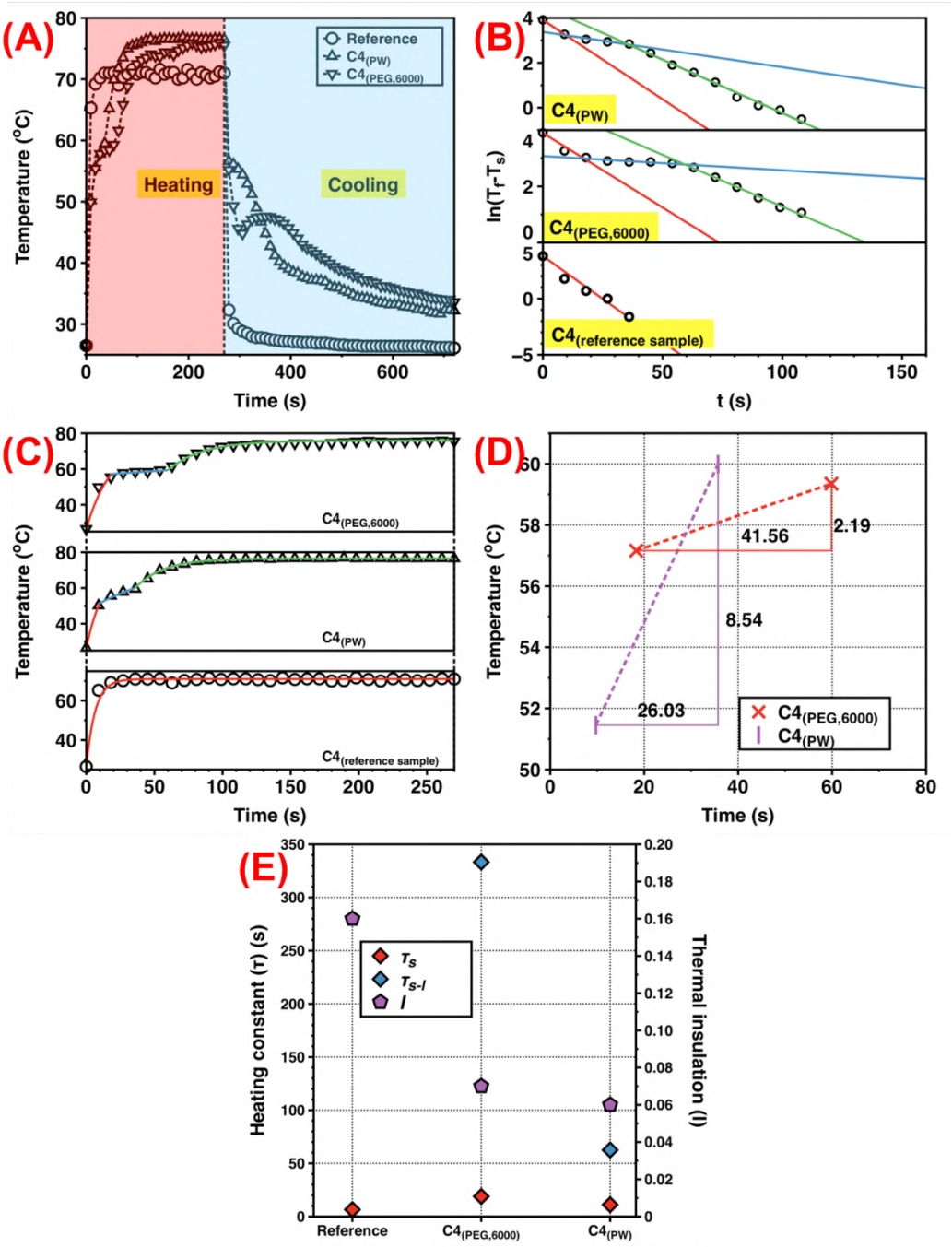

Figure 12 T-history of multi-layer fabrics containing PW and PEG (A), plots of ln [T_f-T_s] against t (B), heating T-history with fitting models (C), estimated phase transition range (D) and evaluation of thermal buffering (E)

5. Enhanced heat transfer efficiency

Different metal microparticles (Cu, Al, Ag, Fe and Zn) are introduced in the PCM-loaded layer to enhance the heat transfer efficiency according to published work (**9.2** and **9.3** in **APPENDIX 1**). The Fe microparticles are the best one of six different

microparticles to be introduced in PCM-loaded layer.

The thermal conductivity values of the Fe-incorporated fibrous multi-layer PCM system ($C4_{(PEG,6000,Fe)}$) are smaller than 0.1 W K^{-1} m^{-1}, which is schemed in **Figure 13 (A)**. Especially, the thermal conductivity of the Fe-incorporated fibrous multi-layer PCM fabrics ($C4_{(PEG,6000,Fe)}$) is 0.0573 W K^{-1} m^{-1}, which is just slightly higher than the fibrous multi-layer PCM fabrics ($C4_{(PEG,6000)}$) with thermal conductivity of 0.0543 W K^{-1} m^{-1}. Besides, the comparison of the Fe-incorporated fibrous multi-layer PCM fabrics with neat PCMs or other PCM-incorporated materials (including PCM containing fibers, MPCMs, carbon-based PCM composites and metal-based PCM composites) is also shown in **Figure 13 (A)** [74,82,89–105] (**Table 10-5** in **APPENDIX 2**), and the Fe-incorporated fibrous multi-layer PCM fabrics have lowest thermal conductivity. The main reason is that the fibrous multi-layer PCM system contains five layers and fours layers are fibrous materials with small thermal conductivity. The used viscose nonwoven fabric has a thermal conductivity of 0.0298 W K^{-1} m^{-1}, and PET fabric with hydrophobic coating has a thermal conductivity of 0.0693 W K^{-1} m^{-1}. Besides, the PCM-loaded layer has a small thermal conductivity. The PEG-coated viscose fabric ($UPEGV_{6000}$) has a small thermal conductivity of 0.0395 W K^{-1} m^{-1}, and the PEG/Fe-coated viscose fabric ($UPEGV_{6000,Fe}$) has a small thermal conductivity of 0.0654 W K^{-1} m^{-1}.

Although the overall thermal conductivity of the Fe-incorporated fibrous multi-layer PCM system is small, the incorporation of Fe microparticles in the PCM-loaded layer enhances the heat transfer efficiency. On one hand, the thermal conductivity of the PCM-loaded layer ($UPEGV_{6000,Fe}$) is increased 65.6%. On another hand, the temperature of $C4_{(PEG,6000,Fe)}$ increases faster than $C4_{(PEG,6000)}$, as shown in **Figure 13 (B)**. **Figure 13 (C)** presented the estimated phase transition range in detail. However, the phase transition range of $C4_{(PEG,6000,Fe)}$ started later and lasted longer than than $C4_{(PEG,6000)}$. The $C4_{(PEG,6000,Fe)}$ has a phase transition for 47.06 s while the temperature is increased 6.52 ^{o}C. The reason is that the heat transfer through the whole fibrous multi-layer PCM system with or without Fe microparticles is indeed non-uniform during phase transition. The surface temperature of the fibrous multi-layer PCM system with or without Fe microparticles is affected by the thermal conductivity, thickness, molten points etc.

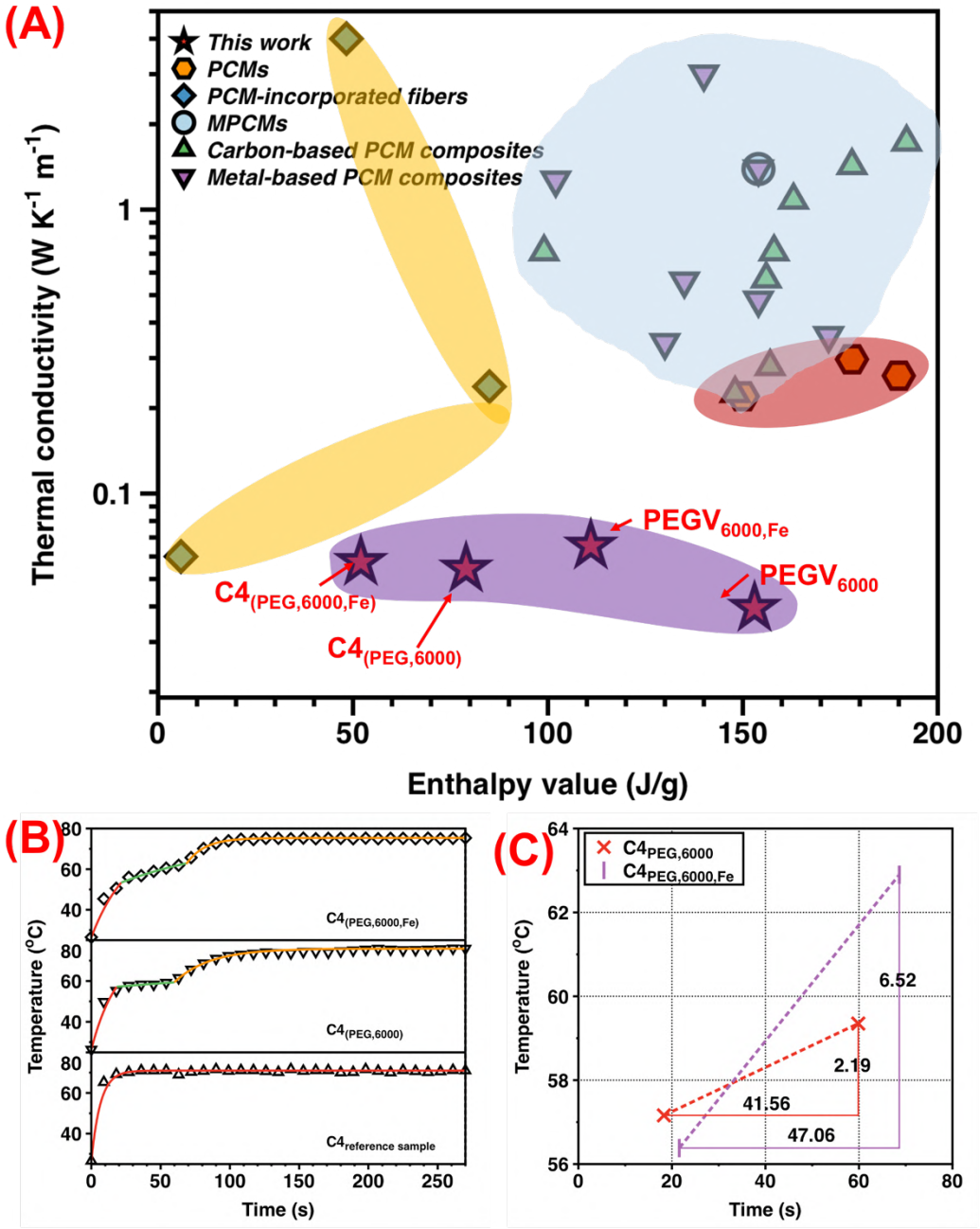

Figure 13 Estimation of thermal conductivity enhancement of Fe-incorporated fibrous multi-layer PCM system (A: comparison with PCM products, B: T-history of Fe-incorporated fibrous multi-layer PCM system, and C: thermal buffering range of Fe-incorporated fibrous multi-layer PCM system)

6. Controlled breathability by modifying PCM-loaded Layer

There is no breathability since PCM-loaded layer is a composite where there is no path for air or water vapor to penetrate. For the fibrous multi-layer PCM system, introduction of air pocket is an alternative to enhance mass transfer and incorporate other materials for functions [106]. To realize breathability, the PCM-loaded layer is

modified and consists of air pocket and PCM pocket (PEG-coated viscose fabric). The PCM pockets are uniformly distributed between two barrier layers with certain air gaps. Since the PCM-loaded layer comprises of PCM pockets and air pockets, as shown in the **Figure 14 (A)**, the possibility of PEG leakage within the PCM-loaded layer must be considered. At first, there was no PEG leakage observed through the fibrous multi-layer PCM system after heating/cooling cycles, either from the vertical or planar direction. As explained in the **Sec. '4'**, The combination of the weak interfacial adhesion between molten PEG and the protection layer (PET fabric with hydrophobic coating) and the use of a PU nanofibrous membrane in the fibrous multi-layer PCM system were responsible for this outcome.

However, it was observed that the diffusion of molten PEG within the PCM pocket inside the fibrous multi-layer PCM system was strongly linked to the amount of loaded PEG. For instance, **Figure 14 (B-i)** displays the leakage phenomena of sample $UPEGV_{10\text{-}1}$ with mass ratio (R_{PEG}) of PEG to viscose fabric of 10:1, where the PEG has dispersed throughout the PCM pocket and air pocket, resulting in obvious leakage. However, when the mass ratio of PEG to viscose fabric in the PCM-loaded layer was reduced to 5:1, the sample $UPEGV_{5\text{-}1}$ exhibited a clear boundary between the PCM pocket and air pocket, and minimal diffusion of molten PEG was detected (**Figure 14 (B-ii**)). The following reasons are found:

- When there was a higher loading amount of PEG in the PCM pocket as shown in **Figure 14 (B-iv)**, some PEGs were located outside of the viscose fabric. Before heating process with pressure, the PCM pocket ideally had a width of D_0 and thickness of L_0. During the heating process with pressure, the PEG outside of the viscose fabric was forced to move along the fabric surface direction because molten PEG was movable. Then after heating process with pressure, the dimension of the PCM pocket was changed and D_0 became D_1 and L_0 became L_1. The D_0 was smaller than D_1 and L_0 was higher than L_1. Consequently, during heating and cooling cycles with pressure, the PEG outside the viscose fabric melted and began to move along the fabric surface direction, leading to leakage phenomena. For example, the $UPEGV_{10\text{-}1}$ had a PEG diffusion and instability of PEG encapsulation.
- However, when the PEG loading amount was limited as shown in **Figure 14 (B-iii)**, the majority of PEG was efficiently adsorbed by the viscose fabric, despite of a very small amount being outside the fabric. It was supposed that the movement of molten PEG inside the viscose fabric was not affected and dimensions including thickness and length were not significantly changed. In details, D_0 and L_0 values

were almost same as D_1 and L_1. After undergoing heating and cooling cycles under pressure, the PEG located outside of the viscose fabric is completely melted, while still remaining within the coverage of the PCM pocket.

Therefore, the optimal PCM-loaded layer for creating a breathable fibrous multi-layer PCM system is the $PEGV_{5\text{-}1}$ with a R_{PEG} ratio of 5:1.

By modifying the size of the PCM pocket and the breathability of the fibrous multi-layer PCM system was modified. When the size of the PCM pocket was decreased from 3 mm to 2 mm, the air permeability of the breathable fibrous multi-layer PCM system was increased from 4.6 mm/s to 9 mm/s under 100 Pa, and water vapor permeability of the breathable fibrous multi-layer PCM system was increased from 31.4 m^2 Pa W^{-1} to 43.4 m^2 Pa W^{-1}. Although the breathability was realized, there is no comparability of the breathable fibrous multi-layer PCM system with other work [107–112], which was shown in **Figure 15Figure 15 (A)** (All values were given in **Table 10-6** in **APPENDIX 2**). This is attributed to the presence of two layers of PU nanofibrous membranes. However, the overall air permeability could be enhanced by having non-uniform placement and form of the PCM pocket inside the fibrous multi-layer PCM system.

Besides, the overall enthalpy value of the breathable fibrous multi-layer PCM system was 7.8 J/g, which was higher than majority of the MPCM-coated fabrics (**Figure 15 (B)**) (All values were given in **Table 10-7** in **APPENDIX 2**). By combining with breathability and use of nanofibrous membrane, the breathable fibrous multi-layer PCM system has a potential in special applications (e.g., mask etc.).

Since there were air pockets and PCM pockets in the breathable fibrous multi-layer PCM system, there was a heterogenous heat transfer through the whole breathable fibrous multi-layer PCM system. As shown in **Figure 14 (C)**, the air pocket faster reached the final stable temperature while it took a longer time for PCM pocket to reach the final stable temperature. Besides, it was found that the phase transition of the PCM pocket always started from the boarder between PCM pocket and air pocket and diffused to the center of PCM pocket from FLIR video. Such phenomena were caused by heterogenous heat transfer through air pocket and PCM pocket. There was only thermal convection for air pocket while there was ideally the thermal conduction for PCM pocket. However, the temperature change rate was higher than PCM pocket when the phase transition starts. Then, the heat transfer from the air pocket to the PCM pocket happened. As a result, the phase transition of PEG at the perimeter of the PCM pocket commenced earlier and exhibited a quicker rate of change due to the coupling of thermal conduction and thermal convection. In contrast, the phase transition of PEG at

the center of the PCM pocket was solely impacted by thermal conduction.

Additionally, the comparative analysis with previous research highlighted the adaptable nature of the permeable fibrous multi-layer PCM system, depicted in **Figure 16 (A-i)**, **(A-ii)** and **(A-iii)**. Therefore, it is recommended that breathable fibrous multi-layer PCM system are suitable for various human body parts (e.g. safeguarding the chest, arms and legs) with optimal compatibility with textiles.

In addition, a PET fabric with hydrophobic coating was utilized as a protective layer, proposing waterproof and self-cleaning capabilities for the breathable fibrous multi-layer PCM system. The majority of dyes were simply drop out as depicted in **Figure 16 (B-i)**, **(B-ii)** and **(B-iii)**, whilst water droplets were efficiently deposited on the fibrous multi-layer PCM system surface as presented in **Figure 16 (C)**. Therefore, in practical application, PEG as phase change material (PCM) could be well safeguarded.

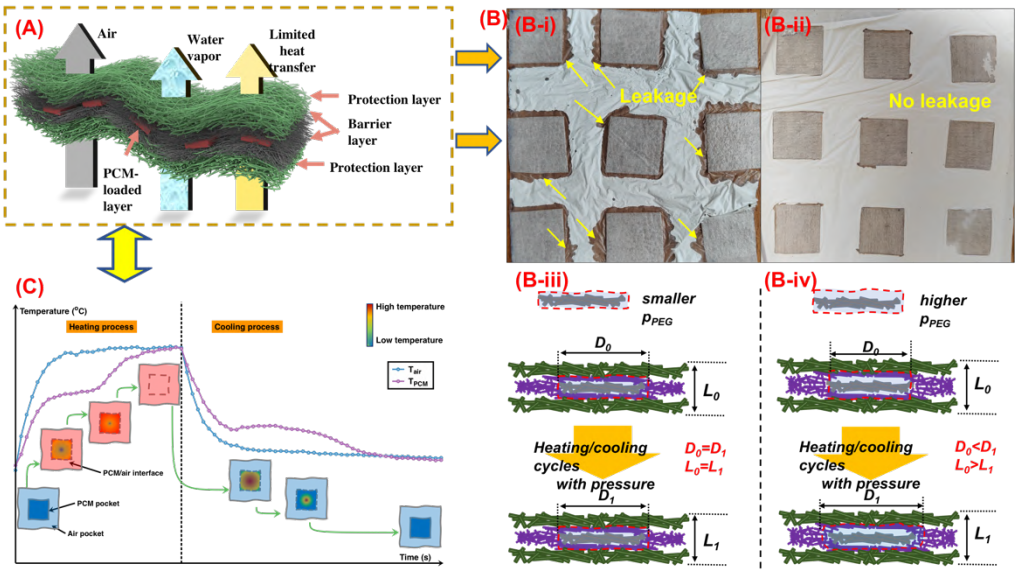

Figure 14 Diagram for breathable fibrous multi-layer PCM system (A), control of leakage phenomena (B), diagram for T-history curves of air pocket and PCM pocket (C)

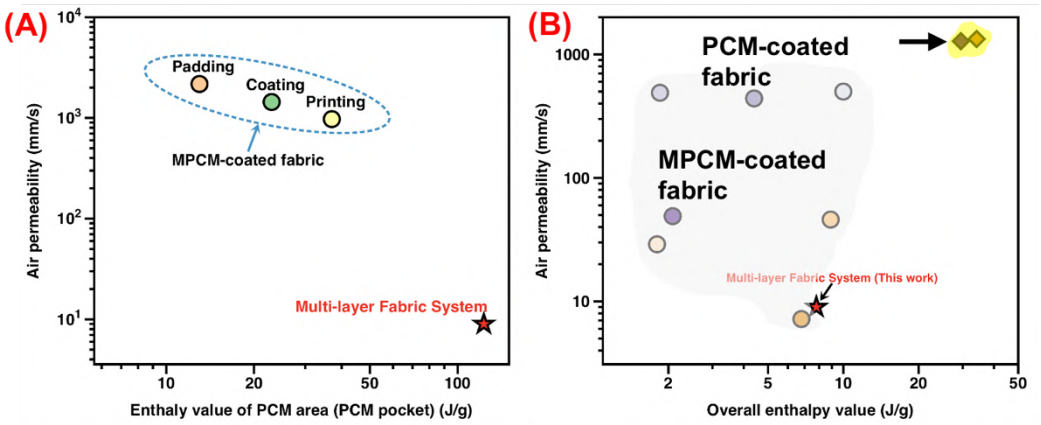

Figure 15 Comparison of this work with air pocket-introduced MPCM-coated fabric (A) and MPCM-coated fabrics without air pocket (B)

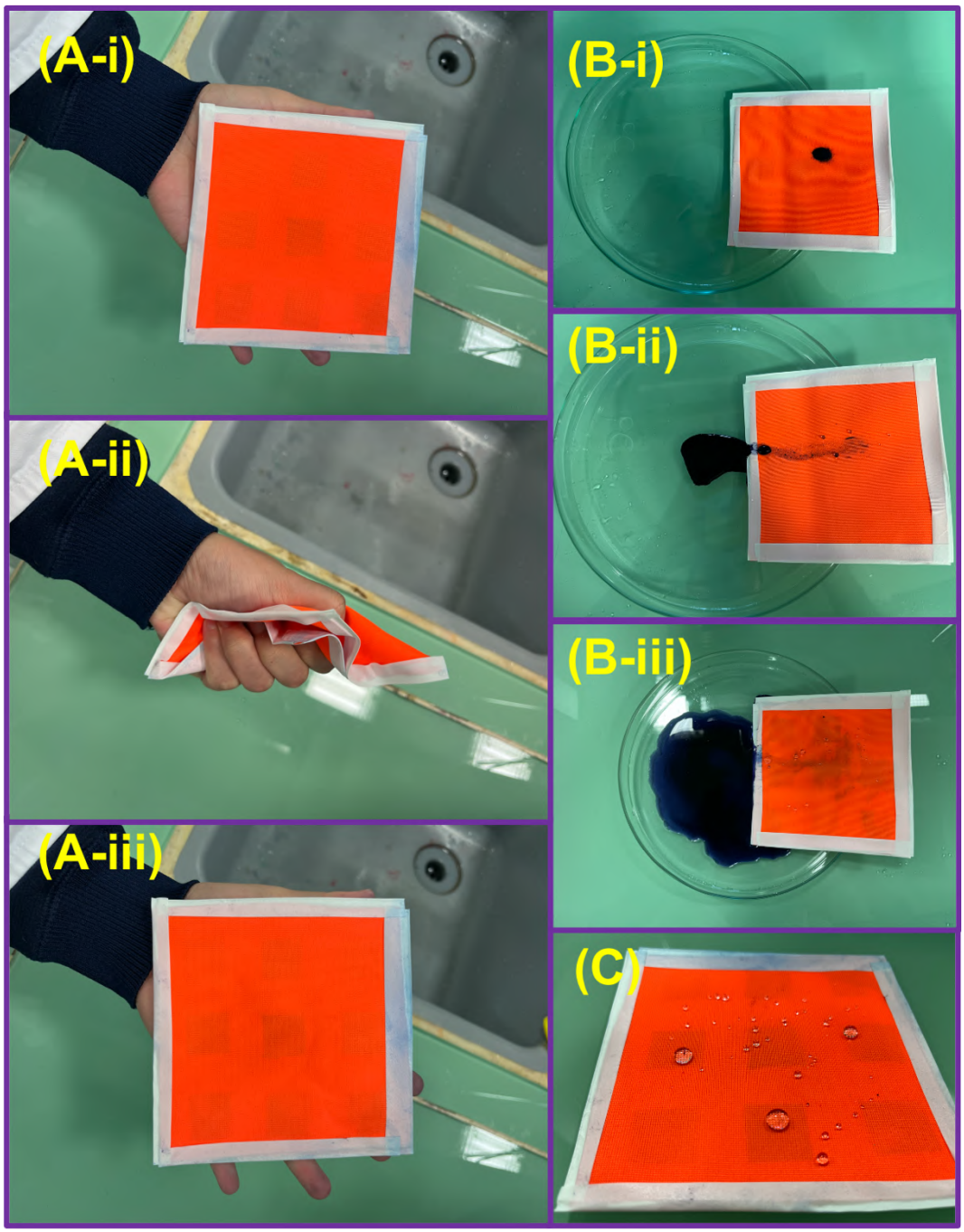

Figure 16 Flexibility (A), self-cleaning property (B) and hydrophobicity (C) of the fibrous multi-layer PCM system

7. Conclusion

This dissertation is conceived as a summary of published scientific and professional works, where the author of this thesis the the first author. In order to emphasize the

topicality of the studies topic, the novelty and author motivation to research activities, the work is supplemented with citations of other research works published in the given area.

The present work established a fibrous multi-layer PCM system. The fibrous multi-layer PCM system consisted of PCM-loaded layer, barrier layer and protection layer. The fibrous multi-layer PCM system could meet various applications and practical situations. The following conclusion have been drawn:

- By controlling the interfacial adhesion of molten PCMs on barrier layer or protection layer, the leakage phenomena were totally avoided. The PEG and paraffin wax were suitable as PCMs in such fibrous multi-layer PCM system. The advantage of the fibrous multi-layer PCM system over other PCM textiles was the PCM loading amount. The maximum loading amount of PCMs in the multi-layer PCM fabric was 45 wt%. The overall enthalpy value of the multi-layer PCM fabric is high as 78 J/g. Besides, the working temperature of the fibrous multi-layer PCM system is easily adjusted by using different PCMs. In addition, the PCM performance of the fibrous multi-layer PCM system could be improved by using the protection layer with small areal density.
- The Newton's cooling law was successfully modified to characterize the heating T-history of the fibrous multi-layer PCM system. Especially, the thermal buffering effect was exactly determined by applying Newton's cooling law. The mathematical prediction of the T-history of fibrous multi-layer PCM system was also realized.
- The thermal enhancement of the fibrous multi-layer PCM system was realized by introducing metal microparticles in the PCM-loaded layer. The overall enthalpy value of the fibrous multi-layer PCM system containing metal microparticles was higher than 50 J/g.
- The breathability of the fibrous multi-layer PCM system was realized by modifying PCM-loaded layer, and the PCM-loaded layer was separated into PCM pocket and air pocket. There was a limitation of PCM loading amount in the PCM pocket of the breathable fibrous multi-layer PCM system. Besides, higher air pocket inside the fibrous multi-layer PCM system resulted in better breathability. However, the breathability was small since there were two layers of nanofibrous membranes inside the fibrous multi-layer PCM system. Still, the introduction of the air pocket provided an alternative to enhance breathability. Besides, the PCM pocket and air pocket had different T-history behaviors because of their different thermal

resistances. It was found that the size of air pocket was strongly connected to the mutual heat transfer between PCM pocket and air pocket.

8. References

[1] N. Zhang, Y. Yuan, X. Cao, Y. Du, Z. Zhang, Y. Gui, Latent Heat Thermal Energy Storage Systems with Solid–Liquid Phase Change Materials: A Review, Adv Eng Mater. 20 (2018) 1700753. https://doi.org/10.1002/adem.201700753.

[2] G. Alva, Y. Lin, L. Liu, G. Fang, Synthesis, characterization and applications of microencapsulated phase change materials in thermal energy storage: A review, Energ Buildings. 144 (2017) 276–294. https://doi.org/10.1016/j.enbuild.2017.03.063.

[3] W. Chalco-Sandoval, M.J. Fabra, A. López-Rubio, J.M. Lagaron, Use of phase change materials to develop electrospun coatings of interest in food packaging applications, J Food Eng. 192 (2017) 122–128. https://doi.org/10.1016/j.jfoodeng.2015.01.019.

[4] C. Zhu, Y. Chen, R. Cong, F. Ran, G. Fang, Improved thermal properties of stearic acid/high density polyethylene/carbon fiber composite heat storage materials, Sol Energ Mat Sol C. 219 (2021). https://doi.org/10.1016/j.solmat.2020.110782.

[5] K. Iqbal, A. Khan, D. Sun, M. Ashraf, A. Rehman, F. Safdar, A. Basit, H.S. Maqsood, Phase change materials, their synthesis and application in textiles—a review, J Text Inst. 110 (2019) 625–638. https://doi.org/10.1080/00405000.2018.1548088.

[6] K. Yang, J. Wiener, M. Venkataraman, Y. Wang, T. Yang, G. Zhang, G. Zhu, J. Yao, J. Militky, Thermal analysis of PEG/Metal particle-coated viscose fabric, Polym Test. 100 (2021) 107231. https://doi.org/10.1016/j.polymertesting.2021.107231.

[7] H. Peng, J. Wang, X. Zhang, J. Ma, T. Shen, S. Li, B. Dong, A review on synthesis, characterization and application of nanoencapsulated phase change materials for thermal energy storage systems, Appl Therm Eng. 185 (2021). https://doi.org/10.1016/j.applthermaleng.2020.116326.

[8] Z.A. Qureshi, H.M. Ali, S. Khushnood, Recent advances on thermal conductivity enhancement of phase change materials for energy storage system: A review, Int J Heat Mass Tran. 127 (2018) 838–856. https://doi.org/10.1016/j.ijheatmasstransfer.2018.08.049.

[9] F. Ran, Y. Chen, R. Cong, G. Fang, Flow and heat transfer characteristics of microencapsulated phase change slurry in thermal energy systems: A review, Renew Sustain Energy Rev. 134 (2020). https://doi.org/10.1016/j.rser.2020.110101.

[10] T. Rehman, H.M. Ali, M.M. Janjua, U. Sajjad, W.-M. Yan, A critical review on heat transfer augmentation of phase change materials embedded with porous

materials/foams, Int J Heat Mass Tran. 135 (2019) 649–673. https://doi.org/10.1016/j.ijheatmasstransfer.2019.02.001.

[11] P. Gadhave, F. Pathan, S. Kore, C. Prabhune, Comprehensive review of phase change material based latent heat thermal energy storage system, Int J Ambient Energy. (2021). https://doi.org/10.1080/01430750.2021.1873848.

[12] A. Safari, R. Saidur, F.A. Sulaiman, Y. Xu, J. Dong, A review on supercooling of Phase Change Materials in thermal energy storage systems, Renew Sustain Energy Rev. 70 (2017) 905–919. https://doi.org/10.1016/j.rser.2016.11.272.

[13] D.G. Prajapati, B. Kandasubramanian, A Review on Polymeric-Based Phase Change Material for Thermo-Regulating Fabric Application, Polym Rev. 60 (2020) 389–419. https://doi.org/10.1080/15583724.2019.1677709.

[14] H. Liu, Z. Wei, W. He, J. Zhao, Thermal issues about Li-ion batteries and recent progress in battery thermal management systems: A review, Energ Convers Manage. 150 (2017) 304–330. https://doi.org/10.1016/j.enconman.2017.08.016.

[15] S.S. Chandel, T. Agarwal, Review of current state of research on energy storage, toxicity, health hazards and commercialization of phase changing materials, Renew Sustain Energy Rev. 67 (2017) 581–596. https://doi.org/10.1016/j.rser.2016.09.070.

[16] N.PAN, P.Gibson, Thermal and moisture transport in fibrous materials, 1st ed., Woodhead Publishing, 2006.

[17] J. Militky, O. Novak, D. Kremenakova, J. Wiener, M. Venkataraman, G. Zhu, J. Yao, A. Aneja, A Review of Impact of Textile Research on Protective Face Masks, Materials. 14 (2021) 1937. https://doi.org/10.3390/ma14081937.

[18] S. Faheem, V. Baheti, M. Tunak, J. Wiener, J. Militky, Flame resistance behavior of cotton fabrics coated with bilayer assemblies of ammonium polyphosphate and casein, Cellulose. 26 (2019) 3557–3574. https://doi.org/10.1007/s10570-019-02296-1.

[19] M. Venkataraman, R. Mishra, J. Militky, X. Xiong, J. Marek, J. Yao, G. Zhu, Electrospun nanofibrous membranes embedded with aerogel for advanced thermal and transport properties, Polym Advan Technol. 29 (2018) 2583–2592. https://doi.org/10.1002/pat.4369.

[20] M.Z. Khan, V. Baheti, J. Militky, A. Ali, M. Vikova, Superhydrophobicity, UV protection and oil/water separation properties of fly ash/Trimethoxy(octadecyl)silane coated cotton fabrics, Carbohyd Polym. 202 (2018) 571–580. https://doi.org/10.1016/j.carbpol.2018.08.145.

[21] T. Yang, X. Xiong, R. Mishra, J. Novák, J. Militký, Sound absorption and compression properties of perpendicular-laid nonwovens, Text Res J. 89 (2019) 612–624. https://doi.org/10.1177/0040517517753634.

[22] K. Yang, A.P. Periyasamy, M. Venkataraman, J. Militky, D. Kremenakova, J. Vecernik, R. Pulíček, Resistance against penetration of electromagnetic radiation for ultra-light Cu/Ni-coated polyester fibrous materials, Polymers-Basel. 12 (2020). https://doi.org/10.3390/polym12092029.

[23] X. Zhang, Z. Jin, L. Hu, X. Zhou, K. Yang, D. Kremenakova, J. Militky, A Silver Yarn-Incorporated Song Brocade Fabric with Enhanced Electromagnetic Shielding, Materials. 14 (2021) 3779. https://doi.org/10.3390/ma14143779.

[24] X. Zhang, Z. Jin, A Kind of Song Brocade Fabric with NFC Data Masking Function Used for Making Purse, Iop Conf Ser Mater Sci Eng. 389 (2018) 012037. https://doi.org/10.1088/1757-899x/389/1/012037.

[25] Y. Wang, V. Baheti, K. Yang, T. Yang, J. Wiener, J. Militký, Utility of whiskerized carbon fabric surfaces in resistive heating of composites, Polym Composite. (2021). https://doi.org/10.1002/pc.26012.

[26] A.P. Periyasamy, K. Yang, X. Xiong, M. Venkataraman, J. Militky, R. Mishra, D. Kremenakova, Effect of silanization on copper coated milife fabric with improved EMI shielding effectiveness, Mater Chem Phys. 239 (2020). https://doi.org/10.1016/j.matchemphys.2019.122008.

[27] C. Wani, P.K. Loharkar, A Review of Phase Change Materials as an Alternative for Solar Thermal Energy Storage, Mater Today Proc. 4 (2017) 10264–10267. https://doi.org/10.1016/j.matpr.2017.06.361.

[28] S.A. Mohamed, F.A. Al-Sulaiman, N.I. Ibrahim, Md.H. Zahir, A. Al-Ahmed, R. Saidur, B.S. Yılbaş, A.Z. Sahin, A review on current status and challenges of inorganic phase change materials for thermal energy storage systems, Renew Sustain Energy Rev. 70 (2017) 1072–1089. https://doi.org/10.1016/j.rser.2016.12.012.

[29] K. Yang, M. Venkataraman, J. Karpiskova, Y. Suzuki, S. Ullah, I.-S. Kim, J. Militky, Y. Wang, T. Yang, J. Wiener, G. Zhu, J. Yao, Structural analysis of embedding polyethylene glycol in silica aerogel, Micropor Mesopor Mat. 310 (2021) 110636. https://doi.org/10.1016/j.micromeso.2020.110636.

[30] L. Pathak, G.V.N. Trivedi, R. Parameshwaran, S.S. Deshmukh, Microencapsulated phase change materials as slurries for thermal energy storage: A review, Mater Today Proc. 44 (2021) 1960–1963. https://doi.org/10.1016/j.matpr.2020.12.101.

[31] S. Sundararajan, A.B. Samui, P.S. Kulkarni, Versatility of polyethylene glycol (PEG) in designing solid–solid phase change materials (PCMs) for thermal management and their application to innovative technologies, J Mater Chem A. 5 (2017) 18379–18396. https://doi.org/10.1039/c7ta04968d.

[32] J.L. Reyez-Araiza, J. Pineda-Piñón, J.M. López-Romero, J.R. Gasca-Tirado, M.A. Contreras, J.C.J. Correa, L.M. Apátiga-Castro, E.M. Rivera-Muñoz, R.R. Velazquez-Castillo, J. de J.P. Bueno, A. Manzano-Ramirez, Thermal Energy Storage by the Encapsulation of Phase Change Materials in Building Elements—A Review, Materials. 14 (2021) 1420. https://doi.org/10.3390/ma14061420.

[33] H. Liu, X. Wang, D. Wu, Innovative design of microencapsulated phase change materials for thermal energy storage and versatile applications: a review, Sustain Energy Fuels. 3 (2019) 1091–1149. https://doi.org/10.1039/c9se00019d.

[34] L. Zhang, W. Yang, Z. Jiang, F. He, K. Zhang, J. Fan, J. Wu, Graphene oxide-modified microencapsulated phase change materials with high encapsulation capacity and enhanced leakage-prevention performance, Appl Energ. 197 (2017) 354–363. https://doi.org/10.1016/j.apenergy.2017.04.041.

[35] A. Shaid, L. Wang, S. Islam, J.Y. Cai, R. Padhye, Preparation of aerogel-eicosane microparticles for thermoregulatory coating on textile, Appl Therm Eng. 107 (2016) 602–611. https://doi.org/10.1016/j.applthermaleng.2016.06.187.

[36] C.E. Tas, O. Karaoglu, B.A. Tas, E. Ertas, H. Unal, H. Bildirir, Improved latent heat storage properties through mesopore enrichment of a zeolitic shape stabilizer, Sol Energ Mat Sol C. 216 (2020) 110677. https://doi.org/10.1016/j.solmat.2020.110677.

[37] J.S. Baruah, V. Athawale, P. Rath, A. Bhattacharya, Melting and energy storage characteristics of macro-encapsulated PCM-metal foam system, Int J Heat Mass Tran. 182 (2022) 121993. https://doi.org/10.1016/j.ijheatmasstransfer.2021.121993.

[38] H. Su, P. Lin, H. Lu, X. Zhao, X. Sheng, Y. Chen, Janus-Type Hydroxyapatite-Incorporated Kevlar Aerogel@Kevlar Aerogel Supported Phase-Change Material Gel toward Wearable Personal Thermal Management, Acs Appl Mater Inter. 14 (2022) 12617–12629. https://doi.org/10.1021/acsami.1c23774.

[39] H. Gao, J. Wang, X. Chen, G. Wang, X. Huang, A. Li, W. Dong, Nanoconfinement effects on thermal properties of nanoporous shape-stabilized composite PCMs: A review, Nano Energy. 53 (2018) 769–797. https://doi.org/10.1016/j.nanoen.2018.09.007.

[40] W. Aftab, X. Huang, W. Wu, Z. Liang, A. Mahmood, R. Zou, Nanoconfined phase change materials for thermal energy applications, Energ Environ Sci. 11 (2018) 1392–1424. https://doi.org/10.1039/c7ee03587j.

[41] K. Yang, X. Zhang, M. Venkataraman, J. Wiener, S. Palanisamy, S. Sozcu, X. Tan, D. Kremenakova, G. Zhu, J. Yao, J. Militky, Structural Analysis of Phase Change Materials (PCMs)/Expanded Graphite (EG) Composites and Their Thermal Behavior under Hot and Humid Conditions, Chempluschem. (2023). https://doi.org/10.1002/cplu.202300081.

[42] K. Yang, M. Venkataraman, X. Zhang, J. Wiener, G. Zhu, J. Yao, J. Militky, Review: incorporation of organic PCMs into textiles, J Mater Sci. 57 (2022) 798–847. https://doi.org/10.1007/s10853-021-06641-3.

[43] A. Karaszewska, I. Kamińska, A. Nejman, B. Gajdzicki, W. Fortuniak, J. Chojnowski, S. Slomkowski, P. Sowinski, Thermal-regulation of nonwoven fabrics by microcapsules of n-eicosane coated with a polysiloxane elastomer, Mater Chem Phys. 226 (2019) 204–213. https://doi.org/10.1016/j.matchemphys.2019.01.029.

[44] Y. Wu, C. Chen, Y. Jia, J. Wu, Y. Huang, L. Wang, Review on electrospun ultrafine phase change fibers (PCFs) for thermal energy storage, Appl Energ. 210 (2018) 167–181. https://doi.org/10.1016/j.apenergy.2017.11.001.

[45] F. Haghighat, S.A.H. Ravandi, M.N. Esfahany, A. Valipouri, Z. Zarezade, Thermal performance of electrospun core-shell phase change fibrous layers at simulated body conditions, Appl Therm Eng. 161 (2019) 113924. https://doi.org/10.1016/j.applthermaleng.2019.113924.

[46] L. Hes, luboshes@vslib.cz, B.I. Lu, Using a Thermal Simulator to Determine the Amount of Time that Humans are Thermally Protected by Fabrics Containing Phase Change Materials, Res J Text Appar. Volume 8 (2004) 51–56. https://doi.org/10.1108/rjta-08-02-2004-b007.

[47] K. Yang, M. Venkataraman, Y.-F. Wang, X.-M. Xiong, T. Yang, J. Wiener, J. Militky, R. Mishra, J. Marek, G.-C. Zhu, J.-M. Yao, Thermal behaviour of multi-layer composite containing PEG and laponite as PCM, in: 2019: pp. 671–676. https://www.scopus.com/inward/record.uri?eid=2-s2.0-85073789344&partnerID=40&md5=b022b850ae171de76f4b12525e6cf9a0.

[48] N. Wang, M. Cai, X. Yang, Y. Yang, Electret nanofibrous membrane with enhanced filtration performance and wearing comfortability for face mask, J Colloid Interf Sci. 530 (2018) 695–703. https://doi.org/10.1016/j.jcis.2018.07.021.

[49] W. Ma, Z. Jiang, T. Lu, R. Xiong, C. Huang, Lightweight, elastic and superhydrophobic multifunctional nanofibrous aerogel for self-cleaning, oil/water separation and pressure sensing, Chem Eng J. 430 (2022) 132989. https://doi.org/10.1016/j.cej.2021.132989.

[50] B. Xiang, G. Shi, P. Mu, J. Li, Eco-friendly WBF/PAN nanofiber composite membrane for efficient separation various surfactant-stabilized oil-in-water emulsions, Colloids Surfaces Physicochem Eng Aspects. 645 (2022) 128917. https://doi.org/10.1016/j.colsurfa.2022.128917.

[51] M. Cao, Y. Hu, W. Cheng, S. Huan, T. Bai, Z. Niu, Y. Zhao, G. Yue, Y. Zhao, G. Han, Lignin-based multi-scale cellular aerogels assembled from co-electrospun nanofibers for oil/water separation and energy storage, Chem Eng J. 436 (2022) 135233. https://doi.org/10.1016/j.cej.2022.135233.

[52] Z. Chu, Y. Li, A. Zhou, L. Zhang, X. Zhang, Y. Yang, Z. Yang, Polydimethylsiloxane-decorated magnetic cellulose nanofiber composite for highly efficient oil-water separation, Carbohyd Polym. 277 (2022) 118787. https://doi.org/10.1016/j.carbpol.2021.118787.

[53] R. Knížek, D. Karhánková, V. Bajzík, O. Jirsák, Lamination of Nanofibre Layers for Clothing Applications, Fibres Text East Europe. 27 (2019) 16–22. https://doi.org/10.5604/01.3001.0012.7503.

[54] R. Bagherzadeh, M. Latifi, S.S. Najar, M.A. Tehran, M. Gorji, L. Kong, Transport properties of multi-layer fabric based on electrospun nanofiber mats as a breathable barrier textile material, Text Res J. 82 (2012) 70–76. https://doi.org/10.1177/0040517511420766.

[55] S. Han, Y. Chen, S. Lyu, Z. Chen, S. Wang, F. Fu, Effects of processing conditions on the properties of paraffin/melamine-urea-formaldehyde microcapsules prepared by in situ polymerization, Colloids Surf. A: Physicochem. Eng. Asp. 585 (2020) 124046. https://doi.org/10.1016/j.colsurfa.2019.124046.

[56] Z. Zhang, Z. Zhang, T. Chang, J. Wang, X. Wang, G. Zhou, Phase change material microcapsules with melamine resin shell via cellulose nanocrystal stabilized Pickering emulsion in-situ polymerization, Chem. Eng. J. 428 (2022) 131164. https://doi.org/10.1016/j.cej.2021.131164.

[57] Y. Konuklu, F. Erzin, Preparation of pentadecane/poly(melamine-urea-formaldehyde) microcapsules for thermal energy storage applications, Int. J. Energy Res. 43 (2019) 6322–6326. https://doi.org/10.1002/er.4346.

[58] A.T. Naikwadi, A.B. Samui, P.A. Mahanwar, Melamine-formaldehyde microencapsulated n-Tetracosane phase change material for solar thermal energy storage in coating, Sol. Energy Mater. Sol. Cells. 215 (2020) 110676. https://doi.org/10.1016/j.solmat.2020.110676.

[59] B. Zhang, S. Li, X. Fei, H. Zhao, X. Lou, Enhanced mechanical properties and thermal conductivity of paraffin microcapsules shelled by hydrophobic-silicon carbide

modified melamine-formaldehyde resin, Colloids Surf. A: Physicochem. Eng. Asp. 603 (2020) 125219. https://doi.org/10.1016/j.colsurfa.2020.125219.

[60] J. Singh, S. Parvate, J.R. Vennapusa, T.K. Maiti, P. Dixit, S. Chattopadhyay, Facile method to prepare 1-dodecanol@poly(melamine-paraformaldehyde) phase change energy storage microcapsules via surfactant-free method, J. Energy Storage. 49 (2022) 104089. https://doi.org/10.1016/j.est.2022.104089.

[61] S.I. Hussain, S. Kalaiselvam, Nanoencapsulation of oleic acid phase change material with Ag2O nanoparticles-based urea formaldehyde shell for building thermal energy storage, J. Therm. Anal. Calorim. 140 (2020) 133–147. https://doi.org/10.1007/s10973-019-08732-5.

[62] E.G. Saraç, E. Öner, M.V. Kahraman, Microencapsulated organic coconut oil as a natural phase change material for thermo-regulating cellulosic fabrics, Cellulose. 26 (2019) 8939–8950. https://doi.org/10.1007/s10570-019-02701-9.

[63] G.N. Kumar, B. Al-Aifan, R. Parameshwaran, V.V. Ram, Facile synthesis of microencapsulated 1-dodecanol/melamine-formaldehyde phase change material using in-situ polymerization for thermal energy storage, Colloids Surf. A: Physicochem. Eng. Asp. 610 (2021) 125698. https://doi.org/10.1016/j.colsurfa.2020.125698.

[64] B. Praveen, S. Suresh, V. Pethurajan, Heat transfer performance of graphene nano-platelets laden micro-encapsulated PCM with polymer shell for thermal energy storage based heat sink, Appl. Therm. Eng. 156 (2019) 237–249. https://doi.org/10.1016/j.applthermaleng.2019.04.072.

[65] X. Wang, C. Zhang, K. Wang, Y. Huang, Z. Chen, Highly efficient photothermal conversion capric acid phase change microcapsule: Silicon carbide modified melamine urea formaldehyde, J. Colloid Interface Sci. 582 (2021) 30–40. https://doi.org/10.1016/j.jcis.2020.08.014.

[66] S. Lu, T. Shen, J. Xing, Q. Song, J. Shao, J. Zhang, C. Xin, Preparation and characterization of cross-linked polyurethane shell microencapsulated phase change materials by interfacial polymerization, Mater. Lett. 211 (2018) 36–39. https://doi.org/10.1016/j.matlet.2017.09.074.

[67] H. Nikpourian, A.R. Bahramian, M. Abdollahi, On the thermal performance of a novel PCM nanocapsule: The effect of core/shell, Renew. Energy. 151 (2020) 322–331. https://doi.org/10.1016/j.renene.2019.11.027.

[68] J.A. Ansari, R. Al-Shannaq, J. Kurdi, S.A. Al-Muhtaseb, C.A. Ikutegbe, M.M. Farid, A Rapid Method for Low Temperature Microencapsulation of Phase Change Materials (PCMs) Using a Coiled Tube Ultraviolet Reactor, Energies. 14 (2021) 7867. https://doi.org/10.3390/en14237867.

[69] R. Pradhan, A.P. Ramaswamy, Encapsulation of paraffin wax by rigid cross-linked poly (styrene divinylbenzene-acrylic acid) and its thermal characterization, SN Appl. Sci. 1 (2019) 859. https://doi.org/10.1007/s42452-019-0891-8.

[70] D. Xu, R. Yang, Efficient preparation and characterization of paraffin-based microcapsules by emulsion polymerization, J. Appl. Polym. Sci. 136 (2019) 47552. https://doi.org/10.1002/app.47552.

[71] F. Haghighat, S.A.H. Ravandi, M.N. Esfahany, A. Valipouri, A comprehensive study on optimizing and thermoregulating properties of core–shell fibrous structures through coaxial electrospinning, J Mater Sci. 53 (2018) 4665–4682. https://doi.org/10.1007/s10853-017-1856-1.

[72] L. Zhao, J. Luo, Y. Li, H. Wang, G. Song, G. Tang, Emulsion-electrospinning n-octadecane/silk composite fiber as environmental-friendly form-stable phase change materials, J Appl Polym Sci. 134 (2017). https://doi.org/10.1002/app.45538.

[73] D. Luo, F. Wei, H. Shao, L. Xiang, J. Yang, Z. Cui, S. Qin, J. Yu, Shape stabilization, thermal energy storage behavior and thermal conductivity enhancement of flexible paraffin/MWCNTs/PP hollow fiber membrane composite phase change materials, J Mater Sci. 53 (2018) 15500–15513. https://doi.org/10.1007/s10853-018-2722-5.

[74] N. Xie, J. Niu, X. Gao, Y. Fang, Z. Zhang, Fabrication and characterization of electrospun fatty acid form-stable phase change materials in the presence of copper nanoparticles, Int J Energ Res. 44 (2020) 8567–8577. https://doi.org/10.1002/er.5543.

[75] H. Ke, Electrospun methyl stearate/PET form-stable phase change composite nanofibres for storage and retrieval of thermal energy, Mater Res Innov. 22 (2018) 150–158. https://doi.org/10.1080/14328917.2016.1266203.

[76] L. Zhou, F. Shi, G. Liu, J. Ye, P. Han, G. Zhang, Fabrication and characterization of in situ cross-linked electrospun Poly(vinyl alcohol)/phase change material nanofibers, Sol Energy. 213 (2021) 339–349. https://doi.org/10.1016/j.solener.2020.11.039.

[77] T. Dong, W. jiang, Y. liu, Y. Wu, Y. Qi, J. Li, Y. Ma, H. Ben, G. Han, A phase change material embedded composite consisting of kapok and hollow PET fibers for dynamic thermal comfort regulation, Ind Crop Prod. 158 (2020). https://doi.org/10.1016/j.indcrop.2020.112945.

[78] W. Feng, Y.-S. Zhang, Y.-W. Shao, T. Huang, N. Zhang, J.-H. Yang, X.-D. Qi, Y. Wang, Coaxial electrospun membranes with thermal energy storage and shape memory functions for simultaneous thermal/moisture management in personal cooling textiles, Eur Polym J. 145 (2021). https://doi.org/10.1016/j.eurpolymj.2020.110245.

[79] E.C.B. Noyan, E. Onder, N. Sarier, R. Arat, Development of heat storing poly(acrylonitrile) nanofibers by coaxial electrospinning, Thermochim Acta. 662 (2018) 135–148. https://doi.org/10.1016/j.tca.2018.02.008.

[80] X. Zhang, J. Qiao, H. Zhao, Z. Huang, Y. Liu, M. Fang, X. Wu, X. Min, Preparation and performance of novel polyvinylpyrrolidone/polyethylene glycol phase change materials composite fibers by centrifugal spinning, Chem Phys Lett. 691 (2018) 314–318. https://doi.org/10.1016/j.cplett.2017.11.041.

[81] Y. Yan, W. Li, R. Zhu, C. Lin, R. Hufenus, Flexible phase change material fiber: A simple route to thermal energy control textiles, Materials. 14 (2021) 1–18. https://doi.org/10.3390/ma14020401.

[82] H. Fang, J. Lin, L. Zhang, A. Chen, F. Wu, L. Geng, X. Peng, Fibrous form-stable phase change materials with high thermal conductivity fabricated by interfacial polyelectrolyte complex spinning, Carbohyd Polym. 249 (2020). https://doi.org/10.1016/j.carbpol.2020.116836.

[83] J. Wu, R. Hu, S. Zeng, W. Xi, S. Huang, J. Deng, G. Tao, Flexible and Robust Biomaterial Microstructured Colored Textiles for Personal Thermoregulation, Acs Appl Mater Inter. 12 (2020) 19015–19022. https://doi.org/10.1021/acsami.0c02300.

[84] Y.-H. Ahn, S.J.A. DeWitt, S. McGuire, R.P. Lively, Incorporation of phase change materials into fibers for sustainable thermal energy storage, Ind Eng Chem Res. (2021). https://doi.org/10.1021/acs.iecr.0c06140.

[85] L. Xiang, D. Luo, J. Yang, X. Sun, J. Jin, S. Qin, Construction and Design of Paraffin/PVDF Hollow Fiber Linear-Phase Change Energy Storage Materials, Energ Fuel. 33 (2019) 11584–11591. https://doi.org/10.1021/acs.energyfuels.9b02852.

[86] H. Qi, T. Zhang, D. Zhang, K. Wang, Y. Wang, Paraffin/chitosan composite phase change materials fabricated by piercing-solidifying method for thermal energy storage, Aip Adv. 10 (2020) 035218. https://doi.org/10.1063/1.5140582.

[87] M. Kenisarin, K. Mahkamov, F. Kahwash, I. Makhkamova, Enhancing thermal conductivity of paraffin wax 53–57 °C using expanded graphite, Sol Energ Mat Sol C. 200 (2019) 110026. https://doi.org/10.1016/j.solmat.2019.110026.

[88] D. Luo, L. Xiang, X. Sun, L. Xie, D. Zhou, S. Qin, Phase-change smart lines based on paraffin-expanded graphite/polypropylene hollow fiber membrane composite phase change materials for heat storage, Energy. 197 (2020). https://doi.org/10.1016/j.energy.2020.117252.

[89] B. Tang, M. Qiu, S. Zhang, Thermal conductivity enhancement of PEG/SiO2 composite PCM by in situ Cu doping, Sol Energ Mat Sol C. 105 (2012) 242–248. https://doi.org/10.1016/j.solmat.2012.06.012.

[90] A.W. Kuziel, G. Dzido, R. Turczyn, R.G. Jędrysiak, A. Kolanowska, A. Tracz, W. Zięba, A. Cyganiuk, A.P. Terzyk, S. Boncel, Ultra-long carbon nanotube-paraffin composites of record thermal conductivity and high phase change enthalpy among paraffin-based heat storage materials, J. Energy Storage. 36 (2021) 102396. https://doi.org/10.1016/j.est.2021.102396.

[91] C. Li, B. Zhang, B. Xie, X. Zhao, J. Chen, Z. Chen, Y. Long, Stearic acid/expanded graphite as a composite phase change thermal energy storage material for tankless solar water heater, Sustain. Cities Soc. 44 (2019) 458–464. https://doi.org/10.1016/j.scs.2018.10.041.

[92] N. Sheng, Z. Rao, C. Zhu, H. Habazaki, Honeycomb carbon fibers strengthened composite phase change materials for superior thermal energy storage, Appl Therm Eng. 164 (2020). https://doi.org/10.1016/j.applthermaleng.2019.114493.

[93] Y. Tang, G. Alva, X. Huang, D. Su, L. Liu, G. Fang, Thermal properties and morphologies of MA–SA eutectics/CNTs as composite PCMs in thermal energy storage, Energy Build. 127 (2016) 603–610. https://doi.org/10.1016/j.enbuild.2016.06.031.

[94] A. Karaipekli, A. Biçer, A. Sarı, V.V. Tyagi, Thermal characteristics of expanded perlite/paraffin composite phase change material with enhanced thermal conductivity using carbon nanotubes, Energy Convers. Manag. 134 (2017) 373–381. https://doi.org/10.1016/j.enconman.2016.12.053.

[95] W. Jin, L. Jiang, L. Chen, T. Yin, Y. Gu, M. Guo, X. Yan, X. Ben, Enhancement of thermal conductivity by graphene as additive in lauric-stearic acid/treated diatomite composite phase change materials for heat storage in building envelope, Energy Build. 246 (2021) 111087. https://doi.org/10.1016/j.enbuild.2021.111087.

[96] J.-L. Zeng, S.-H. Zheng, S.-B. Yu, F.-R. Zhu, J. Gan, L. Zhu, Z.-L. Xiao, X.-Y. Zhu, Z. Zhu, L.-X. Sun, Z. Cao, Preparation and thermal properties of palmitic acid/polyaniline/exfoliated graphite nanoplatelets form-stable phase change materials, Appl. Energy. 115 (2014) 603–609. https://doi.org/10.1016/j.apenergy.2013.10.061.

[97] D.G. Atinafu, C. Wang, W. Dong, X. Chen, M. Du, H. Gao, G. Wang, In-situ derived graphene from solid sodium acetate for enhanced photothermal conversion, thermal conductivity, and energy storage capacity of phase change materials, Sol. Energy Mater. Sol. Cells. 205 (2020) 110269. https://doi.org/10.1016/j.solmat.2019.110269.

[98] X. Zheng, X. Gao, Z. Huang, Z. Li, Y. Fang, Z. Zhang, Form-stable paraffin/graphene aerogel/copper foam composite phase change material for solar energy conversion and storage, Sol. Energy Mater. Sol. Cells. 226 (2021) 111083. https://doi.org/10.1016/j.solmat.2021.111083.

[99] X. Huang, Y. Lin, G. Alva, G. Fang, Thermal properties and thermal conductivity enhancement of composite phase change materials using myristyl alcohol/metal foam for solar thermal storage, Sol. Energy Mater. Sol. Cells. 170 (2017) 68–76. https://doi.org/10.1016/j.solmat.2017.05.059.

[100] J.Y. Do, N. Son, J. Shin, R.K. Chava, S.W. Joo, M. Kang, n-Eicosane-Fe3O4@SiO2@Cu microcapsule phase change material and its improved thermal conductivity and heat transfer performance, Mater. Des. 198 (2021) 109357. https://doi.org/10.1016/j.matdes.2020.109357.

[101] R. Wen, X. Zhu, C. Yang, Z. Sun, L. Zhang, Y. Xu, J. Qiao, X. Wu, X. Min, Z. Huang, A novel composite phase change material from lauric acid, nano-Cu and attapulgite: Preparation, characterization and thermal conductivity enhancement, J. Energy Storage. 46 (2022) 103921. https://doi.org/10.1016/j.est.2021.103921.

[102] B. Zhao, Y. Wang, C. Wang, R. Zhu, N. Sheng, C. Zhu, Z. Rao, Thermal conductivity enhancement and shape stabilization of phase change thermal storage material reinforced by combustion synthesized porous Al2O3, J. Energy Storage. 42 (2021) 103028. https://doi.org/10.1016/j.est.2021.103028.

[103] S. Fan, H. Gao, W. Dong, J. Tang, J. Wang, M. Yang, G. Wang, Shape-Stabilized Phase Change Materials Based on Stearic Acid and Mesoporous Hollow SiO2 Microspheres (SA/SiO2) for Thermal Energy Storage, Eur. J. Inorg. Chem. 2017 (2017) 2138–2143. https://doi.org/10.1002/ejic.201601380.

[104] B. Tang, H. Wei, D. Zhao, S. Zhang, Light-heat conversion and thermal conductivity enhancement of PEG/SiO2 composite PCM by in situ Ti4O7 doping, Sol. Energy Mater. Sol. Cells. 161 (2017) 183–189. https://doi.org/10.1016/j.solmat.2016.12.003.

[105] W. Xia, X. Fei, Q. Wang, Y. Lu, M.T. Innocent, J. Zhou, S. Yu, H. Xiang, M. Zhu, Nano-hybridized form-stable ester@F-SiO<inf>2</inf> phase change materials for melt-spun PA6 fibers engineered towards smart thermal management fabrics, Chem Eng J. 403 (2021). https://doi.org/10.1016/j.cej.2020.126369.

[106] X. Xiong, M. Venkataraman, D. Jašíková, T. Yang, R. Mishra, J. Militký, M. Petrů, An experimental evaluation of convective heat transfer in multi-layered fibrous materials composed by different middle layer structures, J Ind Text. (2019) 152808371987884. https://doi.org/10.1177/1528083719878845.

[107] A. Nejman, M. Cieślak, B. Gajdzicki, B. Goetzendorf-Grabowska, A. Karaszewska, Methods of PCM microcapsules application and the thermal properties of modified knitted fabric, Thermochim Acta. 589 (2014) 158–163. https://doi.org/10.1016/j.tca.2014.05.037.

[108] A. Shahid, S. Miah, A. Rahim, Thermal and breathability management of microencapsulated phase change material (MPCM) incorporated jute fabric, J Eng Fiber Fabr. 16 (2021) 155892502110295. https://doi.org/10.1177/15589250211029564.

[109] T.R. Kar, A.K. Samanta, H.D. Sinnur, M. Kumar, Studies on Effect of Application of Capric Acid and Stearic Acid based Reactive Phase Change Materials (rPCM) with PHAMS Binder on Thermal Comfort of Cotton Khadi Fabric as Thermotropic Smart Textiles., J Nat Fibers. (2021). https://doi.org/10.1080/15440478.2021.1880517.

[110] Y. Shin, D. Yoo, K. Son, Development of thermoregulating textile materials with microencapsulated phase change materials (PCM). IV. Performance properties and hand of fabrics treated with PCM microcapsules, J. Appl. Polym. Sci. 97 (2005) 910–915. https://doi.org/10.1002/app.21846.

[111] K. Choi, G. Cho, Physical and mechanical properties of thermostatic fabrics treated with nanoencapsulated phase change materials, J Appl Polym Sci. 121 (2011) 3238–3245. https://doi.org/10.1002/app.33870.

[112] K. Yang, L. Martinkova, O. Ctibor, X. Zhang, M. Venkataraman, J. Wiener, G. Zhu, G. Zhang, J. Yao, J. Militky, Mass transfer and thermal buffering effect of hydrophobic fabrics with single-side coating of MPCMs, Prog Org Coat. 172 (2022) 107151. https://doi.org/10.1016/j.porgcoat.2022.107151.

[113] H. Wang, L. Zhao, L. Chen, G. Song, G. Tang, Facile and low energy consumption synthesis of microencapsulated phase change materials with hybrid shell for thermal energy storage, J. Phys. Chem. Solids. 111 (2017) 207–213. https://doi.org/10.1016/j.jpcs.2017.08.002.

9. Appendix 1-Full text

9.1 Research journal article-1 (ChemNanoMat, Q2, IF: 3.8)

ACES Asian Chemical Editorial Society

doi.org/10.1002/cnma.202200352

CHEMNANOMAT
Research Article

www.chemnanomat.org

Nanofibrous Membranes in Multilayer Fabrics to Avoid PCM Leakages

Kai Yang,*[a] Xiuling Zhang,[a] Jakub Wiener,[a] Mohanapriya Venkataraman,[a] Yuanfeng Wang,[a] Guocheng Zhu,[b, e] Juming Yao,[c, d, e] and Jiri Militky[a]

Abstract: Incorporating phase change materials (PCMs) into textiles is one facial method to realize personal thermal management (PTM). Despite the significant progress of PCM-incorporated textiles, the incorporation of PCMs into textiles remains an outstanding challenge. In this work, we described a sandwich-like multi-layer PCM fabric, which consisted of nanofibrous membranes as barrier layers and PCM-loaded viscose fabric as a PCM-loaded layer. Three common organic PCMs including polyethylene glycol (PEG), paraffin wax (PW) and myristic acid (MA), and the polyurethane (PU) nanofibrous membranes was used. As a result, we achieved that weak interfacial adhesion between melting PCMs and PU nanofibrous membranes accounted for leakage phenomena. Only the sample (UPWV) with PU nanofibrous membranes as barrier layers and paraffin wax (PW) as PCMs had no leakage. Little confinement of PW crystallization in the UPWV was found. Besides, thermal energy storage, phase transition, and thermal buffering effect of UPWV supported various applications.

Introduction

Personal thermal management (PTM) has been studied for decades.[1] Incorporation of organic phase change materials (PCMs) (e.g., paraffin wax, fatty acid, polyethylene glycol, etc.) into textiles is one facial method for PTM.[2,3] During the phase transition of the PCMs over a certain temperature, the thermal resistance of the PCMs is changeable and the thermal energy is absorbed or released. However, the leakage of the PCMs is the main problem for the practical applications. To avoid leakage, microencapsulated PCMs (MPCMs) and form-stable PCMs (FSPCMs) have been proposed.[4–6] MPCMs have been the most industrial technology and its application in textiles has been studied for decades.[7] The MPCMs consist of supporting materials as shell and PCMs as core, where stability of thermal energy storage and phase transition of MPCMs is enhanced.[8] However, the encapsulation efficiency of MPCMs required modification.[9] FSPCMs are usually prepared by filling PCMs into porous materials (e.g., zeolite, aerogel, foam etc.).[4,10–12] Although the leakage of melting PCMs can be avoided, thermal energy storage and phase transition of final FSPCMs is significantly affected by pores.[13,14] In addition, PCMs are usually coated on fabrics or incorporated into fibers for PTM. For PCM-incorporated fabrics, various methods have been proposed to apply MPCMs or FSPCMs on fabrics, including coating, padding, laminating, printing etc..[2,15,16] However, loss of MPCMs or FSPCMs possibly happens because of mechanical movement (e.g., washing, abrasion). For PCM fibers, the incorporation of the pure PCMs, MPCMs or FSPCMs into fibers is the alternative.[17,18] However, the final thermal energy storage and mechanical property of PCM fibers are affected by PCM contents.

It is noticed that the leakage of PCMs from its coated fabric during heating/cooling cycles is governed by viscosity of melting PCMs and adhesion between melting PCMs and fabrics if the pure PCMs are coated on fabrics directly. From this point of view, the multi-layer fabric structure by using barrier layers covering the PCM-loaded layer (PCM-coated fabrics) is possible to avoid leakage.[19] Especially for the selection of the barrier layers, the nanofibrous membranes are alternative. By controlling porosity and surficial chemistry to obtain hydrophilicity or hydrophobicity or oleophobic property, various nanofibrous membranes have been applied for oil/water separation, air filtration etc..[18,20–30] Besides, the high resistance against mass transfer of nanofibrous membrane-coated fabrics have been proposed.[31] From this point of view, it is an alternative to use the nanofibrous membranes can be used as barrier layer to

[a] K. Yang, X. Zhang, Prof. Dr. J. Wiener, Dr. M. Venkataraman, Y. Wang, Prof. Dr. J. Militky
Department of Material Engineering
Faculty of Textile Engineering
Technical University of Liberec
Studentska, 1402/2, Liberec, 461 17 (Czech Republic)
E-mail: kai.yang@tul.cz

[b] Prof. Dr. G. Zhu
College of Textiles and Engineering
Zhejiang Sci-tech University
No. 5 Second Avenue, Xiasha Education Park,
Hangzhou City, 310018 (P. R. China)

[c] Prof. Dr. J. Yao
School of Materials and Engineering
Zhejiang Sci-tech University
No. 5 Second Avenue, Xiasha Education Park,
Hangzhou City, 310018 (P. R. China)

[d] Prof. Dr. J. Yao
School of Materials Science and Chemical Engineering
Ningbo University
No. 8181 Fenghua Road, Jiangbei District,
Ningbo City, 315211 (P. R. China)

[e] Prof. Dr. G. Zhu, Prof. Dr. J. Yao
Zhejiang-Czech Joint Laboratory of Advanced Fiber Materials
Zhejiang Sci-tech University
No. 5 Second Avenue, Xiasha Education Park,
Hangzhou City, 310018 (P. R. China)

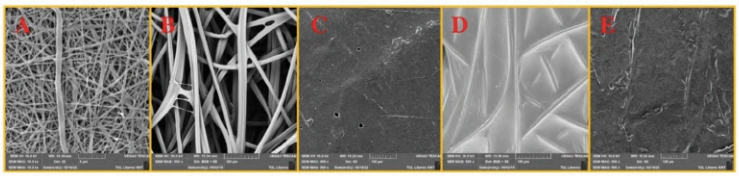

Figure 2. Morphology characterization (A, B, C, D and E: PU nanofibrous membrane, viscose fabric, MA-coated viscose fabric, PEG-coated viscose fabric and PW-coated viscose fabric).

resist against the penetration of melting PCMs by adjusting their interfacial adhesion.

In this work, we first tried to construct a multi-layer fabric structure consisting of PCM-loaded layer and barrier layers. Three common PCMs sharing similar phase transition points were used, including polyethylene glycol (PEG) (M_w = 6,000), myristic acid (MA) and paraffin wax (PW). The polyurethane (PU) nanofibrous membranes as barrier layers and nonwoven viscose fabric was used to load PCMs. After determining on the suitable nanofibrous membranes and PCMs according to leakage test, the thermal energy storage and phase transition of the multi-layer PCM fabrics as well as their thermal buffering effect were investigated.

Results and Discussion

The leakage test results of the PCM-loaded layer and the multi-layer PCM fabrics were shown in Figure 1. Obviously, the leakage of the PCM-loaded layers was found. By combining with morphology in Figure 2, the PCMs filled in the interspaces of viscose fabrics and covered viscose fabric. During heating process, the solid PCMs melt, and porous structure of viscose fabric did not support to hold the melting PCMs. For the multi-layer PCM fabrics, it was found that only sample consisting of PU nanofibrous membrane as barrier layers and PW-coated viscose fabric as PCM-loaded layer had no leakage while other samples had more or less leakage. We propose that the interfacial adhesion between melting PCMs and nanofibrous membranes accounted for the leakage phenomena. The wetting behavior of melting PCMs on nanofibrous membranes characterized by change of contact angle (CA) values of molten PCM droplets on PU nanofibrous membranes with time was shown in Figure 3. In details, the CA values of melting PW on PU nanofibrous membranes were almost constant about 110°, which suggested the stable weak adhesion between melting PW and PU nanofibrous membranes. The CA values of melting PEG or melting MA on PU nanofibrous membranes tended to continuously decrease with time. It took 10s for the melting PEG on PU nanofibrous membranes to have CA values of 90° and took 20s for the melting MA on PU nanofibrous membranes to have 90°. Besides, the porosity of PU nanofibrous membranes also accounted for the leakage. By using IMAGE J software, the surface porosity of PU nanofibrous membrane was measured as 5.07%, and pore size was measured as 356±147 nm. Therefore, the combination of weak adhesion, lower porosity and small pore size of PU nanofibrous membranes increased the difficult for melting PW to penetrate. So, only the sample consisting of PU nanofibrous membranes as barrier layers and PW-coated viscose fabric as PCM-loaded layer was further investigated in the following analysis and labeled as UPWV.

To investigate the thermal energy storage and phase transition of UPWV, DSC measurement of UPWV was performed. It was noticed that UPWV contained viscose fabric and PU nanofibrous membrane, and both thermal property and crystallization behavior of PW in the UPWV may be altered when

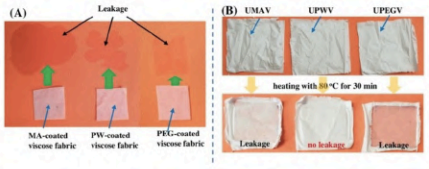

Figure 1. Leakage test results (A: PCM-loaded layer and B: multi-layer PCM fabric).

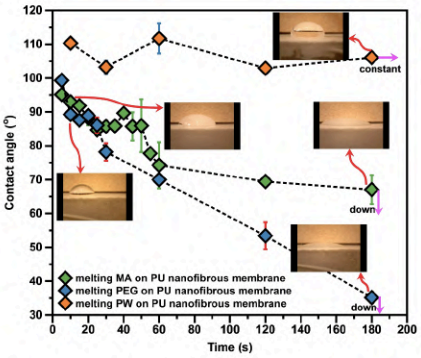

Figure 3. CA values of molten PCMs on surface of nanofibrous membranes.

compared with PW. Therefore, the thermal energy storage and phase transition of PW-coated viscose fabric (labeled as PWV) and the pure PW were also evaluated. All the DSC curves of PW, PWV and UPWV were shown in Figure 4. Two peaks including *peak 1* and *peak 2* were observed for PW, PWV and UPWV. The *peak 1* ranging from 30 °C to 40 °C was caused by solid-solid (SS) phase transition in PW, which generally implicates a rotational motion at the molecular level from the rotator phase α to the non-rotating phase β.[32] The *peak 2* ranging from 50 °C to 60 °C was caused by solid-liquid (SL) phase transition in PW during heating/cooling cycles. The details related to phase transition and thermal energy storage were given in shown in Table 1 and Table 2. From Figure 5, the larger phase transition range and $|\Delta T|$ values of all the samples were increased when higher ϕ values were applied. Besides, both melting enthalpy values and solidifying enthalpy values of all the samples slightly decreased when higher ϕ values were applied. The main reason could be that phase transition of PWs depended on the ϕ values.[33] When higher ϕ values are applied, the time for movement of PW molecule chains becomes shorter and some PW molecule chains do not move in time when the heating or cooling process if finished. Still for all the samples, the differences between the enthapy values with different ϕ values were smaller, which supported the highly-stable phase transition behavior of PW, PW-loaded layer and UPWV.

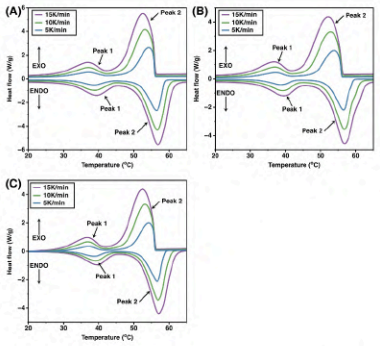

Figure 4. DSC curves with different heating/cooling rates for PW (A), PWV (B) and UPWV (C).

Analysis of SS phase transition

For both SS phase transition, PW, PWV and UPWV had similar T_{pm} and T_{pc} values, which suggested that both viscose fabric and PU nanofibrous membrane little affected α phase and β phase of PW. In addition, it was found that the SS phase transition from α phase to β phase of UPWV and PW started slightly earlier than PW while SS phase transition from β phase to α phase of UPWV and PW started slightly later than PW. Correspondingly, supercooling degree ($|\Delta T_{SS}|$) was changed, and the order of ΔT values was found as PW > PWV > UPWV. Besides, it was found that SS phase transition of PW, PWV and UPWV was almost constant even though different ϕ values were applied. The stable SS phase transition behavior of PW, PWV and UPWV were found. As a result, the PW, PWV and

Table 1. Phase transition and thermal energy storage of *peak 1* (solid-solid phase transition).

Sample code	ϕ [K/min]	T_{om} [°C]	T_{pm} [°C]	T_{em} [°C]	ΔH_m [J/g]	T_{oc} [°C]	T_{pc} [°C]	T_{ec} [°C]	ΔH_c [J/g]	$\lvert\Delta T_{SS}\rvert$ [°C]
PW	5	32.39	38.58	43.14	31.53	41.41	36.84	29.63	27.62	9.02
	10	31.59	38.51	43.84	31.23	41.49	36.82	29.23	28.05	9.9
	15	31.93	39.02	44.22	30.36	41.88	36.47	28.84	27.67	9.95
PWV	5	32.49	38.61	42.55	25.00	40.82	37.06	30.21	22.5	8.33
	10	32.33	39.06	43.43	25.74	40.88	36.61	29.37	22.69	8.55
	15	31.94	39.09	44.07	24.74	40.84	36.41	28.84	21.29	8.9
UPWV	5	32.71	38.73	42.45	24.34	40.62	37.02	30.67	21.86	7.91
	10	32.62	39.12	43.32	24.14	40.67	36.71	29.74	21.03	8.05
	15	32.44	39.19	44.05	23.74	40.74	36.31	29.29	21.29	8.3

Table 2. Phase transition and thermal energy storage of *peak 2* (solid-liquid phase transition).

Sample code	ϕ [K/min]	T_{om} [°C]	T_{pm} [°C]	T_{em} [°C]	ΔH_m [J/g]	T_{oc} [°C]	T_{pc} [°C]	T_{ec} [°C]	ΔH_c [J/g]	$\lvert\Delta T_{SL}\rvert$ [°C]
PW	5	51.7	56.56	58.74	137.88	56	54.21	49.12	138.83	4.3
	10	51.27	56.73	59.97	132.33	56.11	53.22	47.5	133.07	4.84
	15	51.12	56.75	61.2	131.74	56.3	52.71	46.41	132.07	5.18
PWV	5	51.83	56.51	58.64	114.79	56.06	53.87	48.42	115.87	4.23
	10	51.62	56.65	60.2	113.45	56.25	52.97	46.64	115.00	4.63
	15	51.34	56.83	61.65	111.89	56.45	52.37	45.18	113.46	5.11
UPWV	5	52	56.68	58.57	106.55	56.04	54.23	49.14	109.17	4.04
	10	52.05	56.91	60.12	105.39	56.19	53.24	47.67	108.11	4.14
	15	51.77	57.17	61.45	105.04	56.4	52.57	46.43	107.03	4.63

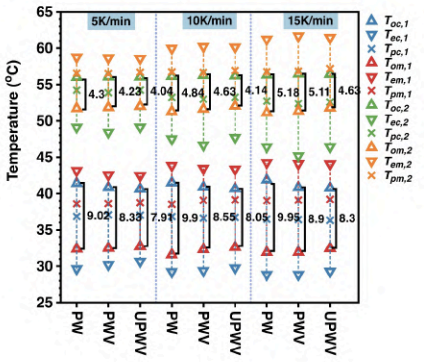

Figure 5. Phase transition range for PW, PWV and UPWV with different heating/cooling rates.

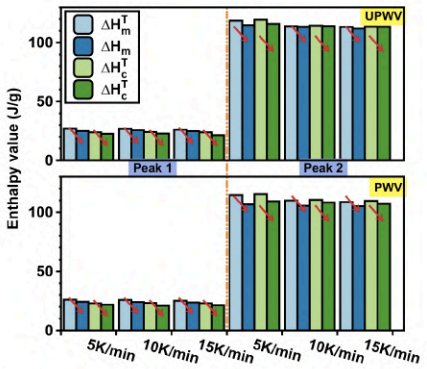

Figure 6. Comparison between measured enthalpy values and theoretical enthalpy values of PW in PWV and UPWV.

UPWV had ΔH_m values of 31 J/g, 26 J/g and 25 J/g, and ΔH_c of 28 J/g, 23 J/g, 22 J/g, respectively.

Analysis of SL phase transition

For SL phase transition, both viscose fabric and PU nanofibrous membrane little affected major crystalline structure of PW after observing T_{pm} and T_{pc} values. Besides, UPWV and PW started melt slightly later than PW while crystalline earlier than PW, which was opposite against SS phase transition. Both viscose fabric and PU nanofibrous membrane altered the crystallization mechanism and α-β phase transition mechanism. Correspondingly, the supercooling degree ($|\Delta T_{SL}|$) for SL phase transition was changed, and the order of ΔT_{SL} values was found as PW > PWV > UPWV. By combining with ΔT_{SS}, the higher thermal energy storage efficiency was found in UPWV when compared with PW and PWV. For thermal energy storage during SL phase transition, the lower enthalpy values were found when ϕ values were equal to or higher than 10 K/min, which suggested more sensitivity of SL phase transition to ϕ values. By taking ϕ value as 10 K/min, the PW, PWV and UPWV had ΔH_m values of 132 J/g, 113 J/g and 105 J/g, and ΔH_c values of 133 J/g, 113 J/g and 108 J/g, respectively.

Besides, it was found that the order of enthalpy values was found as PW > PWV > UPWV for both SS and SL phase transition. We proposed that it was caused by less PW content and altered crystallinity of PW in PWV and UPWV. The theoretical enthalpy values (ΔH^T) were calculated according to equation (1), where ΔH_{PW} was the measured enthalpy values of pure PW. The ΔH^T values of PW in PWV and UPWV were shown in Table 3 and Figure 6. presented comparison between theoretical enthalpy values and measured enthalpy values of PWV and UPWV. All theoretical enthalpy values were higher than corresponding measured enthalpy values for PWV and UPWV. According to equation (2), the relative crystalline degree values (χ) of PW in PWV and UPWV were calculated and χ values were smaller than 100%, which was shown in Figure 7. The crystallinity of PW was confined in viscose fabric structure and PU nanofibrous membrane-incorporated multi-layer fabric structure. However, the χ values were above 90% for both SS transition and SL transition, which supported that the confinement effect of PW crystallization in UPWV was limited. Besides, the SS phase transition was stronger confined than the SL phase transition by observing lower χ values. In addition, the χ values of PW in UPWV were lower than one in PWV. The PU nanofibrous membranes as a barrier layer in multi-layer fabrics

Table 3. Theoretical enthalpy values and relative crystalline degree of PW in PWV and UPWV.

Sample code	ϕ [K/min]	$\Delta H^T_{m,1}$ [J/g]	$\Delta H^T_{c,1}$ [J/g]	$\Delta H^T_{m,2}$ [J/g]	$\Delta H^T_{c,2}$ [J/g]	χ_1 [%]	χ_2 [%]
PWV	5	27.11	23.75	118.58	119,39	92.20	93.01
	10	26.86	24.12	113.81	114.33	95.84	93.13
	15	26.11	24.00	113.29	113.58	94.75	94.21
UPWV	5	26.17	22.92	114.44	115.23	96.81	93.11
	10	25.92	23.28	109.84	110.48	98.81	95.95
	15	25.20	22.97	109.34	109,62	98.76	96.80

Subscript 1 and 2: SL and SS phase transition.

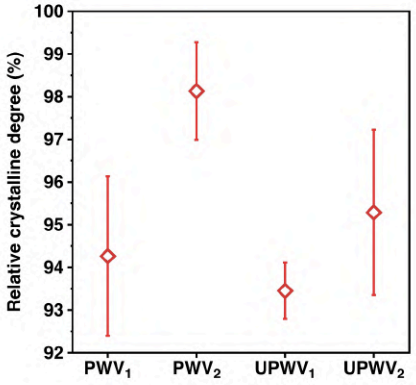

Figure 7. Relative crystalline degree of PW in PWV and UPWV.

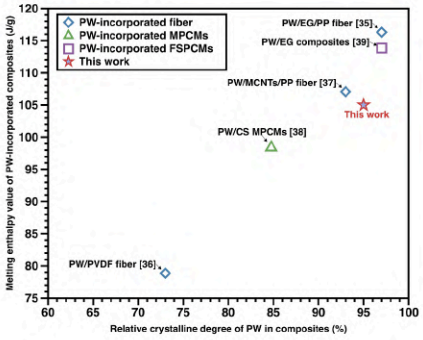

Figure 8. The comparison in relative crystalline degree and thermal energy storage in SL transition of other PW-incorporated composites with this work (The PW type of selected publication was same as the one in this work).

also altered the phase transition of PW. Still, the χ values of PW in UPWV reached 95%, which was higher than other PW-incorporated composite fibers. By comparing with other PW-incorporated composites,[34–38] the UPWV sample had comparable thermal energy storage and relative crystalline degree of PW, which was shown in Table 4 and Figure 8. It was noticed that major research work focused on PW-incorporated composites (e.g., fibers, FSPCMs, MPCMs etc.) and extra processes were necessary for their application in fabrics. So, our work was the facial one to fabricate PCM fabrics.

$$\Delta H^T = \Delta H_{PW} \times p_{PW} \quad (1)$$

$$\chi = \Delta H_m / \Delta H_m{}^T \times 100\% \quad (2)$$

Figure 9(A) presented T-history cures of UPWV and the reference sample consisting of two PU nanofibrous membranes and viscose fabric during heating and cooling process. Obviously, it took much longer time for UPWV to reach final stable temperature than reference sample during heating and cooling processes. For heating process of UPWV, three parts were observed according to phase of PW, including solid phase (including SS phase transition), SL phase transition and liquid phase. Since the enthalpy of SS phase transition was only around 25 J/g and the heating temperature was much higher than phase transition temperature range of SS phase transition, it was hard to observe the platform during heating process. Therefore, the platform in Figure 9(A) was only for SL phase transition. To further characterize the heating process of UPWV and reference sample, Newton's cooling law was used and expressed in equation (3).[39] The T_f (°C) was the final stable surface temperature during heating process, T_s (°C) was the recorded surface temperature of the prepared samples with time, T_i (°C) was the initial surface temperature of the prepared samples, t was the time and τ was the heating constant (s). Higher τ value supported the lower temperature increase rate. By transforming equation (3) to equation (4), the τ values were obtained. As shown in Figure 9(B), one linear relationship for reference sample and two linear relationships between $\ln[(T_f - T_s)]$ and τ were found. As a result, the τ values of solid phase and SL phase transition of UPWV were 18.62 s and 92.59 s, and the τ value of reference sample was 10.74 s. The overall temperature increasing rate of UPWV was lower than reference sample. Both SS phase transition and SL phase transition of UPWV contributed to thermal buffering effect. Besides, the T_f of UPWV was higher than reference sample. The reason was that more still air inside reference sample than

Table 4. The comparison in relative crystalline degree and thermal energy storage in SL transition of other PW-incorporated composites with this work (The PW type of selected publication was same as the one in this work).

PW-incorporated composite fibers or fabrics	χ of PW in PW-based CMs during SL phase transition (%)	ΔH_m of PW-incorporated PCM fabric or fiber (J/g)	Ref.
PU nanofibrous membrane-incorporated multi-layer PW fabrics (UPWV)	95	105	This work
PW/EG/PP fibers	97	116.31	[35]
PW/PVDF fibers	73	78.86	[36]
PW/MCNTs/PP fibers	93	107.06	[37]
PW/CS MPCMs	85	98.4	[38]
PW/EG FSPCMs	97	113.86	[39]

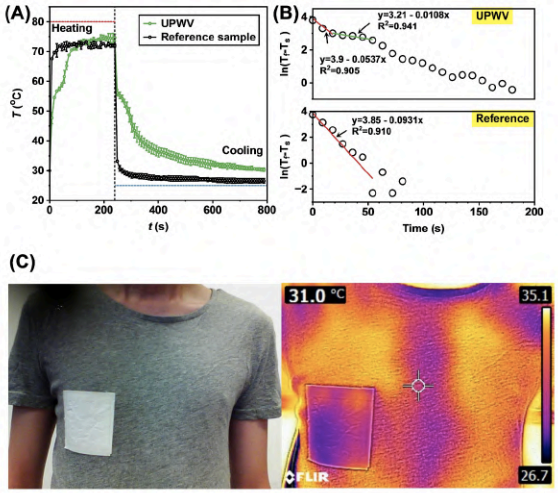

Figure 9. Thermal buffering effect of nanofibrous membrane-incorporated multi-layer fabric with or without PW (A: T-history curve, B: Characterization of heating process according to Newton's cooling law and C: incorporation of UPWV into commercial fabrics) (Error bars in 'A': standard errors, red line and blue line in 'B': the fitting model corresponded to solid phase and SL phase transition, respectively).

sample UPWV resulted in much lower thermal conductivity than UPWV with liquid PW when thermal balance was reached. For cooling process of UPWV, the classic peak was observed, which was caused by release of thermal energy from PW during SL phase transition. Besides, the final measured temperature of UPWV during cooling process was 30 °C, which was higher than reference sample with 26 °C. The main reason could be that SS phase transition of PW ranging from 30 °C to 40 °C took a long time since environment temperature was 25 °C.

$$T_f - T_s = (T_f - T_i)e^{-t/\tau} \quad (3)$$

$$\ln(T_f - T_s) = \ln(T_f - T_i) - t/\tau \quad (4)$$

From the above analysis, the UPWV had a great potential in various applications after investigating leakage, thermal energy storage, phase transition behavior and thermal buffering effect. To apply UPWV in practice, we provided one possibility to incorporate UPWV into textiles by using fabric binders, which was shown in Figure 9(C). The UPWV was well compatible with commercial fabrics. By comparing with other parts without UPWV, the lower temperature of UPWV-covering part was found from thermal infrared camera.

Conclusion

In conclusion, the possibility of nanofibrous membranes as barrier layers in multi-layer PCM fabrics has been systematically investigated. The control of interfacial adhesion between nanofibrous membranes and melting PCMs was significant for leakage results. As a result, the PU nanofibrous membranes successfully resisted against the penetration of melting PW and corresponding multi-layer PCM fabric without leakage was obtained. The final multi-layer PCM fabric had also high thermal energy storage, stable phase transition and thermal buffering effect. The work not only benefits the textile industrial but also support other fields which requires PCMs.

Experimental Section

Materials

Three PCMs including polyethylene glycol (PEG) (M_w = 6,000), myristic acid (MA) and paraffin wax (PW) were purchased from Sigma Aldrich. The polyurethane (PU) nanofibrous membranes (3 g/m^2) were provided from Institute for Nanomaterials, Advanced Technology and Innovation, Technical University of Liberec. Viscose fabric (47 g/m^2) was provided from Department of Material Engineering, Faculty of Textile Engineering, Technical University of Liberec.

Preparation of multi-layer fabrics

The preparation of nanofibrous membrane-incorporated multi-layer PCM fabrics followed the diagram of Figure 10., including two barrier layers and one PCM-loaded layer. The preparation of PCM-loaded layer followed the same process of published work.[39] As a result, three PCM-loaded layers were prepared, including MA-

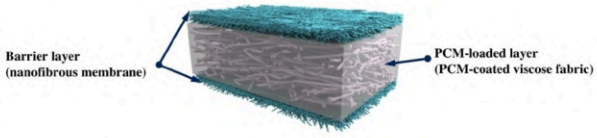

Figure 10. Diagram of nanofibrous membrane-incorporated multi-layer PCM fabrics.

coated viscose fabric, PW-coated viscose fabric and PEG-coated viscose fabric. After having their mass, the weight percentage (p_{PCM}) of PCMs for MA-coated viscose fabric, PW-coated viscose fabric and PEG-coated viscose fabric was 80 wt%, 86 wt% and 88 wt%, respectively. Correspondingly, the multi-layer fabrics with MA-coated viscose fabric, PW-coated viscose fabric or PEG-coated viscose fabric as the PCM-loaded layer were labeled as UMAV, UPWV and UPEGV, respectively.

Materials characterization

Scanning electronic microscopy (SEM) (VEGA TESCAN Inc., Lincoln, NE, USA) was used to characterize the morphology of fibrous materials and PCM-loaded layer. The electronic voltage of 20 kV was applied for SEM measurement. Furthermore, IMAGE J software (Version: 1.53a) (Wayne Rasband, National Institutes of Health, USA) was used to characterize the surface porosity of PU nanofibrous membranes.

Before leakage test, all the samples were taken a photo as the reference. Then, the leakage test was to put all the samples on the surface of commercial fabrics on the stable plate heater with temperature of 80 °C. The usage of commercial polyester fabrics was to avoid possible quick thermal shrinkage of nanofibrous membranes because the high heating temperature was used. After 30 min, the samples were taken a photo, which was compared with reference photo.

The CA values of melting PCMs on PU nanofibrous membranes were measured by following two steps and a custom setup was used (Figure 11):

1) Formation of melting PCMs. All the solid PCMs were put in the breaker. Then, the breakers with solid PCMs were placed on the stable plate heater with temperature of 80 °C till all the PCMs became liquid.
2) Measurement of CA values. The nanofibrous membrane was attached on the stable plate heater with temperature of 80 °C for 5 min to obtain heat transfer balance. To have a homogenous nanofibrous membrane, the adhesive tape was used to avoid deformation of nanofibrous membranes during measurement. Then, the melting PCMs droplets with volume of 25 uL were taken from the breaker and then placed on the surface of the nanofibrous membrane. At the same time, the optical camera (DINO) was used to record the shape of droplets of melting PCMs. As a result, the videos that CA values change with time were obtained.

Differential scanning calorimetry (DSC) (METTLER TOLEDO, Swiss) was used to characterize the thermal energy storage and phase transition of samples. The samples were kept ranging from 5.00 to 10.00 mg for the DSC measurement, and the nitrogen (N_2) gas rate was kept as 50 mL/min during the whole DSC measurement. The different constant heating/cooling rates (φ) were used, including 5 K/min, 10 K/min and 15 K/min. In details, the samples experienced

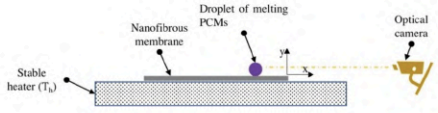

Figure 11. A custom setup to measure melting CA values of melting PCMs on PU nanofibrous membranes.

from 25 °C to 80 °C and was kept at 80 °C for 5 min to erase thermal history. Then, the sample experienced cooling process from 80 °C to 25 °C and following heating process from 25 °C to 80 °C. Both cooling and heating processes were recorded. As a result, the parameters related to phase transition and thermal energy storage were obtained, including onset melting/solidifying temperature (T_{om}/T_{oc}), peak melting/solidifying temperature (T_{pm}/T_{pc}), endset melting/solidifying temperature (T_{em}/T_{ec}) and melting/solidifying enthalpy (ΔH_m/ΔH_c). Besides, the supercooling degree ($|\Delta T|$) was obtained, which was the adsolute difference between T_{om} and T_{oc}.

For the thermal buffering effect, the sample was placed on the stable plate heater with temperature of 80 °C and the surface temperature of the sample was immediately recorded by thermal infrared camera (FLIR, E6) at the same time. Then after 5 min, the heating process of T-history was obtained. Then, the sample was immediately transferred on the surface of the thermal insulation materials with temperature of 25 °C. After 8 min, the cooling process was finished. The T-history measurement was performed under room condition with temperature of 23.5±2 °C and relative humidity of 65%. To further reveal the thermal buffering effect, Newton's cooling law was applied according to our published work.[39] Besides, to reveal the compatility of samples with commercial fabrics, the samples were also fixed on the surface of commercial fabrics by using commercial fabric binders (Korbond Hemming Web) and the temperature of human body was recorded by using thermal infrared camera (FLIR, E6).

Acknowledgements

This work was supported by the project 'Advanced structures for thermal insulation in extreme conditions' (Reg. No. 21-32510M) granted by the Czech Science Foundation (GACR). Additionally, Kai Yang would like to thank Ing. Jana Grabmullerova for her assistance in measuring SEM images, and Dr. Miroslava Pechociakova for her assistance in DSC measurement.

Conflict of Interest

The authors declare no conflict of interest.

Data Availability Statement

The data that support the findings of this study are available from the corresponding author upon reasonable request.

Keywords: fabric · leakage · nanofibrous membrane · PCM · thermal buffering effect

[1] R. Hu, Y. Liu, S. Shin, S. Huang, X. Ren, W. Shu, J. Cheng, G. Tao, W. Xu, R. Chen, X. Luo, *Adv. Energy Mater.* **2020**, *10*, 1903921.
[2] K. Yang, M. Venkataraman, X. Zhang, J. Wiener, G. Zhu, J. Yao, J. Militky, *J. Mater. Sci.* **2022**, *57*, 789–847.
[3] Y. Bao, J. Lyu, Z. Liu, Y. Ding, X. Zhang, *ACS Nano* **2021**, *15*, 15180.
[4] K. Yang, M. Venkataraman, J. Karpiskova, Y. Suzuki, S. Ullah, I.-S. Kim, J. Militky, Y. Wang, T. Yang, J. Wiener, G. Zhu, J. Yao, *Microporous Mesoporous Mater.* **2021**, *310*, 110636.
[5] L. Pathak, G. V. N. Trivedi, R. Parameshwaran, S. S. Deshmukh, *Mater. Today: Proc.* **2021**, *44*, 1960.
[6] S. Sundararajan, A. B. Samui, P. S. Kulkarni, *J. Mater. Chem. A* **2017**, *5*, 18379.
[7] J. L. Reyez-Araiza, J. Pineda-Piñón, J. M. López-Romero, J. R. Gasca-Tirado, M. A. Contreras, J. C. J. Correa, L. M. Apátiga-Castro, E. M. Rivera-Muñoz, R. R. Velazquez-Castillo, J. de J P Bueno, A. Manzano-Ramirez, *Materials* **2021**, *14*, 1420.
[8] L. Zhang, W. Yang, Z. Jiang, F. He, K. Zhang, J. Fan, J. Wu, *Appl Energ* **2017**, *197*, 354.
[9] H. Liu, X. Wang, D. Wu, *Sustain. Energy Fuels* **2019**, *3*, 1091.
[10] C. E. Tas, O. Karaoglu, B. A. Tas, E. Ertas, H. Unal, H. Bildirir, *Sol. Energy Mater. Sol. Cells* **2020**, *216*, 110677.
[11] J. S. Baruah, V. Athawale, P. Rath, A. Bhattacharya, *Int. J. Heat Mass Transfer* **2022**, *182*, 121993.
[12] H. Su, P. Lin, H. Lu, X. Zhao, X. Sheng, Y. Chen, *ACS Appl. Mater. Interfaces* **2022**, *14*, 12617.
[13] H. Gao, J. Wang, X. Chen, G. Wang, X. Huang, A. Li, W. Dong, *Nano Energy* **2018**, *53*, 769.
[14] W. Aftab, X. Huang, W. Wu, Z. Liang, A. Mahmood, R. Zou, *Energy Environ. Sci.* **2018**, *11*, 1392.
[15] A. Karaszewska, I. Kamińska, A. Nejman, B. Gajdzicki, W. Fortuniak, J. Chojnowski, S. Slomkowski, P. Sowinski, *Mater. Chem. Phys.* **2019**, *226*, 204.
[16] K. Iqbal, A. Khan, D. Sun, M. Ashraf, A. Rehman, F. Safdar, A. Basit, H. S. Maqsood, *J. Text. Inst.* **2019**, *110*, 625.
[17] Z. Niu, W. Yuan, *ACS Appl. Mater. Interfaces* **2021**, *13*, 4508.
[18] A. Yang, L. Cai, R. Zhang, J. Wang, P.-C. Hsu, H. Wang, G. Zhou, J. Xu, Y. Cui, *Nano Lett.* **2017**, *17*, 3506.
[19] K. Yang, M. Venkataraman, Y.-F. Wang, X.-M. Xiong, T. Yang, J. Wiener, J. Militky, R. Mishra, J. Marek, G.-C. Zhu, J.-M. Yao, **2019**, pp. 671–676.
[20] W. Ma, Z. Jiang, T. Lu, R. Xiong, C. Huang, *Chem. Eng. J.* **2022**, *430*, 132989.
[21] B. Xiang, G. Shi, P. Mu, J. Li, *Colloids Surfaces Physicochem Eng. Aspects* **2022**, *645*, 128917.
[22] Z. Chu, Y. Li, A. Zhou, L. Zhang, X. Zhang, Y. Yang, Z. Yang, *Carbohydr. Polym.* **2022**, *277*, 118787.
[23] M. S. Shalaby, G. Sołowski, W. Abbas, *Adv. Mater. Interfaces* **2021**, *8*, 2100448.
[24] R. Schneider, M. H. M. Facure, P. A. M. Chagas, R. S. Andre, D. M. dos Santos, D. S. Correa, *Adv. Mater. Interfaces* **2021**, *8*, 2100430.
[25] J. Yong, F. Chen, Q. Yang, J. Huo, X. Hou, *Chem. Soc. Rev.* **2017**, *46*, 4168.
[26] A. Tuteja, W. Choi, M. Ma, J. M. Mabry, S. A. Mazzella, G. C. Rutledge, G. H. McKinley, R. E. Cohen, *Science* **2007**, *318*, 1618.
[27] S.-W. Xiong, P. Fu, Q. Zou, L. Chen, M. Jiang, P. Zhang, Z. Wang, L. Cui, H. Guo, J.-G. Gai, *ACS Appl. Mater. Interfaces* **2020**, *13*, 196–206.
[28] K. R. Melayil, S. K. Mitra, *Langmuir* **2020**, *37*, 2810–2815.
[29] N. Wang, M. Cai, X. Yang, Y. Yang, *J. Colloid Interface Sci.* **2018**, *530*, 695.
[30] Y. Kara, K. Molnár, *J. Ind. Text.* **2021**, 152808372110194.
[31] R. Knížek, D. Karhánková, V. Bajzík, O. Jirsák, *Fibres Text. East. Eur.* **2019**, *27*, 16.
[32] A. Louanate, R. E. Otmani, K. Kandoussi, M. Boutaous, *Phys. Scr.* **2020**, *95*, 105003.
[33] K. Yang, M. Venkataraman, J. Wiener, X. Zhang, M. Stuchlik, G. Zhu, J. Yao, J. Militky, *Thermochim. Acta* **2022**, *710*, 179172.
[34] D. Luo, L. Xiang, X. Sun, L. Xie, D. Zhou, S. Qin, *Energy* **2020**, *197*, 117252.
[35] L. Xiang, D. Luo, J. Yang, X. Sun, J. Jin, S. Qin, *Energ. Fuel* **2019**, *33*, 11584.
[36] D. Luo, F. Wei, H. Shao, L. Xiang, J. Yang, Z. Cui, S. Qin, J. Yu, *J. Mater. Sci.* **2018**, *53*, 15500.
[37] H. Qi, T. Zhang, D. Zhang, K. Wang, Y. Wang, *AIP Adv.* **2020**, *10*, 035218.
[38] M. Kenisarin, K. Mahkamov, F. Kahwash, I. Makhkamova, *Sol. Energy Mater. Sol. Cells* **2019**, *200*, 110026.
[39] K. Yang, J. Wiener, M. Venkataraman, Y. Wang, T. Yang, G. Zhang, G. Zhu, J. Yao, J. Militky, *Polym. Test.* **2021**, *100*, 107231.

Manuscript received: August 4, 2022
Revised manuscript received: August 30, 2022
Accepted manuscript online: August 31, 2022
Version of record online: ■■, ■■

RESEARCH ARTICLE

Control of weak interfacial adhesion between melting PCMs and nanofibrous membranes is significant to obtain a sandwich-like multilayer PCM fabric without leakage duringthe heating/cooling process. Correspondingly, the thermal buffering effect is found in the multilayer PCM fabric.

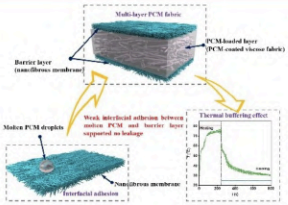

K. Yang, X. Zhang, Prof. Dr. J. Wiener, Dr. M. Venkataraman, Y. Wang, Prof. Dr. G. Zhu, Prof. Dr. J. Yao, Prof. Dr. J. Militky*

1 – 9

Nanofibrous Membranes in Multilayer Fabrics to Avoid PCM Leakages

Check for updates

ChemPhysChem

Research Article
doi.org/10.1002/cphc.202300234

Chemistry Europe
European Chemical Societies Publishing

www.chemphyschem.org

Sandwich Fibrous PEG Encapsulations for Thermal Energy Storage

Kai Yang,*[a] Xiuling Zhang,[a] Mohanapriya Venkataraman,[a] Jakub Wiener,[a] Xiaodong Tan,[a] Guocheng Zhu,[b, e] Juming Yao,[c, d, e] and Jiri Militky[a]

Phase change materials (PCMs) textiles have been developed for personal thermal management (PTM) while limited loading amount of PCMs in textiles reduced thermal buffering effect. In this work, we proposed a sandwich fibrous encapsulation to store polyethylene glycol (PEG) with PEG loading amount of 45 wt%, which consisted of polyester (PET) fabrics with hydrophobic coating as protection layers, polyurethane (PU) nanofibrous membranes as barrier layers and PEG-loaded viscose fabric as a PCM-loaded layer. The leakage was totally avoided by controlling weak interfacial adhesion between protection layer and melting PEG. The sandwich fibrous PEG encapsulations had an overall melting enthalpy value ranging from 50 J/g to 78 J/g and melting points ranging from 20 °C to 63 °C by using different PEGs. Besides, introduction of Fe microparticles in PCM-loaded layer enhanced thermal energy storage efficiency. We believe that the sandwich fibrous PEG encapsulation has a great potential in various fields.

Introduction

Personal temperature management (PTM) has attracted more and more attention since last decades.[1–4] To realize PTM, phase change materials (PCMs) have been an alternative and studied for decades.[5,6] The working principle of PCMs is that the temperature of PCMs can kept over a certain range meantime thermal energy can be stored or released which is determined by difference between temperature of PCMs and surrounding temperature.[7–10] Since inherent solid-liquid phase transition of PCMs during their working, uncontrol of liquid PCMs or PCMs in phase transition state is proposed if there are no supporting materials to store PCMs, correspondingly unstable thermal behavior of PCMs or PCM-incorporated composites is found.

To avoid leakage of PCMs for enhancement in thermal stability, the supporting materials to enclose PCMs are necessary. According to this principle, three strategies are proposed: microencapsulation PCMs (MPCMs),[11,12] solid-solid PCMs (SSPCMs)[13] and form-stable PCMs (FSPCMs).[14–17] MPCMs are shell-core structure, where shell consists of materials with high thermal stability and core consists of PCMs.[18] The PCMs are fully enclosed in the shell structure and leakage can be totally avoided. However, the encapsulation efficiency for MPCMs should be improved. Besides, the mechanical property of MPCMs is up to shell and unexpected destroy of shell in practice may result in leakage of MPCMs. SSPCMs are one of polymer composites, which consists of solid part and soft part.[19] The solid part in SSPCMs has high thermal stability and soft part in SSPCMs is PCMs. During their working temperature, the soft part will be movable and thermal energy storage can be stored. However, the limited thermal energy storage and altered phase transition of SSPCMs are found when compared with pure PCMs, which is caused by limited molecular movement of soft part consisting of PCMs molecules during working temperature. FSPCMs are one group of composites containing the porous materials as supporting materials to contain PCMs.[20] For example, the melting PCMs can be entrapped in porous materials due to capillary force during their working temperature. However, the limited thermal energy storage and phase transition of FSPCMs are found since the molecular movement of PCMs is affected by pores (e.g., pore type, pore size etc.).[21–23] Although there are advantages and disadvantages of present PCMs without leakage, the suitable PCMs for selected applications can suggested. However, to solve PCMs without leakage is not enough for realization of PTM.

The incorporation of PCMs into textiles can be classified into PCM fibers[24,25] and PCM fabrics.[26] For PCM fibers, various methods have been used, including melting spinning, solution, electrospinning, centrifugal spinning, interfacial polyelectrolyte complex spinning etc.[27–30] The thermal energy storage of PCM fibers can be increased by increasing PCM amount. However, mechanical property of PCM fibers is altered with increased PCM amount.[7] For PCM fabrics, the binders are necessary to fix PCMs (e.g., MPCMs or FSPCMs) in fabrics. However, the usage of

[a] K. Yang, X. Zhang, Dr. M. Venkataraman, Prof. Dr. J. Wiener, X. Tan, Prof. Dr. J. Militky
Department of Material Engineering, Faculty of Textile Engineering, Technical University of Liberec
Studentska, 1402/2, Liberec, Czech Republic
E-mail: kai.yang@tul.cz
[b] Prof. Dr. G. Zhu
College of Textiles and Engineering, Zhejiang Sci-tech University
No. 5, Second Avenue, Xiasha Education Park, Hangzhou City, P.R. China
[c] Prof. Dr. J. Yao
School of Materials and Engineering, Zhejiang Sci-tech University
No. 5, Second Avenue, Xiasha Education Park, Hangzhou City, P.R. China
[d] Prof. Dr. J. Yao
School of Materials Science and Chemical Engineering, Ningbo University
No. 8181, Fenghua Road, Jiangbei District, Ningbo City, P.R. China
[e] Prof. Dr. G. Zhu, Prof. Dr. J. Yao
Zhejiang-Czech Joint Laboratory of Advanced Fiber Materials, Zhejiang Sci-tech University
No. 5, Second Avenue, Xiasha Education Park, Hangzhou City, P.R. China

Supporting information for this article is available on the WWW under https://doi.org/10.1002/cphc.202300234

binders may alter the surface chemistry of PCM fabrics. Besides, MPCMs or FSPCMs possibly loss due to mechanical movement (e.g., washing, abrasion etc.).[31] So, it can be included that the limited amount of PCMs and confinements of PCMs in PCM textiles are two significant factors for reduce in thermal energy storage and change of phase transition of PCM textiles. In addition, the way for protection of PCMs in the textiles from unexpected mechanical movement is essential for usage cycles.

In our previous work,[32] a sandwich fibrous PCM encapsulation was successfully proposed to store paraffin wax (PW) as PCMs to realize thermal energy storage and thermal buffering effect, which was a multi-layer PCM fabric consisting of PW-coated viscose fabric as a PCM-loaded layer and PU nanofibrous membranes as a barrier layer. We proved that the low interfacial adhesion between melting PW and PU nanofibrous membranes avoid to penetration of melting PW through the multi-layer fabric structure. Therefore, the sandwich fibrous encapsulation can store various PCMs only if the interfacial adhesion of melting PCMs and barrier layer is low. Besides, PU nanofibrous membranes or other nanofibrous membranes are unsuitable as outer layer for daily usage and should be inner layer in the multi-layer fabric structure. Therefore, common fabrics as protection layer are necessary for such sandwich fibrous PCM encapsulation. Although it is a great process in such application of multi-layer fabrics to store PCMs, the limited PCM types is found and only paraffin wax is acceptable.

Polyethylene glycol (PEG) is one of most common organic PCMs for various application (e.g., textile, constructure, building, solar energy etc.).[33–36] PEG is human friendly with non-toxicity and non-corrosion. The high-stable chemical property and thermal behavior of PEG is also found. The thermal energy storage and phase transition of PEG is only determined by their molecular weight. To extend the application of such multi-layer fabric structure for PEG, the extra protection layer (e.g., common fibrous materials) with weak interfacial adhesion to melting PEG is required according to conclusion from our previous work.[32] Polyester (PET) fabric is one common product in the market for outdoor products (e.g., outwear, bags, tents etc.), which could be protection layer for much-layer PCM fabrics.[37] However, their surface energy may be large enough to attract melting PEG and leakage possibly happens. The hydrophobic coating on PET fabric could realize to reduce surface energy[38] and hydrophobic PET may have weak interfacial adhesion to melting PEG.

In this work, we proposed a sandwich fibrous encapsulation to store PEG. The basic structure of the sandwich fibrous encapsulation consisted of PCM-loaded layer, barrier layer and protection layer. The PEG-coated viscose fabric with 90 wt% PEG loading amount was PCM-loaded layer and PU nanofibrous material was barrier layer. For protection layer, common PET fabric and PET fabric with hydrophobic coating were used as protection layers, respectively. Firstly, the suitable sandwich fibrous PEG encapsulation was determined by investigating leakage phenomena. Then, phase transition, thermal energy storage and thermal buffering effect of sandwich fibrous PEG encapsulation were investigated. Besides, the possibility to obtain thermal-enhanced sandwich fibrous PEG encapsulation was revealed by introducing iron (Fe) microparticles in the PCM-loaded layer. Last but not least, the sandwich fibrous PEG encapsulations with various PEGs of different molecular weights could meet requirement for selected applications.

Results and Discussion

Determination of a Suitable Structure for Sandwich Fibrous PEG Encapsulations

Basic structure of sandwich fibrous PEG encapsulation was shown in Figure 1. (A), which consisted of protection layer, barrier layer and PCM-loaded layer. By taking effect of each layer on leakage phenomena, four sandwich fibrous encapsulations were prepared to store PEG. Here, PEG 6000 was used as PCM in the sandwich fibrous encapsulation to determine the suitable structure. So, four fibrous sandwich PEG encapsulations were prepared, including $C1_{(PEG,n)}$, $C2_{(PEG,n)}$, $C3_{(PEG,n)}$ and $C4_{(PEG,n)}$ (Table 1). The n was M_w of used PEG (In this section was PEG 6000). Figure 1. (B-i) presented the leakage of melting PEG 6000 from four sandwich fibrous encapsulations. There was no leakage from the front side of all samples while leakage of melting PEG 6000 from back side and distribution of melting PEG at interface of inner side of protection layer were different (Figure 1. (B-ii)).

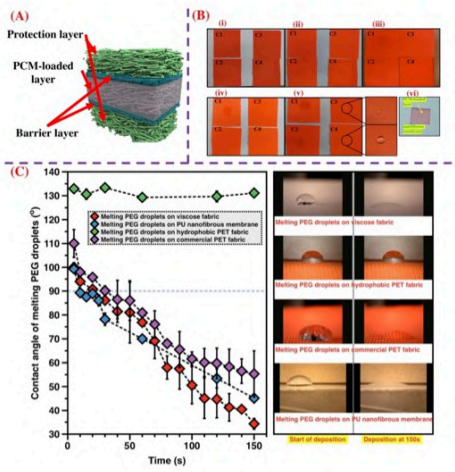

Figure 1. Diagram for structure of sandwich fibrous PEG encapsulation (A), leakage phenomena of different sandwich fibrous PEG encapsulations (B), and wetting behavior of melting PEG droplets on fibrous materials (C) (*i*, *ii*, *iii*, *iv*, *v* and *vi*: macroscopical photo before heating, macroscopical photo for back side of sample after heating, macroscopical photo for inner side of sample after heating, wetting behavior of water droplet on inner side of sample after heating, and adhesion phenomena between PCM-loaded layer and barrier layer) (Here PEG with $M_w = 6{,}000$ was used).

Table 1. Description of four sandwich fibrous PEG encapsulation (n was M_w of used PEG)

Labels	Protection layer	Barrier layer	PCM-loaded layer
$C1_{(PEG,n)}$	PET fabric	–	PEG-coated viscose fabric
$C2_{(PEG,n)}$	PET fabric	PU nanofibrous membrane	PEG-coated viscose fabric
$C3_{(PEG,n)}$	PET fabric with hydrophobic coating	–	PEG-coated viscose fabric
$C4_{(PEG,n)}$	PET fabric with hydrophobic coating	PU nanofibrous membrane	PEG-coated viscose fabric

- For sample $C1_{(PEG,6000)}$ and $C2_{(PEG,6000)}$, obvious leakage phenomena of melting PEG were found by observing back sides, which was shown in Figure 1. (B-iii). In addition, the barrier layer (PU nanofibrous membranes) was well adhered on the PCM-loaded layer (PEG-coated viscose fabric) after leakage testing, which was shown in Figure 1. (B-vi). The SEM image for PU nanofibrous membrane-covering PEG-coated viscose fabric with leakage testing was shown in Supporting Information (Figure S2), and PEG was coated on the PU nanofibrous membranes. So, The PU nanofibrous membrane failed to resisted penetration of melting PEG.
- For sample $C3_{(PEG,6000)}$, a little amount of solid PEG after leakage testing were found on the inner side of protection layer, which was shown in Figure 1. (B-iv). The water droplet on the inner side of protection layer had a significant difference in its shape and angle from ideal complete water droplet on the pure hydrophobic PET fabric, which was shown in Figure 1. (B-v). Correspondingly, the inner side of protection layer (hydrophobic PET fabric) was contaminated by PEG.
- For sample $C4_{(PEG,6000)}$, there was totally no leakage of melting PEG from both front side and back side. No PEG was confirmed on the inner side of protection layer (hydrophobic PET fabric) after testing since the water droplet was stably deposited on the inner side of protection layer with obvious contact angle higher than 90° as shown in Figure 1. (B-v). So, Correspondingly, the PEG was well confined in the PU nanofibrous membrane-covering PCM-loaded layer. Besides, good adhesion between the barrier layer (PU nanofibrous membranes) and the PCM-loaded layer (PEG-coated viscose fabric) was observed after leakage testing, which was similar to sample $C2_{(PEG,6000)}$. Therefore, the PU nanofibrous membranes in the sample $C4_{(PEG,6000)}$ still contributed to leakage phenomena.

We assumed that the interfacial adhesion between melting PEG 6000 and used fibrous materials accounted for the leakage results according to conclusion from our previous work.[32] The measured contact angle of melting PEG 6000 droplet on the used fibrous materials was shown in Figure 1 (C). The melting PEG droplets stably existing on the surface of hydrophobic PET fabric had contact angle higher than 130° after 2.5 min while contact angle value of melting PEG 6000 droplets on other fibrous materials (including viscose fabric, commercial PET fabric and PU nanofibrous membranes) tends to decrease with time and were already smaller than 90° after 10 s. However, the mechanism of weak adhesion seemed not valid for leakage phenomena since leakage was found in sample $C3_{(PEG,6000)}$. A complete diagram for penetration of molten PEG through different multi-layer fabric structures was shown in Figure 2.

- For the leakage of melting PEG 6000 from $C1_{(PEG,6000)}$ and $C2_{(PEG,6000)}$, two main reasons were considered: 1) The good interfacial adhesion between melting PEG 6000 and PU nanofibrous membrane as well as melting PEG 6000 and commercial PET fabric contributed the penetration. 2) The porous structure of fibrous materials provided paths for melting PEG penetration.
- For the leakage of melting PEG 6000 from $C3_{(PEG,6000)}$, it was attributed to the wicking behavior of melting PEG 6000 because of porous structure of the hydrophobic PET fabric although weak interfacial adhesion between melting PEG 6000 and PET fabrics with hydrophobic coating was found.
- For sample $C4_{(PEG,6000)}$, the hydrostatic pressure for melting PEG 6000 to penetrate across the whole $C4_{(PEG,6000)}$ sample was significantly increased because of the PU nanofibrous membrane as the barrier layer between PEG-coated viscose fabric (PCM-loaded layer) and hydrophobic PET fabric (protection layer). Besides, the PCM-loaded layer had a small thickness, which only provided a small pressure to force melting PEG 6000 to penetrate through the whole multi-layer fabric structure even with gravity. So, leakage of melting PEG 6000 from sample $C4_{(PEG,6000)}$ was avoided.

Thermal Energy Storage and Phase Transition Behavior of Sandwich Fibrous PEG Encapsulations

Since encapsulated PEG could not adhere on protection layer (PET fabrics with hydrophobic coating), the thermal energy storage and phase transition behavior of final sandwich fibrous PEG encapsulation were only dependent on barrier layer and PCM-loaded layer. It was found that barrier layer (PU nanofibrous membranes) also affected thermal property of PEG. So, thermal properties of neat PEG, PEG-coated viscose fabric ($PEGV_n$ samples) and PU nanofibrous membrane-covering PEG-

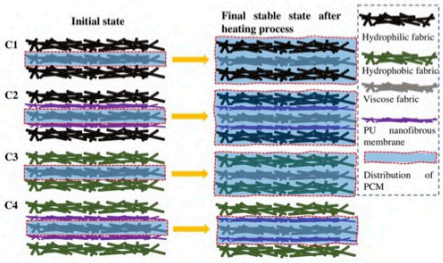

Figure 2. Diagram for leakage of melting PEG through different sandwich fibrous PEG encapsulations during heating process.

coated viscose fabric (UPEGV$_n$ samples) were focused on (*n* was M_w of used PEG, and details of PEGV$_n$ and UPEGV$_n$ samples were given in **Sec. '2'** in **Supporting Information**).

Figure 3. (A-i) presented DSC curves of PEG 6000, PEGV$_{6000}$ and UPEGV$_{6000}$, and details of DSC results were given in **Sec. '3'** in **Supporting Information**. As shown in Figure 3. (B), the phase transition behavior of PEG 6000, PEGV$_{6000}$ and UPEGV$_{6000}$ were different. The PEGV$_{6000}$ and UPEGV$_{6000}$ started to earlier melt when compared with neat PEG 6000, while PEG 6000, PEGV$_{6000}$ and UPEGV$_{6000}$ had a close solidification process. The supercooling degree values (ΔT) were also schemed in Figure 3. (B), and order of ΔT values was UPEGV$_{6000}$ > PEG 6000 > PEGV$_{6000}$. So, the structure of sandwich fibrous encapsulation had an overall side effect on usage cycles from point of thermal energy storage efficiency. It could be caused by the complicated crystallization of PEG confined in PU nanofibrous membrane. Figure 3 (C) presented measured melting/solidifying enthalpy values ($\Delta H_m/\Delta H_c$). The PEG 6000, PEGV$_{6000}$ and UPEGV$_{6000}$ had ΔH_m value of 173 J/g, 152 J/g and 145 J/g, and ΔH_c value of 170 J/g, 152 J/g and 144 J/g, respectively. The order of enthalpy values was PEG 6000 > PEGV$_{6000}$ > UPEGV$_{6000}$. Apart from relative less amount in PEG in the PEGV$_{6000}$ and UPEGV$_{6000}$, the confined crystallization of PEG possibly accounted. The relative crystalline degree (χ) (%) was estimated (Details were in **Sec. '3'** in **Supporting Information**) and schemed in Figure 3. (C). The PEG 6000, PEGV$_{6000}$ and UPEGV$_{6000}$ had χ value of 88%, 86% and 84%, respectively, which supported reduced enthalpy values in PEGV$_{6000}$ and UPEGV$_{6000}$. By taking mass of protection layer into consideration, the overall melting enthalpy of C4$_{(PEG,6000)}$ reached 78 J/g (**Sec. '5'** in **Supporting Information**).

Thermal Buffering Effect of Sandwich Fibrous PEG Encapsulations

Figure 4. (A) presented full T-history (including heating and cooling) of reference sample and sandwich fibrous PEG encapsulation (C4$_{(PEG,6000)}$). During both cooling and heating process, T-history curves of reference sample were simple and reference sample reached final stable temperature within 10s. For sample C4$_{(PEG,6000)}$, a platform was observed during heating process, where thermal energy was absorbed by PEG. During cooling process, the cooling T-history was typical for PCMs, and a peak was observed, where thermal energy was released by PEG. As a result, it took much longer time for sample C4$_{(PEG,6000)}$ than reference sample to reach final stable temperature. For example, it took 6 s for reference sample to reach 60 °C while 70 s for C4$_{(PEG,6000)}$ to reach 60 °C during heating process. Besides, it took 6 s for reference sample to reach 40 °C while 207 s for C4$_{(PEG,6000)}$ to reach 40 °C during cooling process. Especially, three parts could be separated during heating and cooling process, including C4$_{(PEG,6000)}$ with PEG in solid phase, C4$_{(PEG,6000)}$ with PEG in phase transition, and C4$_{(PEG,6000)}$ with PEG in liquid transition phase. Especially, heating T-history could be estimated by Newton's cooling law and three parts could be estimated (**Sec. '4'** in **Supporting Information**). Figure 4. (B) presented the heating T-history of reference sample and sample C4$_{(PEG,6000)}$ after fitting Newton's cooling law. Good fittings were found for all the samples by observing accepted R^2 values (**Table S12** in **Supporting Information**). Figure 4. (D) schemed heating constant (τ) of sample with PEG in solid phase and PEG in phase transition. Higher τ value suggested slower temperature change with time. The sample C4$_{(PEG,6000)}$ had τ_s and τ_{s-l} values higher than reference sample, which supported good thermal buffer-

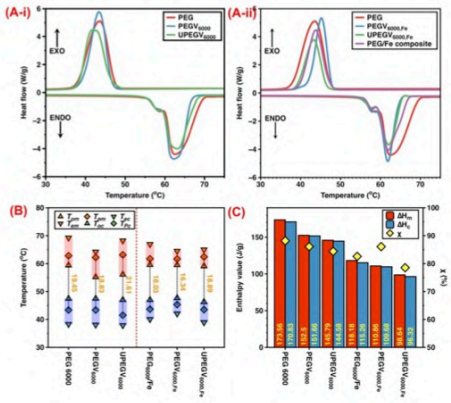

Figure 3. DSC curve (A), phase transition range (B), thermal energy storage and relative crystalline degree (D) of sandwich PEG encapsulation with or without Fe microparticles.

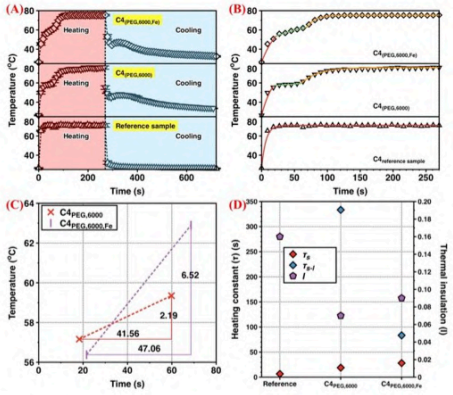

Figure 4. Full T-history curves (A), heating T-history with fitting model (B), heating constant value and thermal insulation (C), and estimated phase transition range of reference sample and sandwich fibrous PEG encapsulation with or without Fe microparticles (D) (red line, blue line and green line: fitting model for solid phase, phase transition and liquid phase).

ing effect. As a result, phase transition range of sample $C4_{(PEG,6000)}$ was estimated and schemed in Figure 4. (C), which lasted 41.56 s while temperature was only increased 2.19 °C. The thermal insulation (*I*) value was also estimated and higher *I* value suggested better thermal insulation. As shown in Figure 4. (D), the sample $C4_{(PEG,6000)}$ had *I* value of 0.07, which was smaller than reference sample with *I* value of 0.12. It was caused by more air content in reference sample.

Enhanced Thermal Properties of Sandwich Fibrous PEG Encapsulations by Introducing Iron (Fe) Particles

To have thermal-enhanced sandwich fibrous PEG encapsulation, the PEG/Fe-coated viscose fabric was used as PCM-loaded layer, which followed previous published work.[39] Better to reveal thermal energy storage efficiency, PEG 6000 was used as PCM. Correspondingly, PEG/Fe-coated viscose fabric was labeled as $PEGV_{6000,Fe}$, and PU nanofibrous membrane-covering PEG/Fe-coated viscose fabric was labeled as $UPEGV_{6000,Fe}$ (Details were in **Sec. '2'** in **Supporting Information**).

By referring SEM images of $PEGV_{6000,Fe}$ and $UPEGV_{6000,Fe}$ (**Figure S3** in **Supporting Information**), Fe microparticles were well dispersed in PCM-loaded layer rather than out of barrier layer. So, introduction of Fe microparticle in sandwich fibrous PEG encapsulations was stable.

Figure 3. (A-ii) presented DSC curves of PEG/Fe composites, $PEGV_{6000,Fe}$ and $UPEGV_{6000,Fe}$, and all details were given in **Sec. '3'** in **Supporting Information**. By comparing with neat PEG 6000, obvious differences in phase transition of PEG/Fe composites, $PEGV_{6000,Fe}$ and $UPEGV_{6000,Fe}$ were found. After introducing Fe particles in PEG or PEG-coated viscose fabric, the phase transition range became obviously narrower and supercooling degree values (ΔT) were smaller, which was shown in Figure 3. (B). Especially, the $UPEGV_{6000,Fe}$ had a ΔT value of 18.89 °C, which was smaller than UPEGV6000 with ΔT value of 21.61 °C and neat PEG 6000 with ΔT value of 19.45 °C. The introduction of Fe microparticles in PEG-coated viscose fabric could support more precise control of phase transition ranges for suitable applications. measured melting/solidifying enthalpy values ($\Delta H_m/\Delta H_c$), and $UPEGV_{6000,Fe}$ had a ΔH_m value of 98 J/g and ΔH_c value of 96 J/g, respectively. By taking mass of protection layer into consideration, the overall melting enthalpy of $C4_{(PEG,6000,Fe)}$ reached 52 J/g (**Sec. '5'** in **Supporting Information**). Besides, the order of enthalpy values was PEG 6000 > PEG/Fe composites > $PEGV_{6000,Fe}$ > $UPEV_{6000,Fe}$. Apart from relative less amount of PEG, the confined crystallization of PEG in PEG/Fe composites or fibrous materials accounted for reduced enthalpy values. The estimated χ values of PEG in the PEG/Fe composites, $PEGV_{6000,Fe}$ and $UPEGV_{6000,Fe}$ were shown in Figure 3. (C). The order of χ value was that PEG/Fe composites > $PEGV_{6000,Fe}$ > $UPEGV_{6000,Fe}$. Then, the introduction Fe microparticles positively enhanced crystallization of PEG in the sandwich fibrous encapsulations.

The thermal energy storage efficiency of $C4_{(PEG,6000,Fe)}$ was revealed by T-history as shown in Figure 4. (A). Similar as $C4_{(PEG,6000)}$, the platform in heating T-history curve and a peak in cooling T-history curve of $C4_{(PEG,6000,Fe)}$ were observed, which was caused by presence of PEG. By applying Newton's cooling law (Details were in **Sec. '4'** in **Supporting Information**), the heating T-history curves with fitted models were shown in Figure 4. (B), and the phase transition range of $C4_{(PEG,6000,Fe)}$ was shown in Figure 4. (C).

The sample $C4_{(PEG,6000,Fe)}$ had τ_s and τ_{s-l} values of 28.03 s and 83.33 s, which was shown in Figure 4. (D). By comparing with sample $C4_{(PEG,6000)}$, the smaller temperature increasing rate in $C4_{(PEG,6000,Fe)}$ with solid PEG phase was found while higher temperature increasing rate in $C4_{(PEG,6000,Fe)}$ with solid PEG phase was expected. From this point, the enhanced thermal energy storage efficiency of $C4_{(PEG,6000,Fe)}$ was found.

However, the phase transition range of $C4_{(PEG,6000,Fe)}$ started later and lasted longer than than $C4_{(PEG,6000)}$, which was shown in Figure 4. (C). $C4_{(PEG,6000,Fe)}$ had a phase transiton for 47.06 s where temperature was incrased 6.52 °C. The reason could be the inherent principle of Newton's cooling law. The three parts were selected according to the observed trends of *T* against *t*. The obvious platform where *T* increases much slower with time is the thermal buffering effect from T-history curve, which is a result of dynamic thermal balance between heat transfer through the sample and heat storage of the sample. Here, the dynamic thermal balance is just a concept and cannot provide more details about phase transition of PCMs. In this case, the thickness, melting range and melting points are responsible for dynamic thermal balance in the T-history. By taking DSC results, the melting range of $C4_{(PEG,6000)}$ was much higher than $C4_{(PEG,6000,Fe)}$. So from this point, the thermal balance of $C4_{(PEG,6000)}$ happend earlier than $C4_{(PEG,6000,Fe)}$. However, smaller melting range and higher thichness of $C4_{(PEG,6000,Fe)}$ than $C4_{(PEG,6000)}$, which may delay the movement of solid-liquid interface of PEG in the $C4_{(PEG,6000,Fe)}$ and occur of phase transition. Besides, the thermal insulation (*I*) value of $C4_{(PEG,6000,Fe)}$ was 0.09, which was only slightly higher than $C4_{(PEG,6000)}$. So, $C4_{(PEG,6000,Fe)}$ had similar final thermal insulation behavior as $C4_{(PEG,6000)}$.

Selected Sandwich Fibrous PEG Encapsulation for Various Applications

To apply the sandwich fibrous PEG encapsulation for various applications, it is proposed to use different PEGs with different molecular weight since thermal properties of PEG are simply dependent on their molecular weight.[40] It was noticed that melting PEGs with different Mw had same interfacial adhesion on fibrous materials, and no leakage was found when C4 structure was used. Then, other four PEGs with different molecular weight were used and encapsulated in C4 structure following **Sec. 'Determination on Suitable Structure of Sandwich Fibrous PEG Encapsulations'**.

Figure 5. (A) presented DSC curves of neat PEG, PEG-coated viscose fabric and PU-covering PEG-coated viscose fabrics (Description of samples were given in **Sec. '2'** in **Supporting Information**, and DSC details of samples were given in **Sec. '3'** in **Supporting Information**). The phase transition of neat PEG, PEG-coated viscose fabric and PU-covering PEG-coated viscose fabrics were shown in Figure 5. (B). Obviously, the phase

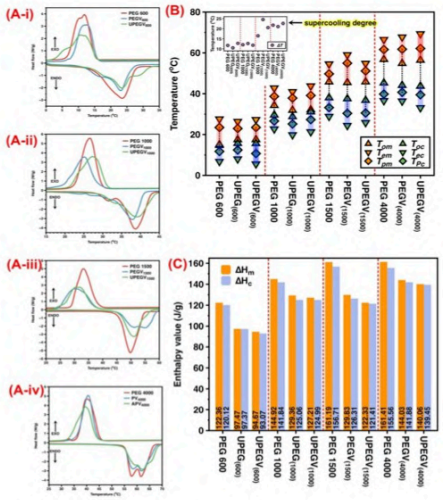

Figure 5. DSC curves (A), phase transition behavior (B) and thermal energy storage (C) of selected sandwich fibrous PEG encapsulation (i, ii, iii and iv: DSC curves of sample with PEG with M_w of 600, 1000, 1500 and 4000) (Subscript number corresponded to M_w value of encapsulated PEG).

transition behavior of PU-covering PEG-coated viscose fabric was different from neat PEG and PEG-coated viscose fabric. The main reason was that both viscose fabric and PU nanofibrous membrane altered self-crystalline behavior of PEG. However, melting points or solidifying points of PU-covering PEG-coated viscose fabric was close to neat PEG. Besides, the supercooling degree values (ΔT) were estimated and schemed in Figure 5. (B). It was hard to conclude positive or negative effect of sandwich fibrous encapsulation on ΔT encapsulated PEG, which was possibly affected by the complicated distribution of PEG in its loaded layer and barrier layer. In addition, both melting enthalpy (ΔH_m) and solidifying enthalpy (ΔH_c) of C4 with different PEGs were shown in Figure 5. (C). Obviously, enthalpy values of PU-covering PEG-coated viscose fabrics were smaller than neat PEG and PEG-coated viscose fabric. Similar as **Sec. 'Thermal Energy Storage and Phase Transition Behavior of Sandwich Fibrous PEG Encapsulations'**, relatively less amount of PEG and confined crystallization of PEG in sandwich fibrous encapsulation accounted for reduced enthalpy values. Still, $UPEGV_{600}$, $UPEGV_{1000}$, $UPEGV_{1500}$, and $UPEGV_{4000}$ had ΔH_m values of 100 J/g, 127 J/g, 122 J/g and 140 J/g, and ΔH_c values of 120 J/g, 125 J/g, 121 J/g, and 139 J/g, respectively. Then, sample $C4_{(PEG,\ 600)}$, $C4_{(PEG,\ 1000)}$, $C4_{(PEG,\ 1500)}$, $C4_{(PEG,\ 4000)}$ had an overall melting enthalpy value of 50 J/g, 67 J/g, 65 J/g and 74 J/g, respectively. As a result, it is potential to use various PEGs in sandwich fibrous PEG encapsulations for selected applications.

Conclusions

In this work, a sandwich fibrous PEG encapsulation was successfully proposed (Figure 1. (A)). The sandwich fibrous PEG encapsulation consisted of PET fabric with hydrophobic coating as protection layers, PU nanofibrous membrane as barrier layers, and PEG-coated viscose fabric as PCM-loaded layer. The leakage phenomena of the sandwich fibrous PEG encapsulation were successfully avoided by controlling weak interfacial adhesion between melting PEG and fibrous materials and using PU nanofibrous membranes. During heating/cooling process, the thermal buffering effect of sandwich fibrous PEG encapsulation was found, and the Newton's cooling law could describe temperature change of heating T-history. Besides, the thermal energy storage efficiency of the sandwich fibrous PEG encapsulation was improved by introduction Fe microparticles. By using different PEGs with different molecular weight, control of melting points and enthalpy values was realized. The overall enthalpy values and melting points of different sandwich fibrous PEG encapsulations were estimated and were schemed in Figure 6. (A), which ranged from 50 J/g to 78 J/g, and 20 °C to 63 °C (**Table S16** in **Supporting Information**). To reveal the advantage of our research work, the sandwich fibrous encapsulations containing PEG 6000 as PCM was selected to compare with other work related to PCM fabrics[30,41–44], which was shown in Figure 6. (A). The sandwich fibrous PEG encapsulation was not the best one while it was possible to have higher overall enthalpy values by using proper protection layer with lower areal density. In addition, the PEG loading amount in our research work was as high as 45 wt%, which was comparable

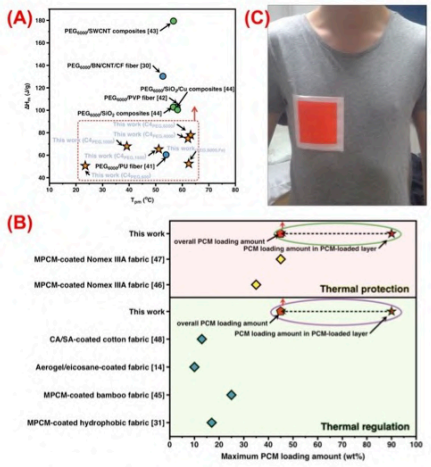

Figure 6. Comparison of our work with other published PEG-incorporate materials in melting points and overall enthalpy value (A) as well as PCM loading amount (B), and compatibility of sandwich fibrous PEG encapsulation with commercial T-shirt (C).

with other PCM fabrics[14,31,45–48] (**Table S17** in **Supporting Information**). As shown in Figure 6. (B), the PEG loading amount was higher than other work related to fabrics for thermal regulation and thermal protection, which supported general applications of sandwich fibrous PEG encapsulations. Besides, the sandwich fibrous PEG encapsulation was the multi-layer fabric structure, which had an advantage over other PEG-incorporated composites or fibers in compatibility with commercial products. To apply the sandwich fibrous PEG encapsulations in practice, it was necessary to keep structure of sandwich fibrous PEG encapsulations stable. Here, we provided one possibility to incorporate suitable sandwich fibrous PEG encapsulation into commercial textiles by using commercial fibrous tape (Korbond hemming web) to fix the structure (Figure 6. (C)).

As a whole, we believe that the sandwich fibrous PEG encapsulations could meet various requirements by using suitable PEGs and adjusting protection layer.

Experimental Section

Materials

Polyethylene glycols (PEGs) (M_w = 600, 1000, 1500, 4000, 6000) (PEG 600, PEG 1000, PEG 1500, PEG 4000 and PEG 6000) were purchased from Sigma Aldrich. The iron (Fe) microparticles were purchased from Kovyachemie company (Czech Republic). Polyurethane (PU) nanofibrous membrane and viscose nonwoven fabric was provided by Department of Material Engineering, Faculty of Textile Engineering, Technical University of Liberec (KMI, FT TUL). The polyester fabrics and polyester fabrics with hydrophobic coating were provided by INOTEX company (Czech Republic). All details of fibrous materials were given in in **Supporting Information** (**Sec. '1'**).

Preparation of Sandwich Fibrous PEG Encapsulations

The basic structure of sandwich fibrous PEG encapsulations was shown in Figure 1. (A), consisting of protection layer, barrier layer and PCM-loaded layer. The protection layer was PET fabric or PET fabric with hydrophobic coating, barrier layer was PU nanofibrous membrane, and PCM-loaded layer was PEG-coated viscose fabric.

The PEG-coated viscose fabric was prepared by following same steps in previous publication[39] and PEG loading amount was 90 wt%. The PEG-coated viscose fabrics with different PEGs were labeled as $PEGV_n$, where n was M_w value of used PEG. For example, $PEGV_{6000}$ was PEG 6000-coated viscose fabric. The details of $PEGV_n$ samples were given in **Supporting Information** (**Table S5**).

Especially, it was noticed that PU nanofibrous membranes could adsorb PEG according to our previous work. The PU nanofibrous membrane could affect thermal property of final thermal property of sandwich fibrous PEG encapsulations. Therefore, PU nanofibrous membrane-covering PEG-coated viscose fabrics were also prepared and were labeled as $UPEGV_n$. The n was M_w value of used PEG. For example, $UPEGV_{6000}$ was PU nanofibrous membrane-covering PEG 6000-coated viscose fabric. The details of $UPEGV_n$ samples were given in **Supporting Information** (**Table S6**).

Four sandwich fibrous PEG encapsulations were prepared as shown in Table 1. To identify the sandwich fibrous encapsulations with different PEGs, the samples were labeled as $C1_{(PEG,n)}$, $C2_{(PEG,n)}$, $C3_{(PEG,n)}$ and $C4_{(PEG,n)}$, where n was Mw value of used PEG. The details of all sandwich fibrous PEG encapsulations were given in **Supporting Information** (**Table S7**).

Preparation of Fe-incorporated Sandwich Fibrous PEG Encapsulations

The Fe-incorporated sandwich fibrous PEG encapsulations were prepared by replacing PEG/Fe-coated viscose fabric with PEG-coated viscose fabric. In this work, the PEG 6000-incorpoareted sandwich fibrous encapsulation was aimed to enhance thermal energy storage efficiency. The PEG/Fe composites were prepared with mass ratio of 72.7 to 27.3 (PEG: Fe) according to previous work.[39] Then, the PEG/Fe composites were coated on viscose fabric with mass ratio of 9 : 1 (PEG/Fe composite: viscose fabric), and PEG/Fe-coated viscose fabric was labeled as $PEGV_{6000,Fe}$. The PU nanofibrous membrane-covering PEG/Fe-coated viscose fabric was labeled as $UPEGV_{6000,Fe}$, and the Fe-incorporated sandwich fibrous PEG encapsulation was labeled as $Cm_{(PEG,6000,Fe)}$, where m was 1, 2, 3 and 4 representing suitable structure.

Tests and Methods

Morphologies of fibrous materials, PCM-loaded layers ($PEGV_n$ samples) and barrier layer-covering PCM-loaded layers ($UPEGV_n$ samples) were characterized by scanning electronic microscopy (SEM) with voltage of 20 kV.

The leakage of sandwich fibrous PEG encapsulations was measured by following previous published work.[32] The photos of sample before and after heating under temperature of 80 °C were taken for comparison to reveal leakage phenomena. Besides, water droplet (25 μL) was deposited on selected fibrous materials after heating/cooling cycles and water contact angles were for validation of leakage phenomena.

The contact angles (CA) between melting PEGs droplets (25 μL) and fibrous materials were recorded by using a custom setup (Figure 7. (A)) according to previous published work.[31,32] Stable heating temperature of 80 °C was used and measurement lasted 2.5 min. The CA values higher than 90° supported weak adhesion and CA values smaller than 90° supported good adhesion.

Phase transition behavior and thermal energy storage of samples was investigated by using differential scanning calorimetry (DSC) (Mettler Toledo) (KMI, FT, TUL). The samples weighting from 3 to 10 mg firstly experienced from 25 °C to 90 °C to erase thermal history and were kept at 90 °C for 5 min. Then, samples experienced cooling process from 90 °C to 0 °C, and then kept at 0 °C for 5 min. Then, samples experienced heating process from 0 °C to 90 °C. Both cooling process and heating process were recorded. During the whole DSC measurement, heating/cooling rate was 10 K/min and nitrogen gas rate was 20 mL/min. The DSC results included onset

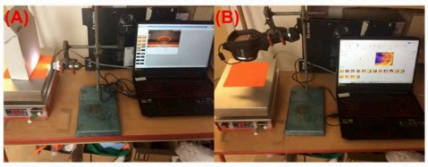

Figure 7. Contact angle of melting PEG droplets on fibrous materials (A) and T-history measurement of sandwich fibrous PEG encapsulations (B).

melting/solidifying point (Tom/Toc), peak melting/solidifying point (T_{pm}/T_{pc}), endset melting/solidifying point (T_{em}/T_{ec}), and melting/solidifying enthalpy ($\Delta H_m/\Delta H_c$). Besides, supercooling degree (ΔT) was difference between T_{pm} and T_{pc}. Besides, relative crystalline degree values were estimated (details were in **Sec '3'** in **Supporting Information**).

T-history curves of sandwich fibrous PEG encapsulations were performed by using a custom setup (Figure 7. (B)) according to previous published work.[32] The heating T-history curve was obtained by placing sample on heater with stable temperature of 80 °C and immediately recording temperature change for 4.5 min. Then, sample was transferred to surface of the flat table with temperature of 23±1 °C and temperature of sample was immediately recorded for 7.5 min. Then, cooling T-history curve was obtained. T-history measurement was performed under room environment with temperature of 24.5±1 °C and relative humidity of 45±2%. T-history measurement was repeated 3 times for same sample to have statistics. The heating T-history curves were characterized by Newton's cooling law (**Sec. '4'** in **Supporting Information**). ALAMBETA device (KMI, FT, TUL)[49] was used to characterize thermal conductivity and thickness of sandwich fibrous PEG encapsulations to support further analysis of T-history.

Supporting Information Summary

Supporting Information included five parts: 1) details of used fibrous materials, 2) description of sandwich fibrous PEG encapsulations, 3) phase transition and thermal energy storage of sandwich fibrous PEG encapsulations from DSC, 4) characterization of thermal buffering effect and 5) comparision of our work with other published work. In addition, all the references in **Supporting Information** were also cited in the manuscript.

Acknowledgements

This work was supported by the project 'Advanced structures for thermal insulation in extreme conditions' (Reg. No. 21-32510M) granted by the Czech Science Foundation (GACR). Additionally, Kai Yang would like to thank Dr. Miroslava Pechociakova for her assistance in DSC measurement.

Conflict of Interests

The authors declare no conflict of interest.

Data Availability Statement

The data that support the findings of this study are available from the corresponding author upon reasonable request.

Keywords: energy conversion · fibrous materials · interfaces · PEG · thermal behavior

[1] X. Zhang, W. Yang, Z. Shao, Y. Li, Y. Su, Q. Zhang, C. Hou, H. Wang, *ACS Nano* **2022**, *16*, 2188–2197.
[2] Y. Song, M. Lei, J. Lei, Z. Li, *Adv. Mater. Technol.* **2020**, *5*, 2000287.
[3] Y. Peng, Y. Cui, *Joule* **2020**, *4*, 724–742.
[4] A. Yang, L. Cai, R. Zhang, J. Wang, P.-C. Hsu, H. Wang, G. Zhou, J. Xu, Y. Cui, *Nano Lett.* **2017**, *17*, 3506–3510.
[5] E. Pakdel, M. Naebe, L. Sun, X. Wang, *ACS Appl. Mater. Interfaces* **2019**, *11*, 13039–13057.
[6] C. Liu, T. Zhang, T. Li, Y. Wang, *Chem. Eur. J.* **2022**, *28*, e202200502.
[7] K. Yang, M. Venkataraman, X. Zhang, J. Wiener, G. Zhu, J. Yao, J. Militky, *J. Mater. Sci.* **2022**, *57*, 798–847.
[8] I. Zahid, M. Farhan, M. Farooq, M. Asim, M. Imran, *Case Stud. Therm. Eng.* **2022**, 102553.
[9] R. K. Mishra, K. Verma, V. Mishra, B. Chaudhary, *J. Energy Storage* **2022**, *50*, 104166.
[10] K. Matuszek, R. Vijayaraghavan, M. Kar, S. Mahadevan, D. R. MacFarlane, *ChemSusChem* **2021**, *14*, 2757–2762.
[11] D. H. Shin, S. Kim, S. W. Karng, Y. Shin, *Int. J. Heat Mass Transfer* **2022**, *183*, 122034.
[12] Y. Yuan, H. Xiang, G. Liu, R. Liao, *Surf. Interfaces* **2021**, *27*, 101516.
[13] Y. Kou, K. Sun, J. Luo, F. Zhou, H. Huang, Z.-S. Wu, Q. Shi, *Energy Storage Mater.* **2021**, *34*, 508–514.
[14] A. Shaid, L. Wang, S. Islam, J. Y. Cai, R. Padhye, *Appl. Therm. Eng.* **2016**, *107*, 602–611.
[15] Y. Zhang, Z. Qiu, H. Zhong, J. Mu, Y. Ma, X. Zhao, W. Huang, *Chem. Eng. J.* **2022**, *429*, 132422.
[16] P. Du, M. Wang, X. Zhong, B. Chen, Z. Li, R. Zhou, Y. Huo, Z. Rao, *J. Energy Storage* **2022**, *56*, 106021.
[17] K. Yang, X. Zhang, M. Venkataraman, J. Wiener, S. Palanisamy, S. Sozcu, X. Tan, D. Kremenakova, G. Zhu, J. Yao, J. Militky, *ChemPlusChem* **2023**, *88*, e202300081.
[18] K. Ghasemi, S. Tasnim, S. Mahmud, *Sustain. Energy Technol. Assess.* **2022**, *52*, 102084.
[19] A. Fallahi, G. Guldentops, M. Tao, S. Granados-Focil, S. V. Dessel, *Appl. Therm. Eng.* **2017**, *127*, 1427–1441.
[20] J. Zhao, J. Sun, Y. Li, R. Xia, W. Zhang, B. Wang, X. Fang, Y. Liu, H. Guo, *J. Mater. Sci.* **2022**, *57*, 3629–3644.
[21] N. Arroyo, S. Balme, F. Picaud, *J. Chem. Phys.* **2021**, *154*, 104901.
[22] K. Yang, M. Venkataraman, J. Karpiskova, Y. Suzuki, S. Ullah, I.-S. Kim, J. Militky, Y. Wang, T. Yang, J. Wiener, G. Zhu, J. Yao, *Microporous Mesoporous Mater.* **2021**, *310*, 110636.
[23] J. Wang, T. Zhang, Y. Shen, B. Yang, J. Lv, Y. Zheng, Y. Wang, *Mater. Today Commun.* **2022**, *32*, 104011.
[24] Z. Niu, S. Qi, S. S. A. Shuaib, W. Yuan, *Compos. Part B. Eng.* **2022**, *228*, 109431.
[25] X. Liu, C. Wang, Z. Cai, Z. Hu, P. Zhu, *J. Energy Storage* **2022**, *53*, 105171.
[26] Y. Su, W. Zhu, M. Tian, Y. Wang, X. Zhang, J. Li, *Appl. Therm. Eng.* **2020**, *174*, 115340.
[27] Y. Wu, C. Chen, Y. Jia, J. Wu, Y. Huang, L. Wang, *Appl. Energy* **2018**, *210*, 167–181.
[28] C. Li, Y. Huang, R. Li, Y. Wang, X. Xiang, C. Zhang, D. Wang, Y. Zhou, X. Liu, W. Xu, *Carbohydr. Polym.* **2021**, *251*, 117037.
[29] W. Xia, H. Xiang, Z. Zhou, X. Fei, M. Zhu, *Compos. Commun.* **2021**, *24*, 100633.
[30] H. Fang, J. Lin, L. Zhang, A. Chen, F. Wu, L. Geng, X. Peng, *Carbohydr. Polym.* **2020**, *249*,116836.
[31] K. Yang, L. Martinkova, O. Ctibor, X. Zhang, M. Venkataraman, J. Wiener, G. Zhu, G. Zhang, J. Yao, J. Militky, *Prog. Org. Coat.* **2022**, *172*, 107151.
[32] K. Yang, X. Zhang, J. Wiener, M. Venkataraman, Y. Wang, G. Zhu, J. Yao, J. Militky, *ChemNanoMat* **2022**, *8*, e202200352.
[33] L. Jiang, Y. Lei, Q. Liu, J. Lei, *Energy* **2020**, *193*, 116802.
[34] F. Lin, X. Zhang, X. Liu, Y. Xu, Z. Sun, L. Zhang, Z. Huang, R. Mi, X. Min, *Polymer* **2021**, *228*, 123894.
[35] S. Sundararajan, A. B. Samui, P. S. Kulkarni, *J. Mater. Chem. A* **2017**, *5*, 18379–18396.
[36] M. Karthikeyan, T. Ramachandran, O. L. S. Sundaram, *J. Ind. Text.* **2014**, *44*, 130–146.
[37] T. Yang, F. Saati, K. V. Horoshenkov, X. Xiong, K. Yang, R. Mishra, S. Marburg, J. Militký, *Text. Res. J.* **2019**, *89*, 3342–3361.
[38] M. R. Abeywardena, M. A. D. H. Yashomala, R. K. W. H. M. K. Elkaduwe, D. G. G. P. Karunaratne, H. M. T. G. A. Pitawala, R. M. G. Rajapakse, A. Manipura, M. M. M. G. P. G. Mantilaka, *Colloids Surf. Physicochem. Eng. Asp.* **2021**, *629*, 127397.
[39] K. Yang, J. Wiener, M. Venkataraman, Y. Wang, T. Yang, G. Zhang, G. Zhu, J. Yao, J. Militky, *Polym. Test.* **2021**, *100*, 107231.

[40] Y. Kou, S. Wang, J. Luo, K. Sun, J. Zhang, Z. Tan, Q. Shi, *J. Chem. Thermodyn.* **2018**, *128*, 259–274.
[41] W. Feng, Y.-S. Zhang, Y.-W. Shao, T. Huang, N. Zhang, J.-H. Yang, X.-D. Qi, Y. Wang, *Eur. Polym. J.* **2021**, *145*, 110245.
[42] X. Zhang, J. Qiao, H. Zhao, Z. Huang, Y. Liu, M. Fang, X. Wu, X. Min, *Chem. Phys. Lett.* **2018**, *691*, 314–318.
[43] T. Qian, J. Li, W. Feng, H. Nian, *Energ. Convers. Manage.* **2017**, *143*, 96–108.
[44] B. Tang, M. Qiu, S. Zhang, *Sol. Energ. Mat. Sol. C.* **2012**, *105*, 242–248.
[45] G. Zhang, C. Cai, Y. Wang, G. Liu, L. Zhou, J. Yao, J. Militky, J. Marek, M. Venkataraman, G. Zhu, *Text. Res. J.* **2019**, *89*, 3387–3393.
[46] Y. Wang, Y. Ma, R. Chen, Y. Su, *Fire. Mater.* **2021**, *45*, 250–260.
[47] Y. Su, W. Zhu, M. Tian, Y. Wang, X. Zhang, J. Li, *Appl. Therm. Eng.* **2020**, *174*,115340.
[48] T. R. Kar, A. K. Samanta, H. D. Sinnur, M. Kumar, *J. Nat. Fibers* **2021**, *19*, 5504–5523.
[49] L. Hes, K. Bal, I. Dolezal, *Fiber. Polym.* **2021**, *22*, 2922–2928.

Manuscript received: March 30, 2023
Revised manuscript received: June 30, 2023
Accepted manuscript online: July 10, 2023
Version of record online: ■■, ■■

RESEARCH ARTICLE

Sandwich fibrous PEG encapsulations were constructed, consisting of a protection layer, a barrier layer and a PCM-loaded layer. Selected applications of the sandwich fibrous PEG encapsulations are available by controlling the PEG types or introducing conductive particles.

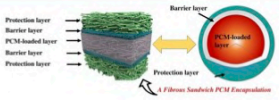

K. Yang, X. Zhang, Dr. M. Venkataraman, Prof. Dr. J. Wiener, X. Tan, Prof. Dr. G. Zhu, Prof. Dr. J. Yao, Prof. Dr. J. Militky*

1 – 10

Sandwich Fibrous PEG Encapsulations for Thermal Energy Storage

9.3 Research journal article-3 (Polymer Testing, Q1, IF: 5.1)

Polymer Testing 100 (2021) 107231

Contents lists available at ScienceDirect

Polymer Testing

journal homepage: www.elsevier.com/locate/polytest

Thermal analysis of PEG/Metal particle-coated viscose fabric

Kai Yang [a,*], Jakub Wiener [a], Mohanapriya Venkataraman [a], Yuanfeng Wang [a], Tao Yang [b], Guoqing Zhang [c], Guocheng Zhu [c], Juming Yao [c], Jiri Militky [a]

[a] Department of Material Engineering, Faculty of Textile Engineering, Technical University of Liberec, Liberec 461 17, Czech Republic
[b] Institute for Nanomaterials, Advanced Technologies and Innovation (CXI), Technical University of Liberec, Liberec 461 17, Czech Republic
[c] College of Materials and Textiles, Zhejiang Sci-tech University, Xiasha Education Park, PR China

ARTICLE INFO

Keywords:
Thermal energy storage
PEG
Metal particle
Viscose fabric
Phase transition
Newton's cooling law

ABSTRACT

The introduction of metal particles (MP) in the phase change materials (PCM) realizes the highly efficient thermal energy storage. However, a suitable carrier is necessary for PCM/MP composites for various applications. In this work, the polyethylene glycol (PEG) was used as PCM, five MPs including copper (Cu), aluminum (Al), silver (Ag), iron (Fe), and zinc (Zn) particles were used, and the viscose fabric was selected as a carrier for coating of PEG/MPs. The PEG was blended with different MPs with the same weight ratio of 72.3:23.7. Then, the PEG/MP-coated viscose fabric was prepared by applying PEG/MP composites on the viscose fabric with the same weight ratio of 90:10 and the PEG-coated viscose fabric (86.7:13.3) was set as reference. The phase transition of the prepared PEG/MP composites and the PEG/MP-coated viscose fabrics was investigated via the differential scanning calorimetry (DSC). The thermal behavior of the PEG/MP-coated viscose fabric was investigated via Alambeta device and the T-history method. The results revealed that the enthalpy of all the PEG/MP-coated viscose fabrics were larger than 100J/g. Besides, only the higher theoretical enthalpy of the PEG in the PEG/MP composites was found, and the MPs assisted in the higher crystallization of PEG. Results from the Alambeta device proved that the thermal conductivity was increased when MPs were introduced in the coated viscose fabric. T-history curves of all the PEG/MP-coated viscose fabric revealed that the heating constant of the phase transition stage mainly accounted for the quick heat transfer.

1. Introduction

Phase change materials (PCMs) are a collection of materials that have an intrinsic capability to absorb and release latent heat during the phase change effect which is a dynamic heat exchange process [1]. The storage of latent heat is based on the transition of materials that undergo a phase change from solid to liquid and vice versa while the temperature of PCMs is unchanged. The application of the PCM included building construction [2], solar energy collection [3], electronic management [4], battery management [4], food storage [5], textile [6] and so on. PCMs were classified into organic PCMs and inorganic PCMs. By comparing with inorganic PCMs, the organic PCMs were non-corrosive and had low or no under-cooling chemical and thermal stability [7]. However, the thermal conductivity of the organic PCMs limited thermal energy storage.

Metals or metal oxides were characterized by high thermal conductivity. For example, Cu, CuO, and ZnO solid were measured to have the thermal conductivity value of 400 ($W K^{-1} m^{-1}$) [8], 33 ($W K^{-1} m^{-1}$) [8], and 50 ($W K^{-1} m^{-1}$) [9] at room temperature, respectively. Various metal-based materials were incorporated into organic PCMs to enhance the thermal conductivity [10], including the metal particles [11], metal foams [12], metal-incorporated PCM capsules [13] and so on. The metal porous foams were also proved to store the PCM to enhance the thermal conductivity as well as protect the leakage of the PCM during the phase transition process [12,14]. However, the heat convection of the PCM in the metal porous foams was suppressed [15]. The pore size and porosity of the metal porous foams also affected thermal storage efficiency [16]. In detail, Yang Xu al et. revealed that there was a maximum filling ratio of the PCM to the porosity by optimizing the PCM location in the porous structure [17]. Xi Meng al et. revealed that the reduced porosity of the copper foam could enhance the overall thermal conductivity of the paraffin-copper foam composite while the heat storage capacity was reduced by about 22.3 kJ when the porosity was increased 2% [18]. Especially, the leakage of the PCM from the porous

* Corresponding author.
E-mail address: kai.yang@tul.cz (K. Yang).

https://doi.org/10.1016/j.polymertesting.2021.107231
Received 16 December 2020; Received in revised form 22 April 2021; Accepted 26 April 2021
Available online 26 May 2021

material-incorporated PCM composites may exist if the pore size was too big. The smaller pore size may result in less adsorption of the PCM by the porous supporting materials [19].

The metal incorporated PCM capsules were also developed for thermal enhancement [13]. However, the compatibility of the PCM capsules with other coating materials remained to be improved. The incorporation of the metal particles into the PCMs was considered as a convenient way to enhance the thermal conductivity [11] although the dispersion of the MPs in the PCM matrix still needed modification. The addition of TiO_2, ZnO, and CuO with 1 wt% in the lauric acid/stearic acid mixture increased thermal conductivity by 34.85%, 46.97%, and 62.12% [20]. Besides, the Al_2O_3, Fe_2O_3, and the SiO_2 with different concentrations in the paraffin, polyethylene glycol (PEG), and eutectics fatty acids also enhanced the thermal performance [21]. Besides, the crystallization of the organic semi-crystalline PCM inside the PCM/MP composites including the crystal growth rate and the crystal growth geometry was affected by the volume ratio of the metal particles to the PCM [22].

The fibrous material was a stable structure consisting of the fibers and the amount of the still air, which was considered as a suitable carrier for the PCM [23] for the aforementioned various applications. The thickness, density, and porosity of the fibrous materials were controllable via various structures, which supported the fibrous materials for various applications [24]. Many methods have been developed for the incorporation of the PCM into the fibrous materials, including spinning, coating, lamination, and so on. Most studies related to the PCM-incorporated fibrous materials focused on the enthalpy and the thermal buffering effect [25–27], while there were few studies directly related to the overall evaluation of the enhanced thermal storage efficiency of the PCM-coated fabric. The metal particles were usually introduced into the PCM fiber for thermal conductivity enhancement [28–30]. However, it was found that the thermal enhanced PCM-incorporated fibers included the PCM, metal particles, and the supporting materials, which meant the enthalpy was significantly reduced when compared with the corresponding pure PCM. Furthermore, the determination of the thermal storage efficiency of the PCM-incorporated fabric was not only limited to the thermal conductivity of the single fiber. The air and the thermal contact between the PCM layer and the coverage layer or the protection layer also affect the heat transfer. The temperature change with time (T-history) of the fabric under the continuous heating or cooling situation provided more details related to the thermal buffering range or the reduced thermal storage time. It was noticeable that Newton's cooling law could describe the T-history of the fabric [31,32] by estimating the heating or cooling constant, which could be also for the PCM-incorporated fabrics.

Polyethylene glycol (PEG) was a common semi-crystalline polymer and used as PCM. By comparing with fatty acid and inorganic PCMs, the PEG was characterized by moderate working temperature range, non-flammability, non-corrosivity, huge heat of fusion, and high thermal stability [33]. The higher molecular weight of the PEG contributed to the higher melting enthalpy. When the molecular weight of the PEG was higher than 6000, the melting enthalpy was around 180 J/g [33]. The hydroxyl group of the PEG supported the compatibility with other materials [34]. In the previous work, the thermal buffering effect of the PEG-coated fabric was realized in the multi-layer fabric systems [35].

In this work, PEG was selected as PCM for the coating on the nonwoven viscose fabric. Five micro metal particles including copper (Cu), aluminum (Al), silver (Ag), iron (Fe), and zinc (Zn) particles were first blended with PEG, respectively. Then the PEG/MP composites were coated on the viscose fabric and the thermal behavior of the PEG/MP-coated viscose fabric was investigated. The melting and solidification process of the PEG/MP composites and the PEG/MP-coated viscose fabric was compared. Newton's cooling law was for the characterization of the T-history of the PEG/MP-coated viscose fabric.

Table 1
Description of metal particles.

Type of metal particles	Mean diameter (μm)	Metal density (g/cm^3)
Cu	35.00	8.96
Al	51.47	2.60
Ag	23.00	10.5
Fe	25.00	7.87
Zn	3.60	7.14

Table 2
Description of the PEG/MP composites.

PEG/MP Code	PEG (wt %)	Cu Particle (wt%)	Al Particle (wt%)	Ag Particle (wt%)	Fe Particle (wt%)	Zn Particle (wt%)
P1	100	0	0	0	0	0
P2	72.7	27.3	0	0	0	0
P3	72.7	0	27.3	0	0	0
P4	72.7	0	0	27.3	0	0
P5	72.7	0	0	0	27.3	0
P6	72.7	0	0	0	0	27.3

2. Experimental

2.1. Material

PEG particles (M_w = 6000) were purchased from Sigma Aldrich. Different five micro metal particles including copper (Cu), aluminum (Al), silver (Ag), iron (Fe), and zinc (Zn) were purchased from Kovya-chemie company. The details of the MPs were shown in Table 1 and the morphology of the MPs were given in **APPENDIX 1**. The viscose fabric (47 g/m^2) was provided by the Department of Material Engineering, Faculty of Textile Engineering, Technical University of Liberec.

2.2. Preparation of PEG/MP composites and the PEG/MP-coated viscose fabric

Before the preparation of the PEG/MP-coated viscose fabrics, the PEG/MP composites had to be prepared in advance. PEG particles were first placed in the oven under 80 °C till PEG particles became molten homogenously. Then MPs were physically blended with the molten PEG till the mixture became homogenous. The mixture was cooled under room temperature to be solid on the glass slide as a film and finally, PEG/MP composites were obtained. Here, all the MPs including Cu, Al, Ag, Fe, and Zn particles were blended with molten PEG separately at the same concentration of 72.7 wt% to 27.3 wt%. Besides, the pure PEG solid was prepared by melting PEG particles with the same method. The description of the prepared PEG/MP composites was shown in Table 2.

Then, the PEG/MP-coated viscose fabric was prepared following the three steps:

1) The prepared PEG/MP composites were firstly pulled into the glass breaker than then placed in the oven under 80 °C till they became molten homogenously.
2) The molten PEG/MP mixture was taken out from the over and the viscose fabric was rapidly introduced into the molten PEG/MP mixture at a weight ratio of 10:90 (viscose fabric: PEG/MP composites). Step '2' was carried out at the environment temperature of 25 °C. When the molten PEG/MP mixture was blended with the viscose fabric, the adsorption of the molten PEG/MP mixture by the viscose fabric was considered because of the high porosity of the fabric whose volume porosity generally was higher than 90%. To keep the molten PEG/MP mixture to adhere on the viscose fabrics, the heating/cooling cycle ranging from 25 °C to 80 °C was to treat the PEG/MP-coated viscose fabrics by using the oven, which was repeated 5 times. After then step '2', the molten PEG/MP mixture

Table 3
Description of the PEG/MP-coated viscose fabric.

Fabric code	Components (wt% (areal density))						
	Viscose nonwoven fabric	PEG	Cu particle	Al particle	Ag particle	Fe particle	Zn particle
C0	100 (47)	–	–	–	–	–	–
C1	13.3 (47)	86.7 (308)	–	–	–	–	
C2	10 (47)	65.6 (308)	24.5 (115)	–	–	–	–
C3	10 (47)	65.6 (308)	–	24.5 (115)	–	–	–
C4	10 (47)	65.6 (308)	–	–	24.5 (115)	–	–
C5	10 (47)	65.6 (308)	–	–	–	24.5 (115)	–
C6	10 (47)	65.6 (308)	–	–	–	–	24.5 (115)

covered the viscose fibers and the pores in the viscose fabrics although the PEG/MP coating layer was not homogenous as expected.

3) The mixture of the PEG/MP and the viscose fabric obtained from step 2 was then kept between the two Teflon layers with a small pressure to kept flat. Then the sample covered by the two Teflon layers was put in the oven at 80 °C. After 5 min, the sample covered by two Teflon fabrics was taken out and then experienced pressure with a rotation of a cylinder glass cup full of water on the surface of the Teflon layers till the sample became solid. Then the sample covered by the two Teflon layers was heated at 80 °C for 10 min again. Both the heating process and rotation process were repeated 5 times to keep the surface of the PEG/MP-coated viscose fabrics even and flat.

The details of the prepared PEG/MP-coated viscose fabrics were shown in Table 3, and the actual weight of the PEG, the MPs, and the viscose fabric was set as 1.20g, 3.21g, and 0.49g, respectively.

In the following studies, the phase transition of the PEG/MP-coated viscose fabric was mainly evaluated by comparing it with the PEG/MP composites.

2.3. Tests and methods

The morphology of the PEG/MP-coated viscose fabric was observed via scanning electronic microscopy (SEM) (VEGA, TESCAN Inc., Licoln, NE, USA) under 20 kV. Besides, the prepared PEG/MP-coated viscose fabrics were evaluated by the Alambeta device to obtain the thickness and the thermal conductivity [36,37]. The basic thermal properties of PEG/MP-coated viscose fabric including thermal conductivity (λ_s), thermal resistance (R_s) and thickness (L_s) were measured by the Alambeta device at 35 °C within several seconds (<60s).

Differential scanning calorimetry (DSC) (METTER TOLEDO) was used to test the thermal properties of PEG/MP (P1, P2, P3, P4, P5, and P6) and PEG/MP-coated viscose fabric (C1, C2, C3, C4, C5, and C6) from 25 °C to 70 °C with a heating rate of 2K/min under N_2 gas purge with a rate of 50 mL/min. After the measurement, all the endothermal and exothermal curves were recorded. By using the built-in software, the melting/cooling enthalpy ($\Delta H_m/\Delta H_c$) of each sample was calculated by choosing the whole phase transition part. To determine the onset of melting/cooling temperature (T_{om}/T_{oc}) and the endset melting/cooling temperature (T_{em}/T_{ec}), the phase transition part in the melting/cooling process of the DSC curve was firstly transferred into the plot of relative amorphous/crystalline part ($W_{m/c}$) vs temperature by using the built-in software according to equation (1), where the H was the enthalpy corresponding to the recorded time t, t_1 was the recorded time for the end of the phase transition and t_0 was the recorded time for the start of the phase transition [38,39]. Then, the T_{om} and T_{oc} were determined by choosing the temperature corresponding to the 1% relative amorphous/crystalline part, and T_{em} and T_{ec} were determined by choosing the temperature corresponding to the 99% relative amorphous/crystalline part [40]. Besides, the melting peak value (T_{pm}) and the solidifying peak value (T_{pc}) were also measured. The supercooling degree (ΔT) was also calculated according to equation (2).

$$W_{m/c} = \frac{\int_{t_0}^{t_1} H dt}{\int_{t_0}^{\infty} H dt} \times 100\% \tag{1}$$

$$\Delta T = T_{pm} - T_{pc} \tag{2}$$

The theoretical meting/cooling enthalpy ($\Delta H_m^T/\Delta H_c^T$) of the PEG inside the composites was calculated according to equation (3) [38,41,42], where p was the weight percentage of the PEG inside the composites following the description in Tables 2 and 3 Besides, the crystalline ratio (χ) (%) was calculated according to equation (4) [43], where ΔH_m was the measured melting enthalpy of the prepared sample and $\Delta H_{m,PEG}^T$ was the theoretical enthalpy of the PEG from equation (3).

$$\Delta H_m^T = \Delta H_m \Delta p \tag{3}$$

$$\chi = \frac{\Delta H_m}{\Delta H_{m,PEG}^T} \times 100\% \tag{4}$$

To reveal the highly efficient thermal energy storage of the prepared PEG/MP-coated viscose fabric, the heating T-history measurement was carried out under room temperature by using a setup shown in Fig. 1. Aim to model the T-history analysis of the multi-layer system containing PCM-incorporated fabrics, the prepared PEG/MP-coated viscose fabric was placed between two Teflon layers (ε = 0.95). In detail, the temperature controller (T_h) was set as 75 °C, whose surface was placed the

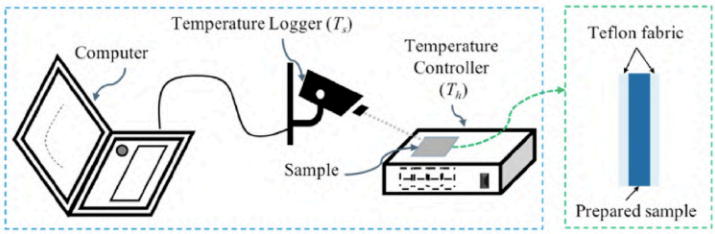

Fig. 1. The setup for the heating T-history to measure the PEG/MP-coated viscose fabrics.

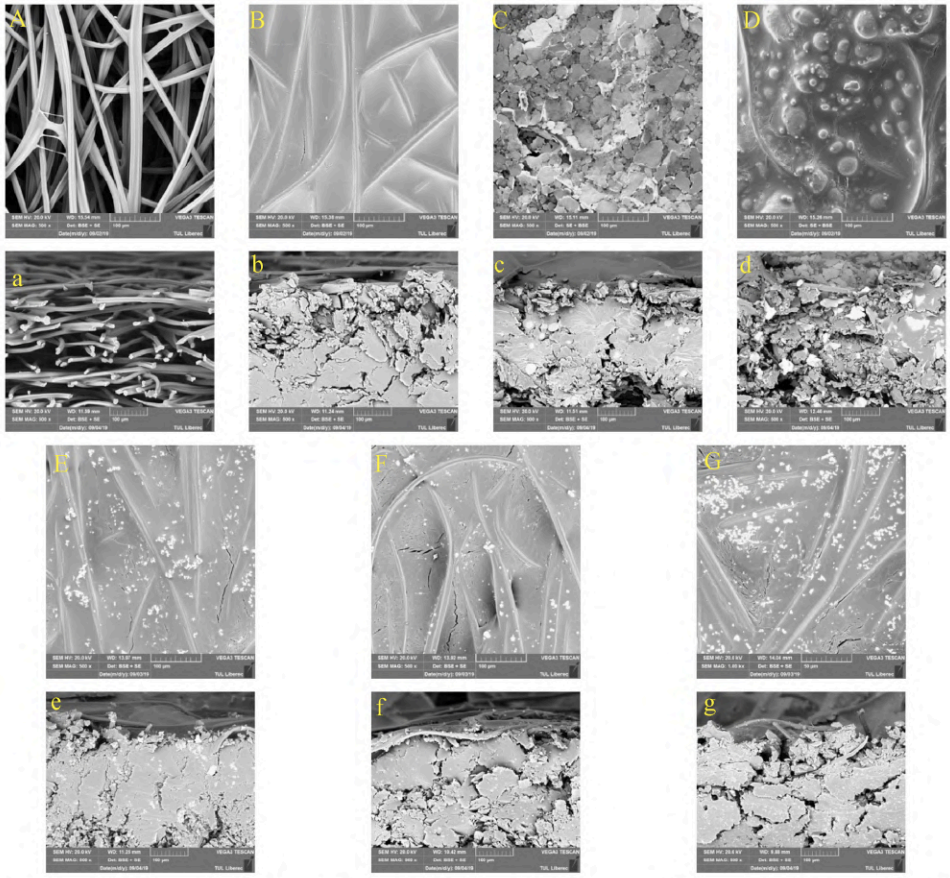

Fig. 2. Morphology of PEG/MP-coated viscose fabrics (A, B, C, D, E, F and G: the surface of C0, C1, C2, C3, C4, C5, and C6; a, b, c, d, e, f and g: cross-section of C0, C1, C2, C3, C4, C5, and C6).

Teflon fabric-covered samples for 5min. By using the temperature logger to record the temperature of the sample (T_s) with the time interval 0.5s. Each sample was measured 5 times.

3. Results and discussion

3.1. Morphology

Fig. 2 provided the morphology of the prepared PEG/MP-coated viscose fabric. It was obvious that the molten PEG and the molten PEG/MP mixture well covered the viscose fabric by observing the filled interspace between viscose fibers in both surface and cross-section images. In detail, it was observed in Fig. 2 (B) and 2 (b) that the PEG covered the viscose fiber, which suggested that the high porosity of the viscose fabric and the capillary force caused by the viscose fiber supported good adsorption of the molten PEG. For the PEG/MP-coated viscose fabric, the MPs were observed and most of them were filled in the PEG matrix by combining the morphology of MPs in APPENDIX 1. Especially, the viscose fiber was fully covered by the PEG/Cu composites, which was different from other samples. The main reason was considered as the significant change of the viscosity of the molten PEG/Cu composites, which was different from other PEG/MP composites.

3.2. Phase transition of the PEG/MP composites and the PEG/MP-coated viscose fabric

DSC curves with change of amorphous/crystalline fraction for all the samples were shown in Fig. 3. It was noticeable that there was one small peak in front of the main peak in the DSC heating curve, which suggested that there were various PEG crystals formed in the composites. Besides, their phase transition was different between all the samples, and the details including the onset melting/cooling temperature (T_{om}/T_{oc}), the melting/cooling peak temperature (T_{pm}/T_{pc}), the endset melting/cooling temperature (T_{em}/T_{ec}) and the melting/cooling enthalpy ($\Delta H_m/\Delta H_c$)

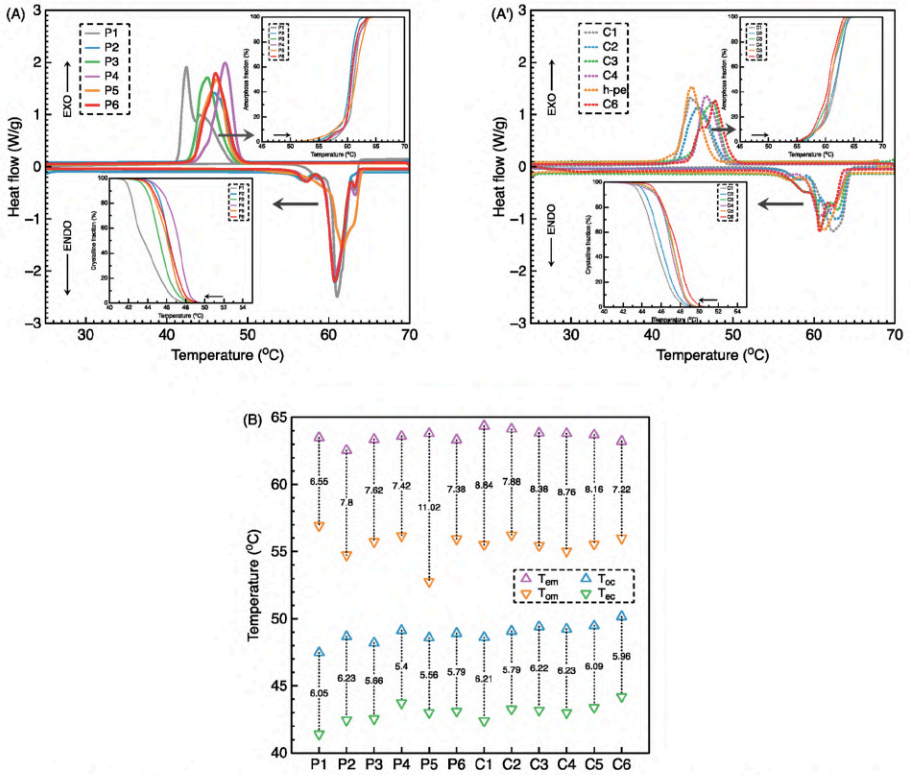

Fig. 3. Evaluation from DSC curves with 2K/min (A and A': heating and cooling process incorporated with amorphous fraction and the crystalline fraction change of PEG/MP composites and PEG/MP-coated viscose fabric, B: overall phase transition temperature range).

Table 4
Summary of the phase transition of the PEG/MP composites and the PEG/MP-coated viscose fabrics calculated from dynamic DSC curves with 2K/min.

Sample Code	T_{om} (°C)	T_{pm} (°C)	T_{em} (°C)	ΔH_m (J/g)	T_{oc} (°C)	T_{pc} (°C)	T_{ec} (°C)	ΔH_c (J/g)	ΔT (°C)	χ (%)
P1	56.93	61.02	63.48	162.99	47.47	42.43	41.42	153.58	18.59	100.00
P2	54.74	60.68	62.54	135.88	48.68	45.85	42.45	135.47	14.83	114.67
P3	55.74	60.75	63.36	144.44	48.20	45.02	42.54	143.71	15.73	121.90
P4	56.17	60.84	63.59	148.40	49.13	47.21	43.73	146.77	13.63	125.24
P5	52.77	61.67	63.79	154.79	48.58	46.22	43.02	145.32	15.45	130.63
P6	55.94	60.78	63.32	152.60	48.91	46.01	43.12	152.24	14.77	128.78
C1	55.52	62.37	64.36	137.01	48.61	44.70	42.40	133.02	17.67	96.96
C2	56.24	62.81	64.12	112.70	49.07	45.70	43.28	109.68	17.11	105.40
C3	55.45	60.18	63.83	104.86	49.41	47.48	43.19	100.59	12.70	98.07
C4	55.03	60.63	63.79	107.00	49.23	46.7	43.00	105.41	13.93	100.07
C5	55.54	61.00	63.70	108.20	49.48	47.21	43.39	109.46	13.79	101.20
C6	56.00	60.10	63.22	110.23	50.16	47.79	44.20	106.93	12.31	103.09

T_{om}: onset melting temperature; T_{pm}: peak melting temperature; T_{em}: endset melting temperature; T_{oc}: onset cooling temperature; T_{pc}: peak cooling temperature; T_{ec}: endset cooling temperature; ΔH_m: melting enthalpy change; ΔH_c: solidification enthalpy change; ΔT: $T_{pm} - T_{pc}$; χ: the crystalline ratio.

were shown in Table 4.

The sigmoid curve plotting the amorphous/crystalline fraction of all the samples as a function of the temperature was observed. In detail, the amorphous fraction plot of all the samples with the temperature was not smooth in the primary stage, while the crystalline fraction plot was much smoother. It was suggested that the various PEG crystals formed in the composites, which was also proved in the DSC curves. During the heating process, the various PEG crystals were melted to release the

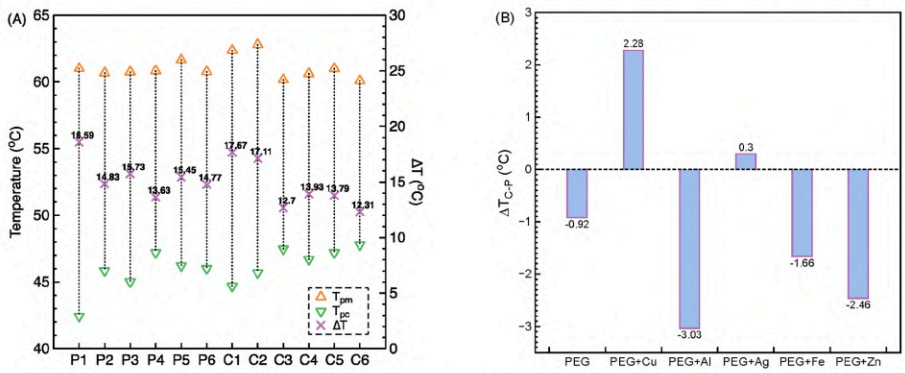

Fig. 4. Supercooling degree of all the prepared composites (A) and effect of viscose fabric on the supercooling degree (B).

corresponding thermal energy at their different activation temperature. For the cooling process, the PEG crystals were formed and experienced nucleation and crystallization, which absorbed the energy step by step. Furthermore, the phase transition of all the prepared PEG/MP composites and the PEG/MP-coated viscose fabrics during the heating and cooling process was also presented. It was found that the solidification had a smaller temperature range when compared with the melting process. The solidification started earlier when there were MPs or viscose fabric in the PEG matrix. The reason may be caused by the different crystallinization of the PEG in the various samples, which was discussed in the following section '3.2.2'.

3.2.1. Supercooling degree (ΔT)

According to equation (2), the supercooling degree (ΔT) of the prepared samples were calculated and shown in Fig. 4 (A). For the PEG/MP composites, the ΔT was narrowed when there were MPs, which was resulted from the increased T_{pc} while the T_{pm} was little affected. The T_{pc} value or the T_{pm} value corresponded to the major PEG crystals in the PEG/MP composites, which was different from the $T_{om/oc}$ or the $T_{em/ec}$. It was suggested that the major PEG crystals were almost the same while the nucleation mechanism was changed. For the PEG/MP-coated viscose fabrics, a similar change was observed in the samples C1, C3, C4, C5, and C6 while the sample C2 was different, which suggested that the major PEG crystals in the sample C2 were altered. Additionally, the narrow ΔT value was reduced when there were the MPs or the viscose fabric in the PEG matrix, the MPs and the viscose fabrics providing the nuclei sites for the PEG crystallization [44] while the change in primary nucleation or the secondary crystallization for the PEG in the composites was not clear, which was not discussed in this work.

Furthermore, the effect of the viscose fabric (ΔT_{C-P}) on the ΔT of the PEG in the composites was investigated according to equation (5) [45], where ΔT_C was the ΔT of the PEG/MP-coated viscose fabrics and the ΔT_P was for the PEG/MP composites. The result is shown in Fig. 4 (B). The ΔT_{C-P} was negative when the PEG was coated on the viscose fabric. Then, the viscose fabric was considered as the nuclei site for the PEG crystallization. A similar trend was observed when viscose fabric was introduced in the PEG/Al, PEG/Fe, and PEG/Zn composite. However, the ΔT_{C-P} was positive when the viscose fabric was in the PEG/Cu and PEG/Ag composite. The different PEG crystallization mechanism in the PEG/MP composites and the PEG/MP-coated viscose fabrics were proposed for the explanation of the difference in the ΔT.

$$\Delta T_{C-P} = \Delta T_C - \Delta T_P \quad (5)$$

Table 5
Theoretical Enthalpy of PEG in the prepared samples.

Sample Type	ΔH^T_{mPEG} (J/g)	ΔH^T_{cPEG} (J/g)
PEG	162.99	153.58
PEG/MP Composite	118.49	111.65
PEG-coated viscose fabric	141.31	133.15
PEG/MP-coated viscose fabric	106.92	100.75

3.2.2. Measured and theoretical enthalpy

The measured melting/solidifying enthalpies ($\Delta H_m/\Delta H_c$) of the PEG/MP composites and the PEG/MP-coated viscose fabrics were shown in Table 4. It was found that the pure PEG (the sample P1) had the highest value in both ΔH_m and ΔH_c, which was 162.99 J/g and 153.58 J/g. For the PEG/MP composites (the sample P2, P3, P4, P5, and P6), both the ΔH_m and the ΔH_c were smaller than the pure PEG. The sample P6 had the highest ΔH_m and the ΔH_c, which was 152.60 J/g and 152.24 J/g. The sample P2 had the lowest ΔH_m and the ΔH_c, which was 135.88 J/g and 135.47 J/g. For the PEG/MP-coated viscose fabrics, both the ΔH_m and the ΔH_c values were smaller than the corresponding PEG/MP composites. The sample C2 had the highest ΔH_m and ΔH_c, which was 112.70 J/g and 109.28 J/g. The sample C3 had the lowest ΔH_m and ΔH_c, which was 104.86 J/g and 100.59 J/g. Furthermore, Table 5 showed the theoretical enthalpy ($\Delta H^T_{m/c\ PEG}$) of the PEG/MP composites and the PEG/MP-coated viscose fabrics according to equation (3). Fig. 5 also presented the difference between the measured and theoretical enthalpy of the PEG/MP composites and the PEG/MP-coated viscose fabrics. Besides, the crystalline ratio (χ) of the PEG inside various prepared composites were calculated according to equation (4) and shown in Table 4. In this case, the estimated χ values of the PEG inside all the prepared PEG/MP composites were higher than 100%. For the PEG/MP-coated viscose fabric, only sample C1 and C3 had the lower χ values of the PEG than 100% while other samples had the higher χ values than 100%. The results from χ values corresponded to the difference between the theoretical enthalpy and measured enthalpy for all the samples. The main reason may be the effect of the MPs and the viscose fabric on the PEG crystallization.

The basic three situations were noticed, including the PEG/MP composites, PEG-coated viscose fabrics, and the PEG/MP-coated viscose fabrics.

1) By comparing the pure PEG (the sample P1) with PEG/MP composites (the sample P2, P3, P4, P5, and P6), both ΔH_m and ΔH_c were higher than the corresponding ΔH^T_{mPEG} and ΔH^T_{cPEG}. The higher enthalpy

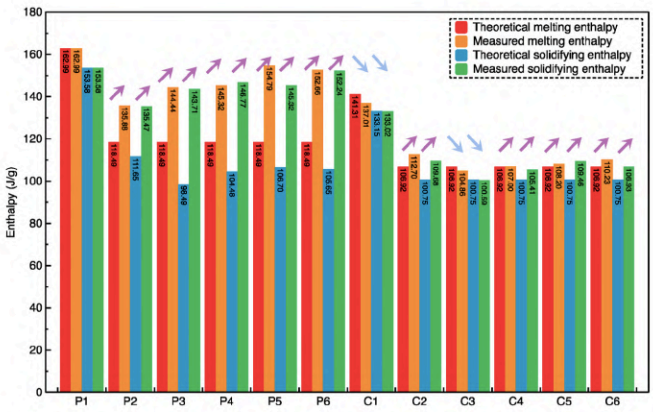

Fig. 5. Measured and theoretical melting and solidifying enthalpies of PEG in the prepared samples (Arrow direction corresponded to the difference between the measured and theoretical melting/solidifying enthalpy).

Table 6
Key parameters to characterize the thermal performance of PEG/MP-coated viscose fabrics via Alambeta device (subscript *s*: the value when the PEG was the solid phase in the samples).

Sample code	λ_s (W K^{-1} m^{-1}) ($\times 10^{-3}$)	a_s (m^2 s^{-1}) ($\times 10^{-6}$)	b_s (W m^{-2} s$^{1/2}$ K^{-1})	r_s (K W^{-1} m^2) ($\times 10^{-3}$)	h_s (mm)	p_s	q_s (K W m^2)
C0	29.860±1.893	0.109±0.020	90.340±2.422	14.90±5.477	0.33±0.022	1.060±0.007	0.349±0.004
C1	39.460±1.274	0.076±0.009	144.800±6.140	31.34±3.578	1.25±0.171	1.624±0.125	0.225±0.022
C2	63.220±3.321	0.044±0.004	244.680±121.092	11.06±0.564	0.69±0.062	1.778±0.213	0.584±0.080
C3	71.960±6.518	0.043±0.008	349.000±47.392	7.00±0.430	0.50±0.022	1.426±0.02	0.635±0.059
C4	66.660±2.507	0.033±0.001	364.800±16.976	6.76±0.304	0.45±0.022	1.630±0.678	0.749±0.028
C5	65.360±3.712	0.035±0.002	351.600±19.870	6.30±0.346	0.42±0.024	1.546±0.049	0.739±0.025
C6	54.740±2.914	0.040±0.006	265.400±32.777	11.72±0.549	0.63±0.033	1.904±0.114	0.600±0.056

corresponded to the higher crystalline ratio. It was known that PEG was the semi-crystalline polymer consisting of the amorphous part and the crystalline part. The PEG/MP composites were considered as binary composites. The strength of the MPs effect on the PEG crystallization strongly depended on the properties of MPs, including the aspect ratio, specific surface area and the type. The addition of the MPs in the PEG matrix not only provided the nucleation sites but also may resulted in the rigid amorphous fraction near the surface of MPs [46]. Although the crystallization mechanism was not so clear, the introduction of MPs in the PEG matrix was assumed a positive effect to improve the crystalline ratio from the aforementioned results.

2) For the PEG-coated viscose fabric (the sample C1), both ΔH_m and ΔH_c were smaller than the corresponding ΔH^T_{mPEG} and ΔH^T_{cPEG}. It was known that the viscose fiber consisted of cellulose. The existence of the viscose fabric in the PEG matrix affected the conformation of the PEG molecular chains due to the hydrogen bonding between the PEG and viscose fiber. Therefore, the incorporation of the viscose fabric was considered as a negative effect to reduce the crystalline ratio.
3) For the PEG/MP-coated viscose fabrics, there was no obvious change trend in the difference between the ΔH_m and ΔH_c and the ΔH^T_{mPEG} and ΔH^T_{cPEG}, respectively. In details, the sample C3 had the lower ΔH_m and ΔH_c than the ΔH^T_{mPEG} and ΔH^T_{cPEG}, while other samples (C2, C4, C5, and C6) had a higher ΔH_m and ΔH_c than the ΔH^T_{mPEG} and ΔH^T_{cPEG}. By combing with the aforementioned analysis '1' and '2', the final positive or negative effect on the PEG crystalline ratio of the PEG/MP-coated viscose fabrics was considered to be strongly related to the ratio between the MPs and the viscose fabric.

3.3. Thermal performance of the PEG/MP-coated viscose fabric before the melting process

Based on the one-dimensional transient heat transfer model, the key parameters including the thermal conductivity (λ_s), thermal diffusivity (a_s), thermal absorptivity (b_s), thermal resistance (r_s), thickness (h_s), the ratio of the maximum and stationary heat flow density (p_s), and the stationary heat flow density (q_s) from the Alambeta device to characterize the thermal performance of the PEG/MP-coated viscose fabric before melting process were shown in Table 6 and shown in Fig. 6.

The λ_s is the quantity of the heat transmitted through a unit thickness in a direction normal to a surface of the unit area, which was usually to characterize the thermal storage enhancement. It was found that the sample C0 had the lowest λ_s value when compared with other samples, which was caused by the still air in the highly porous viscose nonwoven fabric. The sample C1 had a higher λ_s value than the sample C0, which was caused by the coverage of the PEG matrix in the interspace of the viscose nonwoven fabric due to the thermal conductivity of the still air was considered as much lower than other materials. Higher λ_s values of the sample C2, C3, C4, C5, and C6 than the sample C1 were observed, meaning that the introduction of the MPs in the coated viscose fabric enhanced the thermal conduction. In details, the sample C3 had the highest λ_s value as 71.960×10^{-3} $W\,K^{-1}\,m^{-1}$ and the sample C6 had the lowest λ_s value as 54.740×10^{-3} $W\,K^{-1}\,m^{-1}$.

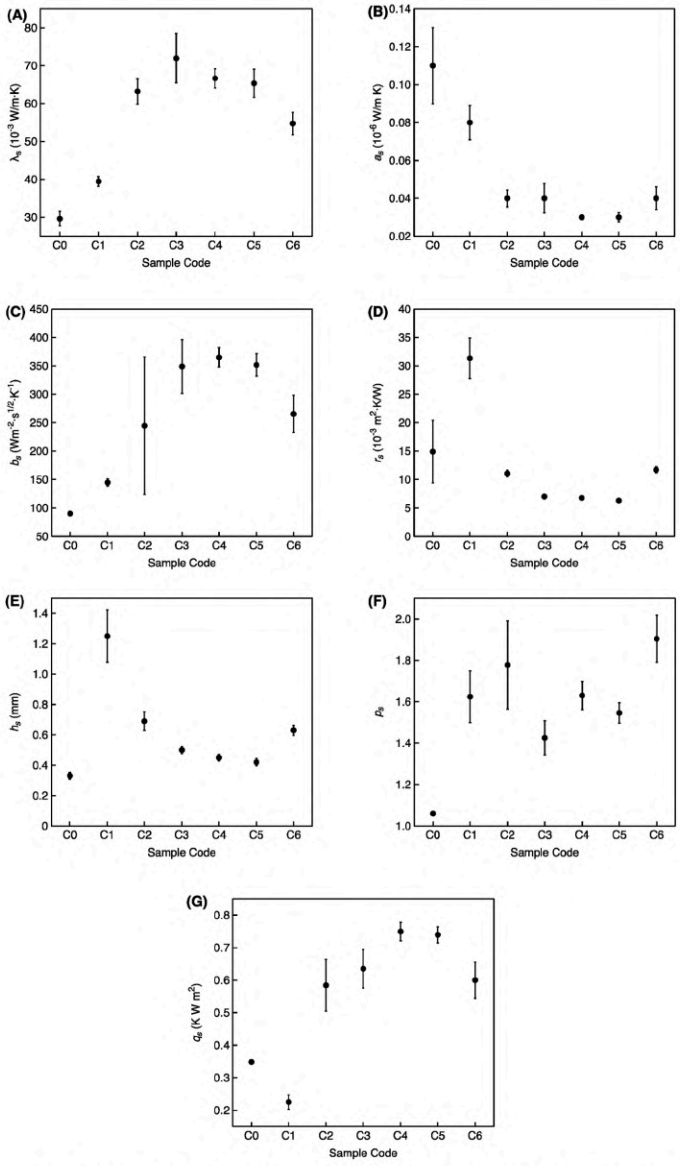

Fig. 6. Thermal performance of the PEG/MP-coated viscose fabric characterized by Alambeta device (A: QUOTE λs *λs*, B: as, C: bs, D: rs, E: hs, F: ps, and G: qs).

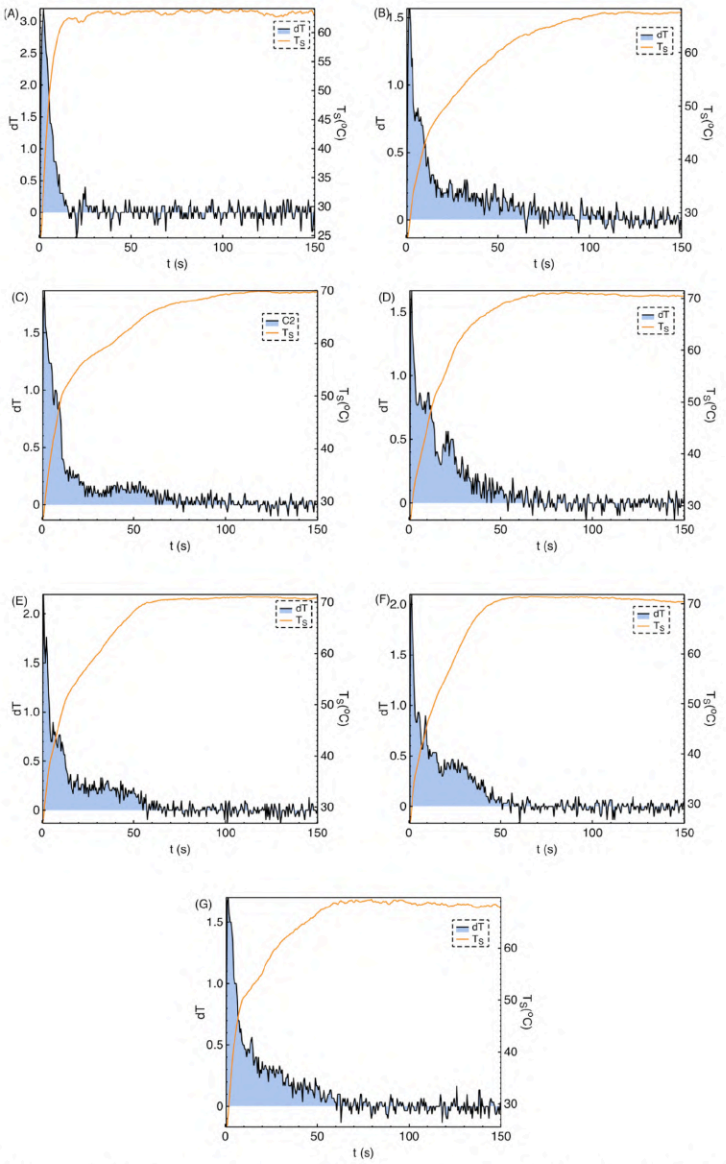

Fig. 7. Heating T-history curves of the prepared samples covered by Teflon layers (A, B, C, D, E, F, and G: the sample C0, C1, C2, C3, C4, C5, and C6).

Table 7
Summary of the thermal performance.

Sample code	T_f (°C)	t_f (s)	I
C0	63.30	16.00	0.22
C1	70.60	110.00	0.08
C2	69.30	115.00	0.11
C3	71.30	80.00	0.07
C4	71.17	60.00	0.07
C5	71.47	55.00	0.07
C6	69.10	70.00	0.11

The a_s is considered as the transient thermal property and related to the velocity of the impulse heat transfer through the thickness of the materials. It was found that the a_s value was reduced when there was the PEG in the viscose fabric by comparing the sample C1 with the sample C0. The a_s value was also reduced when there were MPs in the PEG-coated fabric by comparing the sample C2, C3, C4, C5, and C6 with the sample C1. The main reason accounting for the difference was the change of the overall density and the specific heat capacity of the PEG/MP-coated viscose fabric. The sample C2 had the highest a_s value as $0.044 \times 10^{-6}\ m^2\ s^{-1}$ and the sample C4 had the lowest a_s value as $0.033 \times 10^{-6}\ m^2\ s^{-1}$.

The b_s could be considered as the ability of the maximum heat flow transfer in a short time once two materials contact. The b_s value was strongly related to surface morphology, density, and specific heat capacity. The sample C0 had the lowest b_s value, which was caused by the amount of still air in the sample C0. Besides, the PEG/MP-coated viscose fabrics (the sample C2, C3, C4, C5, and C6) had lower b_s values than the PEG-coated viscose fabrics (the sample C1). The addition of the MP in the coated viscose fabric enhanced the heat transfer ability during the thermal contact. The sample C4 had the highest b_s value as 364.800 W m^{-2} $s^{1/2}$ K^{-1} and the sample C2 had the lowest b_s value as 244.800 W m^{-2} $s^{1/2}$ K^{-1}.

The r_s value was determined by $h_0/(\lambda_s \cdot A)$. It was noticeable that the PEG coating on the viscose fabric increased the r_s values by comparing the sample C1 with C0. The addition of the MPs in the PEG coating on the viscose fabric significantly reduced the r_s values.

3.4. Heating T-history curves of the PEG/MP-coated viscose fabrics

The mean T-history curves with a standard error of the PEG/MP-coated viscose fabrics were shown in **APPENDIX 2**. In the following studies, the mean T-history curves of the prepared samples were used.

3.4.1. Heating T-history curves

It was found that the various samples had different T-history curves but tended to be stable within 150s. In detail, the T-history curves within 150s and the dT values in 0.5s are shown in Fig. 7.

The plots of dT with t were the typical heating curves of the fabrics. The finite dT peak was caused by the frequency response of the amplifier and other causes related to the conditions of the specimen-heat plat boundary. It was also found that the plot of the dT with t of the sample C0 tended to be linear after the finite dT peak while the plots of the dT with t of other samples were much more complicated. Correspondingly, the distorted T-history curves of the samples C1, C2, C3, C4, C5, and C6 were found. The main reason was the phase transition of the PEG during the heating process, which was analyzed in the following section 3.4.2.

In detail, the final stable surface temperature (T_f) (°C) and its corresponding time (t_f) (s) were directly from Fig. 7. Besides, the thermal insulation (I) values of the samples were calculated according to equation (6), where T_h was the heating temperature, T_f was the final stable temperature of the sample and T_r was the room temperature (22.5 °C). The calculated I values were shown in Table 7.

$$I = \frac{T_h - T_f}{T_h - T_r} \tag{6}$$

The T_f value of the viscose fabric was evaluated as the lowest, while the T_f value of the PEG/MP-coated viscose fabric ranged from 69 °C to 72 °C. Correspondingly, the viscose fabric had the highest I value, and the PEG/MP-coated viscose fabric had the much lower I values. The highest I value supported the lower ability for thermal buffering. In this case, the T_f was considered to be determined by the thermal conduction. The amount of the still air in the viscose fabric and the non-stable thermal contacts between the viscose fabric and the Teflon layers coverage contributed to the lower thermal conduction. For the PEG/MP-coated viscose fabric, the molten PEG inside the prepared samples enhanced the thermal contacts with the Teflon fabric coverage, and the thermal conductivity of the molten PEG was proposed to be much lower than the air.

Additionally, the viscose fabric had the t_f value of 16.00s, which was much lower than the other samples. Sample C1 had the t_f value of 110.00s, which was caused by the phase transition of the PEG inside the sample. For the samples C3, C4, C5, and C6, the t_f value was significantly narrowed. The introduction of the Al, Ag, Fe, and Zn particles accelerated the thermal storage efficiency. Sample C5 had the lowest t_f value as 55.00s. For the sample C2, the t_f value was slightly higher than the sample C1 although the λ_s of the sample, C2 was much higher than the sample C1. The main reason was considered as the rough surface of the sample C2. The amount of the Cu particles was on the surface, which resulted in the increase of the non-stable thermal contact between the thermal C2 and the Teflon fabrics. As a result, the unstable heat transfer across the thickness was proposed and the t_f value was expanded.

3.4.2. Evaluation of the heating rate

From the aforementioned analysis, there were three stages including the solid stage, phase transition stage, and the liquid stage in the T-history of the PEG/MP-coated viscose fabric. The heating rate was different in the various stages. According to reference, Newton's cooling heating law was suitable to characterize the T-history of the prepared samples by using equation (7) [47]. The T_f (°C) was the final stable surface temperature, T_s (°C) was the recorded surface temperature of the prepared samples with time, T_i (°C) was the initial surface temperature of the prepared samples, t was the time and τ was the heating constant (s). By transforming equation (7) into equation (8), a linear plot was found.

$$T_f - T_s = (T_f - T_i)e^{-t/\tau} \tag{7}$$

$$\ln(T_f - T_s) = \ln(T_f - T_i) - t/\tau \tag{8}$$

Fig. 8 presented the plots of the $ln(T_f\text{-}T_i)$ vs t of the prepared samples. Here, the time range was determined by referring Fig. 8 and only aimed to show the T-history before the final stable stage. For the sample C0, there was only one main linear part in the plotted curve, which corresponded to the T-history curve in Fig. 7. For the samples C1, C2, C3, C4, C5, and C6, the plots of the $ln(T_f\text{-}T_i)$ vs t were complicated which corresponded to Fig. 7. With time, each linear part corresponded to the solid stage, phase transition stage, and total molten stage. Because of the possible motion of the molten PEG fluid inside the prepared samples during the total molten stage, the unstable thermal behavior was considered by observing the nonlinear part in the last time range of the plots of $ln(T_f\text{-}T_i)$ vs t. Therefore, only the solid stage and the phase transition stage were analyzed.

As a result, the τ determined from the linear part was calculated in Table 8 and shown in Fig. 9 (A). For the solid stage, it was found that the sample C0 had the τ_1 value as 3.759s which was much lower than other samples. Additionally, it was found that the τ_1 value of the sample C3 was higher than the sample C1 while the τ_1 value of the sample C2, C3, C4, C5, and C6 was smaller than the sample C1, although the R_s of the PEG/MP-coated viscose fabrics were much lower than the PEG-coated viscose fabric. The difference was caused by the change of the specific heat capacity and the resistance. For the phase transition stage, the τ_2 of

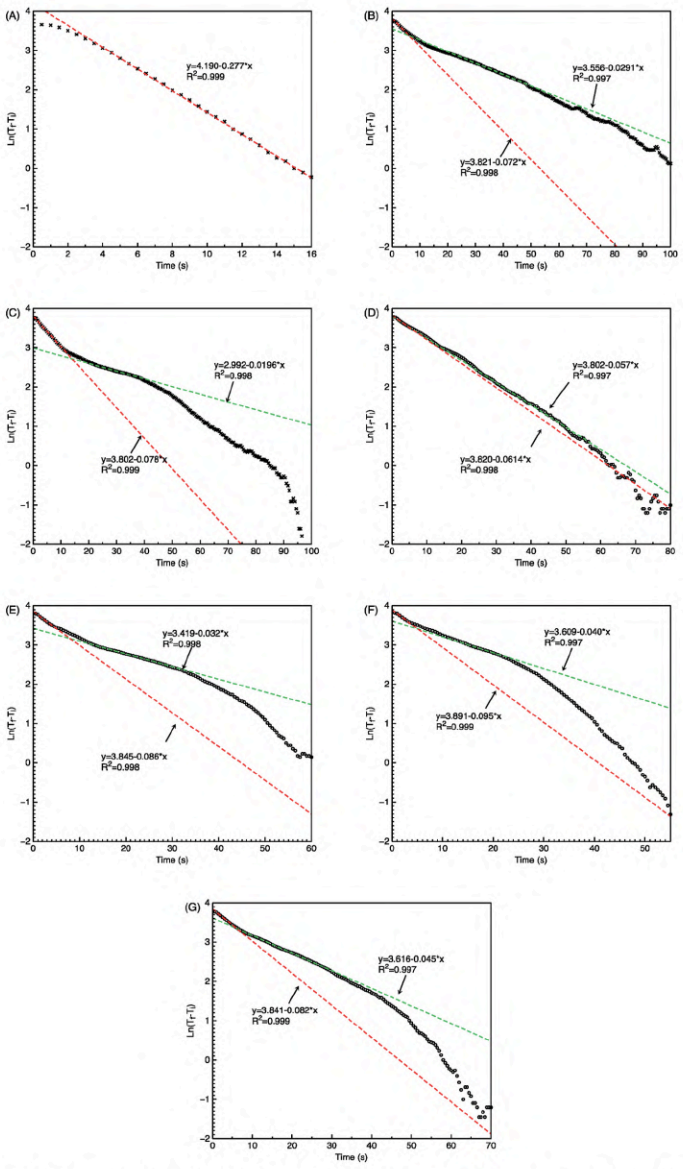

Fig. 8. Plot of QUOTE lnTf-Ts lnTf-Ts vs t (A, B, C, D, E, F, and G: the sample C0, C1, C2, C3, C4, C5, and C6; the red line was for the solid stage and the green line was for the phase transition stage). (For interpretation of the references to colour in this figure legend, the reader is referred to the Web version of this article.)

Table 8
Summary of the key parameters to characterize the T-history curves.

Sample code	$\tau_1{}^a$ (s)	t_1^b (s)	T_1^b (°C)	dT/dt_1^b	$\tau_2{}^a$ (s)	t_2^b (s)	T_2^b (°C)	dT/dt_2^b
C0	3.759	[4.0, 8.0]	[41.90, 56.0]	3.525	N/A	N/A	N/A	N/A
C1	13.889	[0.5, 5.0]	[25.30, 35.30]	2.222	34.483	[21.0, 48.5]	[49.57, 59.60]	0.378
C2	12.821	[0.5, 11.5]	[26.47, 50.63]	2.196	50.000	[20.5, 39.0]	[55.63, 60.23]	0.249
C3	16.393	[0.5, 6.0]	[27.23, 38.67]	2.082	17.544	[24.5, 39.5]	[59.90, 66.43]	0.435
C4	11.628	[0.5, 5.0]	[26.83, 39.77]	2.876	31.250	[12.0, 32.0]	[49.87, 60.57]	0.535
C5	10.526	[0.5, 3.5]	[26.10, 35.57]	3.157	25.000	[12.0, 22.0]	[48.17, 57.57]	0.940
C6	12.195	[0.5, 6.5]	[25.57, 40.97]	2.557	22.222	[7.0, 29.5]	[41.87, 59.37]	0.778

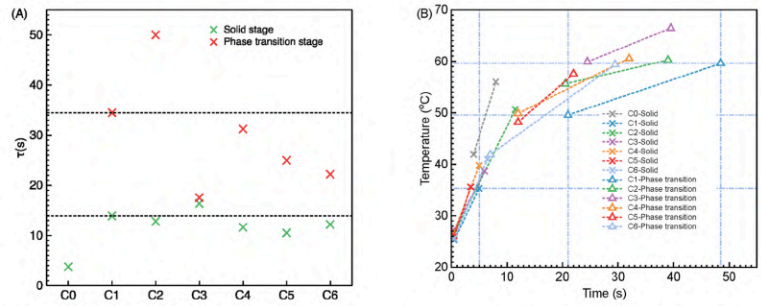

Fig. 9. Evaluated QUOTE τ τ value of prepared samples (A) and the solid stage and phase transition stage range of the prepared samples (B).

the sample C1 was 34.483s. The τ_2 of the sample C3, C4, C5, and C6 was lower than the sample C1 while the τ_2 of the sample, C2 was higher than the sample C1. The addition of the Al, Ag, Fe, and Zn particles accelerated the heat transfer during the phase transition stage while the Cu particles did not. The too many Cu particles inside the sample C2 may result in the difference. The rough surface of the sample C2 caused unstable thermal contact and reduced the heat transfer efficiency during the phase transition process.

Superscript *a*: the values from Fig. 8, and superscript *b*: the values evaluated from Fig. 7 by incorporating the plot from Fig. 8 with a 99% confidence interval.

Subscript *1* and *2*: the solid stage and the phase transition stage, respectively.

3.4.3. Determine the solid stage and the phase transition stage

Based on the analyzed τ_1 and τ_2 value, both the solid stage and the phase transition stage including the time and temperature were determined by using the modeled plot function with a 99% confidence interval. The results were shown in Table 8, and Fig. 9 (B) presented the solid stage range and the phase transition stage.

For the solid stage, the temperature range of the PEG/MP-coated viscose fabric (sample C2, C3, C4, C5, and C6) was higher than the PEG-coated viscose fabric (sample C1). Besides, the time range of the sample C2 and C3 was higher than the sample C1 while the time range of the sample C4, C5, and C6 were lower than the sample C1. The overall evaluated dT/dt_1 values gave the details of the temperature increasing rate. The sample C2 and C3 had a lower dT/dt_1 value than the sample C1 and the sample C4, C5, and C6 had a higher dT/dt_1 than the sample C1. The heat transferability of the sample C2 and C3 during the solid phase stage was considered to reduce, which was different from the analysis in the section '3.3'. The main reason was caused by the different thermal contact between the Teflon fabric coverage and the sample. Although the sample was considered to contact the Teflon fabric well during the preparation process to keep little air inside the multi-layer system, the thermal contact was still unstable and incomparable due to the various surface structure.

Before the analysis of the phase transition stage, it was noticeable that there was a gap between the solid stage and the phase transition stage. In detail, the sample C6 had almost no gap while the other samples had various gap ranges. Since the heating constant τ was based on the assumption that the one-dimensional steady heat transfer was through the samples, the reason for the existence of the gap may be included two points: 1) The change of the thermal contact in the prepared multi-layer systems for the heating T-history measurement, and 2) The PEG matrix inside the samples had to spend time reaching the heat equilibrium. From this point of view, the sample C6 was considered with stable thermal contacts.

For the phase transition stage, the overall evaluated dT/dt_2 value of the sample C1 was 0.378K/s. The sample C3, C4, C5, and C6 had a higher dT/dt_2 value than the sample C1 while the sample C2 had a lower dT/dt_2 value than the sample C1. In this case, the addition of the Al, Ag, Fe, and Zn particles enhanced the heat transfer of the PEG/MP-coated viscose fabric during the phase transition stage.

4. Conclusion

In this work, the PEG/MP composites and the corresponding PEG/MP-coated viscose fabrics were prepared successfully. Two parts including the comparison of the phase transition between the PEG/MP composites and the corresponding PEG/MP-coated viscose fabrics and

the thermal enhancement of the PEG/MP-coated viscose fabrics were investigated.

1) Phase transition comparison. The addition of the MPs in the PEG matrix made the phase transition including the melting process and the solidifying process earlier when compared with the pure PEG, while the T_{pm} was almost the same. The major PEG crystals in the PEG/MP composites were almost the same while the nucleation mechanism was changed. For the PEG/MP-coated viscose fabric, both phase transition and the nucleation mechanism were changed. The MPs were considered as the good nuclei sites for the PEG nucleation while the viscose fiber did not. The ratio between the viscose fiber-based nuclei sites and the MPs-based nuclei sites may account for the various ΔT values. The PEG/MP-coated viscose fabrics had both melting and solidifying enthalpy ranging from 100 to 110 J/g which was smaller than the corresponding PEG/MP composites.
2) Thermal conductivity enhancement. The Alameda device based on the transient heat transfer model revealed the higher thermal conductivity of the PEG/MP-coated viscose fabric. The results from the T-history of the multi-layer system containing PEG/MP-coated viscose fabrics via custom setup were analyzed according to Newton's cooling law. As a result, the higher heating constant τ in the phase transition part was considered as the main reason for the quick heat transfer through the PEG/MP-coated viscose fabric.
3) Discussion of the suitability of Newton's cooling law for the T-history of the PEG/MP-coated viscose fabrics. The principle of Newton's cooling law was based on the major linear part in the plot of $\ln(T_f - T_s)$ vs t. In this work, two major linear parts in the plot of $\ln(T_f - T_s)$ vs t was determined by combining with the T-history curves. From this point of view, the heating constant τ could describe the T-history of the PEG/MP-coated viscose fabrics. However, the phase transition of the PEG (PCM) caused an unexpected nonlinear part after the solid part, which may be caused by the change of the thermal contact and the dynamic balance to reach the thermal equilibrium. So, the heating constant τ was considered for the dynamic balance of the PCM during the phase transition process instead of the initial dynamic phase transition stage.

As a result, we proposed that this work could provide a deeper understanding of the application of the multi-layer system containing PCM-incorporated fabrics. Besides, the ratio between the fibers and the MPs could also initiate the control of semi-crystalline polymer crystals.

CRediT authorship contribution statement

Kai Yang: Conceptualization, Methodology, Software, Validation, Formal analysis, Investigation, Data curation, Writing – original draft, Writing – review & editing, Supervision, Project administration, Funding acquisition. **Jakub Wiener:** Conceptualization, Methodology, Validation, Investigation, Resources. **Mohanapriya Venkataraman:** Validation, Writing – review & editing, Supervision. **Yuanfeng Wang:** Data curation. **Tao Yang:** Data curation. **Guoqing Zhang:** Resources. **Guocheng Zhu:** Project administration, Funding acquisition. **Juming Yao:** Project administration, Funding acquisition. **Jiri Militky:** Validation, Resources, Writing – review & editing, Supervision, Project administration, Funding acquisition.

Declaration of competing interest

The authors declare that they have no known competing financial interests or personal relationships that could have appeared to influence the work reported in this paper.

Acknowledgement

The authors are indebted to Dr. Miroslava Pechociakova for her assistance with DSC measurement and Prof. Lubos Hes for his lecture related to the heat transfer through fabric. This work was supported by the research project (No. SGS-2021-6023) of the Student Grant Competition of Technical University of Liberec granted by the Ministry of Education, Youth and Sports of Czech Republic, the project 'Hybrid Materials for Hierarchical Structures' (HyHi, Reg. No.CZ.02.1.01/0.0/0.0/16_019/0000843) granted by the Ministry of Education, Youth and Sports of the Czech Republic, European Union – European Structural and Investment Funds in the Frames of Operational Programme Research, Development, and Education, the project 'design of multi-layer micro/nanofibrous structures for air filters applications' (Reg. No. 8JCH1064) granted by the Ministry of Education, Youth and Sports of the Czech Republic in the frames of support for researcher mobility (VES19China-mobility, Czech-Chinese cooperation). The work was also supported by the project 'Intelligent thermoregulatory fibers and functional textile coatings based on temperature resistant embedded PCM' SMART-THERM (Project No. TF06000048) granted by the Technology Agency of the Czech Republic (DELTA Programme).

Appendix A. Supplementary data

Supplementary data to this article can be found online at https://doi.org/10.1016/j.polymertesting.2021.107231.

References

[1] K. Iqbal, A. Khan, D. Sun, M. Ashraf, A. Rehman, F. Safdar, A. Basit, H.S. Maqsood, Phase change materials, their synthesis and application in textiles—a review, J. Text. Inst. 110 (2019) 625–638, https://doi.org/10.1080/00405000.2018.1548088.
[2] D. Li, Y. Wu, B. Wang, C. Liu, M. Arıcı, Optical and thermal performance of glazing units containing PCM in buildings: a review, Constr Build Mater, 233 117327 (2020), https://doi.org/10.1016/j.conbuildmat.2019.117327.
[3] A.A.M. Omara, A.A.A. Abuelnuor, H.A. Mohammed, D. Habibi, O. Younis, Improving solar cooker performance using phase change materials: a comprehensive review,, Sol. Energy 207 (2020) 539–563, https://doi.org/10.1016/j.solener.2020.07.015.
[4] C. Liu, D. Xu, J. Weng, S. Zhou, W. Li, Y. Wan, S. Jiang, D. Zhou, J. Wang, Q. Huang, Phase change materials application in battery thermal management system: a review,, Materials 13 (2020) 1–37, https://doi.org/10.3390/ma13204622.
[5] E. Alehosseini, S.M. Jafari, Micro/nano-encapsulated phase change materials (PCMs) as emerging materials for the food industry, Trends Food Sci. Technol. 91 (2019) 116–128, https://doi.org/10.1016/j.tifs.2019.07.003.
[6] D.G. Prajapati, B. Kandasubramanian, A review on polymeric-based phase change material for thermo-regulating fabric application,, Polym. Rev. 60 (2020) 389–419, https://doi.org/10.1080/15583724.2019.1677709.
[7] B. Zalba, J.M. Marín, L.F. Cabeza, H. Mehling, Review on thermal energy storage with phase change: materials, heat transfer analysis and applications, Appl. Therm. Eng. 23 (2003) 251–283, https://doi.org/10.1016/s1359-4311(02)00192-8.
[8] M. Liu, M.C. Lin, C. Wang, Enhancements of thermal conductivities with Cu, CuO, and carbon nanotube nanofluids and application of MWNT/water nanofluid on a water chiller system, Nanoscale Res Lett 6 (2011) 297, https://doi.org/10.1186/1556-276x-6-297.
[9] X. Wu, J. Lee, V. Varshney, J.L. Wohlwend, A.K. Roy, T. Luo, Thermal conductivity of wurtzite zinc-oxide from first-principles lattice dynamics – a comparative study with gallium nitride, sci rep-UK, 6 22504 (2016), https://doi.org/10.1038/srep22504.
[10] R. Agrawal, K.D.P. Singh, M.K. Paswan, Review on enhancement of thermal conductivity of phase change materials with nano-particle in engineering applications, Mater Today Proc. 22 (2020) 1617–1627, https://doi.org/10.1016/j.matpr.2020.02.159.
[11] Z. Khan, Z.A. Khan, P. Sewell, Heat transfer evaluation of metal oxides based nano-PCMs for latent heat storage system application, Int. J. Heat Mass Tran. 144 (2019) 118619, https://doi.org/10.1016/j.ijheatmasstransfer.2019.118619.
[12] T. Rehman, H.M. Ali, M.M. Janjua, U. Sajjad, W.-M. Yan, A critical review on heat transfer augmentation of phase change materials embedded with porous materials/foams,, Int. J. Heat Mass Tran. 135 (2019) 649–673, https://doi.org/10.1016/j.ijheatmasstransfer.2019.02.001.
[13] F. Li, X. Wang, D. Wu, Fabrication of multifunctional microcapsules containing n-eicosane core and zinc oxide shell for low-temperature energy storage, photocatalysis, and antibiosis, Energy Convers. Manag. 106 (2015) 873–885, https://doi.org/10.1016/j.enconman.2015.10.026.

[14] X. Huang, X. Chen, A. Li, D. Atinafu, H. Gao, W. Dong, G. Wang, Shape-stabilized phase change materials based on porous supports for thermal energy storage applications, Chem. Eng. J. 356 (2018) 641–661, https://doi.org/10.1016/j.cej.2018.09.013.
[15] H. Xu, Y. Wang, X. Han, Analytical considerations of thermal storage and interface evolution of a PCM with/without porous media, Int J Numer Method H 30 (2019) 373–400, https://doi.org/10.1108/hff-02-2019-0094.
[16] S. Abishek, A.J.C. King, N. Nadim, B.J. Mullins, Effect of microstructure on melting in metal-foam/paraffin composite phase change materials, Int. J. Heat Mass Tran. 127 (2018) 135–144, https://doi.org/10.1016/j.ijheatmasstransfer.2018.07.054.
[17] Y. Xu, Q. Ren, Z.-J. Zheng, Y.-L. He, Evaluation and optimization of melting performance for a latent heat thermal energy storage unit partially filled with porous media, Appl. Energy 193 (2017) 84–95, https://doi.org/10.1016/j.apenergy.2017.02.019.
[18] X. Meng, L. Yan, J. Xu, F. He, H. Yu, M. Zhang, Effect of porosity and pore density of copper foam on thermal performance of the paraffin-copper foam composite Phase-Change Material, Case Stud Therm Eng, 22 100742 (2020), https://doi.org/10.1016/j.csite.2020.100742.
[19] X. Zhou, H. Xiao, J. Feng, C. Zhang, Y. Jiang, Preparation and thermal properties of paraffin/porous silica ceramic composite, Compos. Sci. Technol. 69 (2009) 1246–1249, https://doi.org/10.1016/j.compscitech.2009.02.030.
[20] S. Harikrishnan, M. Deenadhayalan, S. Kalaiselvam, Experimental investigation of solidification and melting characteristics of composite PCMs for building heating application, Energy Convers. Manag. 86 (2014) 864–872, https://doi.org/10.1016/j.enconman.2014.06.042.
[21] A. Babapoor, G. Karimi, Thermal properties measurement and heat storage analysis of paraffinnanoparticles composites phase change material: comparison and optimization, Appl. Therm. Eng. 90 (2015) 945–951, https://doi.org/10.1016/j.applthermaleng.2015.07.083.
[22] M. D'Haese, F. Langouche, P.V. Puyvelde, On the effect of particle size, shape, concentration, and aggregation on the flow-induced crystallization of polymers, Macromolecules 46 (2013) 3425–3434, https://doi.org/10.1021/ma400318a.
[23] N. Pan, P.W. Gibson, Thermal and Moisture Transport in Fibrous Materials, 2006, https://doi.org/10.1201/9781439824351.
[24] R. Mishra, J. Militky, Nanotechnology in Textiles | ScienceDirect, 2018, https://doi.org/10.1016/C2017-0-02936-1.
[25] Y. Wang, J. Yao, G. Zhu, J. Militky, J. Marek, M. Venkataraman, G. Zhang, A novel method for producing bi-component thermo-regulating alginate fiber from phase change material microemulsion,, Textil. Res. J. 90 (2020) 1038–1044, https://doi.org/10.1177/0040517519886075.
[26] Y. Wang, Y. Ma, R. Chen, Y. Su, Thermal protective performance of firefighting protective clothing incorporated with phase change material in fire environments, Fire Mater. 45 (2021) 250–260, https://doi.org/10.1002/fam.2928.
[27] M. Zhao, The usage of phase change materials in fire fighter protective clothing: its effect on thermal protection, Iop Conf Ser Mater Sci Eng, 274 12136 (2017), https://doi.org/10.1088/1757-899x/274/1/012136.
[28] S.I. Golestaneh, G. Karimi, A. Babapoor, F. Torabi, Thermal performance of co-electrospun fatty acid nanofiber composites in the presence of nanoparticles, Appl. Energy 212 (2018) 552–564, https://doi.org/10.1016/j.apenergy.2017.12.055.
[29] H. Che, Q. Chen, Q. Zhong, S. He, The effects of nanoparticles on morphology and thermal properties of erythritol/polyvinyl alcohol phase change composite fibers,, E-Polymers 18 (2018) 321–329, https://doi.org/10.1515/epoly-2017-0176.
[30] H. Ke, M.U.H. Ghulam, Y. Li, J. Wang, B. Peng, Y. Cai, Q. Wei, Ag-coated polyurethane fibers membranes absorbed with quinary fatty acid eutectics solid-liquid phase change materials for storage and retrieval of thermal energy, Renew. Energy 99 (2016) 1–9, https://doi.org/10.1016/j.renene.2016.06.033.
[31] S.B. Stanković, D. Popović, G.B. Poparić, Thermal properties of textile fabrics made of natural and regenerated cellulose fibers, Polym. Test. 27 (2008) 41–48, https://doi.org/10.1016/j.polymertesting.2007.08.003.
[32] M. Vollmer, Newton's law of cooling revisited, Eur. J. Phys. 30 (2009) 1063–1084, https://doi.org/10.1088/0143-0807/30/5/014.
[33] Y. Kou, S. Wang, J. Luo, K. Sun, J. Zhang, Z. Tan, Q. Shi, Thermal analysis and heat capacity study of polyethylene glycol (PEG) phase change materials for thermal energy storage applications, J. Chem. Thermodyn. 128 (2018) 259–274, https://doi.org/10.1016/j.jct.2018.08.031.
[34] S. Sundararajan, A.B. Samui, P.S. Kulkarni, Versatility of polyethylene glycol (PEG) in designing solid–solid phase change materials (PCMs) for thermal management and their application to innovative technologies, J. Mater. Chem. 5 (2017) 18379–18396, https://doi.org/10.1039/c7ta04968d.
[35] K. Yang, M. Venkataraman, Y.-F. Wang, X.-M. Xiong, T. Yang, J. Wiener, J. Militky, R. Mishra, J. Marek, G.-C. Zhu, J.-M. Yao, Thermal performance of A multi-layer composite containing PEG/laponite as PCMs, J. Fiber Bioeng. Inf. 13 (2020) 61–68, https://doi.org/10.3993/jfbim00330.
[36] X. Xiong, M. Venkataraman, T. Yang, K. Kucerova, J. Militký, K. Yang, G. Zhu, J. Yao, Transport properties of electro-sprayed polytetrafluoroethylene fibrous layer filled with aerogels/phase change materials, nanomaterials-basel, 10 2042 (2020), https://doi.org/10.3390/nano10102042.
[37] T. Yang, X. Xiong, R. Mishra, J. Novák, J. Militký, Acoustic evaluation of Struto nonwovens and their relationship with thermal properties, Textil. Res. J. 88 (2018) 426–437, https://doi.org/10.1177/0040517516681958.
[38] K. Yang, M. Venkataraman, J. Karpiskova, Y. Suzuki, S. Ullah, I.-S. Kim, J. Militky, Y. Wang, T. Yang, J. Wiener, G. Zhu, J. Yao, Structural analysis of embedding polyethylene glycol in silica aerogel, Microporous Mesoporous Mater. 310 (2020) 110636, https://doi.org/10.1016/j.micromeso.2020.110636.
[39] W. Weng, G. Chen, D. Wu, Crystallization kinetics and melting behaviors of nylon 6/foliated graphite nanocomposites, Polymer 44 (2003) 8119–8132, https://doi.org/10.1016/j.polymer.2003.10.028.
[40] A.T. Lorenzo, M.L. Arnal, J. Albuerne, A.J. Müller, DSC isothermal polymer crystallization kinetics measurements and the use of the Avrami equation to fit the data: guidelines to avoid common problems, Polym. Test. 26 (2007) 222–231, https://doi.org/10.1016/j.polymertesting.2006.10.005.
[41] X. Min, M. Fang, Z. Huang, Y. Liu, Y. Huang, R. Wen, T. Qian, X. Wu, Enhanced thermal properties of novel shape-stabilized PEG composite phase change materials with radial mesoporous silica sphere for thermal energy storage, Sci Rep-UK, 5 12964 (2015), https://doi.org/10.1038/srep12964.
[42] R.S. Andriamitantsoa, W. Dong, H. Gao, G. Wang, PEG encapsulated by porous triamide-linked polymers as support for solid-liquid phase change materials for energy storage, Chem. Phys. Lett. 671 (2017) 165–173, https://doi.org/10.1016/j.cplett.2017.01.028.
[43] D. Feng, P. Li, Y. Feng, Y. Yan, X. Zhang, Using mesoporous carbon to pack polyethylene glycol as a shape-stabilized phase change material with excellent energy storage capacity and thermal conductivity, Microporous Mesoporous Mater. 110631 (2020), https://doi.org/10.1016/j.micromeso.2020.110631.
[44] N.S. Murthy, Crystallization in multiphase polymer systems, Undefined (2018) 49–72, https://doi.org/10.1016/b978-0-12-809453-2.00003-7.
[45] A. Safari, R. Saidur, F.A. Sulaiman, Y. Xu, J. Dong, A review on supercooling of Phase Change Materials in thermal energy storage systems,, Renew. Sustain. Energy Rev. 70 (2017) 905–919, https://doi.org/10.1016/j.rser.2016.11.272.
[46] K.P. Črešnar, L.F. Zemljič, L. Papadopoulos, Z. Terzopoulou, A. Zamboulis, P. A. Klonos, D.N. Bikiaris, A. Kyritsis, P. Pissis, Effects of Ag, ZnO and TiO2 nanoparticles at low contents on the crystallization, semicrystalline morphology, interfacial phenomena and segmental dynamics of PLA, Mater Today Commun, 27 102192 (2021), https://doi.org/10.1016/j.mtcomm.2021.102192.
[47] V. Baheti, Y. Wang, Ohmic heating and mechanical stability OF carbon fabric/green epoxy composites after incorporation OF fly ash particles, Mater Today Commun (2020) 101710, https://doi.org/10.1016/j.mtcomm.2020.101710.

9.4 Research journal article-4 (Progress in Organic Coatings, Q1, IF: 6.6)

Progress in Organic Coatings 172 (2022) 107151

Contents lists available at ScienceDirect

Progress in Organic Coatings

journal homepage: www.elsevier.com/locate/porgcoat

Mass transfer and thermal buffering effect of hydrophobic fabrics with single-side coating of MPCMs

Kai Yang [a,*], Lenka Martinkova [b], Ondrej Ctibor [b], Xiuling Zhang [a], Mohanapriya Venkataraman [a], Jakub Wiener [a], Guocheng Zhu [c,d], Guoqing Zhang [e], Juming Yao [d,e,f], Jiri Militky [a]

[a] Department of Material Engineering, Faculty of Textile Engineering, Technical University of Liberec, Liberec, Czech Republic
[b] INOTEX spol. s.r.o., Stefanikova 1208, 544 01 Dvur Kralove nad Labem, Czech Republic
[c] College of Textiles and Engineering, Zhejiang Sci-tech University, Xiasha Education Park, PR China
[d] Zhejiang-Czech Joint Laboratory of Advanced Fiber Materials, Zhejiang Sci-tech University, Xiasha Education Park, PR China
[e] School of Materials and Engineering, Zhejiang Sci-tech University, Xiasha Education Park, PR China
[f] School of Materials Science and Chemical Engineering, Ningbo University, Ningbo City, PR China

ARTICLE INFO

Keywords:
MPCM
Hydrophobicity
Fabric
Breathability
Water transfer
Thermal buffering effect

ABSTRACT

The incorporation of microencapsulated phase change materials (MPCMs) into textiles have been realized for personal temperature regulation. However, the hydrophobicity and breathability of MPCM-incorporated fabrics remained improvement. In this work, four commercial fabrics were first treated with a hydrophobic coating and the MPCMs were coated on the hydrophobic fabrics via pad-dry-curing coating method. The morphology, hydrophobicity, thermal energy storage, thermal buffering effect, moisture transfer, and breathability of the MPCM-coated fabrics were investigated. As a result, the MPCMs were well coated on one side of the hydrophobic fabrics. The water contact angles of the MPCM-coated side of MPCM-coated fabrics were higher than 100°, and the anti-fouling property was found. Besides, the breathability was reduced when an MPCM coating was on the hydrophobic fabric. The one-way moisture transfer behavior was little affected when there was an MPCM coating on the knitted and woven fabrics while significantly reduced when the 3D knitted fabric was the substrate. The thermal energy storage of the MPCM-coated fabrics ranged from 1.89 to 8 J/g, which was related to the used fabric type. Correspondingly, the thermal buffering effect of MPCM-coated fabrics was found, and a better thermal buffering effect was proposed when the MPCM-coated side faced the heating source.

1. Introduction

Personal temperature management has been studied for decades [1,2]. Incorporation of organic phase change materials (PCMs) (e.g., paraffin wax, fatty acid, polyethylene glycol, etc.) into textiles is proposed as an easy method for temperature management [3–7]. During the phase transition of the PCMs over a certain temperature, the thermal resistance of the PCMs is increased and the thermal energy is absorbed or released [6,8,9]. The leakage of the PCMs is the main problem for the practical applications. To avoid leakage, three main methods have been proposed, including form-stable PCMs (FSPCMs), solid-solid PCMs (SSPCMs) and microencapsulated PCMs (MPCMs) [3,10,11]. Especially, the MPCMs as one kind of PCMs consisting of the shell and the core are aimed to support the high thermal stability and avoid the leakage of PCMs during phase transition [12,13]. Compared with FSPCMs and SSPCMs, the MPCMs have stable thermal behavior under various environments (e.g., humidity, etc.) because of their shell-core structure. The incorporation of the MPCMs into textiles has been studied for decades and includes two ways: 1) the fabrication of PCM fibers by incorporating MPCMs into polymer fiber matrix [14–16] and 2) coating of MPCMs on the fabrics [17–20]. For the former one, it is suggested that the higher encapsulation amount of the MPCMs in the PCM fibers could enhance the final thermal energy storage while reducing the mechanical property of the final PCM fibers. Still, there is a limitation for the maximum encapsulation amount of the MPCMs in the PCM fibers. Compared with PCM fibers, the coating of the MPCMs on the fabrics is more convenient, and the MPCM amount is controlled.

To prepare the MPCM-coated fabrics, the pad-dry-curing method is

* Corresponding author.
E-mail address: kai.yang@tul.cz (K. Yang).

https://doi.org/10.1016/j.porgcoat.2022.107151
Received 10 April 2022; Received in revised form 10 August 2022; Accepted 22 August 2022
Available online 7 September 2022

Table 1
Description of the used commercial fabrics.

Sample code	Component	S (g/m^2)	L (mm)	Structure
S1	100%PET	200	0.57 ± 0.01	Warp knit
S2	65%cotton/35%PET	240	0.44 ± 0.01	3/1 twill
S3	57%cotton/41%PET/2% Carbon	170	0.38 ± 0.01	3/1 twill
S4	100%PET	378	2.71 ± 0.10	3D knitting

Table 2
Technical parameter for pad-dry-curing coating method.

Process	T_{in} (°C)	T_{room} (°C)	T_{out} (°C)	$v_{feeding}$ (m/min)
Coating process	30	120	30	0.5
Curing process	30	150	30	0.5

Table 3
Basic information of coated fabrics.

Sample code	Used fabric substrate	S (g/m^2)	L (mm)	p_1 (%)	p_2 (%)
SH1	S1	212	0.54 ± 0.01	6.00	–
SH2	S2	250	0.53 ± 0.01	4.17	–
SH3	S3	178	0.41 ± 0.01	4.71	–
SH4	S4	390	2.76 ± 0.02	3.17	–
SMH1	SH1	232	0.52 ± 0.01	–	10.00
SMH2	SH2	280	0.46 ± 0.01	–	12.50
SMH3	SH3	202	0.38 ± 0.01	–	14.12
SMH4	SH4	457	2.80 ± 0.06	–	17.72

S, L, p_1, and p_2: areal density of the sample, the thickness of the sample, add-on of the hydrophobic coating layer, and add-on of the MPCM layer.

Table 4
Description of reference samples.

Sample code	Used fabric	Coating type	S (g/m^2)	L (mm)
STB1	S1	Thickner + binder	232.81	0.47 ± 0.01
STB2	S2		246.88	0.42 ± 0.01
STB3	S3		192.19	0.36 ± 0.01
STB4	S4		428.13	2.73 ± 0.01
SMTB1	S1	MPCM + thickner + binder	239.06	0.49 ± 0.01
SMTB2	S2		253.13	0.42 ± 0.01
SMTB3	S3		218.75	0.37 ± 0.01
SMTB4	S4		448.44	2.82 ± 0.02

the most popular method, and the binder is necessary for the MPCM coating to enhance thermal stability [21]. For the MPCM-coated fabrics, three main properties were specified, including thermal property, mechanical property, and breathability. Higher MPCMs amount on the fabrics supported higher thermal energy storage and better thermal buffering effect, while reduced the air permeability [22]. Besides, it was revealed that the curing temperature more affected the tensile strength and elongation then MPCM content [23]. The air permeability of MPCM-coated fabrics is reduced while it would be complicated for the water vapor permeability [24,25]. On one hand, the polarity of both MPCMs and binders can enhance the water vapor transmission. On another hand, more content of both MPCMs and binders may also reduce the porosity of the fabric and result in decreased water vapor transmission. Still, the surficial chemistry (e.g. hydrophobicity etc.) of the MPCM-coated fabrics is also significant. The hydrophobicity of the MPCM-coated fabrics could support anti-fouling property, anti-icing property etc. [26,27]. For the MPCM-coated fabrics, the hydrophobicity is determined by inherent hydrophobicity of MPCMs or binders. For example, Fabio Alexandre Pereira Scacchetti et al. made a coating of MPCMs, thyme oil, and monochlorotriazinebeta-cyclodextrin (MCT-β-CD) on cotton fabric. Although MPCMs were hydrophobic, the inherent hydrophilic property of MCT-β-CD had a stronger influence on surface chemistry, and the unstable hydrophobic property was found [28]. M. Karthikeyan et al. made a coating of nano MPCMs on different fabrics by using polyurethane binding agents and revealed that the water absorbance was weakened when there was a nano MPCMs coating on the fabric which was caused by a combination of reduced pores and decreased hydrophilic parts [29,30]. Jun Li et al. fabricated an MPCM consisting of CuO-doped polyurea as shell and n-eicosane as core and coated the fabric using binders [31]. It was revealed that the microstructure constructed by the distribution of MPCMs on fabrics supported the hydrophobic fabric, while the hydrophobicity decreased after 30 washing cycles. Although there has been great progress in the MPCM-coated fabric via the pad-dry-curing method, the hydrophobicity stability remains to be improved.

To support highly stable hydrophobicity of MPCM-coated fabrics, a hydrophobic coating layer as outer layer totally covering MPCM-incorporated textiles is feasible [32,33], while no breathability would be found if the similar method was applied for fabrics. How to support the hydrophobicity and the breathability of the MPCM-coated fabric remains to be revealed. It is noticed that the wicking property of hydrophobic fabrics could support the penetration of liquid by adjusting the viscosity and amount of the solution, fabric structure and external pressure [34]. From this point of view, to make a coating of the MPCMs on the hydrophobic fabric is an alternative to support thermal buffering effect while the hydrophobicity is little affected.

In this work, four commercial fabrics were selected for MPCM coatings according to industrial application. We first made a hydrophobic coating on the commercial fabrics and then made the MPCM coating on the fabricated hydrophobic fabrics via pad-dry-curing coating method. A systematic investigation of the MPCM-coated hydrophobic fabrics was done, including the breathability, hydrophobicity, anti-fouling property, water transfer behavior, thermal energy

Table 5
Areal density of washed samples.

Sample code	Washed fabric	S (g/m^2)
SWH1	SH1	210.94 ± 2.43
SWH2	SH2	248.44 ± 2.73
SWH3	SH3	176.56 ± 2.43
SWH4	SH4	387.50 ± 2.99
SWTB1	STB1	231.25 ± 2.19
SWTB2	STB2	248.44 ± 2.45
SWTB3	STB3	193.75 ± 2.22
SWTB4	STB4	426.56 ± 2.91
SWMH1	SMH1	184.38 ± 2.00
SWMH2	SMH2	221.88 ± 2.31
SWMH3	SMH3	162.50 ± 2.13
SWMH4	SMH4	359.38 ± 2.13
SWMTB1	SMTB1	237.66 ± 2.89
SWMTB2	SMTB2	249.53 ± 2.44
SWMTB3	SMTB3	210.94 ± 2.23
SWMTB4	SMTB4	442.81 ± 2.43

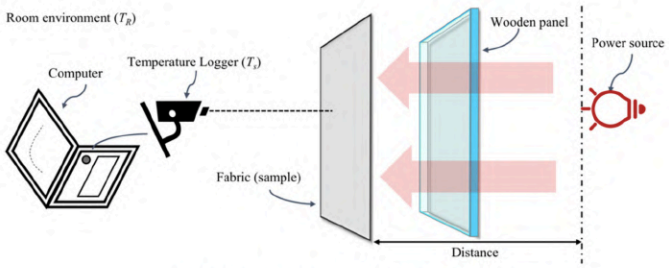

Fig. 1. Schematic diagram of the T-history setup.

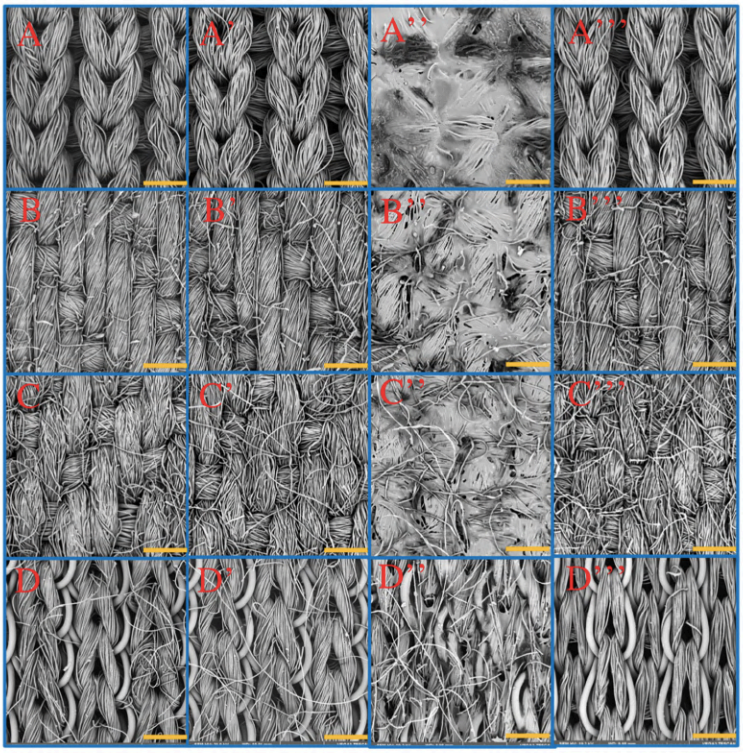

Fig. 2. Morphology of samples (A, B, C, and D: the morphology of pure commercial fabric S1, S2, S3, and S4, respectively; A′, B′, C′ and D′: the morphology of hydrophobic fabric HS1, HS2, HS3, and HS4, respectively; A″, B″, C″ and D″: the morphology of MPCM-coated side of hydrophobic MPCM-coated fabric MHS1, MHS2, MHS3, and MHS4, respectively; A‴, B‴, C‴ and D‴: the morphology of uncoated side of hydrophobic MPCM-coated fabric MHS1, MHS2, MHS3, and MHS4, respectively) (Length of yellow bar: the scale of 500 μm).

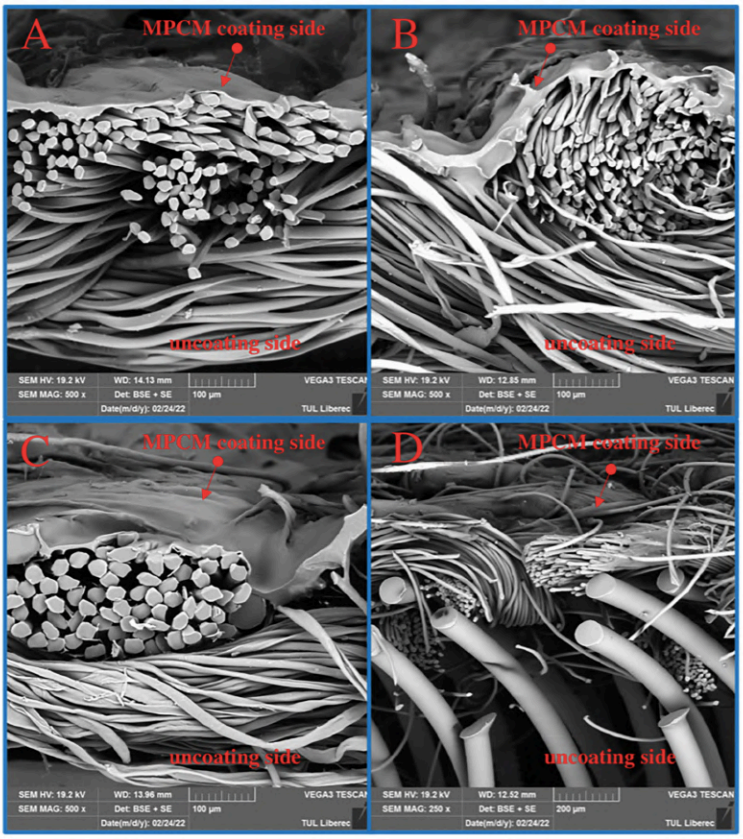

Fig. 3. Cross-section of hydrophobic MPCM-coated fabric (A, B, C, and D: SMH1, SMH2, SMH3, and SMH4, respectively).

storage, and thermal buffering effect.

2. Experimental

2.1. Materials

The details of four commercial fabrics as substrates, including the areal density (S) (g/m^2), the thickness (L) (mm), and the structure, are given in Table 1. The commercial hydrophobic dispersion BCS 01 (C6-based fluorocarbon) was purchased from the BAYGARD company (Einsteinstraat 11, 6716 AC Ede, Netherlands) (https://tanatexchemicals.com/products/baygard-bcs-2/). The chemical code SW3 (1-(1,5-dimethyl-1H-pyrazol-3-yl)methanamine) was purchased from LAMBERTI S.p.A. The MPCMs slurry was provided by Zhejiang Sci-tech University, which contained 35 wt% MPCMs with dodecanol-laurate as core and modified PMMA as shell and 65 wt% mixture of water and emulsifiers [35].

2.2. Preparation of hydrophobic coating

For the hydrophobic coating process, the hydrophobic solution was prepared firstly by physically blending BCS 01 solution with water (10 g/L) till the homogenous solution was obtained. The stirring speed was 500 rpm. Then, the immersion method was used to prepare the hydrophobic fabrics, including the coating and curing processes (Werner-Mathis continuous R2R pilot finishing line) (Table 2). During the coating process, the fabric was immersed in the hydrophobic solution at room temperature (30 °C) and then experienced the drying temperature of 120 °C for 2 min. Then, the 2 min curing process was subsequently for the hydrophobic fabrics with a higher drying temperature of 150 °C. Finally, the hydrophobic fabrics were successfully prepared and labeled according to the fabrics, given in Table 3 in detail.

2.3. Preparation of MPCM coating

Before the MPCM coating process on the hydrophobic fabrics, the MPCM solution was prepared by physically blending with the acrylic thickener (VERSACOL P, Synthesia, a.s. the Czech Republic), SW3 with

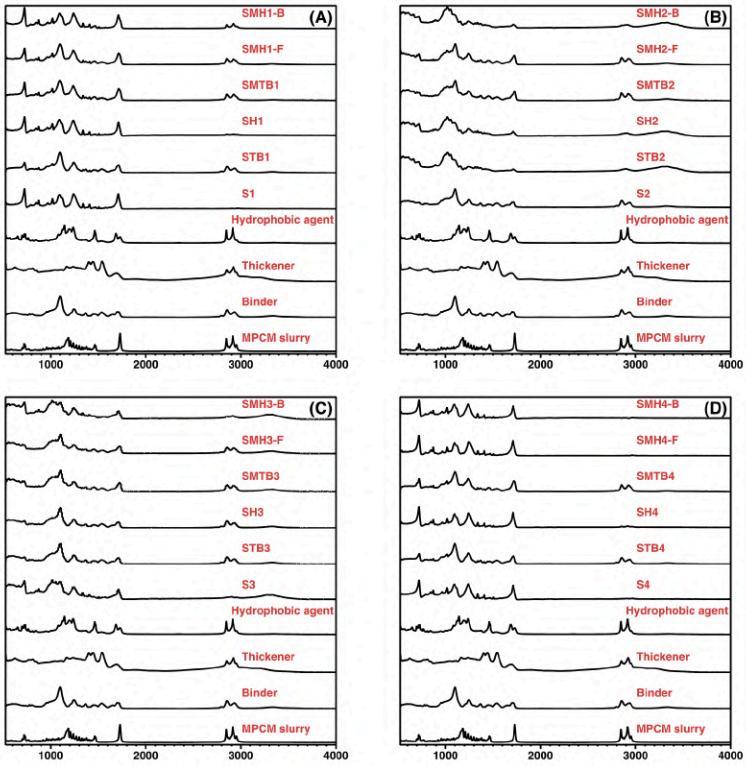

Fig. 4. FTIR curves of MPCM-coated fabrics (A, B, C and D: S1-based samples, S2-bases samples, S3-based samples and S4-based samples).

the MPCM solution. The weight ratio of the SW3 to the MPCM solution was set as 1:1, and a small amount of the thickener (~1 wt% in solution) was added to the SW3/MPCM solution during the physical stirring process with high stirring speed of 500 rpm till the viscosity of the solution reached around 60 dPa s. The prepared MPCM solution was coated on the hydrophobic fabrics via a pad-dry-curing coating process using the coating machine (Werner-Mathis continuous R2R pilot finishing line) and blade coating was used. The parameters of pad-dry-curing process for coating of MPCMs on the hydrophobic fabrics were same as one for the preparation of hydrophobic fabrics, which was given in Table 2. Finally, the MPCM-coated hydrophobic fabrics were successfully prepared and labeled according to the fabrics, which was given in Table 3. Additionally, the add-on of the hydrophobic coating layer (p_1) and add-on of the MPCM layer (p_2) were calculated according to Eqs. (1) and (2), respectively. The subscript S_0, S_1 and S_2 represented the areal density of the fabric without anything, the hydrophobic fabric, and the MPCM-coated hydrophobic fabric. All details of the samples were given in Table 3.

$$p_1 = \frac{S_1 - S_0}{S_0} \times 100\% \quad (1)$$

$$p_2 = \frac{S_2 - S_1}{S_1} \times 100\% \quad (2)$$

To reveal the effect of thickener, binder or MPCMs slurry on the hydrophobicity, the reference samples coated with thickener and binder or with MPCMs, thickener and binder were also prepared by using blade coating and pad-dry-curing process with same parameters. The details of the reference samples were shown in Table 4.

2.4. Preparation of washed MPCM-coated fabrics

To reveal the lifetime of the prepared MPCM-coated fabrics in practice, a washing treatment was for the MPCM-coated fabrics and carried out by washing MPCM-coated fabrics for 1 h with washing powders. Then, the thermal storage property of the washed MPCM-coated fabrics was investigated. Correspondingly, the samples treated with washing treatment were labeled as SWMH1, SWMH2, SWMH3, and SWMH4, which corresponded to the samples SMH1, SMH2, SMH3, and SMH4, respectively. The areal density values of washed samples were given in Table 5.

2.5. Tests and methods

2.5.1. Characterization of morphology

Scanning electronic microscopy (SEM) (VEGA TESCAN Inc., Lincoln, NE, USA) was used to characterize the morphology and the cross-section of the prepared fabrics. The electronic voltage of 20 kV was applied for

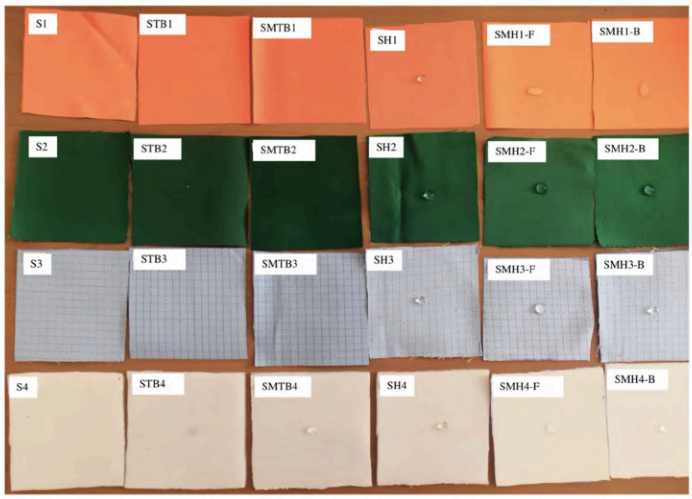

Fig. 5. Wetting behavior of all the samples after 5 min (sample size: 6 cm × 6 cm).

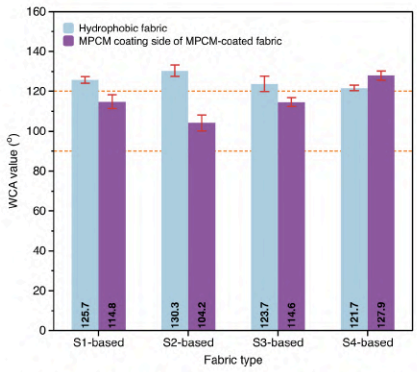

Fig. 6. WCA values of the hydrophobic fabrics and the MPCM-coated side of MPCM-coated fabrics.

SEM measurement. Besides, it was necessary to characterize the morphology of pure MPCMs to compare with the MPCM coating layer on the fabric. In this case, the MPCMs slurry was dropped on the viscose fabric and dried for one week. Then, the MPCM-coated viscose fabric was characterized and only the morphology of MPCMs was focused on.

2.5.2. Characterization of chemical compatibility

The attenuated total reflection-Fourier transforms infrared (ATR-FTIR) spectroscopy was used to characterize the chemical compatibility between various coating layers (including hydrophobic coating and MPCM coating) and fabrics. The machine Thermo Nicolet AVATAR 330 FT-IR was used, and the spectrum was obtained in the spectral region from 4000 cm^{-1} to 525 cm^{-1} with 2 cm^{-1} resolutions.

2.5.3. Characterization of hydrophobicity

The hydrophobic property of the reference fabrics, the hydrophobic fabrics, and the MPCM-coated fabrics was investigated using the droplet method according to standard 27,448:200. 5 μL water droplets were placed on the surface of the reference fabrics, the hydrophobic fabrics and the MPCM-coated side of the MPCM-coated fabrics.

2.5.4. Characterization of anti-fouling property

The anti-fouling property of the samples was evaluated in two steps by using various liquids, including water, coffee, milk, red wine, olive oil, motor oil, mustard, and ketchup: 1) the liquid was dropped on the surface of the sample for 5 min, and 2) the liquid droplet was removed from the surface of the sample. The liquid droplet and wettability on the surface of samples were recorded.

2.5.5. Characterization of breathability

Both the air permeability and the water vapor permeability of the samples were investigated to reveal the effect of the hydrophobic coating and the MPCM coating on the permeability of the fabrics.

The air permeability of the samples was investigated using an FT3300 tester according to ISO 9237. The applied pressure values for measurement were set from 40 Pa to 200 Pa with an interval of 20 Pa. Each measurement was repeated 5 times for each sample, and the statistics were obtained. Furthermore, the *Forchheimer* model was proposed to predict the air permeability of the samples under different pressure, which was expressed in Eq. (3). The Δp was the pressure difference, the L was the fabric thickness, the μ was the dynamic viscosity of the fluid (1.86×10^{-6} Pa·s), the q was the velocity of the flow (1.168 kg/m^3), the ρ was the fluid density, and the k_1 and k_2 were to characterize the permeability related to the porosity properties [36,37]. On the right hand of the equation, the first term ($\frac{\mu}{k_1}q$) represented the viscous energy losses due to friction between the fluid layers. The second term ($\frac{\rho}{k_2}q^2$) represents the kinetic energy losses due to changes in the direction of motion and to acceleration or deceleration of the fluid caused by changes in the flow path (contraction or enlargement of the pore section or pore tortuosity along the flow direction).

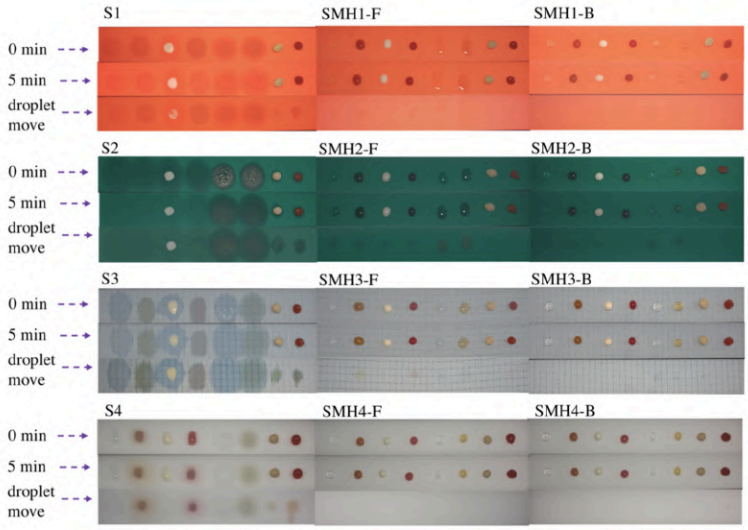

Fig. 7. Antifouling property of samples with or without MPCM coating (used liquid from left to right: water, coffee, milk, red wine, olive oil, motor oil, mustard, and ketchup) (F and B: the MPCM-coated side and uncoated side). (For interpretation of the references to color in this figure legend, the reader is referred to the web version of this article.)

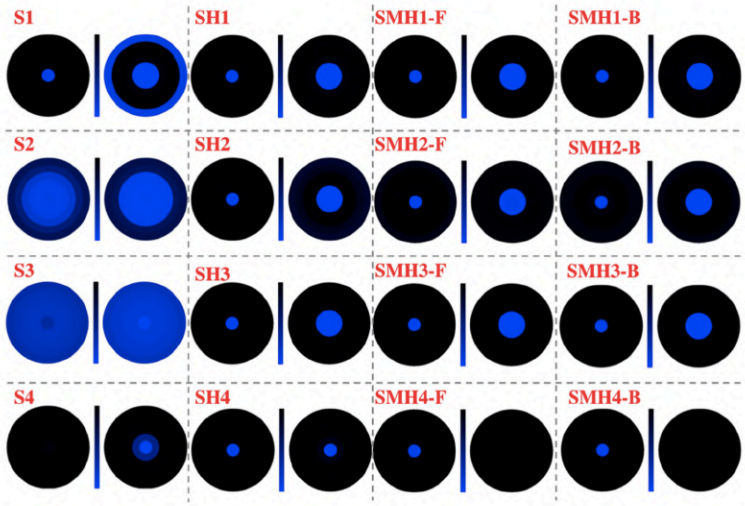

Fig. 8. Wetting areas of the pristine fabric, the hydrophobic fabric, and the MPCM-coated fabric within 2 min after the water penetration with the 30s from MMT measurement (Left image and right image corresponded to the top and bottom water content for each sample; the blue color corresponded to higher water content and the black color corresponded to lower water content; F and B: water transfer from MPCM-coated side to uncoated side and water from uncoated side to MPCM-coated side). (For interpretation of the references to color in this figure legend, the reader is referred to the web version of this article.)

Table 6
Classification of samples from MMT results according to standard ISO 81181.

Sample code	Fabric type
S1	Water penetration fabric
S2	Moisture management fabric
S3	Moisture management fabric
S4	Slow absorbing and slow drying fabric
SH1	Water penetration fabric
SH2	Water penetration fabric
SH3	Water penetration fabric
SH4	Water penetration fabric
SMH1-F	Water penetration fabric
SMH1-B	Water penetration fabric
SMH2-F	Fast absorbing and slow drying fabric
SMH2-B	Water penetration fabric
SMH3-F	Water penetration fabric
SMH3-B	Water penetration fabric
SMH4-F	Water-proof fabric
SMH4-B	Water-proof fabric

$$\frac{\Delta p}{L} = \frac{\mu}{k_1} q + \frac{\rho}{k_2} q^2 \tag{3}$$

The water vapor permeability of the samples was investigated using the PERMETEST instrument (SENSORA, Liberec, Czech Republic) according to ISO 11092. As a result, the water vapor resistance (R_{et}) (Pa m^2/W) was measured following the Eq. (4), where the P_m value was the water vapor saturate partial pressure and the P_a value was the actual partial water vapor pressure during the measurement under a certain temperature, and both q_s and q_0 were the heat flow value without and with a sample, respectively [38,39]. Each sample was measured 5 times, and the statistics were obtained.

$$R_{et} = (P_m - P_a)\left(q_s^{-1} - q_0^{-1}\right) \tag{4}$$

2.5.6. Characterization of moisture transfer behavior

The moisture management tester (MMT) (M290, SDL Atlas) following standard ISO 81181 was used to characterize the moisture transfer [40]. Each sample was measured from both MPCM-coated side and uncoated side. As a result, the classification of the samples was found.

2.5.7. Characterization of thermal energy storage

The differential scanning calorimetry (DSC) (METTLER, Swiss) was used to characterize the thermal energy storage and the phase change temperature range of the MPCM-coated fabrics. All the samples first experienced from 25 °C to 60 °C to erase the thermal history. Then, the sample experienced from 60 °C to 5 °C to have the crystallization process and then was subsequently heated from 5 °C to 60 °C to have the melting process. During the whole DSC process, the heating/cooling rate was set as 10 K/min and nitrogen (N_2) gas rate was set as 50 mL/min. Still, it was necessary to characterize the phase transition behavior of MPCMs via the DSC method. Especially, it was noticed that MPCM slurry was the solution. Then, the MPCM slurry was dropped on a glass slide and dried under room condition for one week to form MPCM film, which consisted of MPCMs and other additives. Finally, the formed MPCM film experienced the same DSC procedure, and only phase transition behavior was focused under the condition that the mass of MPCMs in the formed film was unclear. As a result, 8 parameters of the samples were obtained, including onset melting temperature (T_{om}), peak melting temperature (T_{pm}), endset melting temperature (T_{em}), onset cooling temperature (T_{oc}), peak cooling temperature (T_{pc}), endset cooling temperature (T_{ec}), melting enthalpy change (ΔH_m) and solidification enthalpy change (ΔH_c). Besides, supercooling degree (ΔT) was calculated and equal to $T_{pm} - T_{pc}$.

2.5.8. Characterization of thermal buffering effect

To characterize the thermal buffering effect of the prepared samples, the custom setup was used (Fig. 1), including the temperature data logger (FLIR E6), the radiator heater, and the computer. The measurement was performed by placing the sample away from the radiator heater at a distance of 40 cm, and the room temperature was recorded. Then, the radiator heater was turned on for 2 min; meanwhile, the temperature data logger recorded the surface temperature of the sample. After that, the radiator heater was turned off. The wooden insulation panel was immediately placed between the sample and the radiator heater to avoid the effect of the remaining heat radiation from the radiator heater on the sample. Meantime, the surface temperature of the sample was also continuously recorded by the temperature data logger after 2 min. It was noticed that the waves from radiator heater could penetrate through the samples because of porous structure of the fabrics. From this point of view, the inaccurate results for T-history during heating process may be suitable for characterization of thermal buffering effect. Therefore, only the cooling process was acceptable since there was no effect of the remaining heat radiation to affect the cooling process of the sample because of the existence of the wooden insulation panel. Besides, the overall thermal conductivity (k) (W m^{-1} K^{-1}) and thickness (L) (mm) of the samples were measured via ALAMBETA, which was for the further analysis of the thermal buffering effect [41,42].

3. Results and discussion

3.1. Effect of hydrophobic coating and MPCM coating on the morphology of the fabric

Figs. 2 and 3 presented the morphology of all the samples. The hydrophobic coating had little effect on the morphology since the hydrophobic fabrics had similar morphology as the reference fabrics. For MPCM-coated fabrics, the MPCM coating was well kept on one side of

Table 7
The measured air permeability values of all the samples under different pressure difference.

Sample code	Air permeability (mm/s)								
	40 Pa	60 Pa	80 Pa	100 Pa	120 Pa	140 Pa	160 Pa	180 Pa	200 Pa
S1	287 ± 7	400 ± 8	505 ± 8	596 ± 6	681 ± 8	765 ± 7	843 ± 8	920 ± 13	991 ± 10
S2	38 ± 7	56 ± 2	74 ± 2	93 ± 3	110 ± 3	125 ± 3	143 ± 4	158 ± 4	175 ± 5
S3	49 ± 1	75 ± 1	99 ± 1	123 ± 1	144 ± 4	168 ± 2	190 ± 2	212 ± 2	235 ± 3
S4	611 ± 16	853 ± 18	1070 ± 17	1260 ± 26	1443 ± 32	1627 ± 31	1790 ± 36	1937 ± 47	2103 ± 42
SH1	337 ± 1	459 ± 6	567 ± 7	666 ± 6	760 ± 5	848 ± 6	933 ± 8	1013 ± 11	1090 ± 10
SH2	78 ± 4	115 ± 5	151 ± 8	184 ± 10	216 ± 11	248 ± 13	279 ± 14	308 ± 15	337 ± 16
SH3	57 ± 3	86 ± 4	113 ± 5	138 ± 6	164 ± 7	189 ± 8	207 ± 4	238 ± 10	262 ± 12
SH4	590 ± 14	820 ± 18	1037 ± 25	1213 ± 31	1400 ± 36	1570 ± 36	1737 ± 42	1893 ± 38	2037 ± 42
SMH1	22 ± 1	30 ± 1	38 ± 1	46 ± 1	54 ± 1	62 ± 1	69 ± 1	76 ± 1	83 ± 1
SMH2	13 ± 1	18 ± 1	23 ± 1	29 ± 1	34 ± 1	39 ± 2	45 ± 1	50 ± 2	56 ± 2
SMH3	20 ± 1	30 ± 1	39 ± 1	49 ± 1	58 ± 1	68 ± 1	77 ± 1	87 ± 1	96 ± 1
SMH4	227 ± 3	328 ± 4	410 ± 8	489 ± 3	565 ± 6	635 ± 4	704 ± 2	770 ± 1	832 ± 3

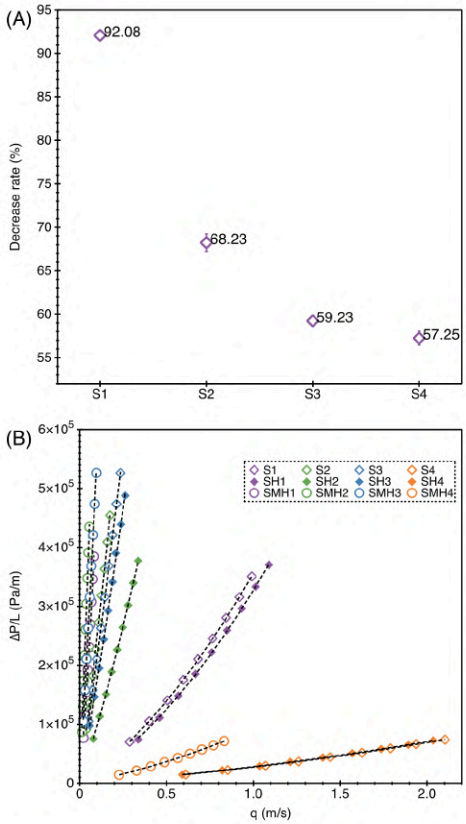

Fig. 9. The decrease rate of the MPCM-coated fabrics when compared with corresponding reference fabrics (A) and the plots of $\Delta P/L$ against q according to Eq. (3) (B) (Error bar: standard values).

Table 8
Estimated k_1, k_2 and R^2 values according to Eq. (3).

Sample code	$k_1(\times 10^{-11})$ (m^2)	$k_2(\times 10^{-5})$ (m)	R^2
S1	9.20	0.76	0.999
S2	0.80	0.07	0.999
S3	0.90	0.14	0.999
S4	93.21	16.02	0.999
SH1	10.65	0.76	0.999
SH2	2.04	0.19	0.999
SH3	1.12	0.14	0.999
SH4	90.16	15.89	0.999
SMH1	0.54	0.01	0.999
SMH2	0.26	0.01	0.999
SMH3	0.35	0.05	0.999
SMH4	34.49	3.03	0.999

the hydrophobic fabrics, and the uncoated side had a similar structure to the hydrophobic fabrics and reference fabrics. The hydrophobic coating activated as a barrier layer to resist the penetration of MPCM solution

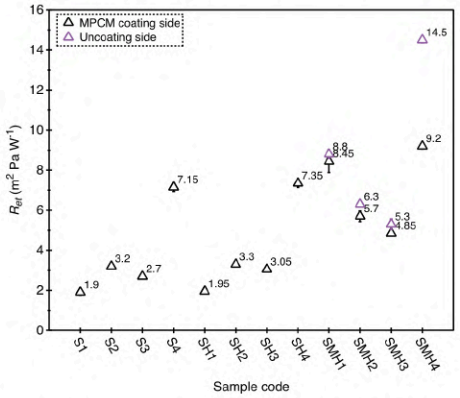

Fig. 10. Water vapor permeability of the fabrics, the hydrophobic fabrics, and the MPCM-coated fabrics.

through the whole hydrophobic fabric during the coating process. Besides, the yarns still can be observed on the MPCM-coated side. Some MPCM solution was adsorbed inside the hydrophobic fabrics because of wicking. Furthermore, no particles corresponding to the MPCMs were observed by referring to the morphology of MPCMs (Appendix 1). On one hand, the MPCMs were embedded in the MPCM coating layer. On another hand, some MPCMs may be destroyed during the preparation of the MPCM solution, although the thickener was added to avoid the destruction of MPCMs [43–45]. Besides, the coverage of the MPCM coating layer on the four hydrophobic fabrics was different from each other, and a much less MPCM coating layer was observed on the surface of SMH4. The 3D knitted fabric had stronger wicking property for MPCM solution than other fabric structures.

ATR-FTIR results provided more details of hydrophobic coatings and MPCM coatings on the fabrics, which was shown in Fig. 4. No new peaks were observed in the hydrophobic fabrics and MPCM-coated hydrophobic fabrics. So, the physical binding between hydrophobic coatings, MPCM coatings and fabrics was proposed. Especially, the unique peaks contributed from MPCMs were almost invisible, which corresponded to morphology analysis and supported that MPCMs were embedded in the coating layer.

3.2. Effect of MPCM coating on the hydrophobicity property and anti-fouling property

Fig. 5 provided wetting behavior of all the samples. By comparing with reference samples fabrics, only the samples with hydrophobic coating had WCA values, the introduction of thickener, binder or MPCM slurry did not support the hydrophobicity. Therefore, the wicking of the MPCM solution into the inner part of hydrophobic fabrics was proposed, where the MPCM coating layer only partially covered the hydrophobic fibers. In details, the hydrophobic fabrics had WCA values higher than $120^{0,}$ and the MPCM-coated fabrics had WCA values higher than 100^{0} (Fig. 6). By combining with morphology analysis, the hydrophobic 3D fabric had better wicking behavior for MPCM solution than other fabrics. The WCA values of the samples SMH1, SMH2, and SMH3 were smaller than the corresponding samples SH1, SH2, and SH3, respectively. Especially for SMH4, the WCA value was slightly increased when compared with SH4. We proposed that the major MPCM coating layer was adsorbed inside the surface of SH4, where the switch between the Wenzel state and Cassie state possibly happened [46]. Correspondingly,

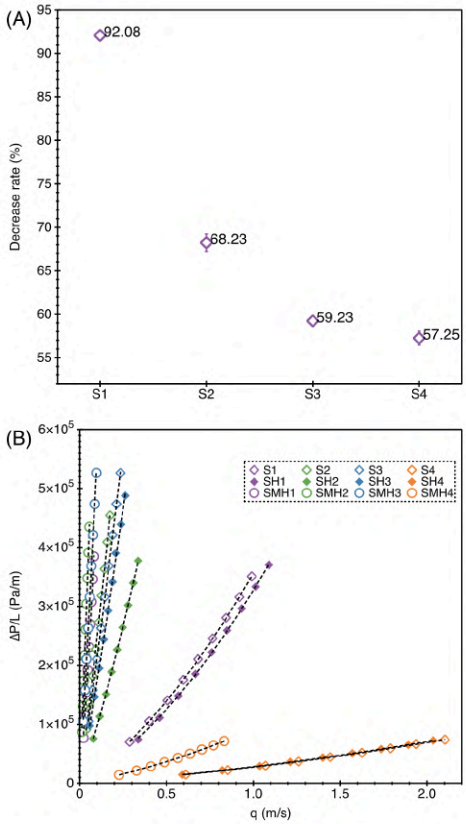

Fig. 9. The decrease rate of the MPCM-coated fabrics when compared with corresponding reference fabrics (A) and the plots of $\Delta P/L$ against q according to Eq. (3) (B) (Error bar: standard values).

Table 8
Estimated k_1, k_2 and R^2 values according to Eq. (3).

Sample code	$k_1(\times 10^{-11})$ (m^2)	$k_2(\times 10^{-5})$ (m)	R^2
S1	9.20	0.76	0.999
S2	0.80	0.07	0.999
S3	0.90	0.14	0.999
S4	93.21	16.02	0.999
SH1	10.65	0.76	0.999
SH2	2.04	0.19	0.999
SH3	1.12	0.14	0.999
SH4	90.16	15.89	0.999
SMH1	0.54	0.01	0.999
SMH2	0.26	0.01	0.999
SMH3	0.35	0.05	0.999
SMH4	34.49	3.03	0.999

the hydrophobic fabrics, and the uncoated side had a similar structure to the hydrophobic fabrics and reference fabrics. The hydrophobic coating activated as a barrier layer to resist the penetration of MPCM solution

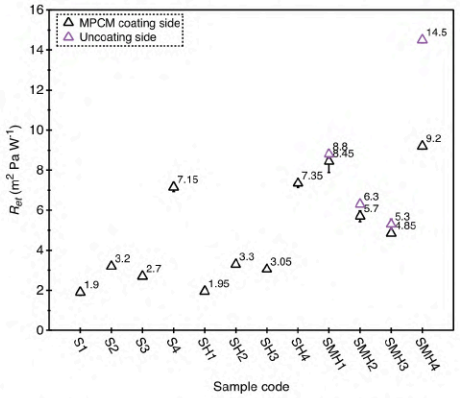

Fig. 10. Water vapor permeability of the fabrics, the hydrophobic fabrics, and the MPCM-coated fabrics.

through the whole hydrophobic fabric during the coating process. Besides, the yarns still can be observed on the MPCM-coated side. Some MPCM solution was adsorbed inside the hydrophobic fabrics because of wicking. Furthermore, no particles corresponding to the MPCMs were observed by referring to the morphology of MPCMs (Appendix 1). On one hand, the MPCMs were embedded in the MPCM coating layer. On another hand, some MPCMs may be destroyed during the preparation of the MPCM solution, although the thickener was added to avoid the destruction of MPCMs [43–45]. Besides, the coverage of the MPCM coating layer on the four hydrophobic fabrics was different from each other, and a much less MPCM coating layer was observed on the surface of SMH4. The 3D knitted fabric had stronger wicking property for MPCM solution than other fabric structures.

ATR-FTIR results provided more details of hydrophobic coatings and MPCM coatings on the fabrics, which was shown in Fig. 4. No new peaks were observed in the hydrophobic fabrics and MPCM-coated hydrophobic fabrics. So, the physical binding between hydrophobic coatings, MPCM coatings and fabrics was proposed. Especially, the unique peaks contributed from MPCMs were almost invisible, which corresponded to morphology analysis and supported that MPCMs were embedded in the coating layer.

3.2. Effect of MPCM coating on the hydrophobicity property and anti-fouling property

Fig. 5 provided wetting behavior of all the samples. By comparing with reference samples fabrics, only the samples with hydrophobic coating had WCA values, the introduction of thickener, binder or MPCM slurry did not support the hydrophobicity. Therefore, the wicking of the MPCM solution into the inner part of hydrophobic fabrics was proposed, where the MPCM coating layer only partially covered the hydrophobic fibers. In details, the hydrophobic fabrics had WCA values higher than $120^{0,}$ and the MPCM-coated fabrics had WCA values higher than 100^{0} (Fig. 6). By combining with morphology analysis, the hydrophobic 3D fabric had better wicking behavior for MPCM solution than other fabrics. The WCA values of the samples SMH1, SMH2, and SMH3 were smaller than the corresponding samples SH1, SH2, and SH3, respectively. Especially for SMH4, the WCA value was slightly increased when compared with SH4. We proposed that the major MPCM coating layer was adsorbed inside the surface of SH4, where the switch between the Wenzel state and Cassie state possibly happened [46]. Correspondingly,

Table 10
Comparison with melting enthalpy of other MPCM-coated fabrics.

Fabric	MPCM type	ΔH_m (J/g)	Ref.
Woven cotton fabric	Glauber's salt/poly(methyl methacrylate) MPCM	12.2	[49]
Woven cotton fabric	N-Hexadecane/poly(n-butyl acrylate) MPCM	9.85	[53]
Woven cotton/PET fabric		29.88	
Woven Jute fabric	Ethyl myristate/poly(methyl methacrylate) MPCM	10.27	[50]
Woven cotton fabric	Paraffin wax based MPCM	4.7–7.6	[54]
Woven PET fabric	Commercial MPCM	16.7–54.4	[55]
Knitted PET fabric		16.6–50.4	
Woven PET fabric	Graphene-modified n-octadecane/ melamine-formaldehyde MPCM	6.1–11	[51]
3D knitted PET fabric	Paraffin-based MPCM	21.78–24.22	[56]
Woven cotton fabric	Poly(diallyldimethylammonium chloride) encapsulated n-octadecane nanocapsules (Cap+)	0.46–1.59	[57]
Knitted PET fabric	Polyurea/dodecanol dodecanoate MPCM	8.89	This work
Woven PET/ cotton fabric		1.80	
Woven PET/ cotton/ carbon fabric		2.08	
3D knitted PET fabric		1.85	

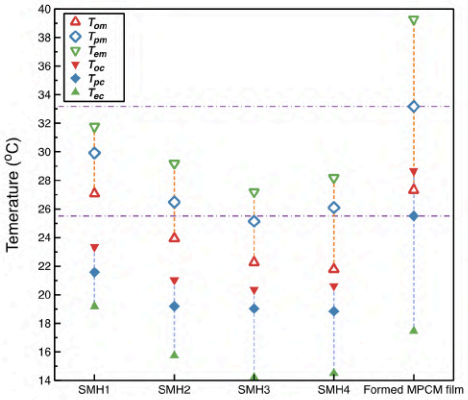

Fig. 12. Comparison of phase transition behavior of MPCM-coated fabrics with formed MPCM film.

the uncoated side. Besides, the samples SMH1, SMH2, and SMH3 were common fabrics with smaller thicknesses. By combining with Section 3.2 analysis, hydrophobic property was considered for the whole MPCM-coated fabric. The capillary force induced the hydrophobic porous fibrous structure supported the one-way water moisture transfer behavior.

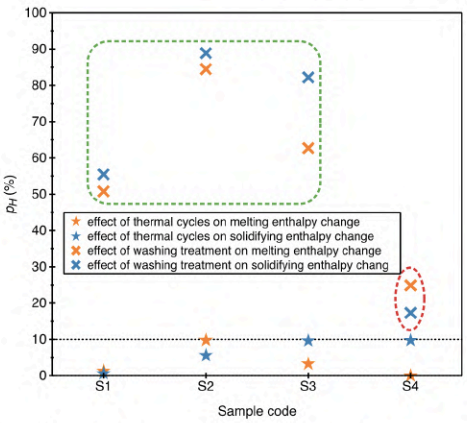

Fig. 13. The effect of the thermal cycles and the washing treatment on the change of the melting/solidifying enthalpy of the MPCM-coated fabrics.

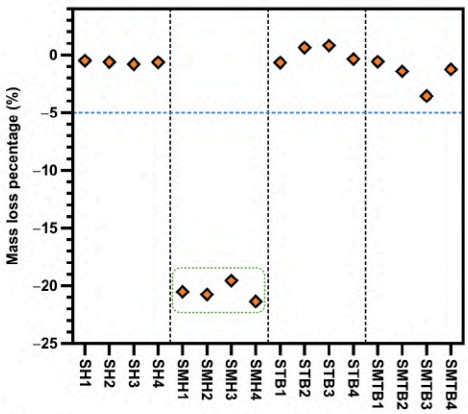

Fig. 14. Add-on percentage change of all the samples after washing treatment.

- For the sample SMH4, a much less MPCM coating layer was observed on the surface, and the MPCMs as well binders filled up the pores of the MPCM-coated side, which significantly reduced the paths of water moisture transfer through both sides

3.4. Effect of the hydrophobic coating and the MPCM coating on the breathability of the fabric

Table 7 provides the measured air permeability values of all the samples. On the one hand, the air permeability values were not generally considered to be decreased after the hydrophobic coating. On the other hand, the air permeability values were significantly reduced when the MPCM coating layer was applied to the hydrophobic fabrics. The fewer paths for the airflow could cause a decrease in the air permeability values by combining with Section 3.1. In detail, the air permeability of

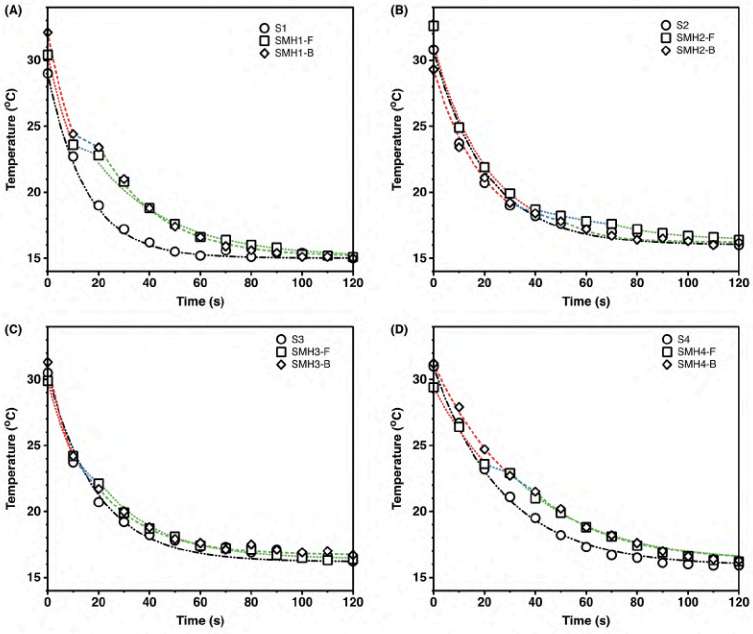

Fig. 15. T-history curves with estimated Newton's cooling law fitting model for the reference fabrics and MPCM-coated fabrics (F and B: the MPCM-coated side and uncoated side towards the radiator; black curve: a fitting model for the reference samples without PCM coating; red curve, blue curve, and green curve: a fitting model for the samples with liquid PCM, the samples with liquid-solid PCM and the samples with solid PCM; large dash and small dash: the F series and B series of samples, respectively). (For interpretation of the references to color in this figure legend, the reader is referred to the web version of this article.)

the sample SMH1, SMH2, SMH3, and SMH4 were decreased by around 92 %, 69 %, 60 % and 61 % compared with corresponding samples S1, S2, S3 and S4, respectively, schemed in Fig. 9 (A). Additionally, the plots of $\Delta P/L$ against q according to Eq. (3) for all the samples were schemed in Fig. 9 (B), and the k_1, k_2, and R^2 were provided in Table 8. All the values were around 0.999, which supported that the *Forchheimer* model could predict air permeability under different pressures. Besides, both k_1, and k_2 values related to the hydrodynamic permeability were significantly reduced when there was the MPCM coating on the fabrics, which corresponded to the air permeability behavior.

Each sample's evaporation resistance (R_{et}) was schemed in Fig. 10. The hydrophobic coating little affected the R_{et} value, while the R_{et} value was significantly increased when both hydrophobic coating and MPCM coating were on the fabric. The proposed much fewer paths for the water vapor transfer through the MPCM-coated fabrics resulted in the higher R_{et} values. Besides, the R_{et} values measured when the water vapor transferred from the uncoated side to the MPCM-coated side were relatively higher than when the water vapor transferred from the MPCM-coated side to the uncoated side. The reason could be the weaker hydrophobic property of the MPCM-coated side compared with the uncoated side.

3.5. Thermal energy storage of MPCM-coated fabrics

Fig. 11 schemed the DSC curves of all the samples, and Table 9 gave the details of the phase transition and the thermal energy storage. Besides, the DSC curves and details of formed MPCM film were shown in Appendix 1.

3.5.1. Thermal energy storage analysis

The ΔH_m and ΔH_c values of samples without water washing treatment were smaller than 10 J/g, which was much less than the thermal energy storage values in other works (Table 10). The main reason could be that the MPCM coating only covered one side of the fabric, and the MPCM content correspondingly was much less. In detail, the sample S1 had the highest ΔH_m and ΔH_c value among all the samples, which was 8.19 J/g and 8.89 J/g, respectively, while other samples without water washing treatment had the ΔH_m and ΔH_c value less than 2 J/g. The main reason could be that the knitted fabric had a better capacity to adsorb the MPCM solution during the coating process than other fabrics (e.g., woven fabric and 3D knitted fabric in this case).

3.5.2. Phase transition analysis

Since the MPCMs were directly incorporated into fabrics using binders during the coating process, the phase transition, including the melting process (e.g., T_{pm}) and solidifying process (e.g., T_{pc}), should be the same or similar to all the MPCM-coated fabrics. However, it was found that all the MPCM-coated fabrics had earlier phase transition behavior than the MPCMs (Fig. 12). Besides, the different MPCM-coated fabrics had different T_{pm} values and T_{pc} values between each other. Correspondingly, the ΔT values of different samples were different. A similar phenomenon was also observed in other research works [49–51]. Indeed, there was no clear reason for such a change of the phase transition. We proposed that some MPCMs were destroyed during the preparation of the MPCM solution and the coating method, which was caused by the poor mechanical property of MPCMs [52].

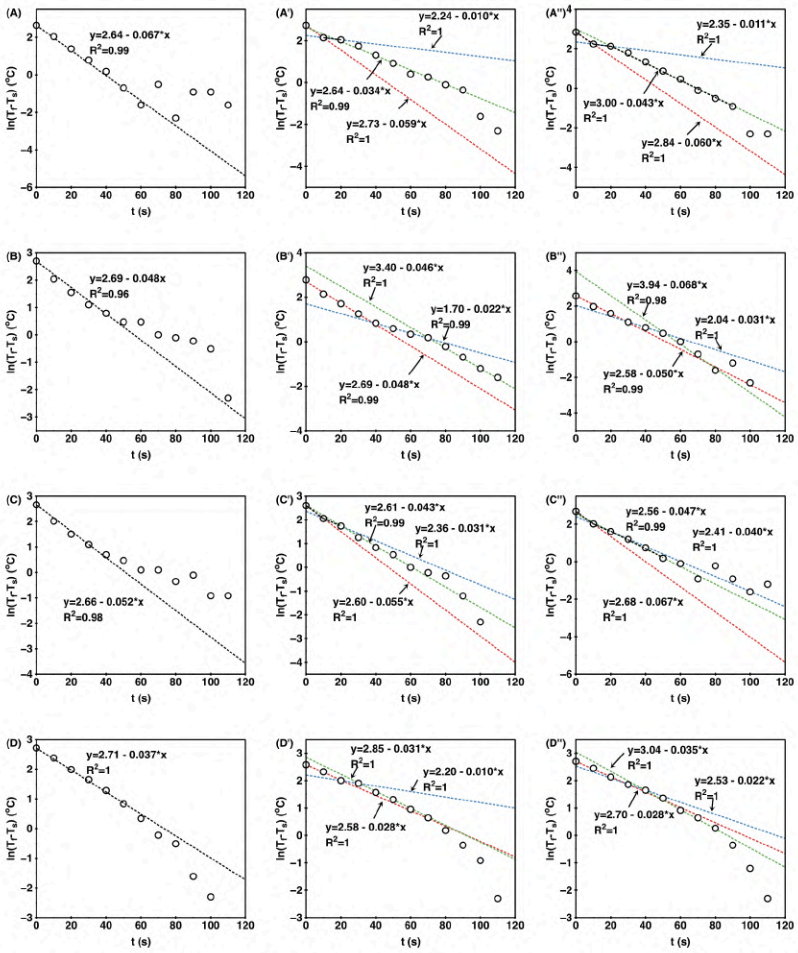

Fig. 16. Plots of $ln(T_f - T_s)$ against t (A, A′ and A″: the sample S1, SMH1-F, and SMH1-B; B, B′ and B″: the sample S2, SMH2-F, and SMH2-B; C, C′ and C″: the sample S3, SMH3-F, and SMH3-B; D, D′ and D″: the sample S4, SMH4-F, and SMH4-B) (Red curve, blue curve, and green curve: the fitting model for the samples with liquid PCM, the samples with liquid-solid PCM and the samples with solid PCM). (For interpretation of the references to color in this figure legend, the reader is referred to the web version of this article.)

3.5.3. *Thermal stability analysis after heating/cooling cycles*

The results of MPCM-coated fabrics from 1st DSC curves and 11th DSC curves have also been schemed in Fig. 11 and Table 9. The Eq. (5) was used to reveal the effect of treatment (heating/cooling cycles and washing treatment) on the thermal energy storage of the MPCM-coated fabrics, where the $\Delta H^t_{m/c}$was the enthalpy value of the sample with treatment, $\Delta H_{m/c}$ was the enthalpy value of the sample under 1st heating/cooling cycle and p_H was the enthalpy decrease rate (%). After 10 heating/cooling cycles in the DSC measurement, a slight decrease in both ΔH_m and ΔH_c value was observed for the samples, which was shown in Fig. 13 and p_H value ranged from 0 to 10 %. Besides, the phase transition process of the samples after 10 heating/cooling processes was similar to the MPCM-coated fabrics during 1st heating/cooling process. From this point of view, the MPCM-coated fabrics had a highly stable thermal energy storage performance after the heating/cooling cycles.

3.5.4. *Thermal stability analysis after washing treatment*

Unlike the heating/cooling cycles, the washing treatment significantly reduced the thermal energy storage and affected the phase transition process. In detail, the ΔH_m and ΔH_c values of the sample S1 reduced from 8.19 J/g and 8.89 J/g to 4.03 J/g and 3.96 J/g after washing treatment, respectively. Samples S2 and S3 had the ΔH_m and

Table 11
Characterization of T-history of samples.

Sample code	T_l (°C)	t_l (s)	τ_l (s)	$T_{l\text{-}s}$ (°C)	$t_{l\text{-}s}$ (s)	τ_{l-s} (s)	T_s (°C)	t_s (s)	τ_s (s)
S1	–	–	–	–	–	–	[29,15]	[0,120]	1.49
SMH1-F	[30.4,23.6]	[0,10]	16.95	[23.6,22.8]	[10,20]	100.00	[22.8,15.1]	[20,120]	29.41
SMH1-B	[32.1,24.4]	[0,10]	16.67	[24.4,23.4]	[10,20]	90.91	[23.4,15]	[20,120]	23.26
S2	–	–	–	–	–	–	[30.8,16]	[0,120]	20.83
SMH2-F	[32.6,18.7]	[0,40]	20.83	[18.7,17.6]	[40,70]	45.45	[17.6,16.4]	[70,120]	21.74
SMH2-B	[29.3,19.9]	[0,30]	20.00	[19.9,18.2]	[30,50]	32.26	[18.2,16.2]	[50,120]	14.71
S3	–	–	–	–	–	–	[30.5,16.2]	[0,120]	19.23
SMH3-F	[29.9,24.2]	[0,10]	18.18	[24.2,22.1]	[10,20]	32.26	[24.2,16.4]	[20,120]	23.26
SMH3-B	[31.3,24.2]	[0,10]	14.93	[24.2,21.7]	[10,20]	25.00	[21.7,16.7]	[20,120]	21.28
S4	–	–	–	–	–	–	[31,15.9]	[0,120]	27.03
SMH4-F	[29.4,23.6]	[0,20]	35.71	[23.6,22.9]	[20,30]	100.00	[22.9,16.2]	[30,120]	32.26
SMH4-B	[31.2,22.7]	[0,30]	35.71	[22.7,21.5]	[30,40]	45.45	[21.5,16.3]	[40,120]	28.57

Subscript *l*, *l-s*, and *s*: the τ value of the samples with liquid PCM, the samples with liquid-solid PCM, and the sample with solid PCM, respectively. (The τ_s was also for the sample without PCMs).

ΔH_c values less than 0.8 J/g after the washing treatment. The sample S4 had the ΔH_m and ΔH_c values of 1.33 J/g and 1.53 J/g after the washing treatment, respectively. The calculated p_H values were shown in Fig. 13. The sample S4 with washing treatment had the lowest p_H value ranging from 10 % to 30 %, while other samples with washing treatment had the p_H values higher than 50 %. The decrease of thermal energy storage of the samples after washing treatment was caused by loss of MPCMs. By comparing weight loss of all the samples (Fig. 14), it was found only the hydrophobic fabrics with MPCMs had more weight loss percentage after washing treatment while other samples had much small weight loss percentage.

It was noticed that there are binders, thickeners, MPCMs and hydrophobic coating in the MPCM-coated hydrophobic fabrics. To reveal which part accounted for the decrease of enthalpy and weight, the mass loss percentage (p_m) of reference samples, hydrophobic fabrics and MPCM-coated hydrophobic fabrics was compared, which was calculated according to Eq. (6). The m_0 was the weight of sample before washing and m_1 was the weight of sample after washing. Fig. 14 provided the p_m values. As a result, the hydrophobic fabrics had smaller weight loss than 2 wt%, the fabrics coated with binders and thickeners almost had same weight, the fabrics coated with MPCMs, binders and thickeners had more weight loss, and MPCM-coated hydrophobic fabrics had highest weight loss. Therefore, weak adhesion between MPCMs and thickeners and binders as well as weak adhesion between MPCMs and hydrophobic coating layers accounted for reduce of thermal energy storage after washing treatment.

$$p_H = \left| \frac{\Delta H'_{m/c} - \Delta H_{m/c}}{\Delta H_{m/c}} \right| \times 100\% \tag{5}$$

$$p_m = \frac{m_0 - m_1}{m_0} \times 100\% \tag{6}$$

3.6. The thermal buffering effect of MPCM-coated fabrics

Fig. 15 presented the T-history results of the samples with or without MPCMs. It took a long time for the MPCM-coated fabrics to cool down compared with the reference fabrics, which supported the thermal buffering effect. Besides, it was found that the initial surface temperatures were different between both sides of the MPCM-coated fabrics. The main reason was that the heating process of the samples was a result of the thermal radiation, which was affected by the porosity, the thickness, the specific heat capacity, etc. Furthermore, there were three parts in the T-history results of MPCM-coated fabrics, which corresponded to the three states of MPCMs, including liquid state, liquid-solid state (phase transition), and solid-state. To characterize the T-history, Newton's cooling law was applied [58] under the condition of small Biot number (*Bi*) (Calculation of *Bi* number was shown in Appendix 2), which was expressed in Eqs. (7) and (8). The T_f was the final stable temperature of the sample, T_s was the recorded temperature of the sample at different times, T_i was the initial time, t was the time, and τ was the cooling constant (s). High τ value corresponded to the lower cooling rate.

$$T_f - T_s = (T_f - T_i)e^{-t/\tau} \tag{7}$$

$$ln(T_f - T_s) = ln(T_f - T_i) - t/\tau \tag{8}$$

Fig. 16 presented the plots of $ln(T_f - T_s)$ against t for all the samples, and Table 11 gave the τ values. The τ_{l-s} value (τ value of samples with liquid-solid PCM) was higher than both τ_l (τ value of samples with liquid PCM) and τ_s (τ value of samples with solid PCM) values, which supported the thermal buffering effect. Additionally, the τ_{l-s} value of the F-side was higher than τ_{l-s} value of the B-side, which supported that the better thermal buffering effect was found when the MPCM-coated side faced towards the heating source.

4. Conclusion

In this work, four commercial fabrics, including two woven fabrics, one knitted fabric, and one 3D knitted fabric, were used for coating of the MPCMs. The pretreatment of the hydrophobic coating for the fabrics activated as the barrier layer for the penetration of MPCM solution, the MPCMs and binders were well deposited on one side. Besides, the wicking of MPCM solution in the surface of hydrophobic fabrics was proposed, and the hydrophobic fibers were on the surface of MPCM-coated side. As a result, the addition of the MPCM coating layer on the hydrophobic fabrics little affected the hydrophobic property, and the anti-fouling property of MPCM-coated fabrics was found. Besides, the one-way directional water moisture transfer behavior was enhanced for the samples with woven fabric structure or knitted fabric while reduced for the samples with 3D knitted fabric structure, which was caused by the difference in the distribution of MPCMs on the coated fabric surface. In addition, the breathability was reduced when there was an MPCM coating on the fabrics. Besides, the thermal enthalpy of the MPCM-coated fabrics ranged from 1 to 10 J/g. Correspondingly, the thermal buffering effect of the MPCM-coated fabrics was found and was better when MPCM-coated side towards the heating source. The heating/cooling cycles little affected the thermal energy storage and phase transition of the MPCM-coated fabrics, while the washing treatment significantly reduced the thermal energy storage. We propose that the prepared MPCM-coated fabrics be applied for personal use (e.g., underwear, jacket, shoes, etc.). Besides, the work is beneficial for the application of hydrophobic porous materials.

CRediT authorship contribution statement

Conceptualization: Kai Yang, Lenka Martinkova and Ondrej Ctibor.
Methodology: Kai Yang, Lenka Martinkova and Ondrej Ctibor.

Software: Kai Yang.

Validation: Kai Yang, Jakub Wiener, Mohanapriya Venkataraman and Jiri Militky.

Formal analysis: Kai Yang, Xiuling Zhang.

Investigation: Kai Yang, Guocheng Zhu and Juming Yao.

Resources: Jakub Wiener, Guoqing Zhang, Jiri Militky.

Data Curation: Kai Yang and Xiuling Zhang.

Writing-Original Draft: Kai Yang.

Writing-Review&Editing: Kai Yang, Xiuling Zhang, Mohanapriya Venkataraman and Jiri Militky.

Supervision: Kai Yang, Mohanapriya Venkataraman and Jiri Militky.

Project administration: Mohanapriya Venkataraman and Jiri Militky.

Funding acquisition: Mohanapriya Venkataraman and Jiri Militky.

Declaration of competing interest

We declare that we do not have any commercial or associative interest that represents a conflict of interest in connection with the work submitted.

Data availability

Data will be made available on request.

Acknowledgement

This work was supported by the project 'Advanced structures for thermal insulation in extreme conditions' (Reg. No. 21-32510M) granted by the Czech Science Foundation (GACR). Additionally, Kai Yang would like to thank Ing. Yuanfeng Wang for his assistance in providing a 3D fabric model, Ing. Jana Grabmullerova for her assistance in measuring SEM images, Ing. Denisa Knizkova for her assistance in the measurement of MMT and breathability, and Dr. Miroslava Pechociakova for her assistance in DSC measurement.

Appendix A. Supplementary data

Supplementary data to this article can be found online at https://doi.org/10.1016/j.porgcoat.2022.107151.

References

[1] S. Zeng, S. Pian, M. Su, Z. Wang, M. Wu, X. Liu, M. Chen, Y. Xiang, J. Wu, M. Zhang, Q. Cen, Y. Tang, X. Zhou, Z. Huang, R. Wang, A. Tunuhe, X. Sun, Z. Xia, M. Tian, M. Chen, X. Ma, L. Yang, J. Zhou, H. Zhou, Q. Yang, X. Li, Y. Ma, G. Tao, Hierarchical-morphology metafabric for scalable passive daytime radiative cooling, Science 373 (2021) 692–696, https://doi.org/10.1126/science.abi5484.

[2] R. Hu, Y. Liu, S. Shin, S. Huang, X. Ren, W. Shu, J. Cheng, G. Tao, W. Xu, R. Chen, X. Luo, Emerging materials and strategies for personal thermal management, Adv. Energy Mater. 10 (2020), 1903921, https://doi.org/10.1002/aenm.201903921.

[3] S. Sundararajan, A.B. Samui, P.S. Kulkarni, Versatility of polyethylene glycol (PEG) in designing solid–solid phase change materials (PCMs) for thermal management and their application to innovative technologies, J. Mater. Chem. A 5 (2017) 18379–18396, https://doi.org/10.1039/c7ta04968d.

[4] L. Xiang, D. Luo, J. Yang, X. Sun, J. Jin, S. Qin, Construction and design of paraffin/PVDF hollow fiber linear-phase change energy storage materials, Energy Fuel 33 (2019) 11584–11591, https://doi.org/10.1021/acs.energyfuels.9b02852.

[5] H. Ke, Morphology and thermal performance of quaternary fatty acid eutectics/polyurethane/Ag form-stable phase change composite fibrous membranes, J. Therm. Anal. Calorim. 129 (2017) 1533–1545, https://doi.org/10.1007/s10973-017-6399-9.

[6] K. Yang, M. Venkataraman, X. Zhang, J. Wiener, G. Zhu, J. Yao, J. Militky, Review: incorporation of organic PCMs into textiles, J. Mater. Sci. (2022) 1–50, https://doi.org/10.1007/s10853-021-06641-3.

[7] K. Yang, M. Venkataraman, J. Wiener, X. Zhang, M. Stuchlik, G. Zhu, J. Yao, J. Militky, Crystallization mechanism of micro flake cu particle-filled Poly(ethylene glycol) composites, Thermochim. Acta (2022), 179172, https://doi.org/10.1016/j.tca.2022.179172.

[8] L. Hes, luboshes@vslib.cz, B.I. Lu, Using a thermal simulator to determine the amount of time that humans are thermally protected by fabrics containing phase change materials, Res. J. Text. Appar. 8 (2004) 51–56, https://doi.org/10.1108/rjta-08-02-2004-b007.

[9] M. Jaworski, Mathematical model of heat transfer in PCM incorporated fabrics subjected to different thermal loads, Appl. Therm. Eng. 150 (2019) 506–511, https://doi.org/10.1016/j.applthermaleng.2019.01.019.

[10] K. Yang, M. Venkataraman, J. Karpiskova, Y. Suzuki, S. Ullah, I.-S. Kim, J. Militky, Y. Wang, T. Yang, J. Wiener, G. Zhu, J. Yao, Structural analysis of embedding polyethylene glycol in silica aerogel, Microporous Mesoporous Mater. 310 (2021), 110636, https://doi.org/10.1016/j.micromeso.2020.110636.

[11] L. Pathak, G.V.N. Trivedi, R. Parameshwaran, S.S. Deshmukh, Microencapsulated phase change materials as slurries for thermal energy storage: a review, Mater. Today Proc. 44 (2021) 1960–1963, https://doi.org/10.1016/j.matpr.2020.12.101.

[12] J.L. Reyez-Araiza, J. Pineda-Piñón, J.M. López-Romero, J.R. Gasca-Tirado, M. A. Contreras, J.C.J. Correa, L.M. Apátiga-Castro, E.M. Rivera-Muñoz, R. R. Velazquez-Castillo, J.de J.P. Bueno, A. Manzano-Ramirez, Thermal energy storage by the encapsulation of phase change materials in building elements—a review, Materials 14 (2021) 1420, https://doi.org/10.3390/ma14061420.

[13] H. Liu, X. Wang, D. Wu, Innovative design of microencapsulated phase change materials for thermal energy storage and versatile applications: a review, Sustain. Energy Fuels 3 (2019) 1091–1149, https://doi.org/10.1039/c9se00019d.

[14] Y. Wu, C. Chen, Y. Jia, J. Wu, Y. Huang, L. Wang, Review on electrospun ultrafine phase change fibers (PCFs) for thermal energy storage, Appl. Energy 210 (2018) 167–181, https://doi.org/10.1016/j.apenergy.2017.11.001.

[15] Y. Wang, J. Yao, G. Zhu, J. Militky, J. Marek, M. Venkataraman, G. Zhang, A novel method for producing bi-component thermo-regulating alginate fiber from phase change material microemulsion, Text. Res. J. 90 (2020) 1038–1044, https://doi.org/10.1177/0040517519886075.

[16] Z. Qin, L. Yi, S. Wang, L. Wang, J. Yao, G. Zhu, J. Militky, M. Venkataramam, M. Zhang, Supercooling suppression and mechanical property improvement of phase change nanofibers by optimizing core distribution, Polymer 233 (2021), 124176, https://doi.org/10.1016/j.polymer.2021.124176.

[17] K. Iqbal, A. Khan, D. Sun, M. Ashraf, A. Rehman, F. Safdar, A. Basit, H.S. Maqsood, Phase change materials, their synthesis and application in textiles—a review, J. Text. Inst. 110 (2019) 625–638, https://doi.org/10.1080/00405000.2018.1548088.

[18] H. Peng, J. Wang, X. Zhang, J. Ma, T. Shen, S. Li, B. Dong, A review on synthesis, characterization and application of nanoencapsulated phase change materials for thermal energy storage systems, Appl. Therm. Eng. 185 (2021), https://doi.org/10.1016/j.applthermaleng.2020.116326.

[19] D.G. Prajapati, B. Kandasubramanian, A review on polymeric-based phase change material for thermo-regulating fabric application, Polym. Rev. 60 (2020) 389–419, https://doi.org/10.1080/15583724.2019.1677709.

[20] J. Gu, W. Wang, D. Yu, Temperature control and low infrared emissivity double-shell phase change microcapsules and their application in infrared stealth fabric, Prog. Org. Coat. 159 (2021), 106439, https://doi.org/10.1016/j.porgcoat.2021.106439.

[21] Y. Su, W. Zhu, M. Tian, Y. Wang, X. Zhang, J. Li, Intelligent bidirectional thermal regulation of phase change material incorporated in thermal protective clothing, Appl. Therm. Eng. 174 (2020), 115340, https://doi.org/10.1016/j.applthermaleng.2020.115340.

[22] F. Salaün, E. Devaux, S. Bourbigot, P. Rumeau, Thermoregulating response of cotton fabric containing microencapsulated phase change materials, Thermochim. Acta 506 (2010) 82–93, https://doi.org/10.1016/j.tca.2010.04.020.

[23] I. Kim, K. Lee, G. Cho, Heat storage/release characteristics and mechanical properties of combat uniform fabrics treated with microcapsules containing octadecane as phase change materials, Fiber Polym. 17 (2016) 1726–1734, https://doi.org/10.1007/s12221-016-6796-x.

[24] T.R. Kar, A.K. Samanta, H.D. Sinnur, M. Kumar, Studies on effect of application of capric acid and stearic acid based reactive phase change materials (rPCM) with PHAMS binder on thermal comfort of cotton khadi fabric as thermo-tropic smart textiles, J. Nat. Fibers (2021), https://doi.org/10.1080/15440478.2021.1880517.

[25] M. Khosrojerdi, S.M. Mortazavi, Impregnation of a porous material with a PCM on a cotton fabric and the effect of vacuum on thermo-regulating textiles, J. Therm. Anal. Calorim. 114 (2013) 1111–1119, https://doi.org/10.1007/s10973-013-3144-x.

[26] Y. Yuan, H. Xiang, G. Liu, R. Liao, Fabrication of phase change microcapsules and their applications to anti-icing coating, Surf. Interfaces 27 (2021), 101516, https://doi.org/10.1016/j.surfin.2021.101516.

[27] Y. Li, G. Wang, Z. Guo, P. Wang, A. Wang, Preparation of microcapsules coating and the study of their bionic anti-fouling performance, Materials 13 (2020) 1669, https://doi.org/10.3390/ma13071669.

[28] F.A.P. Scacchetti, E. Pinto, G.M.B. Soares, Functionalization and characterization of cotton with phase change materials and thyme oil encapsulated in beta-cyclodextrins, Prog. Org. Coat. 107 (2017) 64–74, https://doi.org/10.1016/j.porgcoat.2017.03.015.

[29] M. Karthikeyan, T. Ramachandran, O.L. Shanmugasundaram, Synthesis, characterization, and development of thermally enhanced cotton fabric using nanoencapsulated phase change materials containing paraffin wax, J. Text. Inst. 105 (2014) 1279–1286, https://doi.org/10.1080/00405000.2014.886368.

[30] M. Karthikeyan, T. Ramachandran, O.L.S. Sundaram, Nanoencapsulated phase change materials based on polyethylene glycol for creating thermoregulating cotton, J. Ind. Text. 44 (2014) 130–146, https://doi.org/10.1177/1528083713480378.

[31] J. Li, X. Zhu, H. Wang, P. Lin, L. Jia, L. Li, Y. Chen, Synthesis and properties of multifunctional microencapsulated phase change material for intelligent textiles, J. Mater. Sci. 56 (2021) 2176–2191, https://doi.org/10.1007/s10853-020-05399-4.

[32] G. Li, G. Hong, D. Dong, W. Song, X. Zhang, Multiresponsive graphene-aerogel-directed phase-change smart fibers, Adv. Mater. 30 (2018), https://doi.org/10.1002/adma.201801754.
[33] K. Zhu, X. Li, J. Su, H. Li, Y. Zhao, X. Yuan, Improvement of anti-icing properties of low surface energy coatings by introducing phase-change microcapsules, Polym. Eng. Sci. 58 (2018) 973–979, https://doi.org/10.1002/pen.24654.
[34] H. Wang, W. Wang, H. Wang, X. Jin, J. Li, Z. Zhu, One-way water transport fabrics with hydrophobic rough surface formed in one-step electrospray, Mater. Lett. 215 (2018) 110–113, https://doi.org/10.1016/j.matlet.2017.12.066.
[35] C. Cai, X. Ouyang, L. Zhou, G. Liu, Y. Wang, G. Zhu, J. Yao, J. Militky, M. Venkataraman, G. Zhang, Co-solvent free interfacial polycondensation and properties of polyurea PCM microcapsules with dodecanol dodecanoate as core material, Sol. Energy 199 (2020) 721–730, https://doi.org/10.1016/j.solener.2020.02.071.
[36] D. Bhattacharjee, V.K. Kothari, Prediction of thermal resistance of woven fabrics. Part II: Heat transfer in natural and forced convective environments, J. Text. Inst. 99 (2008) 433–449, https://doi.org/10.1080/00405000701582596.
[37] G. Zhu, Y. Fang, L. Zhao, J. Wang, W. Chen, Prediction of structural parameters and air permeability of cotton woven fabric, Text. Res. J. 88 (2018) 1650–1659, https://doi.org/10.1177/0040517517705632.
[38] A. Razzaque, P. Tesinova, L. Hes, J. Salacova, H.A. Abid, Investigation on hydrostatic resistance and thermal performance of layered waterproof breathable fabrics, Fiber Polym. 18 (2017) 1924–1930, https://doi.org/10.1007/s12221-017-1154-1.
[39] L. Hes, M. Boguslawska-Baczek, M.J. Geraldes, Thermal comfort of bedsheets under real conditions of use, J. Nat. Fibers 11 (2014) 312–321, https://doi.org/10.1080/15440478.2013.867826.
[40] K. Yang, Q. Peng, M. Venkataraman, J. Novotna, J. Karpiskova, J. Mullerova, J. Wiener, M. Vikova, G. Zhu, J. Yao, J. Militky, Hydrophobicity, water moisture transfer and breathability of PTFE-coated viscose fabrics prepared by electrospraying technology and sintering process, Prog. Org. Coat. 165 (2022), 106775, https://doi.org/10.1016/j.porgcoat.2022.106775.
[41] J. Diswat, L. Hes, K. Bal, Thermal resistance of cut pile hand tufted carpet and its prediction, Text. Res. J. 86 (2016) 1759–1767, https://doi.org/10.1177/0040517515612356.
[42] L. Hes, K. Bal, I. Dolezal, Principles of clothing comfort and their use in evaluation of sensorial and thermal comfort of Men's casual jacket, Fiber Polym. 22 (2021) 2922–2928, https://doi.org/10.1007/s12221-021-0425-z.
[43] K. Ghasemi, S. Tasnim, S. Mahmud, PCM, nano/microencapsulation and slurries: a review of fundamentals, categories, fabrication, numerical models and applications, Sustainable Energy Technol. Assess. 52 (2022), 102084, https://doi.org/10.1016/j.seta.2022.102084.
[44] Z. Qiu, X. Ma, P. Li, X. Zhao, A. Wright, Micro-encapsulated phase change material (MPCM) slurries: characterization and building applications, Renew. Sust. Energ. Rev. 77 (2017) 246–262, https://doi.org/10.1016/j.rser.2017.04.001.
[45] M. Delgado, A. Lázaro, C. Peñalosa, J. Mazo, B. Zalba, Analysis of the physical stability of PCM slurries, Int. J. Refrig. 36 (2013) 1648–1656, https://doi.org/10.1016/j.ijrefrig.2013.04.020.
[46] D. Murakami, H. Jinnai, A. Takahara, Wetting transition from the Cassie-Baxter state to the Wenzel state on textured polymer surfaces, Langmuir 30 (2014) 2061–2067, https://doi.org/10.1021/la4049067.
[47] N. Mao, J. Ye, Z. Quan, H. Zhang, D. Wu, X. Qin, R. Wang, J. Yu, Tree-like structure driven water transfer in 1D fiber assemblies for functional moisture-wicking fabrics, Mater. Des. 186 (2020), 108305, https://doi.org/10.1016/j.matdes.2019.108305.
[48] J. Wu, N. Wang, L. Wang, H. Dong, Y. Zhao, L. Jiang, Unidirectional water-penetration composite fibrous film via electrospinning, Soft Matter 8 (2012) 5996–5999, https://doi.org/10.1039/c2sm25514f.
[49] K. Iqbal, D. Sun, Synthesis of nanoencapsulated Glauber's salt using PMMA shell and its application on cotton for thermoregulating effect, Cellulose 25 (2018) 2103–2113, https://doi.org/10.1007/s10570-018-1692-8.
[50] A. Shahid, S. Miah, A. Rahim, Thermal and breathability management of microencapsulated phase change material (MPCM) incorporated jute fabric, J. Eng. Fiber Fabr. 16 (2021), https://doi.org/10.1177/15589250211029564, 1558925021102 95.
[51] A.S. Hicyilmaz, S. Teke, Z.I. Cin, A.C. Bedeloglu, Development of thermo-regulating fabrics with enhanced heat dissipation via graphene-modified n-octadecane microcapsules, Polym. Eng. Sci. (2021), https://doi.org/10.1002/pen.25845.
[52] X. Lin, X. Zhang, J. Ji, L. Zheng, Research progress on preparation, characterization, and application of nanoparticle-based microencapsulated phase change materials, Int. J. Energy Res. 45 (2021) 9831–9857, https://doi.org/10.1002/er.6538.
[53] S. Alay, F. Göde, C. Alkan, Synthesis and thermal properties of poly(n-butyl acrylate)/n-hexadecane microcapsules using different cross-linkers and their application to textile fabrics, J. Appl. Polym. Sci. 120 (2011) 2821–2829, https://doi.org/10.1002/app.33266.
[54] P. Sánchez, M.V. Sánchez-Fernandez, A. Romero, J.F. Rodríguez, L. Sánchez-Silva, Development of thermo-regulating textiles using paraffin wax microcapsules, Thermochim. Acta 498 (2010) 16–21, https://doi.org/10.1016/j.tca.2009.09.005.
[55] A. Nejman, E. Gromadzínska, I. Kamínska, M. Ciéslak, Assessment of thermal performance of textile materials modified with PCM microcapsules using combination of DSC and infrared thermography methods, Molecules 25 (2020), https://doi.org/10.3390/molecules25010122.
[56] V. Skurkyte-Papieviene, A. Abraitiene, A. Sankauskaite, V. Rubeziene, J. Baltusnikaite-Guzaitiene, Enhancement of the thermal performance of the paraffin-based microcapsules intended for textile applications, Polymers-Basel 13 (2021) 1120, https://doi.org/10.3390/polym13071120.
[57] Y. Iamphaojeen, P. Siriphannon, Adjustable thermal barrier of cotton fabric by multilayer immobilization of PCM nanocapsules, Cellulose 25 (2018) 3649–3661, https://doi.org/10.1007/s10570-018-1804-5.
[58] K. Yang, J. Wiener, M. Venkataraman, Y. Wang, T. Yang, G. Zhang, G. Zhu, J. Yao, J. Militky, Thermal analysis of PEG/Metal particle-coated viscose fabric, Polym. Test. 100 (2021), 107231, https://doi.org/10.1016/j.polymertesting.2021.107231.

9.5 Research review article-4 (Journal of Materials Science, Q2, IF: 4.5)

J Mater Sci

Review

Review: incorporation of organic PCMs into textiles

Kai Yang[1,*], Mohanapriya Venkataraman[1], Xiuling Zhang[1], Jakub Wiener[1], Guocheng Zhu[2], Juming Yao[3,4], and Jiri Militky[1]

[1] *Department of Material Engineering, Faculty of Textile Engineering, Technical University of Liberec, Liberec, Czech Republic*
[2] *College of Textile Science and Engineering, Zhejiang Sci-Tech University, Hangzhou, People's Republic of China*
[3] *School of Materials Science and Engineering, Zhejiang Sci-Tech University, Hangzhou, People's Republic of China*
[4] *School of Materials Science and Chemical Engineering, Ningbo University, Ningbo, People's Republic of China*

Received: 12 June 2021
Accepted: 15 October 2021

ABSTRACT

Phase change materials (PCMs) were characterized to adsorb/release the thermal energy during the phase transition process over a certain temperature range. The PCMs had been incorporated into textiles to enhance the thermal property and the products are labeled as PCM textiles. The thermal behavior of the PCM textiles (the PCM fibers, the PCM yarns, and the PCM fabrics) was investigated for decades. The application of the PCM textiles was also extended to various fields. Based on the numerous research work, the publications related to the PCM textiles were already summarized. However, it was found that some reviews tended to describe the application of the microencapsulation PCMs, and some reviews focused on the fabrication of the PCM ultrafine fibers via electrospinning. In addition, there are some novel technologies to fabricate the PCMs, the novel methods to evaluate the PCM textiles, and the novel applications of the PCM textiles in recent years. In this review, the recent research work related to PCM textiles was summarized, which was aimed to deepen the understanding of the PCM textiles.

Handling Editor: Stephen Eichhorn.

Address correspondence to E-mail: kai.yang@tul.cz

https://doi.org/10.1007/s10853-021-06641-3

Published online: 03 January 2022

Springer

GRAPHICAL ABSTRACT

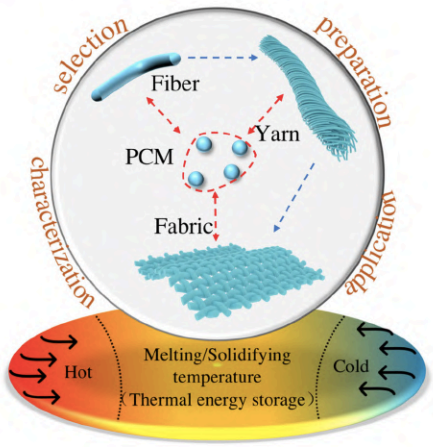

Abbreviations

AC	Active carbon
AMA	Methyl acrylate
BC	Bamboo charcoal
BTCA	Butane tetracarboxylic acid
BN	Boron nitride
BN-OHs	Hydroxylated boron nitride
BS	Butyl stearate
CA	Capric acid
CNF	Cellulose nanofiber
CNT	Carbon nanotube
CS	Chitosan
DMDHEU	Dimethyloldihydroxyethyleneurea
E	Erythritol
EG	Expanded graphite
FK-g-APEG	Feather keratin-g-allyloxy polyethylene glycol
GHP	Galactitol hexa-palmitate
GTL	Glycerol trilaurate
HD	Hexadecanol
LA	Lauric acid
MA	Myristic acid
MC	Mesoporous carbon
MF	Melamine formaldehyde
MP	Methyl palmitate
MWCNT	Multiwalled carbon nanotube
OA	Oleic acid
PA	Palmitic acid
PA 6	Polyamide 6
PALMA	Poly(allyl methacrylate)
PAN	Polyacrylonitrile
P(AN-co-VDC)	Poly(acrylonitrile-co-vinylidene chloride)
PDDA	Poly(diallyldimethylammonium chloride)
PDMS	Polydimethylsiloxane
PEG	Polyethylene glycol
PES	Polyethersulfone
PET	Polyethylene terephthalate
PMIA	Poly(meta-phenylene isophthalamide)
PMMA	Poly(methyl methacrylate)
P(MMA-co-AA)	Poly(methyl methacrylate-co-acrylic acid)

PP	Polypropylene
PSS	Poly-4-styrenesulfonic acid
PUR	Polyurethane
PUA	Polyurea
PVA	Polyvinyl alcohol
PVDF	Polyvinylidene fluoride
PVP	Polyvinylpyrrolidone
rGO	Reduced graphene oxide
SA	Stearic acid
SAN-g-PA	Poly(styrene-co-acrylonitrile)/palmitic acid
SDS	Sodium dodecyl sulfate
SIC	Silicon carbide
SS	Stainless steel
TD	Tetradecyl alcohol
UF	Urea formaldehyde

Symbols

A	The area of the sample through which the heat transfers (m^2)
a	Thermal diffusivity ($m^2\ s^{-1}$)
b	Thermal absorptivity ($W\ s^{1/2}\ m^{-2}\ K^{-1}$)
c_p	Specific heat capacity ($J\ kg^{-1}\ K^{-1}$)
$\dot{g}$	Volumetric generation (W/m^3)
h	Convective heat transfer coefficient ($W\ m^{-2}\ K^{-1}$)
k	Thermal conductivity ($W\ m^{-1}\ K^{-1}$)
L	Distance or thickness of the sample along which the heat transfers (m)
$\dot{q}$	Heat flux (W/m^2)
r	Thermal resistance ($m^2\ K\ W^{-1}$)
T	Temperature (°C or K)
T_w	Temperature of the wall (°C or K)
T_∞	Temperature of the fluid or ambient temperature (°C or K)
ε	Surface emissivity
σ	Stefan–Boltzmann constant ($5.6704 \times 10^{-8}\ W\ m^{-2}\ K^{-4}$)
ρ	Density of the materials (g/m^3)

Introduction

Phase change materials (PCMs) are a group of materials that adsorb/release thermal energy during their phase transition. The PCMs could be applied in various fields, including building materials, solar energy storage, the thermal management of the electronic system, food storage, smart textiles, and so on [1–6]. The discussions

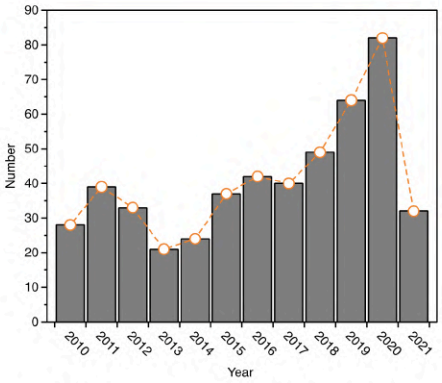

Figure 1 Number of the recorded publications in each year related to 'PCM or phase change material and textiles' in the 'Scopus' (till April 2021) (Searching by selecting keyword 'fabric' or 'fiber' or 'textile,' and 'phase change material').

of the PCMs related to the PCMs classification, the preparation of PCMs, and the application of PCMs were reviewed in various published works [2, 7–14]. Besides, the toxicity, health hazards, and commercialization of PCMs were reviewed by S.S. Chandel et al. [15]. Particularly, the PCM-incorporated thermoregulating textiles had attracted more and more attention (Fig. 1). It is well known that the first introduction of PCM into textiles was realized from NASA in the early 1980s, which was aimed to improve the thermal protection against the extreme temperature fluctuation in the outer space. The basic working principle of PCM textiles was the realization of thermal energy storage when there is a phase transition of PCMs between the solid and liquid phase while the temperature of PCMs during the phase transition was little altered. Besides, the thermal resistance of the PCM textiles was enhanced since there was the phase transition. So, the PCM textiles could be used for thermal regulation or the thermal energy harvesting. Now, there are various commercial PCM textile products over the globe (Table 1). The main reason for the rapid development of the PCM textiles could be two aspects:

1) The first aspect was based on the various applications of textiles. It was noticed that the concept of 'textile' included fiber, yarn, and fabric [16]. Since the successful fabrication of the ultrafine fibers via the advanced technologies, the flexibility of the ultrafine fibers supported

Table 1 Some commercial textiles products containing PCMs

Company	Country	Product
Outlast	USA	Air conditioning thermal fiber
Mid6	USA	Smartskin fabric
Triangle Company	USA	Triangle R&D
Rhodia (Solvay)	Belgium	GaoShushi fiber
Scholler	Swiss	PS-change fiber
Trievira	German	LCAT fiber
Fountain Set	China	Fountain fabric
Hebei Xiongya Textile Group	China	Temperature regulating
Komatsu Seiren	Japan	AirTechnio

the high compatibility with various other materials. Besides, the yarns were considered a special structure where the twist supported the mechanical property. The release/store of the mechanical property in the yarns could be realized. In addition, the fabric was a stable porous structure. By modifying the fabric, various applications were proposed, including the antibacterial property, oil/water separation, particle filtration, thermal regulation, Joule heating property, optical property, EMI shielding, etc. [17–26].

2) The second aspect was based on the usage of the PCM. The usage of the PCM was proposed to enhance the thermal regulation and thermal energy storage and also supported the light radiation–thermal energy conversion, solar–thermal energy conversion, and so on [27].

Although the significant progress for the PCM textiles was made during last century, there were some problems with PCM textiles, like the thermal energy storage efficiency, the thermal energy storage amount, the durability of PCM textiles, the evaluation of PCM textiles, etc. Aimed to modify the thermal behavior of the PCM textiles and extend the application of the PCM textiles in more fields, various research works were done, which were reviewed in the published work [5, 13, 28–30]. It was found that the published reviews related to the PCM textiles were classified into two types: the discussion of PCMs for textiles and the discussion of the PCM fibers. The content of the former mainly focused on the discussion of the encapsulation PCMs (MPCMs) for textiles. However, the other methods (e.g., coatings, lamination, grafting, etc.) for the preparation of PCM-incorporated textiles were not discussed in detail. The content of the latter mainly focused on the PCM fibers prepared via electrospinning. However, there were various methods to prepare the PCM fibers, like traditional spinning methods, centrifugal spinning technology, impregnation, etc. Additionally, the form-stable PCMs (FSPCMs) by using the porous materials as the supporting materials to store the PCM also had a great potential in the application of textile, which was not discussed yet. Furthermore, there were other novel methods to evaluate the thermal behavior of the PCM-incorporated textiles in recent years.

In this work, the recent research works were included and discussed. The main aim of this work was to deepen the understanding of PCM textiles. In detail, the content of the review is classified into the following five sections:

- Sect. 2: PCM classifications. In this section, the suitability of the PCMs for textiles was discussed. In detail, the basic classification of the PCMs was simply presented and the hybrid PCMs were focused on.
- Sect. 3: Preparation of PCM-incorporated textiles. In this section, the discussion included three parts: the preparation of the PCM fibers, the preparation of the PCM yarns, and the preparation of the PCM fabrics. The various technologies for the preparation of PCM textiles were discussed. Particularly, the effect of additives in the PCM fibers on the mechanical property and the usage of the binders in the PCM fabrics were also included.
- Sect. 4: Application of PCM-incorporated textiles. In this section, the specific application of the PCM-incorporated textiles was discussed.
- Sect. 5: Evaluation of PCM textiles. In this section, the methods to evaluate the thermal behavior of the PCM-incorporated textiles were included.
- Sect. 6: Future and challenges. In this section, the main challenges for the PCM textiles were

proposed, which could be the research topic in the following years.

PCM classification

It is well known that the PCMs are classified into three types: inorganic PCMs, organic PCMs, and hybrid PCMs, which were already discussed in various reviews [15, 30, 31]. In this section, the comparison between the inorganic PCMs and organic PCMs was simply described. Different from both the inorganic PCMs and organic PCMs, the existence of hybrid PCMs is aimed to solve the problems of the pristine PCMs, which conceptually contains at least two components. So, the necessity of the hybrid PCMs was focused on in this section.

Inorganic PCMs

The inorganic PCM are generally classified into two groups: salts, salts hydrates, metals, and metal alloys [32]. The melting temperature of the inorganic PCMs could range from 10 to 100 °C, and the melting enthalpy was generally higher than 100 J/g [33]. However, the inorganic PCMs were not proposed to be applied in textiles. The main reasons included the corrosive property, the phase separation after a certain heating–cooling cycle, etc. Recently, there have been some efforts to solve the problems of the inorganic PCMs. It was suggested that the incorporation of the thickening agent and the nucleating agent into the inorganic PCMs could reduce the phase separation and the addition of other supporting materials was necessary to cover the inorganic PCMs to avoid leakage [34]. Besides, the usage of the inorganic PCMs as the core for the MPCMs was the alternative to avoid the disadvantages [35]. However, the inorganic PCMs were still not proposed for the textiles since the suitability of the inorganic PCMs and the MPCMs with the inorganic PCMs for the human being remained to be improved. Therefore, the inorganic PCMs were not discussed in the following sections and the words 'PCMs' shown in the following sections were for the organic PCMs.

Organic PCMs

By comparing with inorganic PCMs, the organic PCMs are considered to have non-corrosion, lower supercooling, high chemical and thermal stability, and moderate working temperature for humans (Table 2). The organic PCMs include paraffin waxes [36], fatty acids [37], PEG [38], etc. The paraffin waxes are the saturated alkanes with the molecular formula C_nH_{2n+2}, where n is the number of carbon atoms in the molecules. The fatty acids are a group of materials sharing a general molecular formula $C_nH_{2n+1}COOH$, where n is the number of carbon atoms in the molecules. The thermal behavior of both paraffin waxes and fatty acids strongly depends on the number of carbon atoms in their molecules, which is shown in Fig. 2A. The PEG is the semi-crystalline polymer with its molecular formula ($HO–[(CH_2)_2O]_n–H$). The thermal behavior of the PEG is dependent on the weighted average molecular weight (M_w), which is shown in Fig. 2B. All the points shown in Fig. 2 are given in Table 3.

For the paraffin waxes, the solid phase only occurs at room temperature when the n is higher than 17. The melting temperature of the solid paraffin waxes ranges from 30 to 80 °C and increases with the increase in carbon atoms in alkanes. The latent heat of fusion of the paraffin waxes ranges from 150 to 280 kJ/kg and changes not much with different carbon atoms in alkanes. The high latent heat of fusion of paraffin waxes is caused by the existence of C–H and C–C bonds leading to high thermal energy absorbed during the melting process and released during the solidification process. No extra functional groups in paraffin waxes support intrinsic chemical stability. Besides, no vapor pressure and little volume change of paraffin during the melting process happen and paraffin is safe and non-corrosive. So, paraffin wax is a suitable PCM for the human body to regulate temperature.

For the fatty acids, the melting temperature increases with a number of C atoms in the molecules, while there is no obvious difference in the latent heat in fatty acids ($n > 11$). By comparing with paraffin waxes, both melting temperature and melting enthalpy are slightly higher.

For the PEG, the melting temperature of PEG increases with a higher molecular weight of PEG from 3 to 67 °C. An increase in melting and crystallization enthalpy is observed when the molecular weight of PEG increases. It was found that the PEG with M_w of 10,000 has the largest melting enthalpy of 182 J/g.

Table 2 Comparison between inorganic PCMs and organic PCMs

Type	Advantages	Disadvantages
Inorganic PCMs	Greater heat fusion	Higher supercooling
	High thermal conductivity	Corrosion
		Phase separation
		Lower thermal stability
Organic PCMs	Non-corrosion	Lower heat fusion
	Lower supercooling	Lower thermal conductivity
	High chemical and thermal stability	Inflammability

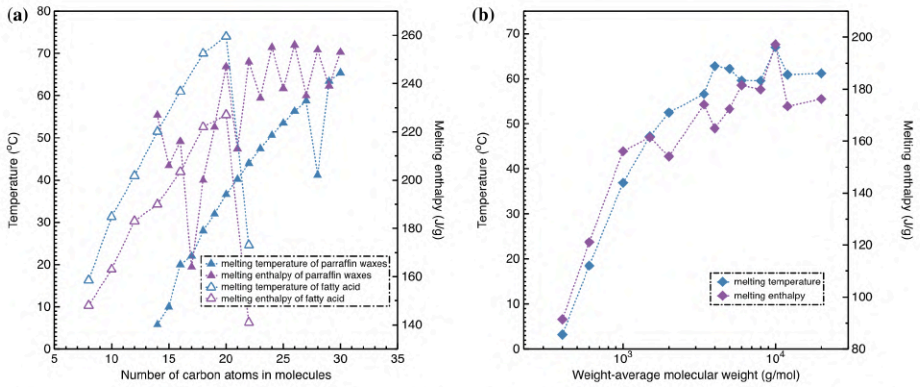

Figure 2 Melting temperature and corresponding melting enthalpy of organic PCMs (A: paraffin waxes and fatty acid, and B: PEG).

Apart from the three types of organic PCMs, there are some other uncommon organic materials for PCMs, including the sugar alcohols [39], the comb-like polymers [40–42], etc. For the sugar alcohols, the phase transition temperature of the sugar alcohols is considered relatively higher than the softening temperature of the many polymers, which indicates that there is a requirement for the polymers as supporting materials for sugar alcohols. For the common comb-like polymers, the enthalpy value and the phase transition range of the comb-like polymers do not support them as PCM. It is feasible to introduce the other bonds to enhance the crystallization process of the common comb-like polymers, which is still necessary to be strictly controlled during the synthetic process.

Hybrid PCMs

The hybrid PCMs could be the organic PCMs eutectics or the inorganic/organic PCMs eutectics. The preparation of the hybrid PCMs is aimed to enhance the thermal stability by avoiding leakage during the phase transition, modify the thermal energy storage efficiency by improving the thermal conductivity, and amend the PCM working situation by adjusting the supercooling degree as well as the phase transition temperature.

Avoiding leakage

The PCMs experience solid–liquid phase change, and the non-stable thermal behavior is suggested if there are no suitable carriers to contain the PCMs. So, some supporting materials are necessary to prohibit the leakage of the PCMs. Many studies focus on the leakage of the PCMs, and most efforts can be concluded into three methods: the microencapsulated PCMs (MPCMs) [2], the solid–solid PCMs (SSPCMs) [46], and the form-stable PCM (FSPCMs) [47]. The MPCMs are a group of materials consisting of the shell and the core. The shell is normally considered a

Table 3 List of the melting behavior of common organic PCMs

PCM type	Melting temperature (°C)	Melting enthalpy (J/g)
n-tetradecane (n = 14)[1]	5.8	227
n-pentadecane (n = 15)[1]	10	206
n-hexadecane (n = 16)[1]	20	216
n-heptadecane (n = 17)[1]	22	164
n-octadecane (n = 18)[1]	28	200
n-nonadecane (n = 19)[1]	32	222
n-eicosane (n = 20)[1]	36.6	247
n-heneicosane (n = 21)[1]	40.2	213
n-docosane (n = 22)[1]	44	249
n-trikozane (n = 23)[1]	47.5	234
n-tetracosane (n = 24)[1]	50.6	255
n-pentacosane (n = 25)[1]	53.5	238
n-hexacosane (n = 26)[1]	56.3	256
n-heptacosane (n = 27)[1]	58.8	235
n-octacosane (n = 28)[1]	41.2	254
n-nonacosane (n = 29)[1]	63.4	239
n-triacontane (n = 30)[1]	65.4	253
CA (n = 10)[2]	31.3	163
LA (n = 12) [2]	41	183
MA (n = 14)[2]	51.5	190
PA (n = 16)[2]	61	203.4
SA (n = 18)[2]	70	222
OA (n = 20)[2]	74	227
PEG (M_w = 400)[3]	3.2	91.4
PEG (M_w = 600)[3]	18.5	121.1
PEG (M_w = 1,000)[4]	36.9	156.1
PEG (M_w = 1,500)[4]	47.23	161.43
PEG (M_w = 2,000)[4]	52.5	154.1
PEG (M_w = 3,400)[4]	56.6	174.1
PEG (M_w = 4,000)[4]	62.8	164.9
PEG (M_w = 5,000)[5]	62.2	172.4
PEG (M_w = 6,000)[4]	59.6	181.5
PEG (M_w = 8,000)[4]	59.54	179.9
PEG (M_w = 10,000)[4]	67	197.2
PEG (M_w = 12,000)[4]	60.93	173.4
PEG (M_w = 20,000)[4]	61.2	176.2

Subscript: 1, 2, 3, 4, and 5: values of the paraffin waxes from [43] and values of the fatty acids from [37], and the values of the PEG from [30, 44], and [45], respectively

polymer with a high melting temperature, and the core is the functional PCM. During the working temperature, the PCM is kept inside the shell. For both FSPCM and SSPCM, the mechanism to avoid leakage of the PCM is based on the chemical or physical interaction between PCM and supporting materials. For the SSPCM, the chemical interaction between PCM and supporting materials plays a significant role to avoid leakage. For the FSPCM, the physical interaction between PCM and supporting materials works to avoid leakage.

A) MPCMs

It is found that the encapsulation technology for PCMs is the main method to avoid the leakage of PCMs [5, 48–50], and the products are named as PCM capsules. PCMs capsules are a group of materials with a core–shell structure, where the PCMs are the core, and the supporting materials were the shell [50, 51]. The shell materials for PCM capsules could be inorganic, organic, or hybrid. The molten PCMs are unable to move out because of the enclosed space

supported by the shell during the work temperature range. The PCM materials for the core are usually the n-eicosane [52], paraffin [53, 54], etc., and the supporting materials are usually the PMMA [35, 55], P(MMA-co-AA) [56], PUR [57], etc. Various methods have been for the preparation of PCM capsules, including suspension-like polymerization, photo-induced microencapsulation, electrospraying technology, etc. [58–61]. According to the size of the obtained PCM capsules, the PCM capsules are classified into microencapsulation PCMs (MPCMs) and PCM nanocapsules (NPCMs) [62]. There were various reviews related to the description of the MPCMs and the NPCMs [30, 63], so only recent research works focusing on the MPCMs especially for the textiles were presented in this review.

It was found that the biomaterials for the preparation of MPCMs attracted more and more attention in recent years. Liang Zhao et al. prepared an MPCM consisting of the n-octadecane as the core and the natural silk fibroin as the shell [64]. By adjusting the n-octadecane/silk fibroin solution weight ratio (w/w%), the phase transition behavior and the encapsulation efficiency of the n-octadecane were modified. The final optimal n-octadecane/silk fibroin MPCMs had a melting temperature of 22.82 °C and a melting enthalpy of 88.23 J/g. Subsequently, Jie Luo et al. revealed that the control of the nonionic, ionic, and mixed surfactants was able to increase the emulsion stability and enhance encapsulating capacity of silk fibroin-based MPCMs [65]. Elif Gozde Sarac et al. selected the organic coconut oil as the core and prepared two MPCMs with PMMA and MF as the shell, respectively [66]. The PMMA/organic coconut oil MPCMs had a melting enthalpy of 39.1 J/g, while the MF/organic coconut oil MPCMs had a melting enthalpy of 81.9 J/g. Additionally, it was noticed that the common methods have difficulties in MPCMs with tunable size, structure, and composition at will, which failed to tailor the thermal properties of MPCMs accurately and flexibly. Recently, the microfluidics encapsulation technology was used to prepare the MPCMs and the tunability of the final MPCMs was realized [67]. Although there were various research works to support the development of the MPCMs, there were several disadvantages of the MPCMs:

1) The mechanical property of the MPCMs shell needed enhancement.
2) The encapsulation efficiency required modification, which was affected by the initiator and the temperature of the polymerization processes [68].
3) The compatibility of the MPCMs with other materials was considered poor, which required improvement.

B) SSPCMs

The SSPCMs retain the solid phase during the working temperature, where the partial crystalline structure or phase is changed. The mechanism of the SSPCMs is classified into two types [46]: 1) the relatively small molecules shift from one crystalline phase to another one (semi-crystalline or amorphous) when the SSPCM absorbs or releases thermal energy; 2) the crystallizable moieties are incorporated through chemical bonding into a secondary structure that prevents them to flow freely when they are in their liquid non-crystalline state (Fig. 3). Particularly, the SSPCMs based on the polymer were realized based on the second mechanism, which could be prepared via grafting, hyper-branching, polymerization, electrospinning, etc. [46]. Alkan et al. prepared different types of PUR via the condensation reaction of PEGs with various diisocyanate [69]. The results showed that the produced PURs had typical solid–solid phase transition properties with high enthalpies reaching 179 J/g, and transition points were between 19 °C and 60 °C. Siyang Mu et al. prepared the SSPCM based on the SAN-g-PA copolymer via chain-grafting [70]. Qi Cao et al. prepared the SSPCM based on hyperbranched PUR [71]. Although the thermal stability of the SSPCMs was found, the final enthalpy of the SSPCMs was much lower than the theoretical pure PCMs, which was caused by the strong limitation of the molecular movement and the soft segment percentage (PCMs). Besides, the final SSPCMs were usually the films or the composites, which had relatively poor compatibility with textiles. To apply the SSPCMs in the textiles, the direct surface modification of the textiles or the fabrication of the PCM fibers was available.

C) FSPCMs

The FSPCMs had attracted more and more attention for thermal energy storage in recent years [72]. For the PCM textiles, the suitable FSPCMs could be classified into two types: the PCM fibers and the PCM-filled porous hybrid materials. The PCM fibers

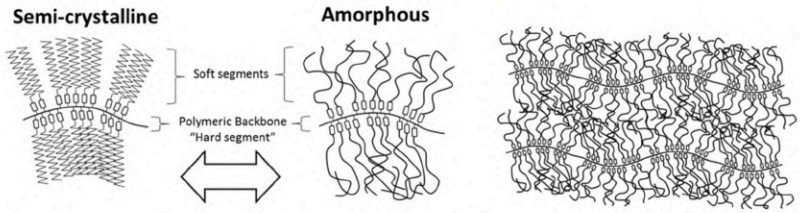

Figure 3 Scheme of the molecular chains of the SSPCMs during the phase transition (Reproduced with permission from [46]. Copyright [2017], [Elsevier]).

here were classified into the FSPCMs because the physical force in the PCM fibers accounted for no leakage in most cases. In detail, the description and preparation of the PCM fibers are shown in the following section "PCM fibers', and only the PCM-filled porous hybrid materials were described here.

The preparation of the PCM-filled porous hybrid materials for thermal energy storage was reviewed in the publication [72]. The porous materials for the storage of the PCM could be the porous foam, the porous powders, and the porous membranes. The principle to encapsulate the PCM in the porous structure is based on the physical interaction (e.g., capillary force, hydrogen bonding, etc.), which avoids the leakage of PCM during the phase transition and supported the thermal stability.

By taking the flexibility and the compatibility of the porous materials with the textiles, the porous powders were suggested. Indeed, various porous powders have been used for the preparation of FSPCMs, including the aerogel [73], the expanded dolomite [74], etc. The main methods for the preparation of the FSPCMs include melting impregnation, vacuum impregnation, dissolving impregnation, the combined technology of dissolving impregnation and the melting impregnation, and so on [73–75]. The usage vacuum impregnation method was proposed to obtain the highest encapsulation ratio. The dissolving impregnation was unable to obtain the high encapsulation ratio, while the adsorption of the PCMs from the solution by the pores was able to be analyzed [75]. Still, the maximum encapsulated PCM content was also affected by the porosity. In detail, Sedat Karaman et al. successfully prepared PEG/diatomite composites as FSPCM via filtration method [74]. The PEG could be retained by 50 wt% into pores of the diatomite without the leakage of melted PEG from the composite. The melting latent heat of the composite PCM was 87.09 J/g, respectively, which was decreased 56.07 J/g when compared with the used PEG. Furthermore, the confined PEG in the diatomite disappeared after the 1000 thermal cycles, which was not clear. Apart from the inorganic porous materials, organic porous materials were available to encapsulate the PCMs. For example, Andriamitantsoa et al. synthesized three types of triamide-linked benzene-based porous polymers and then impregnated them with PEG successfully [76]. The results proposed that the porous polymer by using benzene-1,4-diamine was a suitable framework to encapsulate PEG and the optimized percentage of PEG was suggested to be 85 wt%.

Although the thermal stability of the FSPCMs was found, the final enthalpy of the PCM-filled porous hybrid materials was smaller than the pure PCM. It was suggested that the final thermal behavior of the porous material incorporated FSPCMs was affected by the pore size, pore type, pore structure, etc. [76], 77. In detail, Fang Tian et al. revealed the linear relationship between the pore size and the confined PEG in the silica gel, which could be estimated by the Gibbs–Thomson equation [78] (Fig. 4). Chongyun Wang et al. investigated the thermal behavior of the confined PEG in different carbon-based porous structures (EG, AC, and ordered MC (CMK-5)) [79]. The highest stabilized PEG content was 70wt% for AC and 90wt% for EG and MC. The phase change enthalpy and the PEG crystallinity increased in the order AC < MC < EG at the same PEG content in the composites (Fig. 5). The main reason was found that the pores with micrometer size minimized the enthalpy loss due to the interactions between the pores and the PEG chains, while the mesopores more significantly affected the crystallization of PEG.

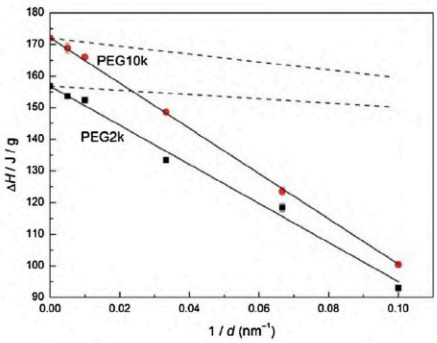

Figure 4 Enthalpy change of the confined PEG in pores with different sizes (ΔH.: enthalpy and d: pore size) (Reproduced with permission from [78]. Copyright [2017], [Elsevier]).

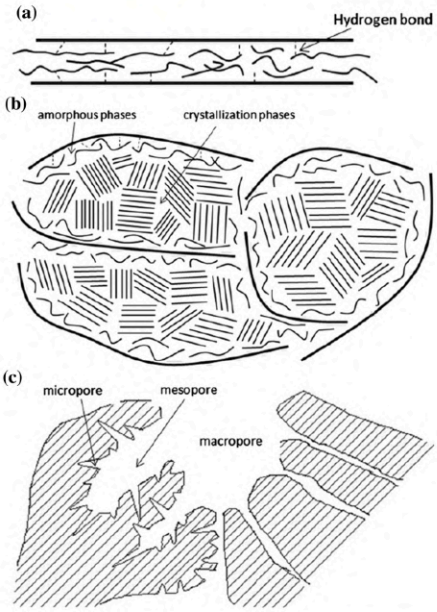

Figure 5 Schematic illustration showing the interactions between PEG and porous carbon materials with different pore diameters: **a** PEG in micropore; **b** PEG in macropore, and **c** pore structure model of AC (Reproduced with permission from [79]. Copyright [2012], [Elsevier]).

Enhanced thermal conductivity (k)

The thermal conductivity (k) of the PCMs is less than 1 W K^{-1} m^{-1}, which resulted in the low thermal energy storage efficiency. For example, the k of the paraffin wax, SA, and PEG (M_w = 6,000) was around 0.43 W K^{-1} m^{-1}, 0.35 W K^{-1} m^{-1}, and 0.21 W K^{-1} m^{-1}, respectively [80–82]. To enhance the overall k, the fillers with high k value were introduced into a polymer matrix, including carbon-based materials and metal-based materials [36, 83, 84].

Tingxian Li et al. modified the k of the SA by introducing carbon-based materials (MWCNT, graphite, and graphene) [85]. It revealed that the graphite-filled SA composites approximately had the k of 3 W K^{-1} m^{-1}, while the MWCNT-filled and the graphene-filled SA composites had the k value less than 1 3 W K^{-1} m^{-1}. Chuyuan Ma et al. investigated the thermal behavior of the EG/metal nanoparticle-filled paraffin [86] and the content of the additives (EG/metal nanoparticle) was less than 3 wt%. The optimized k value of the EG-filled, EG/Cu-filled, EG/Al-filled, EG/Ni-filled, and EG/Fe-filled paraffin was 1.073, 1.95, 1.827, 1.682, and 1.669 W K^{-1} m^{-1}.

Additionally, the k of the hybrid PCMs without leakage was able to be enhanced by introducing metal-based material or carbon-based material in the supporting materials. Nihal Sarier et al. prepared the Ag-incorporated MPCMs which contained the n-hexadecane as the core and n-octadecane as the core, respectively [87]. Jun Li et al. prepared the MPCMs consisting of the n-ecisane as the core and the PUA-CuO as the shell [88]. The maximum encapsulation efficiency of n-ecisane reached 79.4%, and the maximum enthalpy was 162 J/g. Besides, the incorporation of the CuO with the shell could shield the UV radiation, which could act as protection against the damage of the MPCMs from UV.

For both SSPCMs and FSPCMs, the supporting materials or the PCMs are usually to be blended or grafted with carbon-based or metal-based materials. For example, Seyyed Iman Golestaneh et al. added various metal nanoparticles in the PET/fatty acid nanofibers [89]. The thermal conductivity of the hybrid PCM fibers increased with the content of metal nanoparticles. Sriharsha S. Sundarram et al. impregnated the paraffin wax into the Al porous foam, and the optimized k of the paraffin wax-incorporated Al porous foam was the 12 W K^{-1} m^{-1} [90]. It also revealed that the small pores of the Al

porous foam supported the higher k when the encapsulated paraffin wax content was the same. Nan Sheng et al. firstly made a carbon cloth by carbonizing the cotton fabric and then impregnated the paraffin wax into the carbon cloth [91] (Fig. 6). The more sheets supported the higher k value of the paraffin wax-incorporated carbon cloths. Besides, the k of the paraffin wax-incorporated carbon cloths along the thickness direction was higher than the λ of the paraffin wax-incorporated carbon cloths along the yarn direction, and the maximum k was 0.99 W K^{-1} m^{-1}. Chen Li et al. also impregnated the paraffin into the anisotropic rGO/EG aerogels [92]. The thermal conductivity of the paraffin-incorporated rGO/EG aerogel composites increased with the rGO/EG ratio, and the highest k reached 0.8 W K^{-1} m^{-1}.

It was noticed that most studies focused on the improvement of the thermal conductivity by introducing materials with high thermal conductivity into the PCMs, while the final thermal conductivity and the thermal behavior of the final products incorporated with enhanced PCMs were different from the pure enhanced PCMs. Due to the various substrates to carry the enhanced PCMs, the thermal storage energy efficiency can be affected significantly or little.

Adjusting the working temperature

From Fig. 2, it was clear that one of the PCMs had its melting temperature range and the specific melting enthalpy, which failed to meet the requirements of the thermal energy storage system in the complicated environment. So, the eutectic PCMs were prepared for application in various situations. Kinga Pielichowska et al. reviewed the thermal property of the eutectic PCMs [47]. It was found that the melting enthalpy and the supercooling degree of the eutectic PCMs were less than the pure PCMs. The phase transition of the eutectic PCMs started early than the pure PCMs. The components ratio also determined the change of the melting temperature.

The eutectic PCMs were proposed to incorporate into the MPCMs or the FSPCMs. Ming Huang et al. prepared the MPCMs consisting of the binary PCMs as the core and the PALMA as the shell [93]. Meihui Zhou et al. prepared the MPCMs based on the butyl stearate (BS)/hexadecanol (HD) binary system and the AMA was the shell [94]. Dimberu G. Atinafu et al. impregnated the MA-SA eutectic into several porous carbon matrixes [95]. The higher melting temperature, melting enthalpy, and heat storage efficiency of the MA-SA-filled porous carbon matrix were increased when the MA-SA eutectic loading content was increased. Besides, the N-doped carbon matrix supported the more encapsulation of the MA-SA eutectics. Yibing Cai et al. impregnated the capric–myristic–stearic acid ternary eutectic mixture into the porous cellulose acetate fibers [96]. Yibing Cai et al. prepared PET/binary fatty acid fibers as PCM fibers via blending electrospinning [97].

Although the thermal stability and the extended capacity of the thermal storage energy were obtained, there were several points to be noticed.

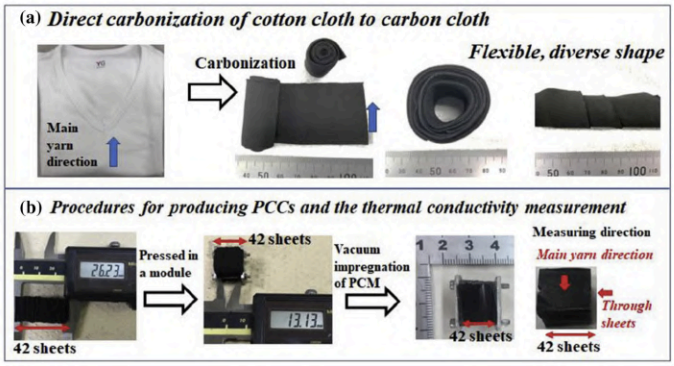

Figure 6 Fabrication of the carbon cloth **a** and the preparation of paraffin wax-filled carbon cloth **b** (Reproduced with permission from [91], Copyright [2020], [Elsevier]).

1) The phase separation possibly occurs if the eutectic PCMs had several melting temperatures which were different from each other [98].
2) The interface between the eutectic PCMs affects the encapsulation efficiency for MPCMs and FSPCMs or the morphology of the PCM fibers.

Preparation of PCM textiles

PCM fibers

Various technologies were used to prepare the PCM fibers, including electrospinning, centrifugal spinning, melting spinning, solution spinning, dry-jet quenching spinning, interfacial polyelectrolyte complex spinning, vacuum impregnation, and injection spinning (Fig. 7). Then, the various polymers were successfully used as the supporting materials for the storage of the different PCMs, including PAN, PET, PVA, PUR, CA, etc.

Blend electrospinning

The blend electrospinning was the basic technology to fabricate the ultrafine PCM fibers (Fig. 8). The PCMs were blended with the polymer solution, and then the mixture of the PCMs and the polymer was fabricated as fibers via electrospinning technology.

Yibing Cai et al. systematically prepared PA 6/LA fibers, PET/LA fibers, and PET/binary fatty acid fibers as PCM fibers via blending electrospinning [97, 100, 101]. Nuray Kizidag systematically prepared the paraffin/PAN composites nanofibers via solution electrospinning [102]. Chao Lin et al. prepared the ultrafine IL/AlN/CoPA phase change composite fibers via electrospinning technology [103]. The maximum PCM weight percentage in the IL/AlN/CoPA phase change composite fibers reached 57.0 wt%, and the enthalpy reached 86.4 J/g. Changzhou Chen synthesized a series of diacid dioctadecyl esters (DADOEs) to enhance the thermal stability of octadecanol and then prepared the DADOE/PET PCM fibers via blend electrospinning [104]. The supercooling degree of the DADOE/PET PCM fibers was significantly reduced, and the encapsulation of DADOEs reached 50 wt% according to the morphology change. Ning Xie et al. prepared a PCM fiber based on fatty acid eutectic of MP and LA and PAN via electrospinning method [105]. It was found that the leakage was avoided in the PCM fibers.

Although the thermal energy storage of the PCM fibers was found, the measured enthalpy was less than the theoretical enthalpy. The hydrogen bonding interactions between PCM and supporting material limited the molecular movement, which resulted in less melting enthalpy. Besides, it was found that the PCM could be on the surface of the outer side or enclosed in the inner part of PCM fiber, while there was no leakage of the PCM during the phase transition. The main reason was the confined effects of the three-dimensional net structure of supporting materials on the movement of the PCMs during the phase transition. Similar results were proved by observing no leakage of the CA which was embedded in the porous cellulose nanofibrous membranes was observed [106].

Additionally, the diameters of the PCM fibers were increased and the strength values of the PCM fibers were reduced when compared with pure fibers

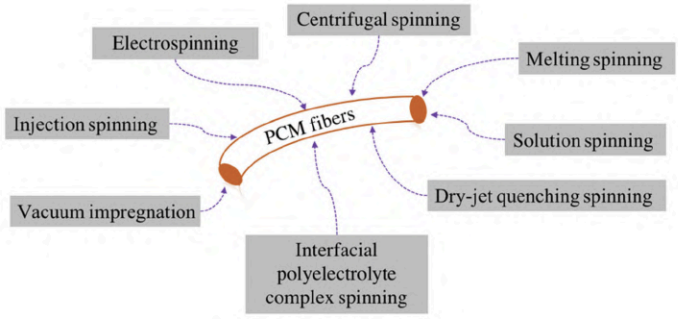

Figure 7 Technologies for preparation of PCM fibers (classification of electrospinning).

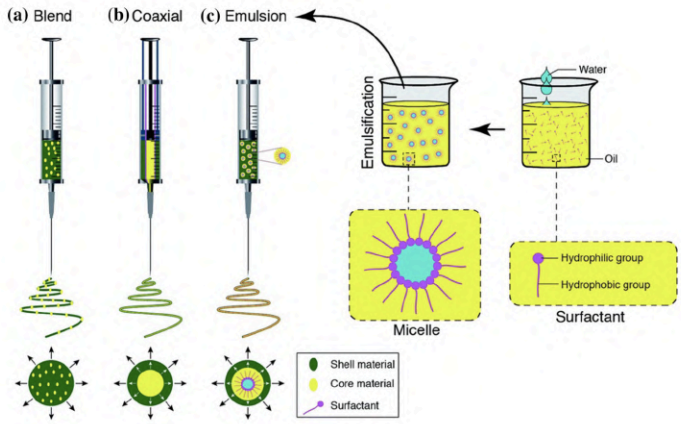

Figure 8 Scheme of different electrospinning technologies **A**: the blend electrospinning, **B**: co-electrospinning, and **C**: emulsion electrospinning) (Reproduced with permission from [99], Copyright [2017], [Royal Society of Chemistry (UK)]).

without PCMs. For example, Changzhong Chen et al. revealed that the diameter of the CA/PEG PCM fibers increased with the more PEG content (Fig. 9), and the ultimate tensile strength of the final CA/PEG PCM fibers was reduced with higher PEG content [107] (Fig. 10). To enhance the mechanical property of the PCM fibers, the additives were proposed to be incorporated into PCM fibers. For example, Thuy Thi Thu Nguyen et al. introduced the fumed silica into the preparation of PVDF/PEG PCM fibers via electrospinning [108]. The tensile strength of the PVDF/PEG/silica PCM fibrous mat was increased from 3.7 to 8.8 MPa. Besides, the type of the PCM also accounted for the ultimate strength. For example, Huizhen Ke investigated the mechanical property of the PET/MES fibers as PCM fibers [109]. The results suggested that entanglements and physical interactions between the MES molecular chains and the PET molecular chains may support the higher ultimate strength.

Besides, the lower k of PCM fibers was modified by introducing the fillers with high k into the PCM fibers. Yinbing Cai et al. added the CNFs in the LA/PA 6 PCM fibers to enhance the thermal conductivity [110]. Ning Xie et al. added the copper nanoparticles into the PCM fibers containing fatty acid eutectic of MP and LA and PAN via the blending electrospinning method [105]. The k of the copper nanoparticle-filled PCM fibers was increased with more copper nanoparticle contents. The maximum k of the copper nanoparticle-filled PCM fibers reached 0.238 Wm^{-1} K^{-1}, which was 2 times the pure PCM fibers.

It was noticed that the PCM fibers were inflammable because the components were organic polymers. To enhance the thermal degradation property of PCM fibers, the incorporation of the nanoinorganic particles was the alternative. For example, Yinbing Cai et al. introduced the nano-SiO_2 particles in the PET/LA PCM fibers [111]. The nano-SiO_2 could generate a physical protective layer on the surface of composite fibers during combustion. Thus, the incorporation of nano-SiO_2 could lead to the increase in initial combustion temperature and the decrease in heat rate release values.

In addition, the incorporation of the MPCMs into the fibers was realized by using blending electrospinning. For example, Sennur Alay et al. prepared the nano-MPCMs consisting of the poly(methyl methacrylate-co-glycidyl methacrylate) as the shell and the n-hexadecane as the core. Then, the MPCMs were introduced into PAN fibers via electrospinning [112]. However, the aggregation of the MPCMs in the PCM fibers was significant, which may result in the uncontrol of the morphology, the mechanical property, and the thermal property of the PCM fibers.

Coaxial electrospinning

The coaxial electrospinning was a modified electrospinning technology by using the inner spinneret and the outer spinneret (Fig. 8). The PCM fibers prepared

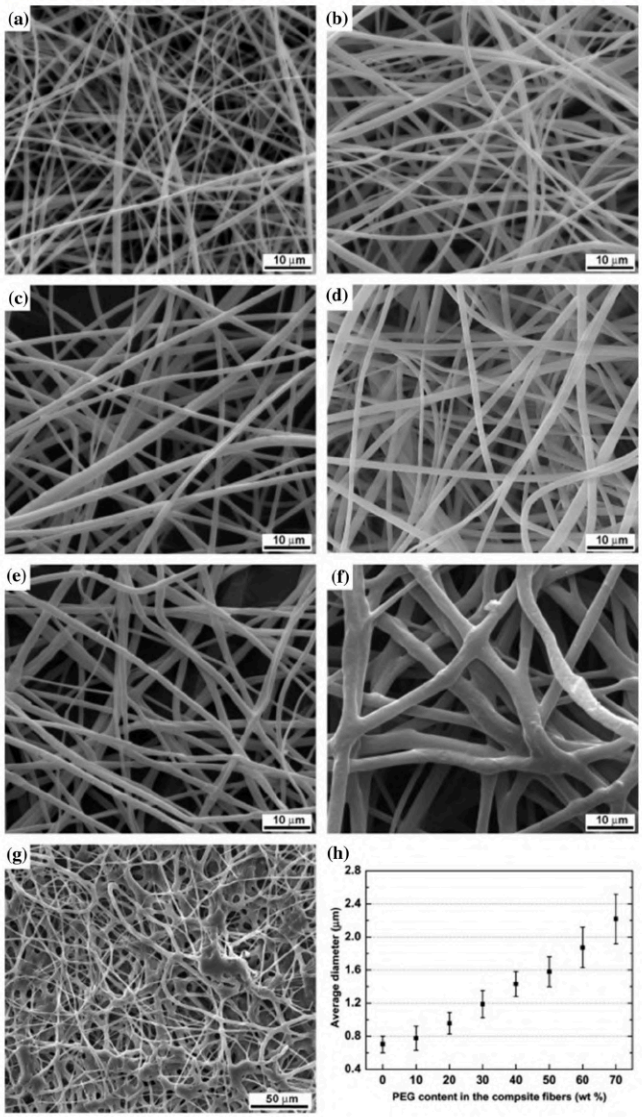

Figure 9 The effect of PEG content on the morphology of PCM fibers (Reproduced with permission from [107], Copyright [2011], [Elsevier]).

via coaxial electrospinning can be obtained by making the PCM solution flow from the inner spinneret and the supporting material solution flow from the outer spinneret. As a result, the PCM fibers consisted of the PCMs as the core and supporting materials as the sheath. By comparing with blend electrospinning,

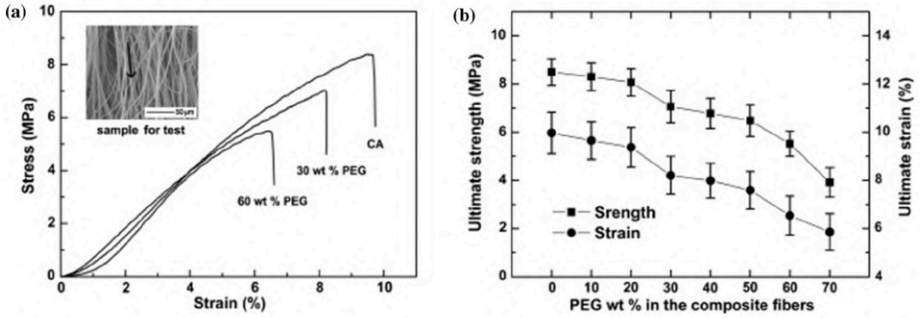

Figure 10 The effect of PEG content on the mechanical property of PCM fibers (Reproduced with permission from [107], Copyright [2011], [Elsevier]).

the PCM fiber prepared via the coaxial electrospinning could have high thermal stability and shape stability [113].

For the fabrication of the PCMs fibers via coaxial electrospinning, there exist some special requirements. The materials for the sheath should have higher thermal stability and higher melting temperature than the PCMs for the core. Usually, the fabrication of the sheath was realized by using the polymer solution instead of the melting polymer, which was also close to the formation of the core from the point of temperature. For the formation of the core, both PCM solution and the melting PCM can be used. The electrospinning with the PCM solution for the formation of the core was labeled as the solution coaxial electrospinning and the electrospinning with the melting PCM for the formation of the core was labeled as the melting coaxial electrospinning. Furthermore, the morphology, mechanical property, and thermal property of the final core–sheath PCM fibers were affected by the interface compatibility and the feed rate ratio between the core solution and the sheath solution as well as the core content. It was found that the flow rate of the core solution and shell solution was significant for the thermal stability, morphology, and mechanical property of the final PCM fibers. The ratio of the core feed rate to the shell feed rate was necessary to optimize. The too higher core feed rate may result in the leakage of the PCM fiber [114], which was confirmed by the change of the water contact angle. Besides, the more content of the PCM inside the core–shell PCM fibers supported the formation of the crystals of the PCM, which restricted the movement of the polymer chains during stretching and exhibited a decrease in fiber elongation [115].

Aziz Babapoor et al. prepared the PCM fibers consisting of the PEG as the core and the PA 6 as the shell via solution coaxial electrospinning [116]. The supercooling degree of the PCM fibers was increased when compared with pure PEG. Wen Feng et al. prepared the PEG/PU fiber via solution coaxial electrospinning [117]. The maximum melting enthalpy of PEG/PU fiber was over 60 J/g. Due to the excellent mechanical property and hydrophobicity of PU, the shape memory and the moisture permeability of the prepared PEG/PU fibrous membranes were observed. Ezgi C. B. Noyan prepared the core/sheath structured ultrafine fibers via solution coaxial electrospinning, The PAN was the sheath, and PEG or PEGME was for the core, respectively [118]. The thermal behavior of the PAN/PEG and PAN/PEGME nanofibers was systematically studied. The encapsulation of the PEG in the PAN was better than the one of the PEGME in the PAN. The final enthalpy of the PEG/PAN nanofibers strongly depended on the weighted average molecular weight of the use PEG. The maximum enthalpy of the PEG/PAM nanofibers reached 133 J/g. Changzhong Chen et al. prepared the PCM fibers consisting of the PEG as the core and the CA as the shell via solution coaxial electrospinning [119]. The ultimate strength and ultimate strain of the PEG/CA PCM fibers were reduced when compared with pure CA fibers. The main reason was that the introduction of PEG weakened the continuous phase structure of CA. We Hu et al. prepared the PCM fibers consisting

of the natural soy wax as the core and the PU as the shell via solution coaxial electrospinning [100]. Besides, the effect of the core content on the final mechanical property of the PCM fibers was investigated [115]. Cao Ruirui et al. also prepared the PCM fiber consisting of GHP as the core and P(AN-co-VDC) as the sheath [120] via the solution coaxial electrospinning. The final enthalpy of the PCM fibers ranged from 27 to 55 J/g, which was dependent on the spinning parameters.

Shuoshuo Wang et al. prepared the PCM fiber with 1-tetradecanol as the core and PVDF as the sheath via melt coaxial electrospinning [121]. The ratio between the shell solution and the core solution and the feeding rate of both core and shell solution affected the morphology of the core–shell PCM fibers. The optimal preparation conditions were determined as the shell solution concentration of 24 wt% and the core feed rate of 0.5 ml/h. The maximum enthalpy of the PVDF@TD PCM fibers reached 108.59 J/g. Fatemeh Haghighat et al. systematically prepared the PCM fibers by embedding the n-octadecane in the PVP, PVDF, and PAN fiber, respectively [122]. As a result, the PVP as the shell material was suitable for the embedding of the n-octadecane according to the small interfacial surface between the n-octadecane and PVP solution. The maximum encapsulation efficiency of the n-octadecane in the PVP fiber reached 35.76%, and the corresponding melting enthalpy was 80.35 J/g.

To enhance the thermal buffering effect of PCM fibers, Nihar Sarier prepared the PEG@PAN hollow PCM fiber by using the PEG@PAN copolymer solution as the shell and the air as the core [123]. The pores were observed, while the PEG@PAN shell was still kept. The final enthalpy of the PEG@PAN hollow PCM fiber depended on the weighted average molecular weight of the used PEG.

In addition, the preparation of the PCM fibers with enhanced thermal conduction was realization. Aziz Babapoor et al. introduced various nanometal particles into the PEG/PA 6 solution, and then the PCM fibers with enhanced thermal conductivity were obtained via coaxial electrospinning [116]. Apart from the expected melting enthalpy and the thermal conductivity increased, the diameter of the prepared PCM fibers was strongly affected by the electrical conductivity of the solution. It also revealed that the introduction of the nanometal particles in the polymer also affected the crystallization structure because

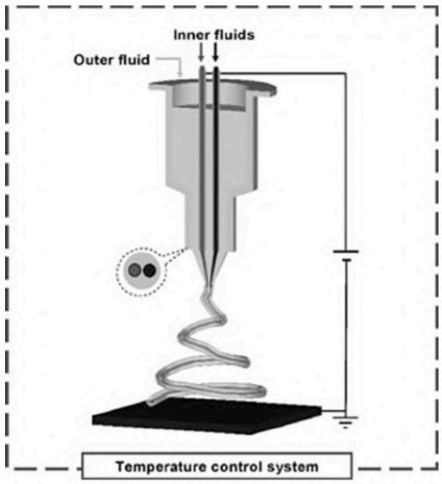

Figure 11 A temperature control multifluidic electrospinning (Reproduced with permission from [124], Copyright [2010], [WILEY-V C H VERLAG GMBH]).

of the interaction between the nanometal particles and the polymer, which altered the final enthalpy of PCM fibers.

Besides, Nu Wang et al. proposed a temperature control multifluidic electrospinning based on the coaxial electrospinning to prepare the multicomponent PCM fibers [124] (Fig. 11). The binary or ternary PCMs were separately enclosed in the composite fibers. Different from the PCM fibers containing the eutectic PCMs, the phase transition of the PCM fibers was only affected by the compatibility between the pure PCM and the supporting materials.

Emulsion electrospinning

The emulsion electrospinning was especially for the incorporation of the MPCMs into the fibers. Different from the MPCM-filled fibers prepared via blending electrospinning, the MPCMs were enclosed in the core part (Fig. 8). Like the coaxial electrospinning, the ratio between the emulsion solution feed rate and the shell feed rate as well as the MPCM loading content in the emulsion solution significantly affected the thermal stability and the morphology of the final PCM fibers. In detail, the higher PCM loadings in the

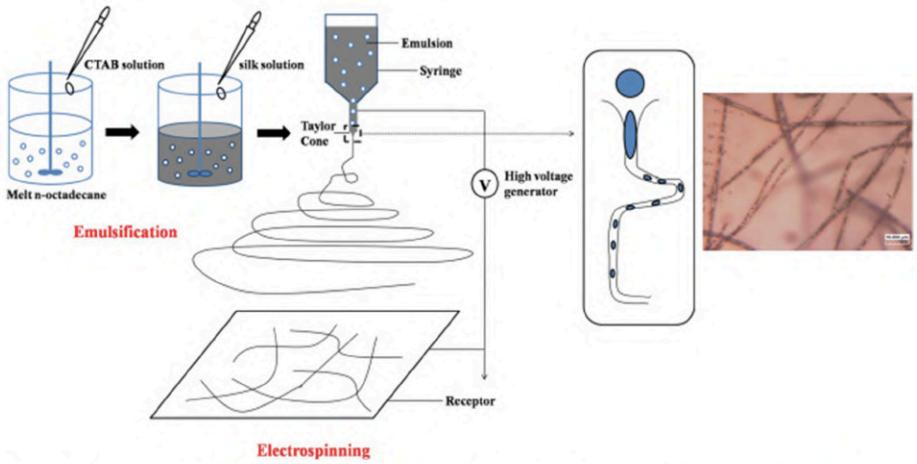

Figure 12 Scheme of the emulsion electrospinning for fabrication of PCM fibers (Reproduced with permission from [126], Copyright [2017], [WILEY]).

nanofibers led to increased fiber diameter, gouged fiber surfaces, and higher heat enthalpies [125].

Liang Zhao et al. prepared the OD/silk PCM fibers via emulsion electrospinning [126] (Fig. 12). The final enthalpy of the OD/silk PCM fibers reached 40.7 J/g. Weiwang Chen et al. prepared the PMIA-based PCM fibers with fatty acid ester via emulsion electrospinning [127]. The encapsulation efficiency of PCM in the PMIA reached 80% and the final PCM fibers had a melting temperature of 36 °C and a melting enthalpy of 26 J/g. Lan Zhou et al. prepared a high chain ester of dodecanol laurate as PCM and fabricated the PCM/PVA fibers via emulsion electrospinning technology [128]. The hydrochloric acid and glutaraldehyde were added to the PCM/PVA mixture solution for the cross-linking reaction to resist the hydrolysis of the PVA-based PCM fibers. The PVA-based PCM fibers with the glutaraldehyde of 8wt% had the water contact angle over 100° and spent at least 30 min in destroying the aqueous situation. Besides, the mechanical property of the PVA-based PCM fibers could be enhanced by the addition of glutaraldehyde.

Co-electrospinning technology

The co-electrospinning technology was realized by using at least two electrospinning devices (Fig. 13). By comparing with the single nozzle electrospinning technology, the production of the co-electrospinning technology was significantly increased. S. I. Golestaneh et al. prepared the PCM fibers consisting of the binary fatty acids as the core and the PET as the shell by using co-electrospinning technology. The increased PCM content in the PCM fibers resulted in the increase in the diameter and the higher melting enthalpy of PCM fibers [129].

Electrospraying technology

The electrospraying technology was a method sharing a similar fabrication mechanism with the electrospinning, and the final product was in the shape of the assembly of particles or the microlayer consisting of the particles [130, 131]. Xiaoman Xiong et al. also prepared the PEG/aerogel/PTFE-coated PP fabric (Fig. 14) [132]. The coating layer was constructed by the microparticles. The increased thermal resistance of the coated PP fabric was found when the sample was placed in the lower temperature, while the thermal energy storage of the coated PP fabric was not clear.

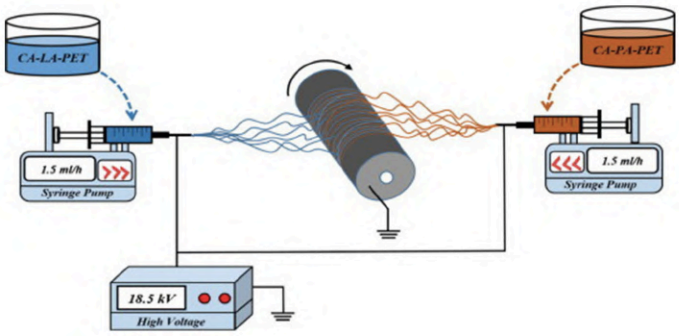

Figure 13 Scheme of the co-electrospinning for fabrication of PCM fibers (Reproduced with permission from [129], Copyright [2016], [Elsevier]).

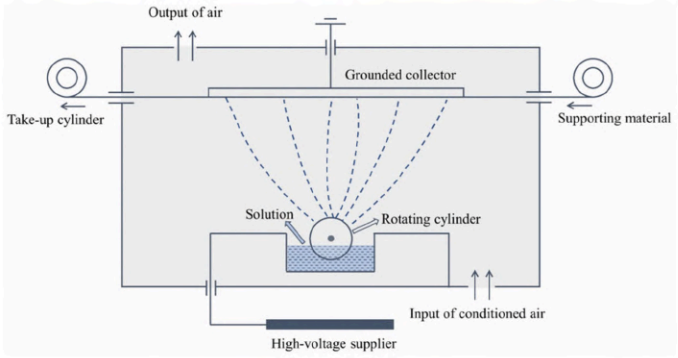

Figure 14 Scheme of electrospraying technology (Reproduced with permission from [132], Copyright [2020], [MDPI]).

Centrifugal spinning

Centrifugal spinning was another method to prepare the ultrafine PCM fibers, which was realized by making use of the centrifugal force [133]. Usually, the preparation of the PCM fibers was realized by using the PCM solution, and the formation of the PCM fibers was caused by the evaporation of the solvent or the movement of the solvent award the coagulating bath [134].

Xiaoguang Zhang et al. prepared PVP/PEG hybrid PCM fibers via centrifugal spinning [135] (Fig. 15). Although there was thermal energy storage and no leakage of the PCM fibers, the thermal property of the

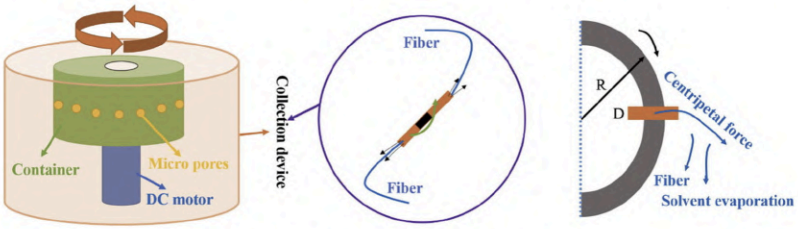

Figure 15 Scheme of centrifugal spinning technology (Reproduced with permission from [135], Copyright [2018], [Elsevier]).

PCM fibers was still considered as not stable due to the hydrophilic property of the PVP and PEG supporting high chemical compatibility with moisture. Guo Chen et al. prepared PAN/PEG-based hybrid PCM fibers via centrifugal spinning [136]. There was no leakage of the PAN/PEG hybrid fibers. Besides, the theoretical melting enthalpy of the PAN/PEG hybrid PCM fibers was less than the experimental melting enthalpy, which was similar to the one via electrospinning technology. The crystalline degree of the PEG encapsulated in the PCM fibers was reduced, while the PEG segments of PAN/PEG fibers were able to crystallize. However, the thermal conductivity of the PAN/PEG fibers was still lower, which was 0.187 Wm^{-1} K^{-1}. Then, Guo Chen et al. continuously prepared the PAN/PEG-based hybrid PCM fibers with nano-SIC fillers via centrifugal spinning [137]. The SIC/PANPEG hybrid PCM fibers had a thermal conductivity of 0.334 Wm^{-1} K^{-1}. Besides, the adding of the nano-SIC fillers slightly increased the fiber diameters. Xueyong Gong et al. prepared the sodium alginate/FK-g-APEG composite phase change fiber via centrifugal spinning [134]. The final enthalpy reached 41.42 J/g and the melting temperature was 47.18 °C.

Melting spinning

The fabrication of the PCM fibers via melting spinning was usually by blending the PCMs with the supporting materials.

US patent US 2011/0027568 A1 developed a spinneret to fabricate multicomponent fibers especially for storage of PCM in the fiber matrix [138]. Wacław Tomaszewski et al. added the paraffin in the PP filament during the melting spinning process [139]. The melting enthalpy of the paraffin/PP filament was increased when the paraffin content was increased, which was caused by the better crystallization ability of the paraffin. Besides, the paraffin occurred on the surface of the PCM filament, and it became obvious when the paraffin content was increased.

Kashif Iqbal et al. incorporated MPCMs into the PP filament during the melting spinning process [140, 141]. The MPCMs were observed in both surface and cross section of the MPCM-filled PP filament. Still, the more MPCM content contributed to the higher latent heat. In detail, the maximum latent heat of the MPCM-filled PP filament reached 9.2 J/g and the corresponding MPCM content was 12 wt%. Furthermore, a linear model was proposed to predict the relationship between the MPCM loading content, the latent heat fusion, and the mechanical property. Fredi et al. prepared PP filaments by blending the paraffin-based MPCMs [142]. In detail, the diameters of the MPCM-incorporated PP filaments strongly depended on the collection speed and the morphology was affected by the MPCM content. The lower mechanical property of the MPCM-incorporated PP filaments was found when the MPCM content was increased.

Besides, the FSPCMs were filled into polymer matrix and then the PCM fibers were obtained. Wei Xia et al. separately introduced the PEG derivatives and the esters into the F-SiO_2 as FSPCMs and then introduced FSPCMs into the PA 6 fibers via melting spinning [143, 144]. Apart from the thermal energy storage, the little effect of the washing cycles on the thermal behavior was found.

Solution spinning

Like the melting spinning, the fabrication of the PCM fibers via solution spinning was usually by blending the PCMs with the supporting materials solution. Besides, the advantage of the solution spinning to prepare the PCMs fibers was to use the biomaterials as the supporting materials.

Weilin Xu et al. prepared PVA/paraffin PCM fibers via the solution spinning method [145]. It was found that the thermal stability and the mechanical property of the prepared PVA/paraffin PCM fibers were reduced when the paraffin content was increased, which was caused by the stronger interaction inside paraffin phases. Zhao Li et al. used the BTCA as the cross-linker to enhance the thermal stability of the PVA/PEG fibers [146]. However, the existence of the new chemical bonding in the PCM fibers limited the movement of the PEG molecules, which resulted in the lower melting temperature and the melting enthalpy.

The MPCMs were also proposed to be introduced in the fibers via solution spinning technology. Meihui Zhou et al. prepared the MPCMs based on the BS/HD binary system and the AMA was the shell. Then, the prepared MPCMs were introduced into the sodium alginate fibers via solution spinning [94]. The final melting enthalpy of the PCM fibers reached 18.79 J/g. Yan Wang et al. prepared the bi-component PCM fiber consisting of alginate and MPCM via

the solution spinning method [147]. The compatibility between the MPCM and the alginate fiber was enhanced when the mixture of the alkylphenol polyoxyethylene and the SDS was transformed into the PCM microemulsion process. The final enthalpy reached 20 J/g with a melting temperature ranging from 25 to 35 °C.

It was found that the PCM fibers prepared via traditional solution spinning technology had small enthalpy. To improve the latent heat, the modified solution spinning technology was used.

Jiawei Wu et al. prepared the silk fibroin/chitosan-based porous fibers via solution freeze-spinning and then filled them with the PEG [148]. To avoid the leakage, the PDMS was used to cover the PEG-filled silk fibroin/chitosan-based porous fibers. The final samples had good mechanical flexibility and thermal regulation. Besides, the PDMS as a covering layer had little effect on the final enthalpy.

Guoqing Wei et al. prepared the core–sheath PCM fibers via the microfluidic method which was based on the solution spinning [149] (Fig. 16). The encapsulation efficiency of the paraffin content in the PCM fibers reached as high as 70%, and the corresponding melting enthalpy of the paraffin-incorporated fibers was 128.2 J/g.

Dry-jet wet quenching spinning

The dry-jet wet quenching spinning technology is a combination of the melting spinning technology and the solution spinning technology [150, 151]. The fiber formation firstly experiences by the dry-jet process or by and then experiences the wet quenching process. The air gap between the dry-jet spinneret and the coagulating bath is set. In detail, the spun fiber first passes through the air gap and then enters the quench bath filled with water. The quenching bath promotes the phase separation to enhance the mechanical property. Then the fiber is collected by wrapping onto a rotating take-up drum. After the collection, the collected fibers are washed for several days or longer to completely remove the pore generator polymer. Then, the water residue in the porous fiber is removed in a solvent exchange process during which the fiber is immersed in pure methanol followed by three batches of fresh hexane. By comparing with blending spinning and solution spinning, the encapsulation efficiency of the MPCMs in the PCM fibers is significantly enhanced.

Yun-Ho Ahn et al. introduced the MPCMs into the polymer fiber via dry-jet wet quenching spinning [152] (Fig. 17). The cellulose acetate, PES, and cellulose were used as the polymer matrix, respectively. Besides, the effect of the parameters on the morphology of the MPCM-incorporated polymer fibers

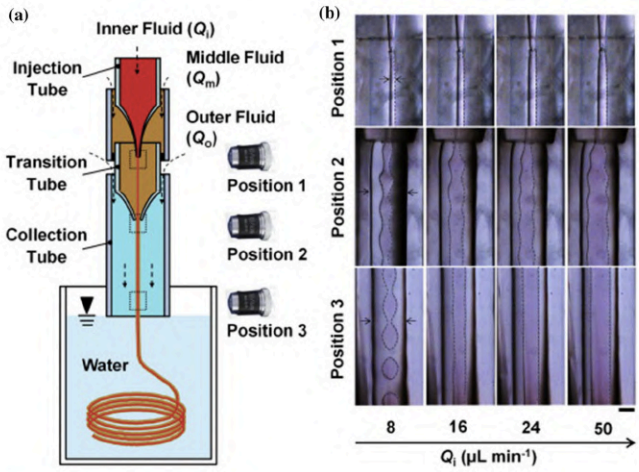

Figure 16 Scheme of the microfluidic method to fabricate the core–sheath PCM fibers (Reproduced with permission from [149], Copyright [2015], [Elsevier]).

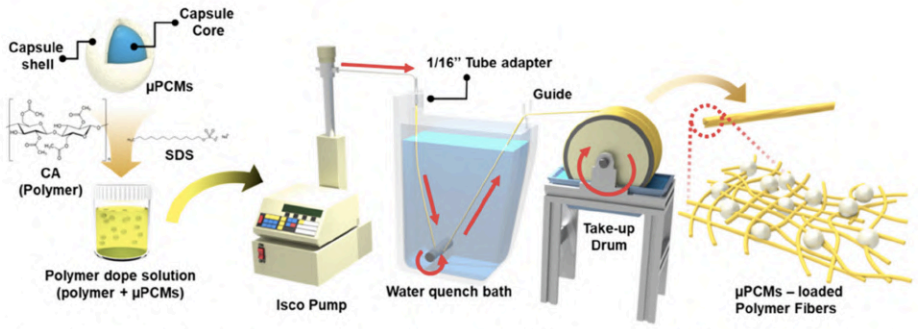

Figure 17 Scheme of the dry-jet wet-quench spinning technology (Reproduced with permission from [152], Copyright [2021], [American Chemical Society]).

and the dispersion of the MPCMs in the polymer fibers were systematically investigated. The thermal energy storage densities of MPCM-incorporated cellulose acetate fibers, MPCM-incorporated PES fibers, and MPCM-incorporated cellulose fibers were over 105 J/g. Particularly for the MPCM-incorporated cellulose fiber as PCMs, it was found that the addition of small content of SDS (less than 1wt% in the dope) supported the well-dispersion of MPCMs in the cellulose fibers. The usage efficiency of the MPCMs during the whole process for the preparation of the PCM fibers reached 94%. Besides, the fiber structure was kept well even the MPCM loading percentage reached 80 wt%.

Injection

The injection method is usually for the PCM-filled hollow fibers, which is realized by using an injector or syringe. Yurong Yan et al. injected the PEG (M_w = 1,000) into the hollow PP filament with a pore size of 0.85 mm by using a microfluidic syringe pump [153]. To avoid the leakage of the molten PEG from the hollow PP filament, two ends of the PP filaments with PEG were sealed. The optimal PCM percentage in the PEG/PP filaments reached 80.0 wt% and the maximum melting enthalpy of the PEG/PP filaments reached 102 J/g. Additionally, the sequence cold drawing treatment of the PEG/PP filaments was expected to enhance the mechanical property, while the melting enthalpy was reduced slightly. To enhance the thermal conductivity of the PCM fibers, Dajun Luo et al. impregnated the paraffin/MWCNTs into the PP hollow fibers [154]. The final maximum adsorption capacity of the paraffin reached 52wt%.

Impregnation (immersion)

Similar to the injection, the impregnation method is also for the incorporation of PCMs into the hollow fibers. Due to the length of the pore along the hollow fibers, the combined effect of the reduced Laplace pressure along the pore and the still air content in the pores reduces the encapsulation efficiency. Therefore, vacuum impregnation is proposed for the enhancement of encapsulation efficiency. Ting Dong et al. filled a fatty acid of MA and TD into the hollow kapok and PET fibers to prepare the PCM fabrics via vacuum impregnation [98]. Particularly, there is no leakage of the PCM from the hollow fiber structure. It was proposed that both capillary forces of the hollow structure and change in surface energy of the MA and TD supported the no leakage.

Besides, the usage of the impregnation method for the incorporation of PCMs with porous fibrous membranes was realized. Jin Zhang et al. impregnated the CA into the porous cellulose nanofibrous membranes [106]. The encapsulation efficiency and the enthalpy of the CA in the porous cellulose nanofibrous membrane were increased with the increased thickness of the pristine porous cellulose nanofibrous membrane. Yibing Cai et al. impregnated the capric–myristic–stearic acid ternary eutectic mixture into the porous cellulose acetate fibers [96]. The highest encapsulation efficiency was higher than 80wt% and no leakage was found.

Still, it was difficult to balance the capillary force and the surface energy of the molten PCM. Therefore, the additional layer was proposed to cover the PCM-incorporated fibers. The fluorocarbon resin was used to cover the PEG/graphene aerogel and paraffin/graphene hybrid fiber was used to store the PEG and paraffin [155], respectively. The final PCM fiber was coated by the fluorocarbon resin to avoid leakage and obtain the hydrophobic property. The optimal encapsulation ratio of the PEG in the PCM fiber reached 84wt% and the melting temperature of the PEG-based PCM fiber was around 59 °C. Besides, the higher electrical conductivity of the PEG/graphene aerogel fibers supported the Joule heating property and the thermal conductivity.

Interfacial polyelectrolyte complex spinning

The interfacial polyelectrolyte complex spinning is based on the interaction of the oppositely charged polyelectrolytes at the interface in aqueous solutions [156]. Since the fiber formation occurs at the ambient temperature by applying the neutral pH and the aqueous solutions, the interfacial polyelectrolyte complex spinning has a great potential to fabricate the biological materials. So, the PCM fibers containing the biological materials as supporting materials are proposed. Hui Fang et al. prepared the PEG/BN/CNF/CS macrofibers via interfacial polyelectrolyte complex spinning (Fig. 18) [157]. The in-situ ionic cross-linking between CNF and CS supported the rapid formation of the fibers. The wrapping effect of cross-linked CNF/CS networks and the strong interfacial interactions contributed to superior shape stability throughout the phase change process. Besides, the homogeneously dispersed BN-OHs in the PCM fibers contributed to the high thermal conductivity.

Summary for preparation of the PCM fibers

In this section, various methods to prepare the ultrafine PCM fibers are reviewed. Their relative properties are given in Table 4. Correspondingly, in Table 5 the advantages and the disadvantages of the various technologies to fabricate the PCM fibers are presented.

Generally, it was summarized that the diameter of the PCM fibers ranged from nanoscale to microscale. The maximum PCM content in the PCM fiber is

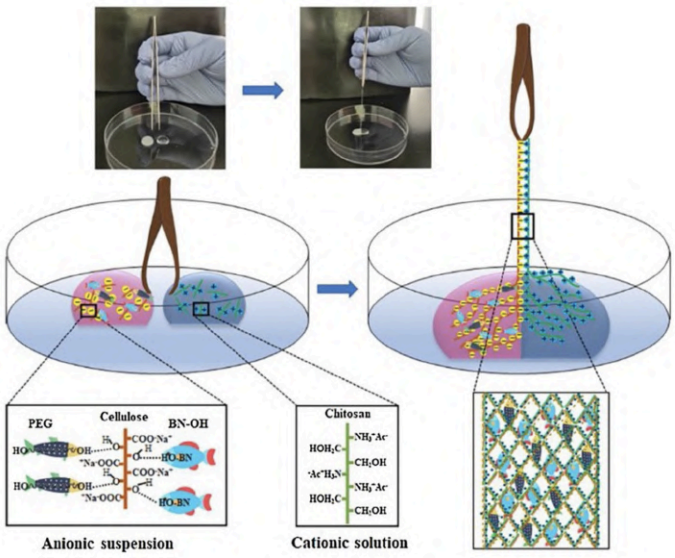

Figure 18 Drawing process of PEG/BN/CNF/CS macrofibers by interfacial polyelectrolyte complex spinning (Reproduced with permission from [157], Copyright [2020], [Elsevier]).

Table 4 Related properties of PCM fibers via different technologies (published from 01.01.2017 to 01.04.2021)

PCM fiber type		Preparation method	Relative properties					
			Diameter range[1] (nm)	Melting temperature range[2] (°C)	Enthalpy value range (J/g)	Thermal conductivity (W m^{-1} K^{-1})	Mechanical property	References
Paraffin waxes based	Paraffin/PAN	Blending electrospinning	301–350	23.53–27.37	11.42–58.75	N/A	N/A	[102]
	n-Octadecane/PVP	Coaxial electrospinning	1577–3728	30.48–30.83	44.57–80.35	N/A	N/A	[122]
	n-Octadecane/silk	Emulsion electrospinning	870–1290	21.16–22.95	15.92–37.58	N/A	N/A	[126]
	Paraffin/MWCNT/PP	Injection	Microscale	53.63–53.64	110.68–113.34	0.21–0.46	78.1–119.9 MPa	[154]
Fatty acid based	MA-LA/PAN fiber	Blending electrospinning	421–700	18.14–20.4	56.45–85.07	0.111	N/A	[105]
	MA-LA/copper nanoparticle/ PAN		~ 669	21.24	85.07	0.183–0.238	N/A	
	MES/PET		300–500	39.84–40.41	58.56–90.43	N/A	5.26–8.95 MPa	[109]
	Fatty acid/PMIA	Emulsion electrospinning	~ 105- ~ 214	36.77	25.89	N/A	N/A	[127]
	Dodecanol laurate/PVA		N/A	28.39–29.24	63.78–65.40	N/A	N/A	[128]
	MAT-TD/kapok/PET	Immersion	1,629,000	24–32.3	76.8	N/A	N/A	[98]
	CA/cellulose	Immersion	N/A	32.5–34.2	122.7–148.0	N/A	N/A1	[106]
PEG-based (including PEG derivatives)	PEG/PA	Blending electrospinning	65–90	~ 38- ~ 42	~ 90- ~ 121	N/A	N/A	[116]
	PEG/PU	Coaxial electrospinning	1780–3230	53.1–53.9	41.1–60.4	N/A	N/A	[117]
	PEG/PAN		424–606	0–57	49–105	0.097–0.099	N/A	[118]
	PEGME/PAN		432–732	0–60	37–45	0.101	N/A	
	PEG/CA		1126–1583	61.7–62.5	52.5–60	N/A	N/A	[119]
	PEG/PVP	Centrifugal spinning	N/A	52.6–52.7	81.4–130.3	N/A	N/A	[135]
	PEG/PAN		N/A	54.45	82.97	0.187	N/A	[136, 137]
	PEG/SiC/PAN		~ 570	39.19–55.95	45.61–69.96	0.334	N/A	
	PEG/silk fibroin/chitosan/ PDMS	Solution-freezing spinning	Microscale	39.5	117.8	0.033 (fabric)	5.5 MPa	[148]
	PEG/PP	Injection	Microscale	37.2–40.2	98.2–102.1	N/A	103–248 MPa	[153]
	PEG/graphene/aerogel	Immersion	70,000–220,000	56–59	33–124	N/A	~ 9- ~ 17 MPa	[155]
	PEG/BN/CNF/CS	interfacial polyelectrolyte complex spinning	Microscale	56.4–58	48.3–103.0	1.705–4.005	N/A	[157]
MPCMs based	Paraffin microcapsule/PP	Melting spinning	70,000–140,000	40–50	13.9–47.5	N/A	2.3 cN/tex	[142]
	BS-HD/AMA/ sodium alginate	Traditional solution spinning	1,755–3,040	23.80	18.79	N/A	3.40 cN/tex	[94]
	MPCM/cellulose	Dry-jet wet-quench spinning	130,000–310,000	18–28	79.02–127.78	N/A	5–30 MPa	[152]
FSPCM based	n-Octadecane/F-SiO_2/PA 6	Melting spinning	Microscale	6.91–9.49	5.87–6.33	~ 0.06	~ 0.78- ~ 1.00	[144]
	PEG (derivatives)/F-SiO_2/PA 6	Melting spinning	Microscale	26.2–27.7	3.9–11.1	N/A	0.89–0.97 cN/ dtex	[143]
Other PCM based	GHP/P(AN-co-VDC)	Coaxial electrospinning	675–796	19.9–22.0	27–55	N/A	N/A	[120]
	FK-g-APEG/sodium alginate	Centrifugal spinning	390,000–450,000	41.78	41.42	N/A	1.5–1.96 cN/dtex	[134]
	Paraffin/MPCM/ alginate	Traditional solution spinning	Microscale	33.83	20.67	N/A	N/A	[147]

Superscript *1* and *2*: the diameter based on average value and the melting peak temperature, respectively

Table 5 Comparison of the different technologies to fabricate PCM fibers

Technology	Advantages	Disadvantages
Blending electrospinning[1]	Very easy to fabricate the ultrafine PCM fibers	Possible failure to encapsulate of PCM component Encapsulation efficiency was not high The final enthalpy of the PCM fiber was much less the pure PCM
Coaxial electrospinning[2]	No leakage of the ultrafine PCM fibers	Interfacial compatibility of the inner flow and the outer flow was necessary to balance
	Encapsulation efficiency was increased	The final enthalpy of the PCM fiber was much less the pure PCM
Emulsion electrospinning[2]	Especially for incorporation of MPCM into fiber	Interfacial compatibility of the MPCM solution and the solution of the supporting materials was necessary to balance
	No leakage of the ultrafine PCM fibers	The diameter of the final fiber strongly depended on the size of MPCM or NPCM
	No effect of the supporting materials on the phase transition of the MPCM	
Co-electrospinning[2]	Very easy to fabricate the ultrafine PCM fibers	Unable to encapsulate of PCM component Encapsulation efficiency was not high
	Higher mechanical property of the fabricated fibrous membrane	The final enthalpy of the PCM fiber was much less the pure PCM
Centrifugal spinning[1]	Very easy to fabricate the ultrafine PCM fibers	Possible failure to encapsulate of PCM component Encapsulation efficiency was not high The final enthalpy of the PCM fiber was much less the pure PCM
Melting spinning[1]	Very easy to fabricate the PCM fibers	Selection of polymer depending on the thermal behavior Encapsulation efficiency was not high The final enthalpy of the PCM fiber was much less the pure PCM
Traditional solution spinning[1]	Very easy to fabricate the PCM fibers	Encapsulation efficiency was not high The final enthalpy of the PCM fiber was much less the pure PCM
Modified solution spinning (solution-freezing spinning, and microfluidic method)[2]	High encapsulating efficiency High latent heat Enhanced mechanical property	Interfacial compatibility required balance
Dry-jet wet quenching spinning[2]	High encapsulation efficiency Enhance mechanical property of PCM fibers without other additives	Relatively complicated process and longer time to fabricate the PCM fibers
Injection	Control of the PCM content in fibers No leakage of the PCM fibers	Limitation for objectives (only for hollow fibers)
Impregnation	Control of the PCM content in fibers No leakage of the PCM fibers	Limitation for objectives (only for porous fibers) Pore size and porosity affected the encapsulation efficiency and the final enthalpy
Interfacial polyelectrolyte complex spinning	Convenient to fabricate PCM fibers	Limitation of objectives (only for the polyelectrolyte solution)

Superscript *1* and 2: the primary spinning technology and the modified spinning technology, respectively

limited and the mechanical property of the PCM fiber is also strongly affected by the PCM content.

In detail, the electrospinning technology was the most popular method to fabricate the ultrafine PCM fibers. It was found that the blending electrospinning technology supported the smaller ultrafine PCM fibers, while the coaxial electrospinning technology and the emulsion electrospinning technology supported the higher thermal stability. Besides, the compatibility between the PCMs and the polymer

solution significantly affected the final property of the ultrafine PCM fibers when the electrospinning technology was applied. In addition, the mechanical property of the fibrous webs consisting of the ultrafine PCM fibers prepared via all the electrospinning technologies is poor. The same consideration was for the ultrafine PCM fibers prepared via centrifugal spinning. To support the dual functions of thermal storage and mechanical properties, the modified traditional fiber spinning technologies or the standard fiber spinning technologies had an advantage over the aforementioned. Furthermore, the interfacial polyelectrolyte complex spinning is more convenient to obtain the PCM fibers without any other setups, while the suitable PCMs type was limited.

PCM yarns

For the PCM fibers, the thermal energy storage, the thermal stability, and the mechanical property were focused. However, the direct incorporation of the PCM fibers into textiles was still a challenge. In some research works, the PCM fibers were directly woven into fabrics with a simple structure. The relative less of the interweaving points of the so-called PCM fabrics and no twist between the PCM fibers did not support the direct usage of the PCM fibers as fabrics. To apply the PCM fibers in the fabrics, it was necessary to fabricate the PCM yarns. Different from the investigation on the basic thermal energy storage of the PCM fibers, how to make the PCM fibers as the PCM yarns was a point.

Traditional yarn spinning technology

The traditional yarn spinning technology is a common method to fabricate PCM yarns. Jia-Horng Lin et al. prepared the PCM yarns by using PCM-incorporated roving for the formation wrap yarns and both SS and BC for the core yarns [158]. In detail, the composite yarns prepared by using both BC roving and PCM roving for the formation wrap yarn had the decreased tenacity when the twist degree was increased. Besides, the yarns whose wrap yarn was formed by using a single component shared the same trend that the tenacity was increased with the higher twist degree.

Traditional polymer fiber spinning technology

The traditional polymer fiber spinning technology is also possible to fabricate the PCM yarns, which is different from the one for the PCM fibers. By comparing with PCM fibers, the PCM yarns could be considered as the tight assembly of the PCM fibers via twisting. The PCM yarns or the PCM multifilament yarns could be labeled when there was an existence of a twist in the PCM multifilaments or fibers. It is suggested that the MPCMs possibly destroyed when they were exposed to the melting polymers for a long time. From this point of view, the design of the spinnerets and the modification of the fiber spinning for the preparation of the PCM multifilaments at one time are the point. Kashif Iqbal et al. developed a specific nozzle to fabricate multifilaments at the same time by overcoming the extrusion problem [159]. Then, the PCM yarns were obtained by twisting multifilaments with 3 turns per inch. Similar to the PCM fibers (filaments), the higher MPCM content in the PCM yarns contributed to the higher thermal energy storage while reduced the strength of the PCM yarns.

Other methods based on electrospinning technology

The twisting electrospinning based on the electrospinning is used for the fabrication of PCM yarns. Rouhollah Semnani Rahbar et al. prepared the PCM yarns via twisting electrospinning technology by using the MPCM consisting of hexadecane as the core material and the melamine–formaldehyde resin as the shell material and the PA 6 as the nanofibers [160]. The major MPCMs were encapsulated inside the PCM fibers, while some MPCMs were still observed on the surface of the PCM yarns. The phenome was caused by the blending of the MPCMs with the PA 6 solution, which was similar to one from the blending electrospinning. Guizhen Ke et al. made a coating of PEG on the cotton/CNT yarns and then used PAN nanofibers to protect the PEG coating layer via twisting electrospinning technology [161]. Weiwang Chen et al. used a multistep twisting setup based on electrospinning to prepare the hybrid yarns with PVA as core and HPCMEs/PMIA PCMs fibers as a sheath. By immersing the prepared hybrid yarns in the hot water to remove the PVA, the ultrathin hollow PCM fibers were obtained [162]. Both the

Table 6 Related properties of PCM yarns prepared via different technologies (01.01.2015–01.04.2021)

PCM yarns	Preparation method	Twist/inch	Melting temperature (°C)	Enthalpy (J/g)	Mechanical property	Ref
SS/BC/PCM yarn	Ring spinning	9–21	N/A	N/A	0.5 ~ 2.4 cN/dtex	[158]
MPCM/PP yarn	Modified fiber polymer spinning	3	~ 28	8.08	~ 18– ~ 32 cN/tex	[159]
MPCM/PA 6 yarn	Twisting electrospinning	N/A	15.39–15.67	0.46–4.28	N/A	[160]
PEG/cotton/CNT/PAN yarn		N/A	56.5–66.3	126.0–35.3	N/A	[161]
PVA/HPCMEs/PMIA yarn	Multistep twisting	N/A	35.27–37.68	21.77–25.07	32.6–36.7	[162]

thermal insulation and the thermal energy storage were realized.

Summary for preparation of the PCM yarns

Table 6 lists the relative properties of some PCM yarns via different methods. The PCM yarns were considered as the assembly of the PCM fibers (filaments). The fabrication of the PCM yarns strongly depended on the mechanical property of the PCM fibers. From this point of view, it was more difficult to prepare the PCM yarns than the PCM fibers. Still, there is the novel technology for fabricating the PCM yarns which is directly based on electrospinning. Besides, the effect of the PCM content in the PCM yarns on the mechanical property of the PCM yarns is like the one of the PCM fibers. What's more, the PCM yarns could have close surface emissivity by controlling the outer layer yarns [163]. However, the PCM yarns seemed only for the fabrication of the PCM fabrics. The great potential of the PCM yarns remained to be discovered.

PCM fabrics

Various methods were used for the creation of the PCM fabrics, which could be classified into two types: 1) the methods to fabricate PCM fabrics by directly using PCM yarns, including weaving, knitting, etc., and 2) the methods to obtain the PCM fabrics via surface modification, including pad–dry–cure coating, grafting, lamination, printing, etc. For the first method, there was successful research work to fabricate the PCM fabrics by directly using PCM yarns [158]; however, it was relatively more difficult since the mechanical property of the PCM yarns or PCM fibers was not high enough according to the aforementioned description. Besides, there was a limitation of the PCM content in the PCM yarns or fibers, which also affected the final thermal enthalpy. For the second method, it was much more convenient to prepare PCM fabric, while the breathability could be strongly affected.

Pad–dry–cure coating method

The pad–dry–cure coating method is suitable for the coating of MPCMs, FSPCMs, and nano-PCM capsules on the fabrics. The thermal energy storage was strongly increased when the MPCM content on the fabric was increased [164].

Abu Shaid et al. made a coating of aerogel/eicosane FSPCM particles on the fabric and the thermal buffering effect was observed [73]. Guocheng Zhu et al. made a coating of n-ecisane-based MPCM on the bamboo fabric by immersing the bamboo fabric in the MPCM emulsions [165]. Sandra Varnaite-Zuravliova et al. made a coating of MPCMs on the knitted fabrics by using auxiliaries during the pad–dry–cure process [166]. The knitted fabrics with complicated structures were able to initially adsorb more MPCMs. However, the washing cycles significantly affected the thermal regulation because there were no binders, where there was a loss of MPCM [166]. Similar results related to the effect of the washing cycles on the final thermal behavior of the MPCM-coated fabrics were found in research work [35]. Sennur Alay Aksoy et al. made a coating of the MPCMs on the cotton fabric by using the NaCl solution to enhance the adhesion between the MPCMs and cotton fabrics [167]. However, it was found that some MPCMs were broken or caved with increasing laundering cycles.

1) Usage of the binder for coating of MPCMs or FSPCMs on the fabric

To solve the problem, the usage of suitable binders to enhance the adhesion between the MPCMs and the fabric is the solution. Apart from the binders, the thickener is also used to enhance the adhesion between the MPCMs and the fabrics.

Yunyi Wang et al. prepared PCM fabrics by using paraffins, PU3630, and HEUR-B via dry coating method [168], and the maximum enthalpy reached 136.9 J/g. Yun Su et al. made a coating of MPCMs on the flame resistance fabric via the dry coating method [169] (Fig. 19). The coating slurry was prepared by mixing microcapsule suspension, thickener, adhesive, and water. The thickener (HEUR-B) was used to mix all components for speeding up the uniform dispersion and maintaining the surface smooth. Agnieszka Karazewska et al. made a coating of n-ecisane-based MPCM on the nonwoven fabric by using a polysiloxane elastomer as a binder [52]. The final loading efficiency of the MPCM on the nonwoven fabric reached 19.2%, and the enthalpy of the PCM fabric was 34.6 J/g. Tapas Ranjan Kar et al. made a coating of the capric acid (CA) and stearic acid (SA) on the cotton fabric with the binder of polyhydroxy-amino-methyl-silicone and the catalyst of $MgCl_2$ via dry coating [170]. The chemical bonding between the cotton fabric and the coating layer was found, which resulted in the enthalpy loss and the lower flexibility of the prepared PCM fabrics. As a result, the maximum melting enthalpy of CA-coated cotton fabric reached 36.5 J/g. Wei Zhang et al. made a coating of PMMA/SiO_2 PCM microcapsules on the denim fabric via the pad–dry–cure coating method [171]. Because the denim fabric was the substrate, the PTF thickener was used for coating. Yuwanda Iamphaojeen et al. made a coating of MPCM on the cotton fabric by using the PSS as the binder [172]. Jun Li et al. prepared MPCMs consisting of the n-ecisane as the core and the PUA-CuO as the shell and made an MPCMs coating on the cotton fabric with binder [88]. The final enthalpy of the MPCMs-incorporated cotton fabric was higher than 36 J/g.

Besides, the nano-PEG capsules were also coated on the fabric by using the binders. M Karthikeyan et al. made a coating of nano-PCM capsule consisting of the paraffin waxes as the core and the UF as the shell on the cotton fabric by using the PUR as the binding agent [57]. However, the final enthalpy of the nano-PCM capsule-coated fabric was less than 2 J/g. M Karthikeyan et al. also made a coating of nano-PCM capsules consisting of the PEG as the core and the UF as the shell on the cotton fabric by using the PUR as the binding agent [173]. However, the final enthalpy of the nano-PCM capsule-coated cotton fabric was less than 1 J/g. From this point of view, the MPCMs and FSPCM powders were usually coated on the fabrics.

By using the binder to fix the MPCMs or FSPCMs on the fabric, the ratio of the binder to the MPCMs was necessary to be controlled. F. Salaün et al. systematically studied the effect of the ratio of the binder to MPCMs on the final thermal behavior of the MPCM-coated fabric [174]. As shown in Fig. 20, the latent heat of the binder/MPCM was reduced with the increased binder, and the linear relationship was found. For the onset melting temperature of the binder/MPCM composites, the lower content of the binder had little effect and was suggested less than 30 wt%. M Karthikeyan et al. also revealed that the binder was unable to pick the nano-PCM capsules when the ratio of the binder to the nano-PCM capsules was higher than 4: 1 (binder: nano-PCM capsules). The main reason may be caused by the viscosity change, and the nano-PCM capsules content was much less.

Besides, both the fabric structure and the fiber materials were considered to affect the initial take-on

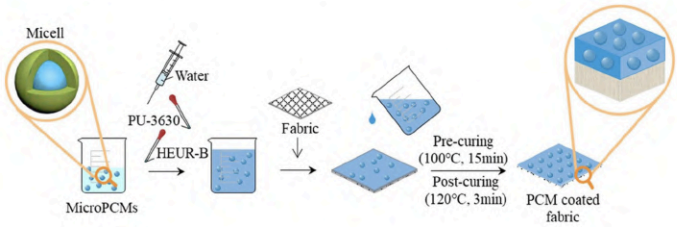

Figure 19 Scheme for preparation of MPCM-incorporated fabrics via pad–dry–curing coating method (Reproduced with permission from [169], Copyright [2020], [Elsevier]).

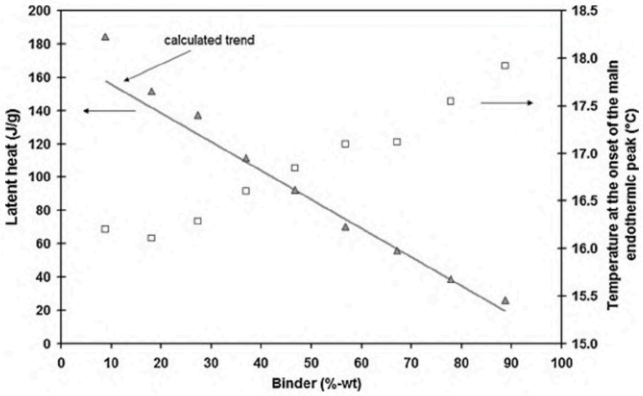

Figure 20 The effect of binder content on the latent heat and the onset melting temperature of the binder/MPCM composites (Reproduced with permission from [174], Copyright [2010], [Elsevier]).

of the mixture of the MPCMs and the additives (blinder and thickener). Luz Sánchez-Silva et al. made a coating of MPCMs (Rubitherm® RT31 microcapsules) on the different fabrics by using WST SUPER-MOR® commercial binder [175]. In the study, the PET/PUR fabric, PET/PA 6/Elastane fabric, PA 6 fabric, PET/PVC fabric, PEG/cotton fabric, PA 6 fabric, and cotton fabric were used. As result, the PET/PUR fabric had the highest MPCM content of 25.6 wt%.

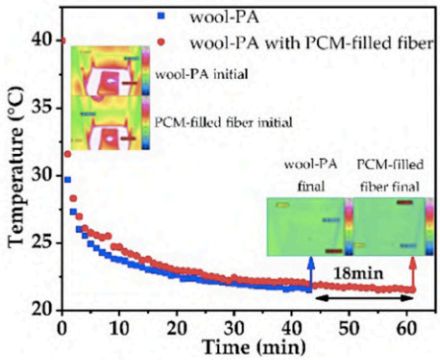

Figure 21 T-history curves of the wool/PA fabric with and without PCM by using infrared camera (Reproduced with permission from [153], Copyright [2021], [MDPI]).

2) The negative effect of PCM fabrics via the pad–dry–cure method by using binders

Although the thermal stability of the MPCM-coated fabrics is obtained by using the binder, the other properties of the fabric are affected, including the permeability and the mechanical property.

The mechanical property of the MPCM-coated fabric including the tensile strength and the elongation at the break was affected by the MPCM content, curing temperature, and curing time [176]. Particularly, the fabric frictional sound, which was caused by the mutual friction between two fabrics, was also influenced by the coating of the MPCMs on the fabric. Inhwan Kim et al. investigated the effect of the curing time and curing temperature on the frictional sound of the MPCM-coated fabrics [177]. It was found that the toughness had a strong relationship with the frictional sound, which was considered to be higher with more MPCM content. Correspondingly, the lower MPCM content on the fabric had less effect on the frictional sound. Additionally, the increased curing time had a more significant effect on the frictional sound by comparing it with the curing temperature. Mostafa Khosrojerdi et al. prepared the FSPCM-coated cotton fabric and the results revealed that the air permeability and water transferability were significantly reduced [74]. Besides, the usage of the binder reduced the water absorbance of the MPCM-coated fabrics [57, 173]. Furthermore, the coating of MPCM on the fabric may also affect the infrared emissivity. Y. M. Park et al. revealed that the infrared emissivity of the MPCM-coated waterproof

breathable nylon fabric was increased from 0.88 to 0.9 and the corresponding emission power was increased from 339 to 345 ($W/m^2 \cdot \mu m$) [178].

3) Modification of permeability of PCM fabrics with binders

It is common for the PCM fabrics with binders to have the small breathability. To modify the breathability of PCM fabric with binders, the control of the coverage area of the PCMs is feasible. US patent US 20,090,100,565 A1 proposed a multilayer structure for PCM fabrics, where the PCMs were adhered at the selected points in the middle fabric layer by using the binders. The final multilayer PCM fabrics were characterized by a soft touch and flexibility [179]. US patent US 9062913B2 reported the incorporation of the PCMs elements into the fabrics, which could enhance the breathability [180]. Besides, the wicking property of the fabric significantly affected the comfortability of wearers. To support the dual functions with wicking property and thermal buffering behavior of the fabrics, US patent US 2020/0146378 A1 proposed to modify the polymeric shell of the MPCMs with an outer shell having a siloxane attached to an exterior surface of the polymer wall by a surfactant. Then, the wicking property of the fabrics coated with modified MPCMs was about 4 times higher than fabrics coated with unmodified MPCMs.

Grafting

The grafting method is used to construct the new chemical bonding between the PCMs and the fabrics.

F. Ghahremanzadeh et al. enhanced the adhesion of PEG to wool fibers by using fluorinated and Chlorine-Hercosett pre-treated wool fabrics followed by reaction with PEG-DMDHEU [181]. Less loss of the melting enthalpy of the PEG-DMDHEU-coated fluorinated and Chlorine-Hercosett pre-treated wool fabrics was observed after 5 washing. D. Bemmoussa prepared the MPCM consisting of the n-hexadecane as the core and the poly(allyl ethylene diamine) as the shell [182]. To reduce the loss of the MPCMs on the cotton fabric, the poly(allyl ethylene diamine) was firstly activated with trichlorotriazine 2,4,6 and then coated on the cotton fabric. Ahmed G. Hassabo prepared a novel material consisting of the different carboxylic acids and different fatty acids based on the esterification reaction between different carboxylic acids and different fatty acids with diglycol compounds [183]. The PCM composites were prepared by blending the novel materials with the octadecane. Then the PCM composites were applied on the surface of the cotton fabric via dry coating. Both capillary force and the chemical bonding between the PCM coating and the cotton fabric supported the thermal stability. Subsequently, Ahem G. Hassbo et al. prepared the pectin-fatty acids PCM composites and pectin–fatty acid–octadecane PCM composites and also applied them on the cotton fabric, respectively [53]. The pectin–fatty acid–octadecane-coated cotton fabric was considered more comfortable than those cotton fabrics coated with pectin-fatty acid composite.

Lamination

Principle of the lamination technology is to incorporate the PCM into polymer film, and then applied the PCM-filled polymer film on the inner side of the fabric [184]. For example, water-blown PUR foam mix intermingled with 20–60% PCM capsules was laminated on the inner side of fabric and then the drying process was applied to remove the water. Although the thermal buffering effect was obtained, the side effect of the lamination on the air permeability and water vapor permeability was more significant than other methods, which did not support the PCM fabric via lamination for personal usage instead of industrial usage. Sanghyun Yoo et al. made the multifunctional composites containing the glass fiber/epoxy/MPCMs, where the epoxy/MPCMs were laminated in the glass fabrics [185]. More content of the MPCMs in the composites supported the higher enthalpy value. However, the overall thermal conductivity of composites was reduced due to the lower thermal conductivity of the microcapsules as well as the non-uniform distribution of micro-PCMs inside the laminations.

Printing

The advantage of the printing technology is to control the coating area on the fabrics. Alicja Nejman et al. made a coating of MPCMs on the PET fabrics by using the printing technology, the coating technology, and the padding technology separately [186]. It was found that the printing was proposed to obtain the largest melting enthalpy of the PCM-incorporated fabrics while resulted in the lowest air permeability.

Knitting or weaving

The knitting or weaving technology is common to obtain the PCM fabrics by using PCM yarns. In this case, the final thermal buffering effect of the PCM fabrics was focused on. Weiwang Chen et al. fabricated the PCM fabric based on the hollow HPCMEs/PMIA PCMs yarns [162]. The obtained PCM fabrics had lower final stable temperature than the commercial fabrics. Besides, it was found that the thermal buffering effect was improved when the density of the PCM yarns in the fabric was increased. Jia-Horng Lin et al. prepared the PCM warp-knitted fabric by using the PCM yarns [158]. US patent US 2019/0017200 A1 also proposed to incorporate PCM yarns into the three-layer circular knitted fabric [187]. The air permeability of the final PCM warp-knitted fabric was strongly based on the fabric structure (e.g., thickness, warp density, weft density, etc.).

Summary for the preparation of PCM fabrics

Table 7 lists the relative properties of the PCM fabrics. Among the aforementioned technologies (pad–dry–cure method, grafting, lamination, and printing), it was found that the MPCMs were usually coated on the fabrics, and the usage of the binder was to avoid leakage. However, the usage of the binder could hinder the permeability of the air and water vapor and also altered the surface chemistry and the mechanical property. From this point of view, it was necessary to modify the coating of MPCMs on the fabrics. Besides, the kitting or weaving method to fabricate the PCM fabric by using PCM yarns supported the breathability. However, the PCM yarns were almost composite yarns where the PCM content was limited, which reduced the final melting enthalpy. Besides, the success of the fabrication of PCM fabrics strongly depended on the mechanical behavior of PCM yarns.

Application of PCM textiles

Since the PCM textiles have the thermal energy storage with little temperature change during the phase transition, the PCM textiles are characterized with a thermal buffering effect. The thermal regulation of the PCM textiles is then considered due to the thermal buffering effect. Besides, the PCM textiles are modified by introducing other materials to obtain other functions except for the thermal regulation, which is proposed to be applied in the textile industry. Therefore, the discussion on the application of the PCM textiles was classified into two parts: the application of PCM textiles based on thermal regulation and the application of the multifunctional PCM textiles suitable.

Thermal regulation of PCM textiles

One of the applications for PCM textiles was to enhance the thermal buffering effect of the firefighter clothing [168, 188, 189]. Fanglong Zhu et al. revealed that the incorporation of the PCM in the multilayer fabrics as firefighting clothing effectively reduced the heat stress [190]. It was noticed that the PCMs are flammable and the aerogel as the thermal insulation layer was proposed to be in the multilayer fabric system for the firefighter clothing. Abu Shaid et al. introduced the aerogel in the multilayer PCM fabric system for the firefight garment [191]. It was found that the aerogel-incorporated multilayer PCM fabric had higher thermal resistance, higher ignition time, and lower flame-spreading speed. Subsequently, Abu Shaid et al. also made a coating of aerogel-eicosane on the fabric, and the thermal buffering effect was found [73]. Hui Zhang et al. studied the position of the thermal liner of the PCM layer and the aerogel layer inside the firefighter clothing [192]. Besides, the PCMs were proposed to apply in the bedding textiles. US patent US 2019/0133349 A1 reported an expandable pillow with PCMs to realize the thermal management [193]. US patent 2019/0053634 A1 also reported an embedding product containing the PCM materials [194]. It was found that all the results proposed the thermal liner should consist of the transitional thermal layer, the aerogel layer, and the PCM layer from the heat source to the skin. Hwasook Yoo et al. proposed that the outer layer of a garment ensemble is the more appropriate position for the effects of the PCM [195]. Seba Demirbag et al. used the clay nanoparticle-doped gelatin/sodium alginate composites as the shell to enclose the n-eicosane [196], which has better flame resistance than the MPCM with the pure polymeric shells. Ana Maria Borreguero et al. investigated the compatibility of the PCM with the footwear industry [197]. It was found that the nonwoven foamed fabric without adhesive and the leather from pig skin allowed incorporating

Table 7 Related properties of PCM fabrics (01.01.2014–01.04.2021) (all the listed parameters were for PCM fabrics)

PCM fabric		Preparation method	Melting temperature (°C)	Enthalpy (J/g)	Air permeability	Thermal conductivity (W m^{-1} K^{-1})	Mechanical property	References
MPCM-incorporated	MPCM-coated protective fabric	Pad–dry–curing	9–55.8	46.7–144.9	0–0.2 mm/s	0.067–0.093	1551–1646 N (warp) 978–1183 N (weft)	[169]
	MPCM (PMMA/SiO_2/paraffin/BS)-coated denim fabric	Pad–dry–curing	37.1–38.9	N/A	N/A	N/A	N/A	[171]
	MPCM (n-Octadecane/PDDA)-coated cotton fabric	Immersion + rising	28.1–28.7	0.46–1.59	N/A	N/A	N/A	[172]
	MPCM (n-ecisane/PUA-CuO)-coated cotton fabric	Coating	39.3	36.8	N/A	N/A	N/A	[88]
	MPCM-coated cotton fabric	Grafting	18.0	N/A	N/A	N/A	N/A	[182]
	Glass fiber/epoxy/MPCMs multilayer fabric composite	Lamination	36.5–37.0	6.70–40.9	N/A	N/A	N/A	[185]
	MPCM-coated knitted PET fabric	Padding	22.9	26.5	~ 1,200 mm/s	N/A	N/A	[186]
		Printing	23.1	28.4	~ 1,000 mm/s	N/A	N/A	
		Coating	22.9	26.6	~ 2,100 mm/s	N/A	N/A	
	MPCM-coated nonwoven PET fabric	Pad–dry–coating	32.9	37.3	3290–3890 mm/s	N/A	N/A	[52]
FSPCM incorporated	Aerogel/eicosane-coated heat protect fabric	Pad–dry–curing	36.55–36.8	N/A	N/A	N/A	N/A	[73]
Paraffin-incorporated	Paraffin-coated Nomex IIIA fabric	Drying coating	26–47	55.3–105.2	N/A	N/A	1493.69–1645.00 N (warp) 1000.38–1185.28 N (weft)	[169]
	CA-coated cotton fabric	Pad–dry–curing	22.6	34.08	232.9–262.3 ft^3/ft2/min	0.0573	1.16–1.48 cN/tex	[170]
	SA-coated cotton fabric	Pad–dry–curing	58.6	29.5	251.6 ft^3/ft2/min	0.0534	1.47 cN/tex	

more MPCM content. Correspondingly, the thermal buffering effect was observed. Besides, the addition of the CNFs in the MPCM coating supported the high thermal energy storage efficiency.

The change of the microenvironment between the masks and the mouth occurred when the mask was worn for a long time, which could cause an uncomfortable feeling. Qi Zhang et al. prepared PCM fibers by impregnating the paraffin into the PP hollow fibers via the impregnation method [198]. The prepared PCM fibers were incorporated into a multilayer fabric system to simulate the mask. There was a temperature plateau (higher than 43 °C) of the PCM-incorporated channel-type mask during the cooling process that lasted for the 2250 s, which supported the potential in the application for allergic rhinitis.

The PCM textiles were incorporated with motorcycle helmets to reduce heat loss. M. Taher Halimi et al. designed a smart motorcycle helmet by incorporating a PCM layer [199]. Kanesalingam Sinnappoo et al. inserted the PCM layer as the interlayer between the scalp and the helmet lining of the motorcycle helmet to control the temperature inside the helmet [200]. The thermal regulation was observed, and the reduction of the temperature of the PCM-incorporated helmet was also affected by the wind speed.

The vests were significantly considered to regulate the comfort of the human since the area of the vests was large and usage of the vests was common. Mariam Itani et al. incorporated PCM with the vests and studied the thermal behavior of the PCM-incorporated cooling vests [201]. The efficiency of the PCM-incorporated cooling vest in controlling the skin temperature was significantly affected by the ambient temperature. The usage of the outer layer covering the cooling vests could enhance the usage efficiency of the PCM-incorporated cooling vests.

Besides, Fusun Doba Kadem et al. prepared the PCM-incorporated denim garment via different methods [202]. It was found that the dip-coating was better for the adsorption of the MPCM on the denim garments. However, the PCM coating influenced the color change when compared with pristine denim garments.

Multifunction of PCM textiles

Fabio Alexandre Pereira Scacchetti et al. prepared the functional cotton fabric with the thermal regulation, the antibacterial property, and the antifungal property by making a coating of MPCMs, thyme oil, and MCT-β-CD on cotton fabric [203]. Subsequently, Fabio A. P. Scacchetti et al. combined the thermal regulation with the antimicrobial property in the cotton fabrics treated with silver-doped zeolites and MPCMs [204]. The existence of the MPCMs in the silver-doped zeolite-treated cotton fabrics improved the overall antimicrobial activities.

Shixiong Yi et al. prepared the thermochromic PCMs composites consisting of the bromocresol purple, boric acid, and tetradecyl alcohol by sol–gel method [205]. Then the prepared thermochromic PCMs composite was applied to the fabric via pad–dry–cure coating. The treated fabrics were proved to have the thermochromic function under different temperatures. Hao Wang et al. introduced the modified thermochromic pigments into the MPCMs, where the oil was the core, the PMMA was the first shell, and the modified thermochromic pigments were the outer layer [206]. As a result, the thermochromic function was realized when the temperature of the MPCMs was higher than the melting temperature. Xiaoye Geng et al. prepared the dual functional fabrics by coating the thermochromic MPCMs [207]. The black MPCMs were found in the lower temperature and the color tended to be white during the phase transition, where the reflection of the solar radiation was changed.

US patent US 20,100,327,247 A1 proposed a nanotube fabric-based composites with PCM and electrical circuit for the Joule heating [208]. Since the high electrical conductivity of the composites, the proposed sample could storage the thermal energy from the Joule heating process. Furthermore, US patent US 9,894,944 B2 also reported a thermal management system by incorporation PCMs into fabric [209]. The combination of the PCMs, the conductive materials, and the voltage source in the fabrics realized the active control of the thermal management. Guangyong Li et al. prepared the PEG@graphene aerogel PCM fibers [155]. Except for the realization of the thermal storage and the enhanced thermal conductivity of the PCM fibers, the Joule heating was also realized due to the high electric conductivity of the PCM fibers. Besides, the fluorocarbon resin as the cover layer also supported the hydrophobic of the PEG@graphene aerogel PCM fibers.

Qisong Shi et al. prepared the PEG/PVP-based PCM fiber with the luminescent property via

electrospinning by doping the Eu in the PEG/PVP solution before the spinning process [210]. Both the thermal energy storage and the luminescent property of Eu@PEG/PVP fibers were observed. Peng Xi et al. prepared PMMA/PUPCM ultrafine fibers via electrospinning. It was revealed that a smaller chance of the luminescent level was found in the PMMA/PUPCM ultrafine fibers when compared with PMMA luminescent fibers [211].

Luxiao Cai et al. prepared the MPCM consisting of the n-eicosane as the core and the crystalline TiO_2 as the shell [212]. Apart from the thermal energy storage, the prepared MPCMs had both the antibacterial property and the photocatalysis property [213].

Chi Zhang et al. made a coating of NPCMs on the filter media by using PU emulsion [214]. The existence of NPCMs supported the thermal buffering time of 60 s. The morphology of the NPCM-coated filter media was kept well under 500 °C. The more content of the NPCMs on the filter media reduced the pore size and the penetration rate of the particles, which enhanced the capture capacity of the filter media.

US patent US 20,080,140,166 A1 developed a therapeutic pack to store the PCM [215]. The designed therapeutic pack allowed the free movement of the PCM bags, which may better treat an injury of the living body. US patent US 10,765,607 B2 also proposed a thermally assisted therapeutic acids for cosmetics and wound treatment by incorporating PCM fabric [216]. The final product with PCM fabric was aimed to adjust the localized temperature, and the lower localized temperature reduced the inflammation and the bacterial growth, and the higher localized temperature supported the blood flow and adsorption rates of therapeutic agents.

US patent US 9,835,986 also reported to use the PCMs to enhance the efficiency of the image transfer products which was based on the printing technology [217].

Evaluation of PCM fabrics

The main parameters to characterize the PCM fabrics includes the melting and solidifying enthalpy, phase transition temperature range, thermal conductivity, the change rate of the temperature of the PCM fabrics, heat flux difference, heating time, and so on. The differential scanning calorimetry (DSC) was a common method to characterize the phase transition of PCM, including the melting temperature, crystallization temperature, melting enthalpy, cooling enthalpy, and supercooling degree [218]. Besides, the relative crystalline degree (X_t) of the PCM material could be evaluated according to Eq. (1), where t_1 and t_2 were the time value corresponding to onset temperature time and the endset temperature, respectively, and ΔH was the enthalpy value change. It was useful to reveal the confined crystalline structure of the PCM materials, which could provide the basic explanation for the difference in both the enthalpy and the phase transition between the PCM textiles and the pure PCMs. Alicja Nejman et al. studied the effect of the heating/cooling rate on the phase transition of MPCM and their coated fabric via the DSC method [219]. The higher heating/cooling rate resulted in the higher supercooling degrees, while had little effect on the enthalpy and melting/crystallization temperature. However, the DSC method was unable to simulate the thermal behavior of the PCM fabrics in practice.

$$X_t = \frac{\int_{t_1}^{t_2} \Delta H dt}{\int_{t_1}^{\infty} \Delta H dt} \times 100\% \quad (1)$$

To characterize the thermal performance of the PCM fabrics, there were various setups based on the steady heat transfer models. The principle of the heat and mass transfer through the PCM-incorporated system (not only for the PCM fabrics) was given in the research work [220], 213. Here, the details related to the evaluation method to characterize the PCM fabric were presented.

The detailed review of mathematical modeling of the latent heat thermal energy storage systems using PCMs based on both the first law and second law of thermodynamics was reported by P.V. Varun and S.K. Singal in 2008. They presented and discussed the important characteristics of different models and their assumptions used as well as the experimental validation of some models.

General principle for heat transfer through PCM fabrics

It is well known that there are three basic heat transfers through the PCM fabric:

- Thermal conduction.

The thermal conduction model is based on the Fourier's law and expressed in Eq. (2). It is noticed that various setups or models to evaluate the thermal behavior of the PCM textiles are based on the 1D steady heat transfer model. The basic equation is expressed in Eq. (3), where the first term in the left side is the rate of change of internal energy due to conduction, the second term in the left side is the rate of energy generation in the element (here it presents for the PCM textiles) and the equation term is the rate of the increase in internal energy over time. Basically, four basic thermal characteristics are proposed, including thermal conductivity, thermal absorptivity, thermal diffusivity, and thermal resistance, which was expressed in Eqs. (2), (6), (7), and (8), respectively. However, they are not suitable to characterize the thermal behavior of the PCM fabrics where the heat transfer is transient and dynamic during the phase change process. By taking into different boundary conditions, various parameters were proposed based on the thermal conduction and were shown in the next section "Experimental methods for thermal performance of PCM fabrics".

- Thermal convection.

The thermal convection model is expressed in Eq. (4). It is noticed that the thermal convection is strongly dependent on the structure of the PCM textiles (here was almost PCM fabrics) and the environment parameters (e.g., temperature difference between PCM fabric and environment, velocity of the air flow, etc.). In the couple of the thermal conduction and thermal convection, the thermal behavior of the PCM fabric could be complicated, which was discussed in some models. The details could be found in the next section "Experimental methods for thermal performance of PCM fabrics".

- Thermal irradiation.

The thermal irradiation model is expressed in Eq. (5). It is well known that the ε mainly determined the amount and the efficiency of the thermal energy storage of the PCM textiles and affected the accuracy of some measurements (e.g., infrared camera-incorporated measurement). The details will be discussed in the next section "Experimental methods for thermal performance of PCM fabrics".

$$\dot{q} = -k\frac{dT}{dL} \tag{2}$$

$$\frac{\partial}{\partial x}\left(k\frac{\partial T}{\partial x}\right)\cdot A\cdot \Delta L + \dot{g}\cdot(A\cdot\Delta L) = \rho(A\cdot\Delta x)c_p\frac{\partial T}{\partial t} \tag{3}$$

$$\dot{q}_{conv} = h(T_w - T_\infty). \tag{4}$$

$$\dot{q}_{rad} = \sigma\varepsilon\left(T_w^4 - T_\infty^4\right). \tag{5}$$

$$b = \sqrt{\mathrm{k}\rho\mathrm{c_p}} \tag{6}$$

$$\mathrm{a} = \frac{\mathrm{k}}{\rho\mathrm{c_p}} \tag{7}$$

$$\mathrm{r} = \frac{\mathrm{L}}{\mathrm{k}}. \tag{8}$$

Experimental methods for thermal performance of PCM fabrics

Experimental method based on thermal conduction

Till now, various parameters were proposed to characterize the thermal behavior of PCM fabrics. In detail, Tables 8 and 9 summarize the main experimental method and developed setups based on the thermal conduction for the PCM fabrics.

The dynamic heat transfer process was first proposed by Pause to measure the thermal barrier function of the PCM textiles [221]. The thermal resistance of the PCM fabric was evaluated according to the end temperature and the heat flux difference. Namely, the dynamic thermal resistance of PCMs fabrics was assumed as a sum of the basic thermal resistance (thermal resistance of textile without PCMs) and dynamic thermal resistance which was provided by the PCM. However, the concept of the thermal resistance of the PCM fabric was simple and inherently erroneous, which was a static concept but was used to characterize the dynamic behavior of PCM materials.

The concept of the *TRF* was proposed by Hittle and Andre, which was derived based on the assumption that the phase process can be roughly approximated by a constant and comparably large heat capacity in the fabric. The theoretical foundation to obtain *TRF* value was based on two assumptions: 1) the heat capacity of the PCM fabric should be high and 2) the thermal conductivity, the density, and the specific heat capacity of the PCM fabric were considered as a constant. As a result, the *TRF* value was a dimensionless number and less than or equal to 1 [222]. The *TRF* value to evaluate the PCM fabrics was

successfully adopted as a standard test method (D7024-04) by ASTM.

Bo-an Ying et al. introduced four indices to characterize the thermal transient process of the PCM fabrics [223], which included the static thermal insulation (I_s), the thermal duration time (Δt_d), the mean of the heat flux delayed by the phase change (I_d), and the thermal psycho-sensory intensity (*TPI*). The I_s value described the static thermal insulation effects of fabric (W m^{-2}), the I_d value was the mean of the heat flux delayed during the phase change period (W m^{-2}), and the *TPI* value represented the thermal perception by the body.

S.X. Wang et al. proposed a bionic skin model to characterize the thermal transient process of the PCM fabrics [224]. The heating time ratio (*HTR*) and the non-heating time ratio (*NHTR*) of each heating/cooling cycle was proposed to characterize the temperature–time curve, and the consumption of the electric power was considered for the evaluation of the heat energy. However, the so-called bionic skin model was considered to describe the heat loss of the PCM fabric. Besides, the skin temperature set in the bionic skin model was fixed, which was unsuitable to simulate the practical situation. X Wan et al. proposed a modified skin model by modifying the exposure environment to characterize the thermal transient process [225]. The exposure environment was simulated by applying a thermal transient process. As a result, four indices were used to characterize the thermal regulating effect of PCM fabrics, including the maximum 'skin' temperature difference due to the phase change, the final 'skin' temperature difference due to the phase change, the duration of the phase change, and the average reduced heat loss due to the phase change. Fabio A. P. Scacchetti et al. evaluated the PCM fabric by using Alambeta [226], while the Alambeta was only suitable to characterize the PCM fabric without phase transition. Lubos Hes et al. also proposed a new measurement based on a modified Alambeta setup for the characterization of the PCM-coated fabric. The concept of the protection time of the PCM fabric was proposed, which was determined by the time value corresponding to the half-maximum rate of heat flow [227].

Besides, it was necessary to characterize the thermal behavior of the PCM fabric under high thermal exposure. Yun Su et al. modified the skin model-based setup for the measurement of the thermal hazardous effect of the multilayer thermal protective clothing with PCMs. In detail, the temperature of the PCM layers was recorded after the thermal exposure of the PCM fabrics to the high temperature [169]. Kai Yang et al. recorded the skin temperature change of the PCM fabric by immersing the PCM fabric into the lower temperature [228]. It revealed that the incorporation of the PCM could absorb the thermal energy from the skin when the PCM fabric with high temperature touched the lower temperature. The concept of *TGP* based on the temperature–time curve was also proposed, which was higher to suggest a better thermal buffering effect. The incorporation of PCM into fabrics supported the temporary heating effect when the PCM fabric was transferred from a warmer environment to a colder environment.

It was noticed that the aforementioned evaluations were based on the steady heat transfer transient process, which was realized by the heat flux sensors and temperature sensors. The results including the heat flux, the heat time, and the surface temperature values were focused. Apart from the methods based on the heat flux sensors and temperature sensors, the usage of the infrared camera was the alternative that was convenient to reveal the thermal buffering effect by recording the temperature–time curves during the heating process. For example, the thermal buffering effect of the knitted wool-PA fabrics with the PEG/PP filaments was investigated and the temperature ranging from 25 to 26 °C was kept for 5 min when the sample was cooling from 40 to 23 °C [153] (Fig. 20). Abu Shaid et al. evaluated the thermal buffering effect of the multilayer firefighter clothing with PCM by recording the temperature of the PCM layer, outer layer, and moisture barrier layer [229]. Zhang et al. revealed the less temperature loss of the PCM-incorporated fabric by using thermal infrared imaging [171]. The thermal insulation value (*I*) was used to characterize the thermal buffering effect [230]. Besides, the temperature change rate with the time of the PCM fabric (dT/dt) was also able to characterize the thermal behavior [231]. The usage of thermal infrared imaging for the characterization of PCM-incorporated fabrics was usually performed with one heater for heating the samples. In another word, one side of the PCM-incorporated fabric faced the heater, and the other side of the PCM-incorporated fabric faced to air. Therefore, Newton's cooling law was also possible to characterize the T-history [6]. As a result, the time of half temperature rising ($t_{1/2}$) and the heating constant were used to characterize the

Table 8 Proposed characterization parameters for PCM fabrics via experimental numerical methods based on dynamic heat transfer process

Model of method	Principle	Proposed parameter	References
Setup based on dynamic heat transfer process	Thermal resistance of the PCM fabric was evaluated according to the end temperature and the heat flux difference	Dynamic thermal resistance	[221]
Setup based on transient heat transfer process	The heat capacity of the PCM fabric should be high The thermal conductivity, the density, and the specific heat capacity of the PCM fabric were considered as a constant	Temperature regulating factor (*TRF*)	[222], Standard ASTM D7024-04
Fabric intelligent hand tester based on thermal transient process	Boundary condition was intercepted All the parameters were determined based on the change of heat flux with time	Static thermal insulation (I_s) Thermal duration time (Δt_d) The mean of the heat flux delayed by the phase change (I_d) Thermal psycho-sensory intensity (*TPI*)	[223]
Bionic skin model based on thermal transient process	Boundary condition was intercepted The skin temperature was considered	Heating time ratio (*HTR*) None heating time ratio (*NHTR*)	[224]
Modified skin model based on thermal transient process	Boundary condition was intercepted	Maximum 'skin' temperature difference due to the phase change Final 'skin' temperature difference due to the phase change Duration of the phase change	[225]
	The skin temperature was considered The exposure of PCM fabric in the environment was evaluated	Average reduced heat loss due to the phase change	
Alambeta based on thermal transient process	Boundary condition was intercepted	Thermal conductivity Thermal resistance	[226]
Modified Alambeta based on thermal transient process	The skin temperature was considered	Protection time	[227]
Setup based on thermal transient process	Simulation for thermal behavior of PCM fabric from high temperature to low temperature	*TGP* parameter Thermoregulating time Thermoregulating capacity Thermoregulating efficiency	[228]
	Temperature–time curve	Minimum temperature that skin temperature can reach	
Temperature–time curve recorded via Infrared camera	Continuous record of surface temperature of PCM fabric under preset heating/cooling temperature	The heating time for the selected temperature (normally higher than melting temperature of PCM) Surficial temperature distribution	[153, 171] and [229]
		Thermal Insulation	[230]
		Temperature change rate with time Newton's cooling law	[231] and [6]
Setup equipped with both infrared camera and mirror		Change of temperature and heat flux with time	[232]

thermal buffering effect of the PCM-incorporated fabrics. Besides, the usage of the thermal infrared camera was able to reveal the heat transfer along the cross-sectional direction. For example, M. Michalak et al. made a setup to measure the cross-sectional thermal conductivity of the fabrics with PCMs [232].

Table 9 Comparison of the measurement methods evaluating the thermal performance of PCM textiles

Measurement	ΔH(J/g)	D (°C)	c_p (J/g K^{-1})	k_s(W/K m)	(W/K m)	k_l. (W/K m)	Characteristics for the function (thermal buffering effect, phase transition, etc.)	Solidifying/melting interface
DSC	×	×	×	-	-	-	-	-
Modified Alambeta	-	-	-	×	-	×	×	-
Skin model	-	-	-	-	-	-	×	-
T-history method	-	-	-	-	-	-	×	-
Numerical Simulation	-	-	-	×	×	×	×	×

ΔH: enthalpy, D: phase transition temperature range, c_p: specific heat capacity, k_s: thermal conductivity of the PCM textiles with the solid phase, k_{s-l}: thermal conductivity of the PCM textiles during phase transition, and k_l: thermal conductivity of the PCM textiles with molten phase.

The incorporation of PCM in the fabrics also delayed the heat transfer along the cross section direction.

It was noticed that the thermal infrared camera could directly record the temperature change of the PCM-incorporated fabrics, which was a convenient method to characterize the T-history. However, there were still several disadvantages:

1) The infrared thermal camera was only able to record the surface temperature, while the temperature change inside the PCM-incorporated fabrics was unable to be recorded.
2) The infrared thermal camera was based on the emissivity (ε) of the fabrics. Normally, ε of the fabrics was 0.95 and it would be changed if there was a fabric with a coating of metal/PCMs on the surface, which was necessary to be checked before the measurement.
3) The infrared thermal camera for characterization of the T-history of the PCM-incorporated fabrics was usually performed by heating one side of the sample. Therefore, the air inside or outside the fabric also affected the final results which were not as accurate as the methods based on the heat flow plate methods, although the thermal buffering effect of PCM-incorporated fabrics could be described [6].

Experimental methods with thermal radiation and thermal convection

It was concluded that the aforementioned methods only considered thermal conduction, while the thermal convection and thermal radiation were ignored. K. Ghali et al. evaluated the thermal buffering effect of the PCM fabrics by applying the thermal convection into consideration [233]. Maciej Jaworski systematically studied the heat transfer in PCM fabrics under various thermal loads including thermal conduction, thermal convection, and thermal radiation and focused on the temporal temperature of PCM fabric [234]. It was noticed that the PCM fabrics could be applied as the firefighter clothing. So, it was also necessary to investigate the thermal performance of the PCM fabrics under high temperatures.

Ergonomic tests

Grazyna Barthowiak et al. systematically investigated the thermal regulation of the PCM-incorporated garment based on the ergonomic tests [235]. The incorporation of the PCM fabric modified the microclimate underneath the impermeable protective clothing. Based on ergonomic tests, the incorporation of the PCM can lead to the sensation of wetness and may therefore be judged as less comfortable instead of the appreciation of coolness [236].

Mathematical models for the thermal performance of PCM fabrics

By comparing with the experimental measurement, the mathematical models had the advantages (Table 9). Yi Li et al. proposed a mathematical model to simulate the heat and moisture transfer through PCM fabrics, which combined the heat transfer model of the MPCMs with the heat the moisture transfer model of the porous fabrics [237]. The initial and boundary conditions of the mathematical model were taken into consideration, and the temperature distribution, the moisture concentration, and the water content of the PCM fabrics were obtained as a result [238]. The mathematical model was proposed to optimize the MPCMs content and the position of the PCM layers of the multilayer fabrics. Erisn Alpetkin et al. numerically simulated 1D coupled transient heat transfer inside the multilayer firefighter protecting clothing by using ANSYS and CFD software [189]. The simulation model revealed that the incorporation of PCM enhanced the protective effect of the PCM-incorporated firefighter clothing and the depth of thermal burn increased for the extended fire exposure durations. Hui Zhang et al. introduced a numerical model for the transient heat transfer in a protective clothing system, which was simulated via ANSYS 15 software [239]. A more sophisticated model for the phase transition in the multilayer fabric system was proposed. In detail, the PCM-incorporated fabrics especially for firefighting clothing would have a longer second-degree burn time when the PCM layer was increased in its specific heat and thickness. Rimanatas Baraukas et al. simulated the radiation heating model for the PCM fabrics [240]. Muhammad Owais Raza Siddiqui et al. developed a plug-in in the Abaqus/CAE software to predict the effective thermal conductivity of MPCMs [241]. The proposed plug-in was able to find the effect of the core content of MPCMs on the final effective thermal conductivity and heating and cooling effect of MPCMs. Kashif Iqbal et al. simulated a model for analysis of the heat transfer through the MPCM-incorporated PP yarns by using ABAQUS software [141]. The proposed model was able to predict the temperature change.

Future and challenges

There was a great progress in the PCM textiles, including the development of the novel PCMs, the preparation of the ultrafine PCM fibers, the fabrication of the PCM yarns, the preparation of the PCM fabrics, the application of the PCM textiles, and their corresponding evaluation methods. However, there were still some challenges for PCM textiles.

- It was suggested that the usage of the MPCMs was considered as the most popular method to prepare the PCM textiles, while the usage of the FSPCMs had attracted more and more attention in recent years since the preparation process was more convenient than the MPCMs. For both MPCMs and FSPCMs, the encapsulation efficiency of the PCMs in MPCMs or FSPCMs remained to be improved. Besides, the modification of the shell materials of the MPCMs or the supporting porous materials of FSPCMs could improve the thermal conductivity and support multifunctions, which enriched the application of FSPCMs and MPCMs in various fields.
- To prepare the PCM textiles, the PCMs, MPCMs, and FSPCMs were incorporated into the fibers, yarns, and fabrics. In detail, the enhancement of the thermal stability of PCM fibers and the fabrication of the ultrafine PCM fibers had been focused on for decades, which was based on the modification of the polymer fiber spinning method. However, the mechanical property of the PCM fibers and the encapsulation efficiency of the PCMs in the fibers remained to be improved.
- For the preparation of the PCM fabrics, the incorporation of MPCMs or FSPCMs with binders into fabrics was the most popular method. However, the usage of the binders could hinder the air permeability of the air and the water vapor permeability, and altered the surface chemistry, etc. It seemed that knitting or weaving method to fabricate PCM fabrics by using PCM yarns could support the thermal storage meanwhile kept the significant permeability. However, it strongly depended on the mechanical property of PCM yarns.
- For the application of the PCM textiles, the major application was still based on the thermal buffering effect. Additionally, the application of the PCM textiles tended to be diversified based on the

thermal energy storage, including the sensors based on the PCM textiles for the detection of the color, humidity, the solar energy storage, the light-thermal energy conversation, the electric-thermal energy conversion, and so on.

- For the evaluation of the PCM textiles, there were already various methods and the standard to evaluate the thermal behavior of the PCM textiles, which was almost based on the thermal conduction. Still, it was also necessary to develop the setups by taking the thermal convection and thermal irradiation into consideration. Besides, the measurement should be specified to provide different parameters of the unique PCM textile for specific usage.

Conclusion

In this review, we systematically reviewed the recent developments of the PCM textiles. In detail, the suitable PCMs for the textiles tended to be diverse, and the methods to obtain the PCM textiles (including the fibers, the yarns, and the fabrics) became various. The application of the PCM textiles almost covered all the engineering fields as well as the energy fields (e.g., the textile industry, the building, the solar energy, etc.). Correspondingly, the main objectives for the preparation of the PCM textiles more strongly related to the actual applications. Besides, the characterization of the PCM textiles was more precise to predict or demonstrate the thermal behavior. Such a great progress in the PCM textiles could optimize the PCM textile industry and support the development of other energy industries.

Acknowledgements

This work was supported by the project 'Hybrid Materials for Hierarchical Structures' (HyHi, Reg. No. CZ.02.1.01/0.0/0.0/16_019/0000843) granted by the Ministry of Education, Youth and Sports of the Czech Republic, European Union – European Structural and Investment Funds in the Frames of Operational Programme Research, Development, and Education, the project 'design of multilayer micro/nanofibrous structures for air filters applications' (Reg. No. 8JCH1064) granted by the Ministry of Education, Youth and Sports of the Czech Republic in the frames of support for researcher mobility (VES19 China-mobility, Czech–Chinese cooperation). The work was also supported by the project 'Intelligent thermoregulatory fibers and functional textile coatings based on temperature resistant embedded PCM' SMARTTHERM (Project No. TF06000048) granted by the Technology Agency of the Czech Republic (DELTA Programme) and the project 'Advanced structures for thermal insulation in extreme conditions' (Reg. No. 21-32510M) granted by the Czech Science Foundation (GACR). Last but not least, Kai Yang would like to thank Mr. Yuanfeng Wang for his assistance in organizing the data and providing 3D fabric model for the final manuscript.

Declarations

Conflict of interest We declare that we do not have any commercial or associative interest that represents a conflict of interest in connection with the work submitted.

References

[1] Zhang N, Yuan Y, Cao X et al (2018) Latent heat thermal energy storage systems with solid-liquid phase change materials: a review. Adv Eng Mater 20:1700753. https://doi.org/10.1002/adem.201700753

[2] Alva G, Lin Y, Liu L, Fang G (2017) Synthesis, characterization and applications of microencapsulated phase change materials in thermal energy storage: a review. Energ Buildings 144:276–294. https://doi.org/10.1016/j.enbuild.2017.03.063

[3] Chalco-Sandoval W, Fabra MJ, López-Rubio A, Lagaron JM (2017) Use of phase change materials to develop electrospun coatings of interest in food packaging applications. J Food Eng 192:122–128. https://doi.org/10.1016/j.jfoodeng.2015.01.019

[4] Zhu C, Chen Y, Cong R et al (2021) Improved thermal properties of stearic acid/high density polyethylene/carbon fiber composite heat storage materials. Sol Energ Mat Sol C. https://doi.org/10.1016/j.solmat.2020.110782

[5] Iqbal K, Khan A, Sun D et al (2019) Phase change materials, their synthesis and application in textiles—a review. J Text Inst 110:625–638. https://doi.org/10.1080/00405000.2018.1548088

[6] Yang K, Wiener J, Venkataraman M et al (2021) Thermal analysis of PEG/metal particle-coated viscose fabric. Polym Test. https://doi.org/10.1016/j.polymertesting.2021.107231

[7] Peng H, Wang J, Zhang X et al (2021) A review on synthesis, characterization and application of nanoencapsulated phase change materials for thermal energy storage systems. Appl Therm Eng. https://doi.org/10.1016/j.applthermaleng.2020.116326

[8] Qureshi ZA, Ali HM, Khushnood S (2018) Recent advances on thermal conductivity enhancement of phase change materials for energy storage system: a review. Int J Heat Mass Tran 127:838–856. https://doi.org/10.1016/j.ijheatmasstransfer.2018.08.049

[9] Ran F, Chen Y, Cong R, Fang G (2020) Flow and heat transfer characteristics of microencapsulated phase change slurry in thermal energy systems: a review. Renew Sustain Energy Rev. https://doi.org/10.1016/j.rser.2020.110101

[10] Rehman T, Ali HM, Janjua MM et al (2019) A critical review on heat transfer augmentation of phase change materials embedded with porous materials/foams. Int J Heat Mass Tran 135:649–673. https://doi.org/10.1016/j.ijheatmasstransfer.2019.02.001

[11] Gadhave P, Pathan F, Kore S, Prabhune C (2021) Comprehensive review of phase change material based latent heat thermal energy storage system. Int J Ambient Energy. https://doi.org/10.1080/01430750.2021.1873848

[12] Safari A, Saidur R, Sulaiman FA et al (2017) A review on supercooling of phase change materials in thermal energy storage systems. Renew Sustain Energy Rev 70:905–919. https://doi.org/10.1016/j.rser.2016.11.272

[13] Prajapati DG, Kandasubramanian B (2020) A review on polymeric-based phase change material for thermo-regulating fabric application. Polym Rev 60:389–419. https://doi.org/10.1080/15583724.2019.1677709

[14] Liu H, Wei Z, He W, Zhao J (2017) Thermal issues about Li-ion batteries and recent progress in battery thermal management systems: a review. Energ Convers Manage 150:304–330. https://doi.org/10.1016/j.enconman.2017.08.016

[15] Chandel SS, Agarwal T (2017) Review of current state of research on energy storage, toxicity, health hazards and commercialization of phase changing materials. Renew Sustain Energy Rev 67:581–596. https://doi.org/10.1016/j.rser.2016.09.070

[16] N.PAN, P.Gibson (2006) Thermal and moisture transport in fibrous materials, 1st ed. Woodhead Publishing

[17] Militky J, Novak O, Kremenakova D et al (2021) A review of impact of textile research on protective face masks. Materials 14:1937. https://doi.org/10.3390/ma14081937

[18] Faheem S, Baheti V, Tunak M et al (2019) Flame resistance behavior of cotton fabrics coated with bilayer assemblies of ammonium polyphosphate and casein. Cellulose 26:3557–3574. https://doi.org/10.1007/s10570-019-02296-1

[19] Venkataraman M, Mishra R, Militky J et al (2018) Electrospun nanofibrous membranes embedded with aerogel for advanced thermal and transport properties. Polym Advan Technol 29:2583–2592. https://doi.org/10.1002/pat.4369

[20] Khan MZ, Baheti V, Militky J et al (2018) Superhydrophobicity, UV protection and oil/water separation properties of fly ash/Trimethoxy(octadecyl)silane coated cotton fabrics. Carbohyd Polym 202:571–580. https://doi.org/10.1016/j.carbpol.2018.08.145

[21] Yang T, Xiong X, Mishra R et al (2019) Sound absorption and compression properties of perpendicular-laid nonwovens. Text Res J 89:612–624. https://doi.org/10.1177/0040517517753634

[22] Yang K, Periyasamy AP, Venkataraman M et al (2020) Resistance against penetration of electromagnetic radiation for ultra-light Cu/Ni-coated polyester fibrous materials. Polymers-basel. https://doi.org/10.3390/polym12092029

[23] Zhang X, Jin Z, Hu L et al (2021) A silver yarn-incorporated song brocade fabric with enhanced electromagnetic shielding. Materials 14:3779. https://doi.org/10.3390/ma14143779

[24] Zhang X, Jin Z (2018) A kind of song brocade fabric with NFC data masking function used for making purse. Iop Conf Ser Mater Sci Eng 389:012037. https://doi.org/10.1088/1757-899x/389/1/012037

[25] Wang Y, Baheti V, Yang K et al (2021) Utility of whiskerized carbon fabric surfaces in resistive heating of composites. Polym Composite. https://doi.org/10.1002/pc.26012

[26] Periyasamy AP, Yang K, Xiong X et al (2020) Effect of silanization on copper coated milife fabric with improved EMI shielding effectiveness. Mater Chem Phys. https://doi.org/10.1016/j.matchemphys.2019.122008

[27] Wani C, Loharkar PK (2017) A review of phase change materials as an alternative for solar thermal energy storage. Mater Today Proc 4:10264–10267. https://doi.org/10.1016/j.matpr.2017.06.361

[28] Mondal S (2008) Phase change materials for smart textiles—an overview. Appl Therm Eng 28:1536–1550. https://doi.org/10.1016/j.applthermaleng.2007.08.009

[29] Wu Y, Chen C, Jia Y et al (2018) Review on electrospun ultrafine phase change fibers (PCFs) for thermal energy storage. Appl Energ 210:167–181. https://doi.org/10.1016/j.apenergy.2017.11.001

[30] Sarier N, Onder E (2012) Organic phase change materials and their textile applications: an overview. Thermochim Acta 540:7–60. https://doi.org/10.1016/j.tca.2012.04.013

[31] Purohit BK, Sistla VS (2021) Inorganic salt hydrate for thermal energy storage application: a review. Energy Storage. https://doi.org/10.1002/est2.212

[32] Xie N, Huang Z, Luo Z et al (2017) Inorganic salt hydrate for thermal energy storage. Appl Sci. https://doi.org/10.3390/app7121317

[33] Mohamed SA, Al-Sulaiman FA, Ibrahim NI et al (2017) A review on current status and challenges of inorganic phase change materials for thermal energy storage systems. Renew Sustain Energy Rev 70:1072–1089. https://doi.org/10.1016/j.rser.2016.12.012

[34] Kazemi Z, Mortazavi SM (2014) A new method of application of hydrated salts on textiles to achieve thermoregulating properties. Thermochim Acta 589:56–62. https://doi.org/10.1016/j.tca.2014.05.015

[35] Iqbal K, Sun D (2018) Synthesis of nanoencapsulated Glauber's salt using PMMA shell and its application on cotton for thermoregulating effect. Cellulose 25:2103–2113. https://doi.org/10.1007/s10570-018-1692-8

[36] Bose P, Amirtham VA (2016) A review on thermal conductivity enhancement of paraffinwax as latent heat energy storage material. Renew Sustain Energy Rev 65:81–100. https://doi.org/10.1016/j.rser.2016.06.071

[37] Yuan Y, Zhang N, Tao W et al (2014) Fatty acids as phase change materials: a review. Renew Sustain Energy Rev 29:482–498. https://doi.org/10.1016/j.rser.2013.08.107

[38] Sundararajan S, Samui AB, Kulkarni PS (2017) Versatility of polyethylene glycol (PEG) in designing solid–solid phase change materials (PCMs) for thermal management and their application to innovative technologies. J Mater Chem A 5:18379–18396. https://doi.org/10.1039/c7ta04968d

[39] Che H, Chen Q, Zhong Q, He S (2018) The effects of nanoparticles on morphology and thermal properties of erythritol/polyvinyl alcohol phase change composite fibers. E-Polymers 18:321–329. https://doi.org/10.1515/epoly-2017-0176

[40] Wang H, Shi H, Qi M et al (2013) Structure and thermal performance of poly(styrene-co-maleic anhydride)-g-alkyl alcohol comb-like copolymeric phase change materials. Thermochim Acta 564:34–38. https://doi.org/10.1016/j.tca.2013.04.025

[41] Zhang Z, Zhang X, Shi H et al (2016) Thermo-regulated sheath/core submicron fiber with poly(diethylene glycol hexadecyl ether acrylate) as a core. Text Res J 86:493–501. https://doi.org/10.1177/0040517515592815

[42] Li S, Wang H, Mao H et al (2019) Light-to-thermal conversion and thermoregulated capability of coaxial fibers with a combined influence from comb-like polymeric phase change material and carbon nanotube. Acs Appl Mater Inter 11:14150–14158. https://doi.org/10.1021/acsami.9b02387

[43] Sharma A, Tyagi VV, Chen CR, Buddhi D (2009) Review on thermal energy storage with phase change materials and applications. Renew Sustain Energy Rev 13:318–345. https://doi.org/10.1016/j.rser.2007.10.005

[44] Kou Y, Wang S, Luo J et al (2018) Thermal analysis and heat capacity study of polyethylene glycol (PEG) phase change materials for thermal energy storage applications. J Chem Thermodyn 128:259–274. https://doi.org/10.1016/j.jct.2018.08.031

[45] Du X, Wang H, Cheng X, Du Z (2016) Synthesis and thermal energy storage properties of a solid–solid phase change material with a novel comb-polyurethane block copolymer structure. Rsc Adv 6:42643–42648. https://doi.org/10.1039/c6ra02559e

[46] Fallahi A, Guldentops G, Tao M et al (2017) Review on solid-solid phase change materials for thermal energy storage: Molecular structure and thermal properties. Appl Therm Eng 127:1427–1441. https://doi.org/10.1016/j.applthermaleng.2017.08.161

[47] Pielichowska K, Pielichowski K (2014) Phase change materials for thermal energy storage. Prog Mater Sci 65:67–123. https://doi.org/10.1016/j.pmatsci.2014.03.005

[48] Keyan K, Ramachandran T, Shumugasundaram OL et al. (2012) Microencapsulation of PCMs in textiles: A review. J Textile Appar Technol Manag 7

[49] Reyez-Araiza JL, Pineda-Piñón J, López-Romero JM et al (2021) Thermal energy storage by the encapsulation of phase change materials in building elements—a review. Materials 14:1420. https://doi.org/10.3390/ma14061420

[50] Liu H, Wang X, Wu D (2019) Innovative design of microencapsulated phase change materials for thermal energy storage and versatile applications: a review. Sustain Energy Fuels 3:1091–1149. https://doi.org/10.1039/c9se00019d

[51] Zhao CY, Zhang GH (2011) Review on microencapsulated phase change materials (MEPCMs): fabrication, characterization and applications. Renew Sustain Energy Rev 15:3813–3832. https://doi.org/10.1016/j.rser.2011.07.019

[52] Karaszewska A, Kamińska I, Nejman A et al (2019) Thermal-regulation of nonwoven fabrics by microcapsules of n-eicosane coated with a polysiloxane elastomer. Mater Chem Phys 226:204–213. https://doi.org/10.1016/j.matchemphys.2019.01.029

[53] Hassabo AG, Mohamed AL (2017) Enhancement the thermo-regulating property of cellulosic fabric using encapsulated paraffins in modified pectin. Carbohyd Polym 165:421–428. https://doi.org/10.1016/j.carbpol.2017.02.074

[54] Liu C, Xu Z, Song Y et al (2019) A novel shape-stabilization strategy for phase change thermal energy storage. J Mater Chem A 7:8194–8203. https://doi.org/10.1039/c9ta01496a

[55] Zhou J, Zhao J, Li H et al (2020) Enhanced thermal properties for nanoencapsulated phase change materials with functionalized graphene oxide (FGO) modified PMMA. Nanotechnology 31:295704. https://doi.org/10.1088/1361-6528/ab898b

[56] Alkan C, Aksoy SA, Anayurt RA (2015) Synthesis of poly(methyl methacrylate-co-acrylic acid)/n-eicosane microcapsules for thermal comfort in textiles. Text Res J 85:2051–2058. https://doi.org/10.1177/0040517514548751

[57] Karthikeyan M, Ramachandran T, Shanmugasundaram OL (2014) Synthesis, characterization, and development of thermally enhanced cotton fabric using nanoencapsulated phase change materials containing paraffin wax. J Text Inst 105:1279–1286. https://doi.org/10.1080/00405000.2014.886368

[58] Ma Y, Zong J, Li W et al (2015) Synthesis and characterization of thermal energy storage microencapsulated n-dodecanol with acrylic polymer shell. Energy 87:86–94. https://doi.org/10.1016/j.energy.2015.04.096

[59] Jamekhorshid A, Sadrameli SM, Farid M (2014) A review of microencapsulation methods of phase change materials (PCMs) as a thermal energy storage (TES) medium. Renew Sustain Energy Rev 31:531–542. https://doi.org/10.1016/j.rser.2013.12.033

[60] Zhang S, Campagne C, Salaün F (2020) Preparation of n-Alkane/Polycaprolactone phase-change microcapsules via single nozzle electro-spraying: characterization on their formation. Struct Propert Appl Sci 10:561. https://doi.org/10.3390/app10020561

[61] Moghaddam MK, Mortazavi SM (2015) Preparation, characterisation and thermal properties of calcium alginate/n-nonadecane microcapsules fabricated by electro-coextrusion for thermo-regulating textiles. J Microencapsul 32:737–744. https://doi.org/10.3109/02652048.2015.1073388

[62] Shi J, Wu X, Sun R et al (2019) Nano-encapsulated phase change materials prepared by one-step interfacial polymerization for thermal energy storage. Mater Chem Phys 231:244–251. https://doi.org/10.1016/j.matchemphys.2019.04.032

[63] Alehosseini E, Jafari SM (2020) Nanoencapsulation of phase change materials (PCMs) and their applications in various fields for energy storage and management. Adv Colloid Interfac. https://doi.org/10.1016/j.cis.2020.102226

[64] Zhao L, Luo J, Wang H et al (2016) Self-assembly fabrication of microencapsulated n-octadecane with natural silk fibroin shell for thermal-regulating textiles. Appl Therm Eng 99:495–501. https://doi.org/10.1016/j.applthermaleng.2015.12.111

[65] Luo J, Zhao L, Yang Y et al (2016) Emulsifying ability and cross-linking of silk fibroin microcapsules containing phase change materials. Sol Energ Mat Sol C 147:144–149. https://doi.org/10.1016/j.solmat.2015.12.012

[66] Saraç EG, Öner E, Kahraman MV (2019) Microencapsulated organic coconut oil as a natural phase change material for thermo-regulating cellulosic fabrics. Cellulose 26:8939–8950. https://doi.org/10.1007/s10570-019-02701-9

[67] Han X, Kong T, Zhu P, Wang L (2020) Microfluidic encapsulation of phase-change materials for high thermal performance. Langmuir 36:8165–8173. https://doi.org/10.1021/acs.langmuir.0c01171

[68] Carreira AS, Teixeira RFA, Beirão A et al (2017) Preparation of acrylic based microcapsules using different reaction conditions for thermo-regulating textiles production. Eur Polym J 93:33–43. https://doi.org/10.1016/j.eurpolymj.2017.05.027

[69] Alkan C, Günther E, Hiebler S et al (2012) Polyurethanes as solid–solid phase change materials for thermal energy storage. Sol Energy 86:1761–1769. https://doi.org/10.1016/j.solener.2012.03.012

[70] Mu S, Guo J, Yu C et al (2015) A novel solid-solid phase change material based on Poly(styrene-co-acrylonitrile) grafting with palmitic acid copolymers. J Macromol Sci Part 52:617–624. https://doi.org/10.1080/10601325.2015.1050633

[71] Cao Q, Liu P (2006) Hyperbranched polyurethane as novel solid–solid phase change material for thermal energy storage. Eur Polym J 42:2931–2939. https://doi.org/10.1016/j.eurpolymj.2006.07.020

[72] Huang X, Chen X, Li A et al (2018) Shape-stabilized phase change materials based on porous supports for thermal energy storage applications. Chem Eng J 356:641–661. https://doi.org/10.1016/j.cej.2018.09.013

[73] Shaid A, Wang L, Islam S et al (2016) Preparation of aerogel-eicosane microparticles for thermoregulatory coating on textile. Appl Therm Eng 107:602–611. https://doi.org/10.1016/j.applthermaleng.2016.06.187

[74] Khosrojerdi M, Mortazavi SM (2013) Impregnation of a porous material with a PCM on a cotton fabric and the effect of vacuum on thermo-regulating textiles. J Therm Anal Calorim 114:1111–1119. https://doi.org/10.1007/s10973-013-3144-x

[75] Yang K, Venkataraman M, Karpiskova J et al (2021) Structural analysis of embedding polyethylene glycol in

silica aerogel. Micropor Mesopor Mat. https://doi.org/10.1016/j.micromeso.2020.110636

[76] Andriamitantsoa RS, Dong W, Gao H, Wang G (2017) PEG encapsulated by porous triamide-linked polymers as support for solid-liquid phase change materials for energy storage. Chem Phys Lett 671:165–173. https://doi.org/10.1016/j.cplett.2017.01.028

[77] Gao H, Wang J, Chen X et al (2018) Nanoconfinement effects on thermal properties of nanoporous shape-stabilized composite PCMs: a review. Nano Energy 53:769–797. https://doi.org/10.1016/j.nanoen.2018.09.007

[78] Tian F, Zhang S, Zhai M et al (2017) Thermal properties of nano-sized polyethylene glycol confined in silica gels for latent heat storage. Thermochim Acta 655:211–218. https://doi.org/10.1016/j.tca.2017.05.006

[79] Wang C, Feng L, Li W et al (2012) Shape-stabilized phase change materials based on polyethylene glycol/porous carbon composite: the influence of the pore structure of the carbon materials. Sol Energ Mat Sol C 105:21–26. https://doi.org/10.1016/j.solmat.2012.05.031

[80] Bayram Ü, Aksöz S, Maraşlı N (2014) Temperature dependency of thermal conductivity of solid phases for fatty acids. J Therm Anal Calorim 118:311–321. https://doi.org/10.1007/s10973-014-3968-z

[81] Kenisarin M, Mahkamov K, Kahwash F, Makhkamova I (2019) Enhancing thermal conductivity of paraffin wax 53–57 °C using expanded graphite. Sol Energ Mat Sol C 200:110026. https://doi.org/10.1016/j.solmat.2019.110026

[82] Zahir MH, Rahman MM, Irshad K, Rahman MM (2019) Shape-stabilized phase change materials for solar energy storage: MgO and Mg(OH)2 mixed with polyethylene glycol. Nanomaterials-basel 9:1773. https://doi.org/10.3390/nano9121773

[83] Kibria MA, Anisur MR, Mahfuz MH et al (2015) A review on thermophysical properties of nanoparticle dispersed phase change materials. Energ Convers Manage 95:69–89. https://doi.org/10.1016/j.enconman.2015.02.028

[84] Fan L, Khodadadi JM (2011) Thermal conductivity enhancement of phase change materials for thermal energy storage: a review. Renew Sustain Energy Rev 15:24–46. https://doi.org/10.1016/j.rser.2010.08.007

[85] Li T, Lee J-H, Wang R, Kang YT (2014) Heat transfer characteristics of phase change nanocomposite materials for thermal energy storage application. Int J Heat Mass Tran 75:1–11. https://doi.org/10.1016/j.ijheatmasstransfer.2014.03.054

[86] Ma C, Zhang Y, Chen X et al (2020) Experimental study of an enhanced phase change material of paraffin/expanded graphite/nano-metal particles for a personal cooling system. Materials 13:980. https://doi.org/10.3390/ma13040980

[87] Sarier N, Onder E, Ukuser G (2015) Silver incorporated microencapsulation of n-hexadecane and n-octadecane appropriate for dynamic thermal management in textiles. Thermochim Acta 613:17–27. https://doi.org/10.1016/j.tca.2015.05.015

[88] Li J, Zhu X, Wang H et al (2021) Synthesis and properties of multifunctional microencapsulated phase change material for intelligent textiles. J Mater Sci 56:2176–2191. https://doi.org/10.1007/s10853-020-05399-4

[89] Golestaneh SI, Karimi G, Babapoor A, Torabi F (2018) Thermal performance of co-electrospun fatty acid nanofiber composites in the presence of nanoparticles. Appl Energ 212:552–564. https://doi.org/10.1016/j.apenergy.2017.12.055

[90] Sundarram SS, Li W (2014) The effect of pore size and porosity on thermal management performance of phase change material infiltrated microcellular metal foams. Appl Therm Eng 64:147–154. https://doi.org/10.1016/j.applthermaleng.2013.11.072

[91] Sheng N, Rao Z, Zhu C, Habazaki H (2020) Enhanced thermal performance of phase change material stabilized with textile-structured carbon scaffolds. Sol Energ Mat Sol C. https://doi.org/10.1016/j.solmat.2019.110241

[92] Li C, Zhang D, Ren W (2021) Phase change materials composite based on hybrid aerogel with anisotropic microstructure. Materials 14:777. https://doi.org/10.3390/ma14040777

[93] Huang M, Luo Y, Zhong Y et al (2017) Preparation and characterization of microencapsulated phase change materials with binary cores and poly (allyl methacrylate) (PALMA) shells used for thermo-regulated fibers. Thermochim Acta 655:262–268. https://doi.org/10.1016/j.tca.2017.07.006

[94] Zhou M, Luo Y, Du J (2020) Temperature-regulated seaweed fibers based on MPCMs using binary system of Butyl Stearate/Hexadecanol. Fiber Polym 21:1956–1964. https://doi.org/10.1007/s12221-020-9960-2

[95] Atinafu DG, Dong W, Huang X et al (2018) Introduction of organic-organic eutectic PCM in mesoporous N-doped carbons for enhanced thermal conductivity and energy storage capacity. Appl Energ 211:1203–1215. https://doi.org/10.1016/j.apenergy.2017.12.025

[96] Cai Y, Liu M, Song X et al (2015) A form-stable phase change material made with a cellulose acetate nanofibrous mat from bicomponent electrospinning and incorporated capric-myristic-stearic acid ternary eutectic mixture for thermal energy storage/retrieval. Rsc Adv 5:84245–84251. https://doi.org/10.1039/c5ra14876f

[97] Cai Y, Ke H, Lin L et al (2012) Preparation, morphology and thermal properties of electrospun fatty acid eutectics/

polyethylene terephthalate form-stable phase change ultrafine composite fibers for thermal energy storage. Energ Convers Manage 64:245–255. https://doi.org/10.1016/j.enconman.2012.04.018

[98] DongJiang Liu TWY et al (2020) A phase change material embedded composite consisting of kapok and hollow PET fibers for dynamic thermal comfort regulation. Ind Crop Prod. https://doi.org/10.1016/j.indcrop.2020.112945

[99] Nikmaram N, Roohinejad S, Hashemi S et al (2017) Emulsion-based systems for fabrication of electrospun nanofibers: food, pharmaceutical and biomedical applications. Rsc Adv 7:28951–28964. https://doi.org/10.1039/c7ra00179g

[100] Hu W, Yu X (2012) Encapsulation of bio-based PCM with coaxial electrospun ultrafine fibers. Rsc Adv 2:5580–5584. https://doi.org/10.1039/c2ra20532g

[101] Cai Y, Ke H, Zhang T et al (2011) Preparation, morphology and properties of electrospun lauric acid/pet form-stable phase change ultrafine composite fibres. Polym Polym Compos 19:773–780. https://doi.org/10.1177/096739111101900907

[102] Kizildag N (2021) Smart composite nanofiber mats with thermal management functionality. Sci Rep-uk 11:4256. https://doi.org/10.1038/s41598-021-83799-5

[103] Lin C, Li W, Yan Y et al (2021) Ultrafine electrospun fiber based on ionic liquid/AlN/copolyamide composite as novel form-stable phase change material for thermal energy storage. Sol Energ Mat Sol C. https://doi.org/10.1016/j.solmat.2020.110953

[104] Chen C, Liu S, Liu W et al (2012) Synthesis of novel solid–liquid phase change materials and electrospinning of ultrafine phase change fibers. Sol Energ Mat Sol C 96:202–209. https://doi.org/10.1016/j.solmat.2011.09.057

[105] Xie N, Niu J, Gao X et al (2020) Fabrication and characterization of electrospun fatty acid form-stable phase change materials in the presence of copper nanoparticles. Int J Energ Res 44:8567–8577. https://doi.org/10.1002/er.5543

[106] Zhang J, Yang Q, Cai Y et al (2017) Fabrication and characterization of electrospun porous cellulose acetate nanofibrous mats incorporated with capric acid as form-stable phase change materials for storing/retrieving thermal energy. Int J Green Energy 14:1011–1019. https://doi.org/10.1080/15435075.2017.1354298

[107] Chen C, Wang L, Huang Y (2011) Electrospun phase change fibers based on polyethylene glycol/cellulose acetate blends. Appl Energ 88:3133–3139. https://doi.org/10.1016/j.apenergy.2011.02.026

[108] Nguyen TTT, Park JS (2011) Fabrication of electrospun nonwoven mats of polyvinylidene fluoride/polyethylene glycol/fumed silica for use as energy storage materials. J Appl Polym Sci 121:3596–3603. https://doi.org/10.1002/app.34148

[109] Ke H (2018) Electrospun methyl stearate/PET form-stable phase change composite nanofibres for storage and retrieval of thermal energy. Mater Res Innov 22:150–158. https://doi.org/10.1080/14328917.2016.1266203

[110] Cai Y, Xu X, Gao C et al (2012) Effects of carbon nanotubes on morphological structure, thermal and flammability properties of electrospun composite fibers consisting of lauric acid and polyamide 6 as thermal energy storage materials. Fiber Polym 13:837–845. https://doi.org/10.1007/s12221-012-0837-x

[111] Cai Y, Ke H, Dong J et al (2011) Effects of nano-SiO2 on morphology, thermal energy storage, thermal stability, and combustion properties of electrospun lauric acid/PET ultrafine composite fibers as form-stable phase change materials. Appl Energ 88:2106–2112. https://doi.org/10.1016/j.apenergy.2010.12.071

[112] Alay S, Göde F, Alkan C (2010) Preparation and characterization of poly(methylmethacrylate-coglycidyl methacrylate)/n-hexadecane nanocapsules as a fiber additive for thermal energy storage. Fiber Polym 11:1089–1093. https://doi.org/10.1007/s12221-010-1089-2

[113] Rezaei B, Ghani M, Askari M et al (2016) Fabrication of thermal intelligent core/shell nanofibers by the solution coaxial electrospinning process. Adv Polym Tech. https://doi.org/10.1002/adv.21534

[114] Dang TT, Nguyen TTT, Chung OH, Park JS (2015) Fabrication of form-stable poly(ethylene glycol)-loaded poly(vinylidene fluoride) nanofibers via single and coaxial electrospinning. Macromol Res 23:819–829. https://doi.org/10.1007/s13233-015-3109-y

[115] Hu W, Yu X (2014) Thermal and mechanical properties of bio-based PCMs encapsulated with nanofibrous structure. Renew Energ 62:454–458. https://doi.org/10.1016/j.renene.2013.07.047

[116] Babapoor A, Karimi G, Golestaneh SI, Mezjin MA (2017) Coaxial electro-spun PEG/PA6 composite fibers: fabrication and characterization. Appl Therm Eng 118:398–407. https://doi.org/10.1016/j.applthermaleng.2017.02.119

[117] Feng W, Zhang Y-S, Shao Y-W et al (2021) Coaxial electrospun membranes with thermal energy storage and shape memory functions for simultaneous thermal/moisture management in personal cooling textiles. Eur Polym J. https://doi.org/10.1016/j.eurpolymj.2020.110245

[118] Noyan ECB, Onder E, Sarier N, Arat R (2018) Development of heat storing poly(acrylonitrile) nanofibers by coaxial electrospinning. Thermochim Acta 662:135–148. https://doi.org/10.1016/j.tca.2018.02.008

[119] Chen C, Zhao Y, Liu W (2013) Electrospun polyethylene glycol/cellulose acetate phase change fibers with core-sheath structure for thermal energy storage. Renew Energ 60:222–225. https://doi.org/10.1016/j.renene.2013.05.020

[120] Ruirui C, Dongfang P, Shuqin L et al (2019) Electrospinning of thermo-regulated sheath/core submicrometer fiber with galactitol hexa palmitate as a core. Text Res J 89:354–363. https://doi.org/10.1177/0040517517743740

[121] Wang S, Yi L, Fang Y et al (2021) Reversibly thermochromic and high strength core-shell nanofibers fabricated by melt coaxial electrospinning. J Appl Polym Sci. https://doi.org/10.1002/app.50465

[122] Haghighat F, Ravandi SAH, Esfahany MN, Valipouri A (2018) A comprehensive study on optimizing and thermoregulating properties of core–shell fibrous structures through coaxial electrospinning. J Mater Sci 53:4665–4682. https://doi.org/10.1007/s10853-017-1856-1

[123] Sarier N, Arat R, Menceloglu Y et al (2016) Production of PEG grafted PAN copolymers and their electrospun nanowebs as novel thermal energy storage materials. Thermochim Acta 643:83–93. https://doi.org/10.1016/j.tca.2016.10.002

[124] Wang N, Chen H, Lin L et al (2010) Multicomponent phase change microfibers prepared by temperature control multifluidic electrospinning. Macromol Rapid Comm 31:1622–1627. https://doi.org/10.1002/marc.201000185

[125] Zdraveva E, Fang J, Mijovic B, Lin T (2015) Electrospun Poly(vinyl alcohol)/Phase change material fibers: morphology, heat properties, and stability. Ind Eng Chem Res 54:8706–8712. https://doi.org/10.1021/acs.iecr.5b01822

[126] Zhao L, Luo J, Li Y et al (2017) Emulsion-electrospinning n-octadecane/silk composite fiber as environmental-friendly form-stable phase change materials. J Appl Polym Sci. https://doi.org/10.1002/app.45538

[127] Chen W, Ni S, Weng W, Fu M (2018) The preparation and characterization of ultrafine fatty acid Ester/Poly(meta-phenylene isophthalamide) phase change fibers designed for thermo-regulating protective clothing. Fiber Polym 19:498–506. https://doi.org/10.1007/s12221-018-7180-9

[128] Zhou L, Shi F, Liu G et al (2021) Fabrication and characterization of in situ cross-linked electrospun Poly(vinyl alcohol)/phase change material nanofibers. Sol Energy 213:339–349. https://doi.org/10.1016/j.solener.2020.11.039

[129] Golestaneh SI, Mosallanejad A, Karimi G et al (2016) Fabrication and characterization of phase change material composite fibers with wide phase-transition temperature range by co-electrospinning method. Appl Energ 182:409–417. https://doi.org/10.1016/j.apenergy.2016.08.136

[130] Venkataraman M, Yang K, Xiong X et al (2020) Preparation of electrosprayed, microporous particle filled layers. Polymers-basel. https://doi.org/10.3390/polym12061352

[131] Peng Q, Yang K, Venkataraman M et al (2021) Preparation of electrosprayed composite coated microporous filter for particulate matter capture. Nano Sel. https://doi.org/10.1002/nano.202100186

[132] Xiong X, Venkataraman M, Yang T et al (2020) Transport properties of electro-sprayed polytetrafluoroethylene fibrous layer filled with aerogels/phase change materials. Nanomaterials-basel 10:1–14. https://doi.org/10.3390/nano10102042

[133] Li C, Huang Y, Li R et al (2021) Fabrication and properties of carboxymethyl chitosan/polyethylene oxide composite nonwoven mats by centrifugal spinning. Carbohyd Polym 251:117037. https://doi.org/10.1016/j.carbpol.2020.117037

[134] Gong X, Dang G, Guo J et al (2019) Sodium alginate/feather keratin-g-allyloxy polyethylene glycol composite phase change fiber. Int J Biol Macromol 131:192–200. https://doi.org/10.1016/j.ijbiomac.2019.02.168

[135] Zhang X, Qiao J, Zhao H et al (2018) Preparation and performance of novel polyvinylpyrrolidone/polyethylene glycol phase change materials composite fibers by centrifugal spinning. Chem Phys Lett 691:314–318. https://doi.org/10.1016/j.cplett.2017.11.041

[136] Chen G, Xu Y, Shi T et al (2019) Preparation and properties of polyacrylonitrile/polyethylene glycol composite fibers phase change materials by centrifugal spinning. Mater Res Express. https://doi.org/10.1088/2053-1591/ab2d0a

[137] Chen G, Shi T, Zhang X et al (2020) Polyacrylonitrile/polyethylene glycol phase-change material fibres prepared with hybrid polymer blends and nano-SiC fillers via centrifugal spinning. Polymer. https://doi.org/10.1016/j.polymer.2019.122012

[138] Anna N, Inge G, Bengt H (2011) Multi-component fibres

[139] Tomaszewski W, Twarowska-Schmidt K, Moraczewski A et al (2012) Nonwovens with thermal storage properties based on paraffin-modified polypropylene fibres. Fibres and Textiles in Eastern Europe 96:64–69

[140] Iqbal K, Sun D (2014) Development of thermo-regulating polypropylene fibre containing microencapsulated phase change materials. Renew Energ 71:473–479. https://doi.org/10.1016/j.renene.2014.05.063

[141] Iqbal K, Sun D, Stylios GK et al (2015) FE analysis of thermal properties of woven fabric constructed by yarn incorporated with microencapsulated phase change materials. Fiber Polym 16:2497–2503. https://doi.org/10.1007/s12221-015-5607-0

[142] Fredi G, Bruenig H, Vogel R, Scheffler C (2019) Melt-spun polypropylene filaments containing paraffin microcapsules

for multifunctional hybrid yarns and smart thermoregulating thermoplastic composites. Express Polym Lett 13:1071–1087. https://doi.org/10.3144/expresspolymlett.2019.93

[143] Xia W, Xiang H, Zhou Z et al (2021) Hybridizing rational designed hydrophobic PEG-based derivatives into nanoporous F-SiO_2 as form-stable phase change materials for melt-spun PA6 phase change fibers with a superior washing durability. Compos Commun. https://doi.org/10.1016/j.coco.2021.100633

[144] Xia W, Fei X, Wang Q et al (2021) Nano-hybridized form-stable ester@F-SiO_2 phase change materials for melt-spun PA6 fibers engineered towards smart thermal management fabrics. Chem Eng J. https://doi.org/10.1016/j.cej.2020.126369

[145] Xu W, Lu Y, Wang B et al (2013) Preparation and characterization of high latent heat thermal regulating fiber made of PVA and paraffin. J Eng Fiber Fabr 8:44–49. https://doi.org/10.1177/155892501300800205

[146] Li Z, He W, Xu J, Jiang M (2015) Preparation and characterization of in situ grafted/crosslinked polyethylene glycol/polyvinyl alcohol composite thermal regulating fiber. Sol Energ Mat Sol C 140:193–201. https://doi.org/10.1016/j.solmat.2015.04.014

[147] Wang Y, Yao J, Zhu G et al (2020) A novel method for producing bi-component thermo-regulating alginate fiber from phase change material microemulsion. Text Res J 90:1038–1044. https://doi.org/10.1177/0040517519886075

[148] Wu J, Hu R, Zeng S et al (2020) Flexible and Robust Biomaterial Microstructured Colored Textiles for Personal Thermoregulation. Acs Appl Mater Inter 12:19015–19022. https://doi.org/10.1021/acsami.0c02300

[149] Wen G-Q, Xie R, Liang W-G et al (2015) Microfluidic fabrication and thermal characteristics of core–shell phase change microfibers with high paraffin content. Appl Therm Eng 87:471–480. https://doi.org/10.1016/j.applthermaleng.2015.05.036

[150] Pesek SC, Koros WJ (1994) Aqueous quenched asymmetric polysulfone hollow fibers prepared by dry/wet phase separation. J Membrane Sci 88:1–19. https://doi.org/10.1016/0376-7388(93)e0150-i

[151] Gan YX, Gan JB (2020) Porous Fiber Processing and Manufacturing for Energy Storage Applications. Chemengineering 4:59. https://doi.org/10.3390/chemengineering4040059

[152] Ahn Y-H, DeWitt SJA, McGuire S, Lively RP (2021) Incorporation of phase change materials into fibers for sustainable thermal energy storage. Ind Eng Chem Res. https://doi.org/10.1021/acs.iecr.0c06140

[153] Yan Y, Li W, Zhu R et al (2021) Flexible phase change material fiber: A simple route to thermal energy control textiles. Materials 14:1–18. https://doi.org/10.3390/ma14020401

[154] Luo D, Wei F, Shao H et al (2018) Shape stabilization, thermal energy storage behavior and thermal conductivity enhancement of flexible paraffin/MWCNTs/PP hollow fiber membrane composite phase change materials. J Mater Sci 53:15500–15513. https://doi.org/10.1007/s10853-018-2722-5

[155] Li G, Hong G, Dong D et al (2018) Multiresponsive graphene-aerogel-directed phase-change smart Fibers. Adv Mater. https://doi.org/10.1002/adma.201801754

[156] Wan ACA, Cutiongco MFA, Tai BCU et al (2016) Fibers by interfacial polyelectrolyte complexation – processes, materials and applications. Mater Today 19:437–450. https://doi.org/10.1016/j.mattod.2016.01.017

[157] Fang H, Lin J, Zhang L et al (2020) Fibrous form-stable phase change materials with high thermal conductivity fabricated by interfacial polyelectrolyte complex spinning. Carbohyd Polym. https://doi.org/10.1016/j.carbpol.2020.116836

[158] Lin J-H, Huang Y-T, Li T-T et al (2016) Bamboo charcoal/phase change material/stainless steel ring-spun complex yarn and its far-infrared/anion-releasing elastic warp-knitted fabric: Fabrication and functional evaluation. J Ind Text 46:624–642. https://doi.org/10.1177/1528083715595007

[159] Iqbal K, Sun D (2015) Development of thermal stable multifilament yarn containing micro-encapsulated phase change materials. Fiber Polym 16:1156–1162. https://doi.org/10.1007/s12221-015-1156-9

[160] Rahbar RS, Maleki H, Kalantari B (2016) Fabrication of electrospun nanofibre yarn based on nylon 6/microencapsulated phase change materials. J Exp Nanosci 11:1402–1415. https://doi.org/10.1080/17458080.2016.1233582

[161] Ke G, Jin X, Cai G et al (2021) A novel composite cotton yarn with phase change and electrical conductivity functions. J Ind Text. https://doi.org/10.1177/15280837211003166

[162] Chen W, Fu M, Weng W (2020) Electrospinning of continuous nanofiber hollow yarns for thermal storage and insulation by a multi-step twisting method. Text Res J 90:1045–1056. https://doi.org/10.1177/0040517519886023

[163] Huang C-L, Huang Y-T, Li T-T et al (2016) Composite processing and property evaluation of far-infrared/electromagnetic shielding bamboo charcoal/phase change material/stainless steel elastic composite fabrics. J Polym Eng 36:211–220. https://doi.org/10.1515/polyeng-2015-0080

[164] Liu X, Lou Y (2015) Preparation of microencapsulated phase change materials by the sol-gel process and its application on textiles [Przygotowanie materiałów zmiennofazowych w mikrokapsułkach za pomocą procesu zol-żel i ich zastosowanie w tekstyliach]. Fibres and Textiles in Eastern Europe 23:63–67

[165] Zhang G, Cai C, Wang Y et al (2019) Preparation and evaluation of thermo-regulating bamboo fabric treated by microencapsulated phase change materials. Text Res J 89:3387–3393. https://doi.org/10.1177/0040517518813681

[166] Varnaitė-Žuravliova S, Stygienė L, Krauledas S et al (2015) The dependance of effectiveness of incorporated microencapsulated phase change materials on different structures of knitted fabrics. Fiber Polym 16:1125–1133. https://doi.org/10.1007/s12221-015-1125-3

[167] Aksoy SA, Alkan C, Tözüm MS et al (2017) Preparation and textile application of poly(methyl methacrylate-co-methacrylic acid)/n-octadecane and n-eicosane microcapsules. J Text Inst 108:30–41. https://doi.org/10.1080/00405000.2015.1133128

[168] Wang Y, Ma Y, Chen R, Su Y (2021) Thermal protective performance of firefighting protective clothing incorporated with phase change material in fire environments. Fire Mater 45:250–260. https://doi.org/10.1002/fam.2928

[169] Su Y, Zhu W, Tian M et al (2020) Intelligent bidirectional thermal regulation of phase change material incorporated in thermal protective clothing. Appl Therm Eng. https://doi.org/10.1016/j.applthermaleng.2020.115340

[170] Kar TR, Samanta AK, Sinnur HD, Kumar M (2021) Studies on Effect of Application of Capric Acid and Stearic Acid based Reactive Phase Change Materials (rPCM) with PHAMS Binder on Thermal Comfort of Cotton Khadi Fabric as Thermo-tropic Smart Textiles. J Nat Fibers. https://doi.org/10.1080/15440478.2021.1880517

[171] Zhang W, Hao S, Zhao D et al (2020) Preparation of PMMA/SiO2 PCM microcapsules and its thermal regulation performance on denim fabric. Pigm Resin Technol 49:491–499. https://doi.org/10.1108/prt-01-2020-0003

[172] Iamphaojeen Y, Siriphannon P (2018) Adjustable thermal barrier of cotton fabric by multilayer immobilization of PCM nanocapsules. Cellulose 25:3649–3661. https://doi.org/10.1007/s10570-018-1804-5

[173] Karthikeyan M, Ramachandran T, Sundaram OLS (2014) Nanoencapsulated phase change materials based on polyethylene glycol for creating thermoregulating cotton. J Ind Text 44:130–146. https://doi.org/10.1177/1528083713480378

[174] Salaün F, Devaux E, Bourbigot S, Rumeau P (2010) Thermoregulating response of cotton fabric containing microencapsulated phase change materials. Thermochim Acta 506:82–93. https://doi.org/10.1016/j.tca.2010.04.020

[175] Sánchez-Silva L, Rodríguez JF, Romero A, Sánchez P (2012) Preparation of coated thermo-regulating textiles using Rubitherm-RT31 microcapsules. J Appl Polym Sci 124:4809–4818. https://doi.org/10.1002/app.35546

[176] Kim I, Lee K, Cho G (2016) Heat storage/release characteristics and mechanical properties of combat uniform fabrics treated with microcapsules containing octadecane as phase change materials. Fiber Polym 17:1726–1734. https://doi.org/10.1007/s12221-016-6796-x

[177] Kim I, Lee K, Cho G (2016) Response surface methodology for optimizing treatment condition of military combat uniform fabrics with phase change microcapsules to minimize fabric frictional sound and maximize the heat property. Fiber Polym 17:1305–1310. https://doi.org/10.1007/s12221-016-6383-1

[178] Park YM, Shin JW (2011) Surface properties studies of MPCMs containing fabrics for thermo-regulating textiles. Fiber Polym 12:384–389. https://doi.org/10.1007/s12221-011-0384-x

[179] Peter G, Hans R, Oliver S (2009) Elastic, soft and punctiformly bound non-woven fabric provided with filler particles and method for production and the use thereof

[180] Christophter A, Blackford ME (2015) Cooling fabrics

[181] Ghahremanzadeh F, Khoddami A, Carr CM (2010) Improvement in fastness properties of phase-change material applied on surface modified wool fabrics. Fiber Polym 11:1170–1180. https://doi.org/10.1007/s12221-010-1170-x

[182] Benmoussa D, Molnar K, Hannache H, Cherkaoui O (2018) Novel Thermo-Regulating Comfort Textile Based on Poly(allyl ethylene diamine)/n-Hexadecane Microcapsules Grafted onto Cotton Fabric. Adv Polym Tech 37:419–428. https://doi.org/10.1002/adv.21682

[183] Hassabo AG (2014) New approaches to improving thermal regulating property of cellulosic fabric. Carbohyd Polym 101:912–919. https://doi.org/10.1016/j.carbpol.2013.10.006

[184] Paul R (2014) Functional Finishes for Textiles Improving Comfort. Woodhead Publishing, Performance and Protection

[185] Yoo S, Kandare E, Shanks R et al (2016) Thermophysical properties of multifunctional glass fibre reinforced polymer composites incorporating phase change materials. Thermochim Acta 642:25–31. https://doi.org/10.1016/j.tca.2016.09.003

[186] Nejman A, Cieślak M, Gajdzicki B et al (2014) Methods of PCM microcapsules application and the thermal properties of modified knitted fabric. Thermochim Acta 589:158–163. https://doi.org/10.1016/j.tca.2014.05.037

[187] Eugene AJ (2019) Cooling Fabric
[188] Zhao M (2017) The usage of phase change materials in fire fighter protective clothing: its effect on thermal protection. Iop Conf Ser Mater Sci Eng 274:012136. https://doi.org/10.1088/1757-899x/274/1/012136
[189] Alptekin E, Ezan MA, Gül BM et al (2017) Numerical investigation of thermal regulation inside firefighter protective clothing. Tekstil Ve Mühendis 24:94–100. https://doi.org/10.7216/1300759920172410606
[190] Zhu F, Feng QQ, Liu R et al (2015) Enhancing the thermal protective performance of firefighters' protective fabrics by incorporating phase change materials [Polepszenie właściwości termicznych odzieży ochronnej strażaków poprzez zastosowanie materiałów zmiennofazowych]. Fibres and Textiles in Eastern Europe 23:68–73
[191] Shaid A, Wang L, Fergusson SM, Padhye R (2018) Effect of Aerogel Incorporation in PCM-Containing Thermal Liner of Firefighting Garment. Cloth Text Res J 36:151–164. https://doi.org/10.1177/0887302x18755464
[192] Zhang H, Song G, Su H et al (2017) An exploration of enhancing thermal protective clothing performance by incorporating aerogel and phase change materials. Fire Mater 41:953–963. https://doi.org/10.1002/fam.2435
[193] Michael F (2019) Sleep products having adjustable firmness levels and adjustable heights
[194] Kevin C, Mackenzie P, Sheri M, Brian A (2019) Three dimensional polymeric fiber matrix layer for bedding products
[195] Yoo H, Lim J, Kim E (2013) Effects of the number and position of phase-change material-treated fabrics on the thermo-regulating properties of phase-change material garments. Text Res J 83:671–682. https://doi.org/10.1177/0040517512461700
[196] Demirbağ S, Aksoy SA (2016) Encapsulation of phase change materials by complex coacervation to improve thermal performances and flame retardant properties of the cotton fabrics. Fiber Polym 17:408–417. https://doi.org/10.1007/s12221-016-5113-z
[197] Borreguero AM, Talavera B, Rodriguez JF et al (2013) Enhancing the thermal comfort of fabrics for the footwear industry. Text Res J 83:1754–1763. https://doi.org/10.1177/0040517513481872
[198] Zhang Q, He Z, Fang X et al (2017) Experimental and numerical investigations on a flexible paraffin/fiber composite phase change material for thermal therapy mask. Energy Storage Mater 6:36–45. https://doi.org/10.1016/j.ensm.2016.09.006
[199] Halimi MT, Hassen MB, Sakli F (2012) Design of a novel comfort liner for a motorcycle helmet. Int J Sustain Eng 5:128–134. https://doi.org/10.1080/19397038.2011.602438
[200] Sinnappoo K, Nayak R, Thompson L, Padhye R (2020) Application of sustainable phase change materials in motorcycle helmet for heat-stress reduction. J Text Inst. https://doi.org/10.1080/00405000.2020.1715606
[201] ltani M, Ghaddar N, Ghali K (2017) Innovative PCM-desiccant packet to provide dry microclimate and improve performance of cooling vest in hot environment. Energ Convers Manage 140:218–227. https://doi.org/10.1016/j.enconman.2017.03.011
[202] Kadem FD, Saraç EG (2017) An experimental application on denim garment to give thermal regulation property. J Text Inst 108:353–360. https://doi.org/10.1080/00405000.2016.1166822
[203] Scacchetti FAP, Pinto E, Soares GMB (2017) Functionalization and characterization of cotton with phase change materials and thyme oil encapsulated in beta-cyclodextrins. Prog Org Coat 107:64–74. https://doi.org/10.1016/j.porgcoat.2017.03.015
[204] Scacchetti FAP, Pinto E, Soares GMB (2018) Thermal and antimicrobial evaluation of cotton functionalized with a chitosan–zeolite composite and microcapsules of phase-change materials. J Appl Polym Sci. https://doi.org/10.1002/app.46135
[205] Yi S, Sun S, Deng Y, Feng S (2015) Preparation of composite thermochromic and phase-change materials by the sol–gel method and its application in textiles. J Text Inst 106:1071–1077. https://doi.org/10.1080/00405000.2014.965501
[206] Wang H, Luo J, Yang Y et al (2016) Fabrication and characterization of microcapsulated phase change materials with an additional function of thermochromic performance. Sol Energy 139:591–598. https://doi.org/10.1016/j.solener.2016.10.011
[207] Xy G, Y G, N W, et al (2021) Intelligent adjustment of light-to-thermal energy conversion efficiency of thermo-regulated fabric containing reversible thermochromic MicroPCMs. Chem Eng J 408:127276. https://doi.org/10.1016/j.cej.2020.127276
[208] Ward JW, Thomas R, Mitchell M, Segal BM (2010) Method and system of using nanotube fabrics as joule heating elements for memories and other applications
[209] Brooks L, Lettow J, Scheffer D (2018) Personal thermal management system
[210] Shi Q, Liu Z, Jin X et al (2015) Electrospun fibers based on polyvinyl pyrrolidone/Eu-polyethylene glycol as phase change luminescence materials. Mater Lett 147:113–115. https://doi.org/10.1016/j.matlet.2015.02.040
[211] Xi P, Zhao T, Xia L et al (2017) Fabrication and characterization of dual-functional ultrafine composite fibers with

phase-change energy storage and luminescence properties. Sci Rep-uk. https://doi.org/10.1038/srep40390

[212] Chai L, Wang X, Wu D (2015) Development of bifunctional microencapsulated phase change materials with crystalline titanium dioxide shell for latent-heat storage and photocatalytic effectiveness. Appl Energ 138:661–674. https://doi.org/10.1016/j.apenergy.2014.11.006

[213] Verma P, Varun SSK (2008) Review of mathematical modeling on latent heat thermal energy storage systems using phase-change material. Renew Sustain Energy Rev 12:999–1031. https://doi.org/10.1016/j.rser.2006.11.002

[214] Zhang C, Chang S, Song G et al (2021) Study on a novel filter media incorporating with core shell nanoencapsulated phase change material: fabrication and evaluation. Process 9:731. https://doi.org/10.3390/pr9050731

[215] L VHK, W VHE, Diana VH (2008) Therapeutic pack

[216] Aldo L (2020) Thermally assisted therapeutic aids for cosmetics and wound treatment

[217] Brideges S, Shuman SR, Asplund P (2016) Image transfer product including a phase change materials

[218] Nejman A, Gromadzínska E, Kamínska I, Ciéslak M (2020) Assessment of thermal performance of textile materials modified with PCM microcapsules using combination of DSC and infrared thermography methods. Molecules. https://doi.org/10.3390/molecules25010122

[219] Nejman A, Cieślak M (2017) The impact of the heating/cooling rate on the thermoregulating properties of textile materials modified with PCM microcapsules. Appl Therm Eng 127:212–223. https://doi.org/10.1016/j.applthermaleng.2017.08.037

[220] Bergman TL, Lavine AS, Incropera FP, Dewitt DP (2011) Fundamentals of heat and mass transfer, 7th edn. Wiley

[221] Pause B (1995) Development of heat and cold insulating membrane structures with phase change material. J Ind Text 25:59–68. https://doi.org/10.1177/152808379502500107

[222] Bendkowska W, Tysiak J, Grabowski L, Blejzyk A (2005) Determining temperature regulating factor for apparel fabrics containing phase change material. Int J Cloth Sci Tech 17:209–214. https://doi.org/10.1108/09556220510590902

[223] Ying B, Kwok Y, Li Y et al (2004) Assessing the performance of textiles incorporating phase change materials. Polym Test 23:541–549. https://doi.org/10.1016/j.polymertesting.2003.11.002

[224] Wang SX, Li Y, Hu JY et al (2006) Effect of phase-change material on energy consumption of intelligent thermal-protective clothing. Polym Test 25:580–587. https://doi.org/10.1016/j.polymertesting.2006.01.018

[225] Wan X, Fan J (2009) A new method for measuring the thermal regulatory properties of phase change material (PCM) fabrics. Meas Sci Technol 20:025110. https://doi.org/10.1088/0957-0233/20/2/025110

[226] Scacchetti FAP, Soares GMB (2019) Chemical characterization and thermal comfort properties of cotton finished with phase change materials and antimicrobial agents. Cell Chem Technol 53:363–371. https://doi.org/10.35812/cellulosechemtechnol.2019.53.37

[227] Hes L, Lu BL (2004) Using a thermal simulator to determine the amount of time that humans are thermally protected by fabrics containing phase change materials. Res J Text Appar 8:51–56. https://doi.org/10.1108/rjta-08-02-2004-b007

[228] Yang K, Jiao M, Wang S et al (2018) Thermoregulation properties of composite phase change materials in high temperature environmental conditions. Int J Cloth Sci Tech 30:507–516. https://doi.org/10.1108/ijcst-11-2017-0173

[229] Shaid A, Wang L, Padhye R (2016) The thermal protection and comfort properties of aerogel and PCM-coated fabric for firefighter garment. J Ind Text 45:611–625. https://doi.org/10.1177/1528083715610296

[230] Yang K, Venkataraman M, Wang YF et al (2020) Thermal performance of a multi-layer composite containing peg/laponite as pcms. J Fiber Bioeng Informatics 13:61–68. https://doi.org/10.3993/jfbim00330

[231] Haghighat F, Ravandi SAH, Esfahany MN et al (2019) Thermal performance of electrospun core-shell phase change fibrous layers at simulated body conditions. Appl Therm Eng 161:113924. https://doi.org/10.1016/j.applthermaleng.2019.113924

[232] Michalak M, Felczak M, Wiecek B (2008) A new method of evaluation of thermal parameters of textile material. Proc 2008 Int Conf Quantitative Infrared Thermography. https://doi.org/10.21611/qirt.2008.11_04_05

[233] Ghali K, Ghaddar N, Harathani J, Jones B (2004) Experimental and numerical investigation of the effect of phase change materials on clothing during periodic ventilation. Text Res J 74:205–214. https://doi.org/10.1177/004051750407400304

[234] Jaworski M (2019) Mathematical model of heat transfer in PCM incorporated fabrics subjected to different thermal loads. Appl Therm Eng 150:506–511. https://doi.org/10.1016/j.applthermaleng.2019.01.019

[235] Bartkowiak G, Da browska A, Marszałek A, (2013) Analysis of thermoregulation properties of PCM garments on the basis of ergonomic tests. Text Res J 83:148–159. https://doi.org/10.1177/0040517512460299

[236] Tiest WMB, Kosters ND, Kappers AML, Daanen HAM (2012) Phase change materials and the perception of wetness. Ergonomics 55:508–512. https://doi.org/10.1080/00140139.2011.645886

[237] Li Y, Zhu Q (2004) A model of heat and moisture transfer in porous textiles with phase change materials. Text Res J 74:447–457. https://doi.org/10.1177/004051750407400512

[238] Li Y, Zhu Q (2003) A model of coupled liquid moisture and heat transfer in porous textiles with consideration of gravity. Numer Heat Transf Part Appl 43:501–523. https://doi.org/10.1080/10407780307318

[239] Zhang H, Liu X, Song G, Yang H (2020) Effects of microencapsulated phase change materials on the thermal behavior of multilayer thermal protective clothing. J Text Inst. https://doi.org/10.1080/00405000.2020.1832363

[240] Barauskas R, Sankauskaite A, Rubeziene V et al (2020) Investigation of thermal properties of spacer fabrics with phase changing material by finite element model and experiment. Text Res J 90:1837–1850. https://doi.org/10.1177/0040517520902063

[241] Siddiqui MOR, Sun D (2017) Development of plug-ins to predict effective thermal conductivity of woven and microencapsulated phase change composite. J Compos Mater 51:733–743. https://doi.org/10.1177/0021998316655202

10. APPENDIX 2-details for comparison

Table 10-1 Comparison of this work with MPCMs in enthalpy values and encapsulation efficiency

MPCMs type	Method	Encapsulation efficiency (%)	Enthalpy (J/g)	Ref.
This work (PW as PCMs)	Fibrous multi-layer fabric system	26.5	73	This work with protection layer
This work (PW as PCMs)	Fibrous multi-layer fabric system	65.8	108	This work without protection layer
This work (PEG as PCMs)	Fibrous multi-layer fabric system	44.8	78	This work with protection layer
Paraffin/MUF MPCMs	In-situ polymerization	77.1	134	[55]
N-octadecane/MF MPCMs		84.3	185.1	[56]
Pentadecane/MUF MPCMs		50.6	84.5	[57]
N-tetracosane/MF MPCMs		72.4	134.7	[58]
Paraffin/H-SiC-modifed MF MPCMs		65.1	93.2	[59]
1-dodecanol/MPF MPCMS		88.6	169.5	[60]
Oleica acid/Ag_2O-UF MPCMs		54.8	71.7	[61]
Coconut oil/MF MPCMs		76.2	81.9	[62]
1-dodecanol/MF MPCMs		40.9	79.5	[63]
Paraffin/nanoplatelets laden/UF MPCMs		55.1	110.7	[64]
Caprylic/UF MPCMs		59	93.9	[65]
Methyl laurate/nano-TiO_2-PU	Interfacial polymerization	83.3	147.71	[66]
Paraffin/PU		80.2	153.9	[67]
Paraffin/crosslinked PMMA	Suspension polymerization	66.5	93.1	[68]
Paraffin/poly(styrene		41.1	62.4	[69]

divinylbenzene-acrylic acid)				
N-octadecane/PMMA MPCMs	Emulsion	70	102.7	[113]
Paraffin/PMMA		72.5	75.6	[70]

Table 10-2 Comparison of this work with PCM containing fibers in enthalpy values and encapsulation efficiency (The sample with maximum encapsulation efficiency are selected)

PCM containing fibers type	Method	Encapsulation efficiency (%)	Enthalpy (J/g)	Loading amount (wt%)	Ref.
This work (PW as PCMs)	Fibrous multi-layer fabric system	55.3	73	45	This work with protection layer
This work (PW as PCMs)	Fibrous multi-layer fabric system	78.9	105	83	This work without protection layer
This work (PEG as PCMs)	Fibrous multi-layer fabric system	31.6	78	45	This work with protection layer
N-octadecane/PVP	Coaxial electrospinning	35.65	80	-	[71]
N-OCTADECANE/silk	Emulsion electrospinning	37.6	20	44	[72]
Parrffin/MWCNT/PP	Injection	52.8	74	-	[73]
MP-LA/PAN fiber	Blending electrospinning	47.5	89	-	[74]
MES/PET nanofiber	Blending electrospinning	44	90	-	[75]
Dodecanol laurate/PVA	Emulsion electrospinnin	33.8	65	-	[76]

nanofiber	g				
MA-TD/kapok/PET	Immersion	39	77	-	[77]
PEG/PU	Coaxial electrospinning	33.3	60	41	[78]
PEG/PAN	Coaxial electrospinning	49	70	-	[79]
PEG/PVP	Centrifugal spinning	67.3	130	-	[80]
PEG/silk fibroin/CS/PDMS	Solution-freezing spinning	-	118	86	[83]
PEG/PP	Injection	75.7	102	83	[81]
PEG/BN/CNF/CS	Interfacial polyelectrolyte complex spinning	58.5	103	71	[82]
MPCM/cellulose	Dry-jet wet-quench spinning	-	129	78	[84]

Table 10-3 Comparison of this work with PCM-incorporated composites in relative crystalline degree ratio

Sample	Relative crystalline degree ratio (%)	Overall melting enthalpy value (J/g)	Ref.
$C4_{(PEG,6000)}$	98	78	This work
$C4_{(PW)}$	95	73	This work
UPWV	95	105	This work
PW/EG/PP fiber	97	116	[73]
PW/PVDF fiber	73	79	[85]
PW/MCNTs/PP fiber	93	107	[73]
PW/CS MPCMs	85	98	[86]
PW/EG composites	97	114	[87]
PEG/PU fiber	81	60	[78]
PEG/PVP fiber	94	130	[80]
PEG/BN/CNF/CS fiber	82	103	[82]

Table 10-4 Comparison of this work with PCM-incorporated composites in overall enthalpy and phase transition range

Sample	Melting point (°C)	Overall melting enthalpy value (J/g)	Ref.
$C4_{(PEG,6000)}$	63.14	78	This work
$C4_{(PEG,4000)}$	62.13	75	
$C4_{(PEG,1500)}$	51.14	65	
$C4_{(PEG,1000)}$	39.13	68	
$C4_{(PEG,600)}$	23.48	52	
$C4_{(PEG,6000,Fe)}$	62.42	53	
$C4_{(PW)}$	56.91	73	
PEG/PU fiber	53.9	60	[78]
PEG/BN/CNT/CF fiber	58	103	[82]
PEG/PVP fiber	52.7	130	[80]
PEG/SWCNT composites	56.68	179	[73]
PEG/SiO_2 composites	56.6	103	[89]
PEG/SiO_2/Cu composites	58.2	100	[89]
PW/EG/PP fiber	53.73	116	[73]
PW/PVDF fiber	57.79	79	[85]
PW/MCNTs/PP fiber	53.64	107	[73]
PW/CS MPCMs	61.8	98	[86]
PW/EG composites	57.19	114	[87]
PW/MCNTs/PP fiber	93	107	[73]
Outlast fabric-1	29.13	13.24	From our lab
Outlast fabric-2	30.07	36.4	
Outlast fabric-3	30.59	23.69	

Table 10-5 Comparison of this work with other reported work in thermal conductivity

Sample	Thermal conductivity (K W^{-1} m^{-1})	Overall enthalpy value (J/g)	Ref.
$C4_{(PEG,6000)}$	0.0543	78	This work
$C4_{(PEG,6000,Fe)}$	0.0573	52	This work
$PEGV_{6000}$	0.0395	153	This work
$PEGV_{6000,Fe}$	0.0654	111	This work
PEG	0.297	178	[89]

PW	0.22	150	[90]
SA	0.26	190	[91]
PW/carbon fiber	1.73	192	[92]
PW/carbon nanotubes	0.71	158	[90]
MA/SA/carbon nanotubes	0.225	148	[93]
N-eicosane/carbon nanotubes	0.28	157	[94]
LA/SA graphene/diatomite	0.71	99	[95]
Palmitic acid/melamine/EG	1.08	163	[96]
Dodecanoic acid/graphene	0.57	156	[97]
PEG/GO/GN	1.43	178	[97]
PW/graphene aerogel/copper foam	3	140	[98]
Myristyl alcohl/copper foam	0.48	154	[99]
n-Eicosane/Fe_3O_4/SiO_2/Cu nanoparticles MPCMs	1.39	154	[100]
LA/Cu	0.36	172	[101]
PW/Al	1.27	102	[102]
SA/SiO_2	0.56	135	[103]
PEG/Ti_4O_7	0.34	130	[104]
MA-LA/copper nanoparticle/PAN nanofiber	0.238	85	[74]
PEG/BN/CNF/CS fiber	4	48	[82]
PEG/F-SiO_2/PA 6 nanofiber	0.06	6	[105]

Table 10-6 Comparison of PCM pocket of breathable SFPEs with MPCM coating area of air pocket-incorporated MPCM-coated knitted fabric [107]

Sample	PCM pocket (J/g)	Overall air permeability (mm/s)
Breathable fibrous multi-layer PCM systems	123	4.6 to 9
MPCM-coated knitted fabric via printing	37	973

MPCM-coated knitted fabric via coating	23	1440
MPCM-coated knitted fabric via padding	13	2173

Table 10-7 Comparison of overall enthalpy values of reported PCM textiles with this work

Sample	Overall enthalpy values (J/g)	Air permeability (mm/s)	Reference
Breathable fibrous multi-layer PCM systems	4.8 to 7.8	4.6 to 9	This work
MPCM-coated jute fabric	10	500	[108]
MPCM-coated hydrophobic PET knitted fabrics	8.9	46	[112]
MPCM-coated hydrophobic PET/cotton woven fabrics	1.8	29	[112]
MPCM-coated PET/cotton/carbon woven fabric	2.08	49	[112]
MPCM-coated PET 3D knitted fabric	1.85	489	[112]
CA-coated cotton fabric	34.1	1333	[109]
SA-coated cotton fabric	29.5	1280	[109]
MPCM-coated PET knitted fabric	4.4	440	[110]
MPCM-coated fabric	6.8	7.2	[111]

11. Future prospects

- The thermochromic multi-layer PCM fabrics will be prepared by incorporating thermochromic pigments on the protection layer. The potential applications are the fibrous visual temperature indicators.
- The multi-layer PCM fabrics will be realized the electric-thermal energy conversation by using conductive fabrics as protection layers. It can save the electrical power for Joule heating because the excess heat is stored by PCMs.
- To construct a multi-layer fabric to store fatty acid by controlling interfacial adhesion between used fibrous materials and molten fatty acid.
- The thermal enhancement of the multi-layer fabric remains to be improved although there has an achievement in the introduction of metal particles in the multi-layer fabric.

12. List of publications

12.1 Journal publications

[1] **K. Yang**, X. Zhang, M. Venkataraman, J. Wiener, X. Tan, G. Zhu, J. Yao, J. Militky, Sandwich Fibrous PEG Encapsulations for Thermal Energy Storage, **ChemPhysChem**. (2023). https://doi.org/10.1002/cphc.202300234. **(Q2, IF: 2.9)**

[2] **K. Yang**, X. Zhang, J. Wiener, M. Venkataraman, Y. Wang, G. Zhu, J. Yao, J. Militky, Nanofibrous Membranes in Multilayer Fabrics to Avoid PCM Leakages, **ChemNanoMat**. (2022). https://doi.org/10.1002/cnma.202200352. **(Q2, IF: 3.8)**

[3] **K. Yang**, J. Wiener, M. Venkataraman, Y. Wang, T. Yang, G. Zhang, G. Zhu, J. Yao, J. Militky, Thermal Analysis of PEG/Metal Particle-coated Viscose Fabric, **Polym Test**. (2021) 107231. https://doi.org/10.1016/j.polymertesting.2021.107231. (**Q1, IF: 5.1**)

[4] **K. Yang**, L. Martinkova, O. Ctibor, X. Zhang, M. Venkataraman, J. Wiener, G. Zhu, G. Zhang, J. Yao, J. Militky, Mass transfer and thermal buffering effect of hydrophobic fabrics with single-side coating of MPCMs, **Prog Org Coat.** 172 (2022) 107151. https://doi.org/10.1016/j.porgcoat.2022.107151. (**Q1, IF: 6.6**)

[5] **K. Yang**, Q. Peng, M. Venkataraman, J. Novotna, J. Karpiskova, J. Mullerova, J. Wiener, M. Vikova, G. Zhu, J. Yao, J. Militky, Hydrophobicity, water moisture transfer and breathability of PTFE-coated viscose fabrics prepared by electrospraying technology and sintering process, **Prog Org Coat**. 165 (2022) 106775. https://doi.org/10.1016/j.porgcoat.2022.106775. (**Q1, IF: 6.6**)

[6] **K. Yang**, M. Venkataraman, X. Zhang, J. Wiener, G. Zhu, J. Yao, J. Militky., Review: incorporation of organic PCMs into textiles, **Journal of Materials Science** (2021). doi: https://doi.org/10.1007/s10853-021-06641-3. **(Q2, IF: 4.5)**

[7] **K. Yang**, M. Venkataraman, J. Karpiskova, Y. Suzuki, S. Ullah, I.-S. Kim, J. Militky, Y. Wang, T. Yang, J. Wiener, G. Zhu, J. Yao, Structural analysis of embedding polyethylene glycol in silica aerogel, **Micropor Mesopor Mat**. 310 (2021). https://doi.org/10.1016/j.micromeso.2020.110636. **(Q1, IF: 5.2)**

[8] **K. Yang**, X. Zhang, M. Venkataraman, J. Wiener, S. Palanisamy, S. Sebnem, X. Tan, D. Kremenakova, G. Zhu, J. Yao, J. Militky, Structural Analysis of Phase Change Materials (PCMs)/Expanded Graphite (EG) Composites and Their Thermal Behavior under Hot and Humid Conditions, **ChemPlusChem**. (2023). https://doi.org/10.1002/cplu.202300081. **(Q2, IF: 3.4)**

[9] **K. Yang**, M. Venkataraman, J. Wiener, X. Zhang, M. Stuchlik, G. Zhu, J. Yao, J. Militky, Crystallization Mechanism of Micro Flake Cu Particle-filled

Poly(ethylene glycol) Composites, **Thermochim Acta**. (2022) 179172. https://doi.org/10.1016/j.tca.2022.179172. **(Q2, IF: 3.5)**

[10] **K. Yang**, A.P. Periyasamy, M. Venkataraman, J. Militky, D. Kremenakova, J. Vecernik, R. Pulíček, Resistance against penetration of electromagnetic radiation for ultra-light Cu/Ni-coated polyester fibrous materials, **Polymers-Basel**. 12 (2020). https://doi.org/10.3390/polym12092029. **(Q1, IF: 5)**

[11] X. Zhang, **K. Yang**, D. Kremenakova, J. Militky, Luminance bahavior and tensile property of twisted side-emitting polymer optical fibers bundles, polymer testing. (2022) 108016. https://doi.org/10.1016/j.polymertesting.2023.108016. **(Q1, IF: 5.1**)

[12] Y. Wang, V. Baheti, **K. Yang**, T. Yang, J. Wiener, J. Militký, Utility of whiskerized carbon fabric surfaces in resistive heating of composites, Polym Composite. (2021). https://doi.org/10.1002/pc.26012. **(Q1, IF: 5.2)**

[13] X. Tan, Q. Peng, **K. Yang**, T. Yang, J. Saskova, J. Wiener, M. Venkataraman, J. Militky, W. Xiong, J. Xu, Preparation and Characterization of corn husk nanocellulose coating on electrospun polyamide 6, Alexandria Eng J. (2021). https://doi.org/10.1016/j.aej.2021.10.011. **(Q1, IF: 6.8)**

[14] A.P. Periyasamy, **K. Yang**, X. Xiong, M. Venkataraman, J. Militky, R. Mishra, D. Kremenakova, Effect of silanization on copper coated milife fabric with improved EMI shielding effectiveness, Mater Chem Phys. 239 (2020). https://doi.org/10.1016/j.matchemphys.2019.122008. **(Q2, IF: 4.6)**

[15] Y. Wang, V. Baheti, M.Z. Khan, M. Vikova, **K. Yang**, T. Yang, J. Militky, A facile approach to develop multifunctional cotton fabrics with hydrophobic self cleaning and UV protection properties using ZnO particles and.pdf, The Journal of The Textile Institue. (2021). https://doi.org/10.1080/00405000.2021.1975905. **(Q2, IF: 1.7)**

[16] X. Zhang, Z. Jin, L. Hu, X. Zhou, **K. Yang**, D. Kremenakova, J. Militky, A Silver Yarn-Incorporated Song Brocade Fabric with Enhanced Electromagnetic Shielding, Materials. 14 (2021) 3779. https://doi.org/10.3390/ma14143779. **(Q1, IF: 3.4)**

[17] T. Yang, F. Saati, K.V. Horoshenkov, X. Xiong, **K. Yang**, R. Mishra, S. Marburg, J. Militký, Study on the sound absorption behavior of multi-component polyester nonwovens: experimental and numerical methods, Text Res J. 89 (2019) 3342–3361. https://doi.org/10.1177/0040517518811940. **(Q2, IF: 2.3)**

[18] X. Xiong, M. Venkataraman, T. Yang, K. Kucerova, J. Militký, **K. Yang**, G. Zhu, J. Yao, Transport properties of electro-sprayed polytetrafluoroethylene fibrous

layer filled with aerogels/phase change materials, Nanomaterials-Basel. 10 (2020) 1–14. https://doi.org/10.3390/nano10102042. **(Q1, IF: 5.3)**

[19] Y.F. Wang, V. Baheti, **K. Yang**, M. Venkataraman, T. Yang, J. Militky, Study on ohmic heating behavior of fly ash filledarbon woven/epoxy resin composite?, J Fiber Bioeng Informatics. 13 (2020) 1–11. https://doi.org/10.3993/jfbim00329.

[20] Q. Peng, **K. Yang**, M. Venkataraman, X. Tan, X. Xiong, J. Novotna, J. Karpiskova, J. Hruza, M. Stuchlík, J. Militky, Preparation of electrosprayed composite coated microporous filter for particulate matter capture, Nano Sel. (2021). https://doi.org/10.1002/nano.202100186.

[21] **K. Yang**, X. Zhang, M. Venkataraman, K. Chen, Y. Wang, J. Wiener, G. Zhu, J. Yao, J. Militky, Thermal Behavior of Flexible and Breathable Sandwich Fibrous Polyethylene Glycol (PEG) Encapsulations, **Textile Research Journal**. (2023) **(Submitted) (Q2, IF: 2.3)**

12.2 Conferences

[1] **K. Yang**, Q. Peng, M. Venkataraman, J. Novotna, X. Xiong, J. Wiener, Y. Wang, X. Tan, G. Zhu, J. Yao, J. Militky, Hydrophobic Breathable Fabric via Electrospraying Technology. **Autex Conference 2021**.

[2] **K. Yang,** M. Venkataraman, Y. Wang, J. Wiener, J. Milikty. Preparation of Polyamide 6 Nanofibrous Membranes Coated with Polyethylene Glycol. **47th Textile Research Symposium 2019**.

[3] **K. Yang**, M. Venkataraman, Y.-F. Wang, X.-M. Xiong, T. Yang, J. Wiener, J. Militky, R. Mishra, J. Marek, G.-C. Zhu, J.-M. Yao, Thermal behaviour of multi-layer composite containing PEG and laponite as PCM, in: 2019: pp. 671–676.

[4] S. Hu, D. Wang, **K. Yang**, Y.-F. Wang, T. Yang, Q.-Y. Peng, X.-D. Tan, D. Kremenakova, J. Militky, M. Venkataraman, A.P. Periyasamy, Copper coated textiles for inhibition of virus spread, in: 2020: pp. 84–91.

[5] Q.-Y. Peng, S.-L. Xiao, X.-D. Tan, **K. Yang**, Y.-F. Wang, T. Yang, D. Wang, S. Hu, X.-M. Xiong, M. Venkataraman, J. Militky, Dendrimer-grafted PLGA nanofibrous matrix-mediated gene delivery systems, in: 2020: pp. 152–158.

[6] Y.-F. Wang, J. Militky, A.P. Periyasamy, M. Venkataraman, V. Baheti, **K. Yang**, S. Hu, D. Wang, X.-D. Tan, T. Yang, Q.-Y. Peng, Disinfection mechanisms of UV light and ozonization, in: 2020: pp. 173–180.

[7] Y.-F. Wang, D. Karthik, **K. Yang**, T. Yang, X.-M. Xiong, V. Baheti, J. Militký, Electrical heating properties of carbon fabric/green epoxy composites filled with fly ash, in: 2019: pp. 44–51.

[8] Y.-F. Wang, V. Baheti, **K. Yang**, S. Hu, D. Wang, X.-D. Tan, T. Yang, J. Militký, Electrical heating properties of various carbonized textile structures, in: 2020: pp. 99–106.

[9] A.P. Periyasamy, **K. Yang**, X. Xiong, M. Venkatraman, J. Militky, R. Mishra, D. Kremenakova, Influence of EMI Shielding on Silane-coated Conductive Fabric, in: 2019: pp. 67–71.

[10] X.-D. Tan, Q.-Y. Peng, **K. Yang**, J. Saskova, A.P. Periyasamy, J. Militky, J. Wiener, Influence of UV light and ozonization on microbes, in: 2020: pp. 159–166.

[11] Q.-Y. Peng, M. Venkataraman, **K. Yang**, J. Militky, Kinetic model for disinfection with photo-oxidation, in: 2020: pp. 68–75.

[12] M. Venkataraman, **K. Yang**, A.P. Periyasamy, X. Xiong, J. Militky, R. Mishra, Modification of electromagnetic property of copper coated milife fabrics, in: 2019: pp. 694–700.

[13] T. Yang, F. Saati, X.-M. Xiong, Y.-F. Wang, **K. Yang**, R. Mishra, J. Militký, M. Petrů, Numerical modelling of the acoustic properties of polyester non-woven, in: 2019: pp. 767–776.

[14] M. Venkataraman, R. Mishra, K. Yang, J. Militky, D. Kremenakova, G. Zhu, J. Yao, Preparation of Electrosprayed Microporous Membranes, in: 2018. https://doi.org/10.1088/1757-899x/460/1/012017.

[15] X.-D. Tan, Q.-Y. Peng, **K. Yang**, Y.-F. Wang, T. Yang, D. Wang, S. Hu, X.-M. Xiong, J. Saskova, J. Wiener, M. Venkataraman, J. Militky, The effect of electrode materials and ultrasound on electrochemical reduction, in: 2020: pp. 554–560.

[16] D. Wang, S. Hu, D. Kremenakova, J. Militky, M. Venkataraman, Y.-F. Wang, **K. Yang**, Q. Peng, X.-D. Tan, Virology of SARS-CoV-2, in: 2020: pp. 49–55.

[17] M. Venkataraman, X.-M. Xiong, T. Yang, **K. Yang,** Y.-F. Wang, R. Mishra, J. Militký, Thermal performance of Kevlar woven fabrics coated with silica aerogel, in: 2019: pp. 687–693.

12.3 Book chapters

[1] **K. Yang**, X. Zhang, M. Venkataraman, J. Wiener, J. Militky. Phase Change Materials in Textiles for Thermal Regulation, in Advanced Multifunctional Materials from Fibrous Structure. Springer, 2023: 27-47.

https://doi.org/10.1007/978-981-99-6002-6_2.

[2] **K. Yang**, M. Venkataraman, J. Wiener, J. Militký, Photoluminescence PCMs and their potential for thermal adaptive textiles, in multifunctional Phase Change Materials. Elsevier, 2023: pp. 255-277. https://doi.org/10.1016/B978-0-323-85719-2.00006-7.

[3] **K. Yang**, X. Zhang, M. Venkataraman, J. Militký, Characterization of Polymer Crystallization by Using Thermal Analsys, in: Polymer Crystallization: Methods, Characterization and Applications, Wiley, 2023: 13-31. https://onlinelibrary.wiley.com/doi/10.1002/9783527839247.ch2.

[4] **K. Yang**, M. Venkataraman, J. Militký, Textiles and Their Use in Microbial Protection, in: Fundamental Principles for Moisture Harvesting System and Its Design of Fabric, 1st ed., CRC Press, 2021: pp. 283–298. https://doi.org/10.1201/9781003140436-17.

[5] **K. Yang**, M. Venkataraman, J. Militky, J. Wiener. A review of PCM and their application in textile, in: Recent trends in fibrous material science. 2020.